Stationary and Temporal Structure of Antibody Titer Distributions to Human Influenza A Viruses in Southern Vietnam

A thesis submitted for the degree of

Doctor of Philosophy in Clinical Medicine

by

Nguyen Thi Duy Nhat

September 30, 2017

Nuffield Department of Medicine, University of Oxford, United Kingdom

Oxford University Clinical Research Unit, Ho Chi Minh City, Vietnam

Hospital for Tropical Diseases, Ho Chi Minh City, Vietnam

Abstract

(Part of this abstract was published in the publication titled "Structure of the general-population antibody titers distributions in influenza virus" published in *Nature Scientific Reports* on July 20, 2017 (PMID: 28729702))

Seroepidemiology aims to understand population-level exposure and immunity to infectious disease. Serological results are normally presented as binary outcomes describing the presence or absence of antibody, despite the fact that many assays measure continuous quantities. A population's antibody titers may include information on multiple serological states – naiveté, recent infection, non-recent infection, childhood infection – not just seropositivity or seronegativity. In the first part of this thesis, I investigate 20,152 general-population serum samples from southern Vietnam collected between 2009 and 2013 from which I report antibody titers to the influenza virus HA1 protein using a continuous titer measurement from a protein microarray assay. I describe titer distributions to subtypes 2009 H1N1 and H3N2, and using a model selection approach for mixture distributions, I determine that 2009 H1N1 is best described by four titer subgroups while H3N2 is best described by three titer subgroups. For H1N1, my interpretation is that the two highest-titer subgroups correspond to recent and historical infection, which is consistent with pandemic attack rates. For H3N2 however, right-censoring of titers makes interpretations difficult to validate. To move beyond this stationary interpretation of titers, I developed two methods for analyzing this serum collection as a time series. First, I attempted to analyze mixture categories in individual time windows. This approach did not lead to a consistent temporal picture of titer

change; results differed by site and were sensitive to assumptions in the mixture fitting. Second, I attempted to fit a hybrid-dynamical model with free incidence parameters. This inference was robust to parameter assumptions, consistent across sites, and in agreement with the incidence reported in Vietnam's influenza surveillance network. In addition, my new approach showed evidence that there was a second silent wave of the 2009 influenza pandemic that was not recorded in national surveillance, which is this thesis' main novel result.

Acknowledgements

To my DPhil advisor, Prof. Maciek Boni, I could not thank you enough for the academic advice and guidance that have motivated me throughout my entire course of research and thesis writing. Maciek took me into his lab as a fresh-from-school engineer with nothing but unrelated chemical process modelling background, introduced me to infectious disease, lent me his Rohani book, taught me the basic probability theories and the concept of random variables, and helped me put together my very first maximum likelihood optimization in C++. From the Boni lab, I learned about the existence of other programing languages besides Matlab. Java has saved me and this thesis, and I am very certain that we will stay friends for many more years to come. Without Maciek's continuous support and encouragement, I would have not been able to make it this far.

I want to thank Professor Marion Koopmans, Head of the Department of Viroscience at Erasmus Medical Centre (EMC) in the Netherlands, and Erwin de Bruin who has been leading the development of microarray technology in Prof Koopmans' research group. Prof Koopmans' research team at EMC and the RIVM were very generous in sharing their awesome microarray technology that they developed (printing thousands of slides for the work in this thesis!) and their collaboration and support since the very first days of my DPhil. I also want to thank Dr Janko van Beek for writing the original scripts for titer fitting as these were used to develop the analyses in Chapter 2 of this thesis.

To my co-advisors, Prof. Steve Baker and Prof. Cameron Simmons, I want to express my gratitude to Cam for his help setting up this SSE study and making this work a possibility, and to Steve for reminding me that it is important for a mathematical modeler to have deep epidemiological understanding of the underlying mechanism.

I would like to acknowledge the financial support from the Prize Studentship from Oxford University Clinical Research Unit, The Wellcome Trust Major Overseas Programme, and Nuffield Department of Medicine at Oxford University for funding all research and travel expenses during the course of my DPhil, and the the Li Ka

Shing foundation for providing the computing clusters being used in some analyses of this thesis.

To my current and former gang from the Boni Lab and Room 305, I would like to thank you all for the stimulating discussions and hundreds of afternoon tea, coffee, and milk tea over the years. I am so thankful for Thu's presence in the group in particular; the quality of my research has grown up exponentially since she joined Room 305 because I was always well fed. My heartfelt gratitude especially goes to Lam, Thanh, Thao, Vy, Giang, and Quan for processing thousands of samples and analyzing thousands of slides – the kind of work that requires utter attention to details. I wish to thank Stacy for her valuable clinical inputs, for giving me access to her clinical data, and for reminding me to step out of my modelling bubble and look at the big picture. Without any one of you, there would be no data-fitting component in this thesis (and everybody knows (quietly) that I am neither the best programmer nor a good theorist).

To my dearest friends and partners in crime for life – Quyen, Khanh, Tuyet Anh, and Duong, thank you for reminding of a life outside the lab, for always keeping your spirit and faith up even when I lost mine, and for sending food over despite living half of the city away. To my Organicare teammates – the "Anh" triplet, thank you for showering me with group messages that I cannot even keep up with; your patience, and care over the years.

Last but not least, I want to express my deepest gratitude to my beloved parents for their constant consolation in my pursuit of an academic path, for their unconditional love and support over the last three decades of my life, and for being the best parents anybody could ever ask for. Of course, I have to duly thank my furry little brother – Bao, for his complimentary stress-relieving therapy.

To my fiancé – M., I am so grateful for all the morning and midnight coffee, dishwashing, clam linguine, and BBQ that I was entitled to. Thank you for all your love and patience, especially for rushing to the study room to pick up my pen or turning on the lights during the last couple stressful months of my thesis writing.

My life has been so blessed with love and joy, a loving family, a down-to-earth gang, a supportive partner, and a fruitful education. I must have been the

luckiest girl on earth. This thesis may bear my name on it, but the entire voyage was a team effort. This long journey has brought to my life people that will stay as lifelong friends and companions. I want to sincerely thank each and every one of you from the bottom of my heart for helping me grow, academically and personally, over the last four years and for making this thesis a reality.

(The following passage is in Vietnamese and is dedicated to my beloved parents.)

Con thật là đứa trẻ may mắn được sinh ra trong gia đình mình, được lớn lên trong tình thương và sự hi sinh vô bờ bến của ba má trong suốt 30 năm qua. Vậy là con đường học hành dài đăng đẵng của con từ Berkeley đã sắp kết thúc ở Oxford, lúc nào cũng có ánh mắt lo lắng của ba má dõi theo.

Cảm ơn ba đã dạy cho con biết từ nhỏ giá trị của lao động không mệt mỏi và kiên trì theo đuổi đam mê trong cuộc sống. Từ những bài toán khó ba vẫn giải cho con qua điện thoại khi công tác xa nhà cho đến lời dặn dò "ba biết con sẽ làm được nếu con thực sự muốn" trước ngày con bắt đầu đi học xa, tấm bằng này con đã thay ba hoàn thành ước mơ của cả hai ba con mình rồi.

Cảm ơn má đã luôn yêu thương và lắng nghe con trong suốt những năm tháng xa nhà; Bé Mập và Duy Nhất sẽ luôn là hai người bạn thân thiết.

Khi con chuẩn bị nộp bài thầy đã hỏi sau này luận văn được xếp trong thư viện trường con có muốn đề tên tiếng Anh là "Nhất Nguyễn" không? Con nói muốn được in tên trên luận văn là Nguyễn Thị Duy Nhất để đề tặng ba má. Con luôn biết ơn cuộc đời này vì được làm con của ba và má.

Table of Contents

Abstract ii

Acknowledgements iv

List of Figures xi

List of Tables xv

List of Abbreviations xvii

1 Chapter 1: Background and Introduction 1

1.1 Influenza viruses 1

1.2 The global epidemiology of influenza A 8

1.3 Influenza serology 12

1.4 Influenza serological surveillance 13

1.5 Influenza in Vietnam 15

1.6 Objectives 17

2 Chapter 2: Methods 20

2.1 Background 20

2.2 Serial Serological Epidemiological (SSE) Influenza Surveillance in Southern Vietnam 22

2.2.1 Data collection 22

2.2.2 Serological assays using protein microarray 24

2.2.3 Slide preparation and processing 25

2.2.4 Slide scanning and analysis 25

2.3 Mapping luminescence values to titers using luminescence values at four dilutions 26

2.3.1 Four-parameter log-logistic curve 26

2.3.2 Defining maximum error tolerance to identify monotonic quartet 28

2.4 Standardization against H1N1 Pdm 2009 International Standard (IS) 30

2.4.1 Standard procedure 32

2.4.2 Advanced correction procedure 33

2.5 Mapping luminescence to titers for two testing dilutions 34
2.5.1 Possible dilution pairs 35
2.5.2 Comparing mapping models 35
2.6 Titer reproducibility 37
2.7 Age-dependent titer cut-offs to define positivity 38
2.8 Discussion 41

3 Chapter 3: Stationary Structure of General-Population Antibody Titer Distributions to Influenza A Virus 44
3.1 Background 44
3.2 Data 48
3.3 Methods 49
3.3.1 Maximum likelihood framework 49
3.3.2 Model selection 52
3.4 Results 52
3.4.1 Representativeness of sample collection versus census data 52
3.4.2 Choosing bin width to discretize the normal distribution 54
3.4.3 Comparisons of Gamma, Weibull, and Normal distribution 55
3.4.4 Multimodal patterns of the general population antibody titers distribution against H1N1 and H3N2 60
3.4.5 Four-component mixture models for H1N1 Pdm 2009 strain 64
3.4.5.1 Sub-sampling data according to the age-group proportions and age bands in the general population 70
3.4.5.2 Stratifying data by collection years 72
3.4.5.3 Stratifying data by samples' ages 74
3.4.5.4 Multi-lineage hypothesis for H1N1 78
3.4.6 Three-component mixture models for geometric mean titers of H3N2 2009 and 2011 strains 80
3.4.7 ROC for the four-component mixture model for H1-09 88
3.5 Discussion 89

4 Chapter 4: Serological Dynamics For 2009 H1N1 Using Mixture Components 94
4.1 Background 94
4.2 Data 97
4.2.1 Serological data 97
4.2.2 Sentinel data 97
4.3 Methods 98
4.3.1 Fixing parameters in mixture fits 98
4.3.2 Comparison of w_4 and $w_4 + w_3$ time series to monthly ILI+ cases from sentinel data 100
4.3.3 Comparison of $w_3 + w_4$ time series to the cumulative ILI+ cases from sentinel data 102
4.4 Results 102
4.4.1 BIC comparison among the four fitting scenarios 102
4.4.2 Back-mapped time series w_4 vs. monthly ILI+ cases from sentinel data 107
4.4.3 Time series of $w_3 + w_4$ vs. monthly ILI+ cases from sentinel data 113
4.4.4 Time series $w_3 + w_4$ vs. cumulative ILI+ cases from sentinel data 118
4.5 Discussion 122

5 Chapter 5: Sero-Dynamics Using Individual Weekly Incidence Parameters 128
5.1 Background 128
5.2 Data 131
5.2.1 Serological data 131
5.2.2 Sentinel data 133
5.3 Methods 133
5.3.1 Model description 133
5.3.2 Antibody waning 136
5.3.3 Post-infection seroconversion 138
5.3.4 Reduced susceptibility 139

5.3.5 Likelihood framework 140
5.3.5.1 Multinomial distribution of discrete titer values 141
5.3.5.2 Normal likelihood of individual titer observations 142
5.3.5.3 Gamma likelihood of individual titer observations 143
5.4 Results 143
5.4.1 Dak Lak 145
5.4.1.1 Inferred antibody waning and post-infection seroconversion rates 146
5.4.1.2 Inferred biweekly incidences vs. sentinel data 149
5.4.2 Kien Giang 152
5.4.2.1 Inferred antibody waning and post-infection seroconversion rates 153
5.4.2.2 Inferred biweekly incidences vs. sentinel data 155
5.4.3 Hue 157
5.4.3.1 Inferred antibody waning and post-infection seroconversion rates 158
5.4.3.2 Inferred biweekly incidences vs. sentinel data 160
5.5 Discussion 162
5.6 Additional Figures 167

6 Chapter 6: Discussion 182
6.1 Motivation 182
6.2 Key results 188
6.3 Limitations and challenges 193
6.4 Areas for further exploration 197

7 References 201

List of Figures

Figure 1.1 Sentinel data for detrended number of weekly ILI+ cases by regions in Vietnam. 17

Figure 2.1 Geographic locations of ten collection sites.. 23
Figure 2.2 An example of the 64-pad protein microarray slide..... 25
Figure 2.3 Four-parameter log-logistic curve..... 27
Figure 2.4 Examples of a non-monotonic luminescence quartet… 28
Figure 2.5 Mean of luminescence differences in $\log_{10}$ units between two duplicated spots grouped by luminescence range..... 30
Figure 2.6 Four-dilution titers vs. luminescence at each dilution from 1:20 to 1:1280 34
Figure 2.7 Two-dilution titers obtained from cubic spline surface map vs. four-dilution titers for different pairs of dilutions..... 38
Figure 2.8 Titer reproducibility for human and ISH2 sera from eleven duplicates… 38
Figure 2.9 Age-specific seroprevalence for post-pandemic data and the Ha Nam cohort 40
Figure 2.10 Pre-pandemic titers in $\log_2$-units by age groups.. 41

Figure 3.1 Collected sample population versus Vietnam national housing census in 2009 for different sites….. 53
Figure 3.2 Comparing model fits between Normal, Gamma, and Weibull distributions for aggregated titers against H1-09. 57
Figure 3.3 Comparing model fits between Normal, Gamma, and Weibull distributions for aggregated titers against seasonal H3N2 strains… 58
Figure 3.4 Population-level antibody titer histograms H1-09 and H3N2 grouped by age groups.. 61
Figure 3.5 QQ-plot comparisons among different collection sites for H1-09 titers…62
Figure 3.6 QQ-plot comparisons among different collection sites for H3N2 titers….63

Figure 3.7 Fit results different number of mixture components for H1-09 grouped by collection sites. 68
Figure 3.8 Visualization of model selection process for 2009 H1N1 titer-distribution models from Figure 3.7 69
Figure 3.9 Model fits for H1-09 titers for four random sub-samples 71
Figure 3.10 Model fits for H1-09 titers for aggregated data stratified by collection years 73
Figure 3.11 An additional visualization of age structure in the titer distributions against H1-09 and H3N2 76
Figure 3.12 Model fits for titer distributions against H1-09 grouped by different age groups 77
Figure 3.13 Model fits to validate multi-lineage hypothesis for H1-09 79
Figure 3.14 Model fits for titer distributions against H3N2 grouped by different collection sites 84
Figure 3.15 Visualization of model selection process for H3N2 titer distributions from Figure 3.14 85
Figure 3.16 Model fits for titer distributions against H3N2 grouped by different age groups 86
Figure 3.17 Antibody titer histograms against all H1N1 and H3N2 strains on the protein microarrays 87
Figure 3.18 ROC curves for H1N1 using four mixture components for aggregated data and individual sites. 89

Figure 4.1 Model fits different fitting scenarios grouped by collection site 105
Figure 4.2 Bimonthly time series of w_4 for different fitting scenarios 106
Figure 4.3 Monthly time series of w_4 back-distributed by **3 months** 108
Figure 4.4 Monthly time series of w_4 back-distributed by **6 months** 109
Figure 4.5 Monthly time series of w_4 back-distributed by **9 months** 110
Figure 4.6 Monthly time series of w_4 back-distributed by **12 months** 111

Figure 4.7 Monthly time series of w_3+w_4 for data grouped by collection site in which w_4 was back-distributed by **6 months,** and w_3 was back-distributed by **12 months…**.. 114
Figure 4.8 Monthly time series of w_3+w_4 for data grouped by collection site in which w_4 was back-distributed by **6 months,** and w_3 was back-distributed by **18 months…**.. 115
Figure 4.9 Monthly time series of w_3+w_4 for data grouped by collection site in which w_4 was back-distributed by **9 months,** and w_3 was back-distributed by **12 months…**.. 116
Figure 4.10 Monthly time series of w_3+w_4 for data grouped by collection site in which w_4 was back-distributed by **9 months,** and w_3 was back-distributed by **18 months…**..... 117
Figure 4.11 Bimonthly time series of w_3+w_4 vs. bimonthly cumulative ILI+ cases from sentinel data..... 121

Figure 5.1 Time series (MM/YY) of antibody titers against H1N1 Pdm 2009. 132
Figure 5.2 Compartmental models for equations (5.1) – (5.6). 134
Figure 5.3 Antibody waning function as a function of time in which ω = 90.0 (days) and a 30-day delay in R_7 for different values of c..... 137
Figure 5.4 Proportion of post-infection titers seroconverted into different R-Classes for different values of λ..... 139
Figure 5.5 Reduced susceptibility as a function of titer values with $T50$ = 80.0 and β varies from 0.3 to 1.5..... 140
Figure 5.6 Optimization results for **Dak Lak** using the gamma likelihood function..... 148
Figure 5.7 Comparing biweekly seroincidence from **Dak Lak** using gamma likelihood function to sentinel data..... 151
Figure 5.8 Optimization results for **Kien Giang** using gamma likelihood function.154
Figure 5.9 Comparing biweekly seroincidence from **Kien Giang** using gamma likelihood function to sentinel data..... 156
Figure 5.10 Optimization results for **Hue** using gamma likelihood function..... 159

Figure 5.11 Comparing biweekly seroincidence from **Hue** using gamma likelihood function to sentinel data…… 161
Figure 5.12 Optimization results for **Dak Lak** using multinomial likelihood function…… 168
Figure 5.13 Optimization results for **Dak Lak** using normal likelihood function….169
Figure 5.14 Comparing biweekly seroincidence from **Dak Lak** using multinomial likelihood function to sentinel data…… 170
Figure 5.15 Comparing biweekly seroincidence from **Dak Lak** using normal likelihood function to sentinel data…… 171
Figure 5.16 Optimization results for **Kien Giang** using multinomial likelihood function…… 172
Figure 5.17 Optimization results for **Kien Giang** using normal likelihood function…..
…… 173
Figure 5.18 Comparing biweekly seroincidence from **Kien Giang** using multinomial likelihood function to sentinel data…… 174
Figure 5.19 Comparing biweekly seroincidence from **Kien Giang** using normal likelihood function to sentinel data. …… 175
Figure 5.20 Optimization results for **Hue** using multinomial likelihood function.
…… 176
Figure 5.21 Optimization results for **Hue** using normal likelihood function. …….. 177
Figure 5.22 Comparing biweekly seroincidence from **Hue** using multinomial likelihood function to sentinel data. …… 178
Figure 5.23 Comparing biweekly seroincidence from **Hue** using normal likelihood function to sentinel data…… 179
Figure 5.24 Smoothed spline fit to the age-stratified GMT timer series against H1-09 by collection site…… 180

List of Tables

Table 2.1 List of hospital laboratories where samples were collected..... 23
Table 2.2 List of all influenza strains tested on the protein microarrays..... 24
Table 2.3 Summary of ISH2 performance against all antigens 32
Table 2.4 The age-specific 95th, 90th, and 80th percentile titers for pre-pandemic dataset against H1-09 39

Table 3.1 LLH optimization results for different bin widths..... 55
Table 3.2 Change in BIC scores for aggregated data against H1-09..... 59
Table 3.3 Change in BIC scores for aggregated data against H3N2..... 59
Table 3.4 Change in BIC scores for H1-09 data grouped by collection sites 66
Table 3.5 Estimates with 95% confidence intervals in parentheses, for means, variances, and weight parameters, for one-component to four-component mixture models of H1N1 titers plotted in Figure 3.7 and 3.8..... 67
Table 3.6 Change in BIC scores for model fits to H1-09 titers for four random subsamples.. 70
Table 3.7 Estimates and confidence intervals for weight parameters in post-pandemic (January to June 2010) analysis for four-component models..... 75
Table 3.8 Change in BIC scores for H1-09 data grouped by age groups 75
Table 3.9 Change in BIC scores for H3N2 models fits grouped by collection site..... 82
Table 3.10 Change in BIC scores for H3N2 models grouped by age group..... 82
Table 3.11 Estimates with 95% confidence intervals in parentheses, for mean, variance, and weight parameters, for one-component to four-component mixture models of H3N2 titers plotted in Figure 3.14 and 3.15. 83

Table 4.1 Change in BIC scores for four-component mixture model for four fitting scenarios..... 103
Table 4.2 Spearman's correlations and p-values for different fitting scenarios grouped by collection site for different values of *m* ranging from 2 to 12 months..112

Table 4.3 Spearman's correlation and p-values for different fitting scenarios described in Figure 4.11 grouped by collection sites. 118

Table 5.1 Model parameters 136
Table 5.2 AIC values for the Dak Lak data 146
Table 5.3 Inferred antibody waning and post-infection seroconversion patterns for Dak Lak using gamma likelihood function 147
Table 5.4 AIC values for Kien Giang data 152
Table 5.5 Inferred antibody waning and post-infection seroconversion patterns for Kien Giang using gamma distribution 153
Table 5.6 AIC values for Hue data 157
Table 5.7 Inferred antibody waning and post-infection seroconversion patterns for Hue using gamma likelihood function 158
Table 5.8 Inferred antibody waning and post-infection seroconversion patterns for Dak Lak using gamma likelihood function for different values of ω 181

List of Abbreviations

AIC	Akaike Information Criterion
ADS	Age-dependent Seroconversion
BIC	Bayesian Information Criterion
DL	Dak Lak province, Vietnam
GMT	Geometric Mean Titer
KG	Kien Giang province, Vietnam
KH	Khanh Hoa province, Vietnam
H1-09	H1N1 Pandemic 2009
HC	Ho Chi Minh City, Vietnam
HI	Hemagglutination Inhibition
HU	Thua Thien Hue province, Vietnam
IAR	Infection Attack Rate
ILI	Influenza-Like Illness
IS	International Standard
ISH2	2nd International Standard against H1N1 Pandemic 2009 Virus
LLH	Log-Likelihood
MLE	Maximum Likelihood Estimate
MN	Micro Neutralization
NIHE	National Institute of Hygiene and Epidemiology
OAS	Original Antigenic Sin
OUCRU	Oxford University Clinical Research Unit, Ho Chi Minh City, Vietnam
Pdm	Pandemic
PM	Protein Microarray Assay
SSE	Serial Seroepidemiology
WHO	World Health Organization

CHAPTER 1

1 Background and Introduction

1.1 Influenza viruses

Human influenza viruses – sometimes called seasonal influenza viruses – cause upper respiratory tract infections in humans, commonly known as 'flu' infections. Influenza infections are not usually severe, causing a range of common symptoms including fever, headache, cough, rhinorrhea, myalgia, and dyspnea. Influenza transmission from human to human occurs via aerosol droplets from coughing, sneezing, or other direct or indirect contact with infected individuals (WHO 2016). The infection is self-limiting and typically lasts between two and seven days. A minority of infections will result in severe disease and may require hospitalization. Individuals with comorbidities, immune-suppressed individuals, infants, and the elderly are susceptible to severe symptoms and hospitalization resulting from an influenza infection.

The four influenza pandemics in the last century killed more than 50 million people worldwide (Fodor and Brownlee 2002), and the most recent H1N1 pandemic in 2009 caused a global estimate of 1 million deaths due to influenza-associated clinical outcomes during the first year of virus circulation (Dawood et al. 2012). Seasonal influenza is also associated with annual morbidity and mortality. In the

United Kingdom, there are an estimated 28,000 influenza-attributable hospitalizations and 7,000 influenza-attributable deaths every year (Matias et al. 2016), with the highest hospitalization rates observed in individuals over the age of 75. Globally, the World Health Organization has estimated that there are between three and five million severe cases of influenza every year, and approximately 250,000 to 500,000 deaths, most of which are among infants and the elderly (WHO 2016).

Influenza is a member of the viral family *Orthomyxoviridae*. At the next lower taxonomic level, influenza virus is separated into *types* A, B, and C according to differences in antigenic properties of their internal proteins, nucleoprotein (NP), and matrix protein (M). Among the three types of influenza viruses, the genomes of influenza A and B are much closer to each other than they are to the genome of influenza C, and flu A and B are responsible for the majority of the human influenza burden. Influenza A is primarily an avian disease that also infects mammals (Webster et al. 1992; Nicholson, Wood, and Zambon 2003). The natural reservoirs of influenza A viruses include wild and domestic aquatic birds. Influenza A is enzootic in domestic pigs, and commonly causes infections in horses, dogs, cats, and a range of other mammals (Webster et al. 1992). Influenza B is primarily a human infection and has not been found in any avian hosts. Influenza C is a human infection and is associated with milder clinical symptoms than flu A or flu B. Since influenza A is the most common and most severe form in humans, the motivations, data collection, and analyses presented in this thesis will all relate to influenza A.

Influenza virus is an enveloped, segmented, negative-sense, single-stranded RNA virus. The influenza A genome consists of eight RNA segments that code for ten proteins – the two basic subunits of the polymerase protein (PB1 and PB2), the acidic subunit of the polymerase protein (PA), haemagglutinin (HA), nucleoprotein (NP), neuraminidase (NA), two matrix proteins (M1 and M2), and two nonstructural proteins (NS1 and NS2), among which the most immunogenic ones are HA and NA (Webster et al. 1992). On the surface of the viral particle HA is approximately three times as abundant as NA (Wilson and Cox 1990). While HA antigen is responsible for binding and fusion of the influenza virion onto the host cell, NA cleaves the viral particle from the host cell and allows for further viral replication within the host (Webster et al. 1992; Schrauwen and Fouchier 2014). Because of selection pressure exerted by host immunity, these two surface proteins evolve much more quickly than the internal proteins (Gorman et al. 1990).

The differences in the surface HA and NA viral proteins which determine the viral replication mechanism, range of infecting hosts, transmissibility, and pathogenicity are used to classify influenza into different *subtypes*. There are 18 HA subtypes and 11 NA subtypes identified in influenza A viruses (Schrauwen and Fouchier 2014). However, only 3 HA subtypes (H1, H2, and H3) and 2 NA subtypes (N1 and N2) have been able to sustain stable human-to-human transmission since 1918. The finer taxonomy of influenza A subtypes is described by influenza *variants* and *strains*. Typically, within one subtype two genotypes are considered as different *variants* if they confer *partial cross-immunity* on one another. Two different

genotypes of the same variant are labeled as different *strains* if infection with one strain confers complete protection against the other.

During a course of a natural influenza infection, a number of defense mechanisms are involved. The innate immune response reacts quickly to an influenza virus and is effective in controlling viral replication and clearing infected cells (Cox, Brokstad, and Ogra 2004). The cellular immune response mediated by virus-specific T cells then activates cytotoxic T Lymphocytes (CTL) and is responsible for clearing the virus (Kreijtz, Fouchier, and Rimmelzwaan 2011). The main target of the CTL are NP, M1, and PA proteins – the more conserved part of the influenza virus. Even though the post-infection virus-specific CTL response is known to induce broad protection even across different subtypes (Jameson, Cruz, and Ennis 1998; McMichael et al. 1983), it does not correlate with susceptibility to future infections (Cox, Brokstad, and Ogra 2004). The humoral immune response forms a second line of defense by facilitating the production of subtype-specific antibody against the HA and NA viral proteins of the virus (C. Potter and Oxford 1979; Gerhard 2001). The HA-specific antibodies attach themselves onto the globular head of the HA viral surface proteins to inhibit attachment of the viral particles onto host cells, resulting in virus neutralization (Cox, Brokstad, and Ogra 2004). In addition, binding of the HA antibody to proteins presented on the surface of infected cells facilitates the antibody-dependent cell cytotoxicity (ADCC) process and allows the natural killer cells to recognize and lyse infected cells (Arnon et al. 2001). Natural infection with a given influenza virus is known to lead to long-lasting immunity against that particular variant, and presence of HA-specific antibodies is

considered evidence of past exposure to a given influenza virus (Hobson et al. 1972). On the other hand, NA-specific antibodies inhibit enzymatic activities facilitated by NA viral proteins and thus limit within host replication, resulting in moderate neutralization of the viral population (Cox, Brokstad, and Ogra 2004; Kreijtz, Fouchier, and Rimmelzwaan 2011). Results from a rabbit model showed that NA antibodies cannot fully neutralize influenza virus to confer protection against future infection (Kilbourne et al. 1968), but these NA-specific antibodies worked to reduce the viral load and severity in both animal and human challenge studies (Kilbourne et al. 1968; Murphy, Kasel, and Chanock 1972). The three major antibody isotopes produced by the humoral immune response are IgG, IgM, and IgA. IgA and IgM virus-specific antibodies are produced rapidly following an infection and play a major role in neutralizing the infected virus during primary infection. They peak at around two weeks after infection onset and are indicative of a recent influenza infection (Rothbarth et al. 1999; Couch and Kasel 1983). IgGs are generally produced about two to four weeks following an infection and are usually long lived (Murphy and Clements 1989).

In addition to immunity against strains of the same infected subtype known as *homosubtypic* response (Freeman et al. 2016), the humoral immune response induces a weaker cross-protection against influenza strains of different subtypes, known as *heterosubtypic* response (Jameson, Cruz, and Ennis 1998; McMichael et al. 1983; Hillaire et al. 2011; Schulman and Kilbourne 1965; Freeman et al. 2016; Todd 2016). There is serological evidence that the body mounts elevated antibody responses against the first influenza infection experienced early in life that remains

detectable for decades; this phenomenon is referred to as the *original antigenic sin* (OAS) (Francis 1960; Davenport, Hennessy, and Francis 1953). Antibody responses against infections experienced later in life are less well-understood due to variations in individuals' infection history – the age at infection (Lessler et al. 2012), the level of cross-reaction between the infected virus and those previously experienced (Kucharski et al. 2015), whether antibodies are acquired through natural infection or vaccination (Couch and Kasel 1983), and the rate at which an individual loses antibody naturally over time (Todd 2016; Couch and Kasel 1983).

Unlike other acute viral infections, one-time exposure to a particular influenza subtype does not preclude the possibility of future reinfections of the same subtype (Kilbourne 1978; Lessler et al. 2012; Sonoguchi et al. 1986; Camacho and Cazelles 2013). The reason for this is that influenza antigens are continuously evolving through a process called *antigenic drift* – a result of accumulated point mutations on the antigenic sites of the viral HA globular head (Smith et al. 2004). *Antigenic drift* alters the viral antigenicity and its binding affinity to the host cells allowing the virus to escape host immunity and causes seasonal epidemics (Wilson and Cox 1990; Hampson 2002). Occurring much less frequently than antigenic drift is another evolutionary mechanism called *antigenic shift* – a process that happens when a currently circulating strain reassorts with an animal influenza strain to form a novel subtype that can cause an influenza pandemics (Scholtissek 2002).

The primary intervention to reduce influenza incidence is through influenza vaccination. In 2001, 250 million influenza vaccine doses were manufactured globally (Stöhr 2002) and by 2015 this number increased to 486 million (Palache et

al. 2017). According to statistics from the International Federation of Pharmaceutical Manufacturers and Association (IFPMA) Influenza Vaccine Supply International Task Force (IVS), countries outsides of the European, American, and Western-Pacific regions where 50% of the world's population currently resides only received 5% influenza vaccine doses from 2004 to 2015 (Palache et al. 2017). In Southeast Asia before the 2009 pandemic influenza, the importance of influenza vaccination was underappreciated and vaccine sales were low (Gupta et al. 2012); the pandemic's one positive impact was that it raised public awareness regarding influenza vaccination in some countries in the region.

Due to the continuous and unpredictable evolutionary path of influenza viruses, human immune responses mounted to a particular influenza infection may not be protective against influenza viruses that circulate a few years later. Thus, WHO updates its recommendation for vaccine composition twice a year in February and September for the Northern and Southern hemisphere based on antigenic and virological data provided by the WHO Global Influenza Surveillance Network (WHO GISN 2017). The current recommendation for seasonal influenza vaccines includes two influenza A subtypes – H1N1 and H3N2, and one influenza B strain (WHO GISN 2016). The two kinds of licensed influenza vaccines that are being used are inactivated influenza vaccines (IIVs) and live-attenuated influenza vaccines (LAIVs). IIVs are known to induce serum strain-specific antibodies targeting the globular head of the HA proteins (Kreijtz, Fouchier, and Rimmelzwaan 2011). LAIVs initially were believed to confer a broader protection because they induce both humoral (serum and mucosal) response and cellular immunity (Chirkova et al. 2011; Jang et

al. 2012; Isakova-sivak, Rudenko, and Isakova-sivak 2015). The degree of conferred protection by vaccination depends on a number of factors – the antigenic match between the vaccine strains and the circulating strains, the age of the recipient, as well as the individual's health status and exposure history (Kreijtz, Fouchier, and Rimmelzwaan 2011; Cox, Brokstad, and Ogra 2004). Therefore, current research interests focus on two goals: predicting the next antigenic variant for vaccine recommendation as well as the development of a universal vaccine targeting the more conservative part of the viral proteins (Kreijtz, Fouchier, and Rimmelzwaan 2011; de Vries, Altenburg, and Rimmelzwaan 2015; Hampson 2002).

1.2 The global epidemiology of influenza A

Influenza viruses circulate globally (Bahl et al. 2011; Bedford et al. 2010; 2015) with predictable wintertime epidemics in temperate zones and less predictable patterns of persistence and irregular epidemics in tropical areas (Tamerius et al. 2013; Deyle et al. 2016). In general, influenza infections manifest themselves as local or regional epidemics with the traditional non-linear dynamics expected from acute immunogenic infections. The influenza epidemic has a classic epidemic shape with early exponential growth, a brief peak, followed by a reduction in the number of new cases generated, and a subsequent decline in the number of infections. In temperate zones, influenza is a wintertime infection, and the inter-epidemic periods are characterized by zero or near-zero influenza transmission. The virus is re-introduced exogenously at the beginning of each winter season, although RNA sequence data have demonstrated a few exceptions to this rule with the rare

isolation of summertime influenza viruses (Boni 2008; Patterson Ross et al. 2015). In tropical and sub-tropical regions, inter-epidemic transmission is better characterized as 'low circulation' as viruses tend to be isolated year-round even when influenza and other respiratory disease activity is low.

In temperature zones, the cause for influenza seasonality is likely a combination of climate and social factors. Cold and dry air are favorable conditions for influenza transmission, as shown in recent epidemiological and modeling studies in the US (Shaman and Kohn 2009; Shaman et al. 2010; Shaman, Goldstein, and Lipsitch 2011) and in the guinea pig model (Lowen et al. 2007). Indoor crowding during winter is commonly cited as a likely cause of increased respiratory virus transmission (Cauchemez et al. 2008; 2009; Tamerius et al. 2011). An alternative explanation is that the reduced exposure to solar radiation in the wintertime causes vitamin D deficiency and inhibits host immunity to respiratory viruses (Hope-Simpson 1981; Cannell et al. 2006; Tamerius et al. 2011).

Seasonality of influenza in the tropics and sub-tropics is more complex. Despite a renewed interest in tropical influenza over the past decade (Viboud, Alonso, and Simonsen 2006; Ng and Gordon 2015), it is still not clear whether tropical influenza has a single annual epidemic cycle with year-to-year variation (Moura, Perdigão, and Siqueira 2009; Alonso et al. 2007; Ly et al. 2017), two-distinct seasons (Chew and Ling 1998; Koul et al. 2014; Chow et al. 2006; Cheng et al. 2012; Cheng et al. 2013; Wong et al. 2006), or significant circulation year-round (Tamerius et al. 2013; Alonso et al. 2007; Azziz Baumgartner et al. 2012). In some countries, influenza epidemics were observed to coincide with the rainy season (Moura,

Perdigão, and Siqueira 2009; Tamerius et al. 2013). The disagreement of how different climate factors such as absolute/relative humidity, temperature, and precipitation affect influenza seasonality across different latitudes is now being acknowledged in the mainstream academic literature (Tamerius et al. 2013; Deyle et al. 2016; Alonso et al. 2007). These conflicting results are due to the low quality and short duration of studies (Koul et al. 2014; Waicharoen et al. 2008; Nguyen et al. 2007) and also the absence of routine virological surveillance in some part of the tropics, especially in Africa. The majority of these studies look at influenza percentages only (Azziz Baumgartner et al. 2012) – i.e. the percent of patient swabs taken that are positive for influenza virus – or absolute counts of successful influenza virus isolations (Alonso et al. 2007; Deyle et al. 2016; Moura, Perdigão, and Siqueira 2009; Tamerius et al. 2013; Chew and Ling 1998; Bloom-Feshbach et al. 2013). These are not appropriate methods for determining influenza prevalence as they ignore the critical denominator in this scenario: the number of patients attending clinics/hospitals with influenza-like illness (ILI) and who are likely to be given a diagnostic test for influenza virus. This is crucial in the tropics as it is now known that ILI incidence does not correlate with influenza incidence (Nguyen et al. 2009; Nguyen et al. 2013, Lam et al. 2017), which means that the percentage of positive influenza isolations can be high when ILI is low. Some studies of influenza in the tropics aggregate data across seasons (Chadha et al. 2015; Saha et al. 2014) giving the appearance of an influenza season where there is none. At a minimum, it is fair to say that the evidence supporting annual influenza transmission in the tropics is weak.

A second important characteristic of tropical influenza epidemiology is whether the viruses truly persist year-round. Phylogenetic evidence of viral persistence for longer than one year has been demonstrated in Vietnam (Le et al. 2013) and West Africa (Nelson et al. 2014). When sufficient molecular surveillance data are available from tropical regions, they are sometimes (Viboud, Alonso, and Simonsen 2006; Alonso et al. 2007, Nguyen et al. 2010) but not always (Cheng et al. 2013; Pollett et al. 2015) consistent with patterns of long-term persistence. The persistence question is critical, because year-round persistence is the epidemiological feature that would allow the tropics to act as an ecological source seeding influenza epidemics to other parts of the world (Boni 2008; Russell et al. 2008; Rambaut et al. 2008; Bedford et al. 2010). In addition, long persistence patterns have been shown, in mathematical models, to correlate positively with immune-escape evolution (Boni et al. 2006). An alternative hypothesis explaining global influenza circulation is that no single region acts as a global source, and that the global viral meta-population moves into and out of different parts of the world based on immunity, climate, and proximity (Bahl et al. 2011).

Finally, the biggest disruptor to seasonal influenza dynamics is the sporadic epidemiological swell known as an influenza pandemic. During the 20th century, influenza pandemics were recorded four to five times starting with the catastrophic "Spanish" Flu in 1918 by an H1N1 strain causing an estimated of 20–40 million deaths worldwide (Taubenberger and Reid 2002). In 1957, the "Asian" Pandemic H2N2 strain replaced the H1N1 1918 strain in the population. Just eleven years after that, the "Hong Kong" H3N2 pandemic strain replaced the H2N2 "Asian" strain in

1968. In 1977, the "Russian" H1N1 strain that had previously circulated in the 1950s was released accidentally (either as a laboratory accident or as a result of human infection trials) and began spreading again. Since 1977, H3N2 and H1N1 have been the predominant influenza A strains circulating in the human population. Influenza pandemics are triggered by the generation of a new influenza subtype (sometimes, by an existing subtype that is antigenically very distant to the currently circulating variants, as in 2009). The most likely explanation of the appearance of these pandemic strains was reassortment between an avian strain and the currently circulating human strain; phylogenetic evidence showed that the 1957 H2N2 "Asian" strain, the 1968 H3N2 "Hong Kong" strain (Scholtissek 2002), and the H1N1 Pdm 2009 strain (Schrauwen and Fouchier 2014) originated via this mechanism. Another possible way that a pandemic strain can appear is by an avian or mammalian influenza strain evolving to become human-transmissible. It is believed that the 1918 "Spanish" flu evolved this way (Taubenberger and Reid 2002). This hypothesis has uncertainty since the precursor virus that the "Spanish" strain would have evolved from was not available for analysis.

1.3 Influenza serology

In influenza serology, the concentration of antibody in the blood directed against the hemagglutinin (HA) surface glycoprotein of the influenza virus is known to correlate positively with the immune status of the body (Kilbourne 1978; Smith et al. 2004; Potter and Oxford 1979). The gold standard serological tests to detect the presence of antibody against a particular influenza virus are Haemagglutination

Inhibition (HI) and Microneutralization (MN) assays (Potter and Oxford 1979; Hobson 1974; WHO GISN 2011), which give discrete readouts – from 10 to 2560 depending on the testing purposes. Single HI titers of 40 for cross-sectional samples (Van Kerkhove et al. 2010; Wood et al. 1994) and four-fold increase in paired acute/convalescent samples are viewed to be indicative of past infection, but concerns about errors (Cauchemez et al. 2012) and repeatability (Wood et al. 1994) have limited the ability of the HI assay to give accurate estimates of past infection. Modern serological techniques developed over the past decade have aimed to address some of the shortcomings of HI and MN assays: (*i*) the large amount of serum required to test for presence of antibodies to multiple viruses, (*ii*) discrete titer readouts, (*iii*) limited titer reproducibility, and (*iv*) lack of standardization across laboratories. Improvements in these areas can be seen in novel high-throughput assays developed in the recent years for both human (Li et al. 2017, Koopmans et al. 2012) and poultry subjects (Watson et al. 2009; Freidl et al. 2014). All of the results in this thesis used serological readouts from the protein microarray (PM) assay developed by Koopmans et al. 2012.

1.4 Influenza serological surveillance

WHO established the Global Influenza Surveillance Network (GISN) with participation of 92 countries amounting to 121 national centres and 5 collaborating centres to keep track of global influenza epidemics (WHO GISN 2016). Serological surveillance had been widely used both in influenza research and as part of the national surveillance in many of these countries to understand the underlying

epidemiology of influenza viruses as well as monitoring viral circulation. The study design and sampling methods vary depending on the outcomes of interest. Year-round symptomatic surveillance via routine hospital sampling or convenience sampling from blood donors for non-influenza related purposes, either at a single time point or continually (Hien et al. 2010; Wu et al. 2010; 2011; Nguyen et al. 2013), are sometimes employed to assess population-level immunity; however, longitudinal data from cohort studies (Hayward et al. 2014; Horby et al. 2012; Chen et al. 2010; Todd 2016) provide a more detailed picture at the individual level.

The optimal way to gain understanding of how protective antibody titer against a particular influenza virus changes over time is to analyze sera from individuals from a cohort, repeatedly collected at different time points. However, such a serological study is expensive to set up at a large-scale, and difficult to carry out and maintain in the long-term. Therefore, time series cross-sectional serological data have been used as an alternative to infer the age-specific infection attack rates (IAR) for influenza A H1N1 pandemic 2009 virus, by taking one or more cross-sectional samples after an epidemic period and testing for the presence or absence of virus-specific antibodies (Baguelin et al. 2011; Iwatsuki-Horimoto et al. 2011; McLeish et al. 2011; Soh et al. 2012; Wu et al. 2010; 2011). This approach is easily interpretable in a post-epidemic or post-pandemic period (Miller et al. 2010; Broberg, Nicoll, and Amato-Gauci 2011) as the seropositive individuals are those that were infected recently. However, in tropical countries, the timing of epidemics is irregular and difficult to predict (Yang et al. 2015, Lam et al. 2017), and analysis of cross-sectional serological data would need to take into account that samples may

not have been collected during a period that follows an epidemic. Difference in culture and demography is also important, Asian families generally have more children, and multi-generation households are more common, which is particularly favorable for virus spread (Ng and Gorgon 2015). Thus, studies that focus on longitudinal transmission within household have proven themselves particularly useful for the understanding of tropical influenza (Cauchemez 2014; Tsang et al. 2014; 2016).

1.5 Influenza in Vietnam

Vietnam is a long thin country located between 8°N and 24°N latitude in Southeast Asia with an estimated population size of 86 million in 2009 (Vietnam Housing and Population Census 2009). Despite being very close to the equator, the difference in latitudes causes the weather patterns to vary considerably across the country. In the southern and middle parts of the country (where most of the hospitals participating in this study are located), there are two distinct seasons: the dry season (from January to May) and the rainy season (from June to December). The northern part of the country has a sub-tropical climate with clear seasonal patterns.

The Vietnamese population is relatively young. Indeed, 68% of the population is in the 15-64 working-age bracket, and only 7% of the population is older than 65 (Vietnam Housing and Population Census 2009). The average population density is 259 persons/km^2 with the highest density reaching 3399 persons/km^2 in Ho Chi Minh City (the biggest financial and economic center in the

south. Socioeconomically, Vietnam gained middle-income country status in the past decade and is ranked 115th by the Human Development Index of the United Nations Development Programme (United Nations Human Development Report 2016) with public health spending reaching 7.1% of the national GDP in 2014 (World Health Organization Global Health Expenditure Database 2014).

Vietnam is within the Tropical Asian Influenza Vaccination Zone and is recommended to use the Southern Hemisphere formulation for seasonal vaccines (WHO GISN 2017). However, there is no national vaccination campaign as well as no recommended time of vaccination for influenza. Influenza vaccine sales figures in Vietnam (obtained privately, IMS Health Vietnam) indicate that about 0.7% to 0.8% of the Vietnamese population is vaccinated annually. A portion of these sales are likely to go to foreign nationals living in Vietnam, and the remainder are likely distributed in the major metropolises of Hanoi and Ho Chi Minh City (internal conversations, Ministry of Health, Vietnam). During the pandemic H1N1 2009, the Vietnamese government declined the monovalent H1N1 Pdm 2009 vaccine donation from WHO despite being eligible for the program (Gupta et al. 2012). As a recipient of 4.2 million USD from WHO's incentive to transfer vaccine manufacturing technology to developing countries, Vietnam has now completed building a manufacturing plant for H1N1 and H5N1 vaccines (Gupta et al. 2012; Vuong et al. 2013) and is currently conducting clinical trials for these vaccines. It is not known when they will be available to the public.

The National Influenza Surveillance System (NISS) located at the National Institute of Hygiene and Epidemiology (NIHE) started routine collection in 2016

from fifteen sentinel sites and four regional laboratories (Vuong et al. 2013) (Figure 1.1). Year-round circulation of different seasonal strains with co-circulation of influenza A and B peaking at different time was observed (Nguyen et al. 2009; Nguyen et al. 2013; Todd 2016). The most detailed results to date in Vietnam show that influenza-like illness (ILI) is seasonal in the sub-tropical zones of Vietnam but not in tropical zones (Thai et al. 2015). In tropical Ho Chi Minh City, daily ILI data collected from community clinics over six years demonstrate that in fact non-annual forcing is stronger than annual forcing and ILI activity does not correlate with influenza case numbers (Lam et al. 2017).

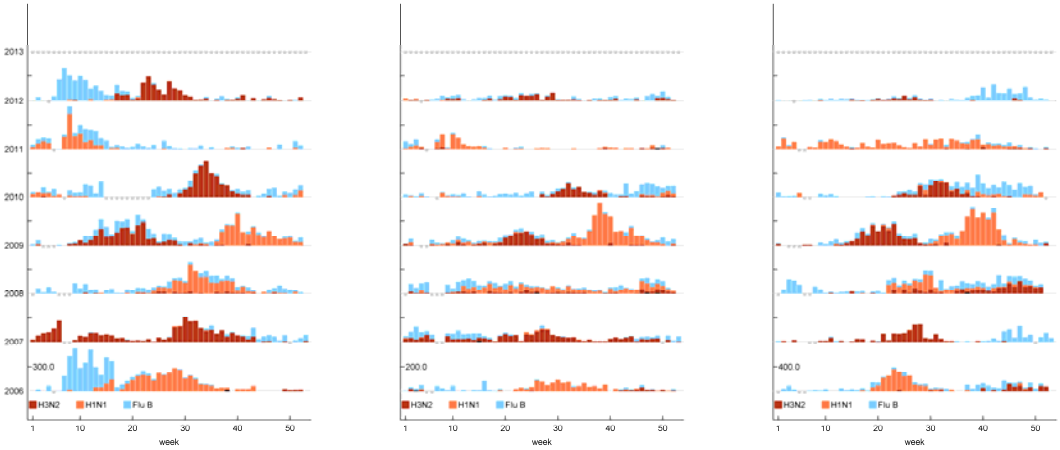

Figure 1.1 Sentinel data for detrended number of weekly ILI+ cases by regions in Vietnam. Y-axes show weekly ILI+ cases color-coded for influenza A subtypes H1N1 (orange) and H3N2 (red), and influenza B (blue) for three different regions in Vietnam (from left to right: North, Central, and South). Reproduced from Thai (2014). This is the aggregated dataset of the sentinel data used for comparison to our SSE analyses in Chapter 4 and 5.

1.6 Objectives

The time series serological data being used in this thesis came from an ongoing study that has been collecting cross-sectional, residual human sera

periodically at different locations spanning southern Vietnam since 2009 (see Figure 2.1 for geographical locations of all collection sites). We will refer to this type of time series serological data as serial seroepidemiological (SSE) data for the rest of this thesis. The primary objective of this research is to look at the stationary and temporal patterns of human influenza antibody titers at a population level using SSE data. The uniqueness of our dataset is the substantial proportion of the infants and young children groups that were missing in previous serological studies (Iwatsuki-Horimoto et al. 2011; McLeish et al. 2011; Soh et al. 2012; Wu et al. 2011, Hobson et al. 1972), a large number of collection sites, and a relatively long period of collection time.

Chapter 2 presents a systematic approach to compute and standardize PM titers values that could be applied to all future studies looking to use this protein microarray assays.

To take advantage of the continuous PM titer measurements and move away from the conventional binary classifications in influenza serology, the aim of Chapter 3 is to systematically describe the underlying structure of a general-population antibody-titer distributions against H1N1 Pandemic (Pdm) 2009 (H1-09) strain and seasonal H3N2 strains using a mixture of distributions approach.

Using the proposed interpretation of individual mixture components defined in Chapter 3, Chapter 4 explores the time series analysis of the proportion of recently infected and/or historically infected individuals to determine if the dynamics of serological states can be used in a meaningful way to reconstruct the population epidemic history.

Moving away from the *ad hoc* analyses developed in the previous two chapters, Chapter 5 focuses on reconstructing the dynamics of the first wave of H1N1 Pdm 2009 in southern Vietnam by using a hybrid dynamical SEIR model and maximum likelihood inference. The novel aspect of this work is that rather than using a forcing term like in conventional SEIR models, the bi-weekly incidences are independent parameters that shape the model's dynamics. The results from this thesis are meant to contribute to the body of tropical influenza research looking at population-level influenza dynamics, and answer two basic questions: *i*) is influenza circulation in Vietnam grouped into discrete epidemics, or does the virus simply circulate year-round? and *ii*) could serological surveillance be used as a proxy to monitor tropical influenza activities?

CHAPTER 2

2 Methods

This chapter makes up part of the supplementary materials for the publication titled "Structure of the general-population antibody titers distributions in influenza virus" published in *Nature Scientific Reports* (7:6060, 2017). Chapter 3 contains the main article text and main figures of this publication.

2.1 Background

The emergence of the H1N1 Pdm 2009 highlighted the need for timely serological investigation to estimate the spread and severity during the early phase of the pandemic. The gold standard Haemagglutination Inhibition (HI) and Microneutralization (MN) assays widely used in influenza serology were discussed in detail along with their drawbacks in Section 1.3 & 1.6. In this study, we adopted a newly developed serological assay known as the *protein microarray* (PM), which allows simultaneous testing of different influenza strains with as little as ten micro-liters of serum (Koopmans et al. 2012). This high throughput assay could ultimately help solving the problem of profiling a large number of samples in a timely manner in responding to an emerging pandemic (Wu et al. 2011; Broberg, Nicoll, and Amato-Gauci 2011). This technology could help increase the underrepresented contribution

of infants and young children groups from whom large volumes of blood are not normally taken-(Iwatsuki-Horimoto et al. 2011; McLeish et al. 2011; Soh et al. 2012; Wu et al. 2010; 2011; Ng et al. 2013; Gillim-Ross and Subbarao 2006). The additional advantages of this technique include the continuous and reproducible titer values, and the ability to standardize and correct the results for any inter-technician and inter-laboratory variations. Traditional HI assays target the complete HA proteins which contains both HA1 and HA2 subunits; thus, making the HI titers less specific compared to the MN titers (Veguilla et al. 2011). The PM assay only measures subtype-specific antibodies against the more antigenic HA1 subunit and is less prone to cross-reaction.

As mentioned in section 1.6, this chapter is dedicated to the analytical development of a high throughput mapping and standardization of the fluorescence responses for different influenza antigens to PM titers as an advance from the methods in Koopmans et al. (2012). Unlike the long-established HI test, there exists no universal titer threshold for the PM titers to define seropositivity which makes meaningful comparison of various epidemiological and serological estimates between PM and HI studies difficult. The increasing use of the protein microarray among recent serological studies (Baguelin et al. 2011; Huijskens et al. 2013; Baas et al. 2013; Boni et al. 2013; Steens et al. 2011; te Beest et al. 2014a; 2014b; 2017) highlights the need of a systematic approach to define titer thresholds for seropositivity, the beginnings of which are addressed in this chapter. At the end of this chapter, I present a short analysis showing why applying the conventional binary approach using a single titer threshold to classify individuals as seropositives

and seronegatives is not appropriate for this dataset. Taking advantage of the continuous nature of the titer measurements could allow us to go beyond the traditional binary classification.

2.2 Serial Serological Epidemiological (SSE) Influenza Surveillance in Southern Vietnam

2.2.1 Data collection

Residual serum samples were collected from ten provincial hospital laboratories in southern Vietnam (Figure 2.1) from July 1, 2009 to December 30, 2013 on a bimonthly basis. Every collection included 200 samples from all age groups (neonates to elderly individuals in their 90s). Samples were anonymized, delinked, and labeled with age, gender, originating hospital ward (HIV wards were excluded) (Table 2.1 for list of collection wards), and date of collection. An independent analysis (not shown here) showed that the samples collected from the respiratory/chest ward of some hospitals tended to have lower titers compared to other wards; no other wards showed this effect. Samples were collected from both inpatients and outpatients and are believed to represent the hospital-going population in their respective provinces. This assumption is currently being tested and will continue to be tested as different antibody assays are performed on the sample set. The study was approved by the Scientific and Ethical Committee of the Hospital for Tropical Diseases in Ho Chi Minh City and the Oxford Tropical Research Ethics Committee at the University of Oxford.

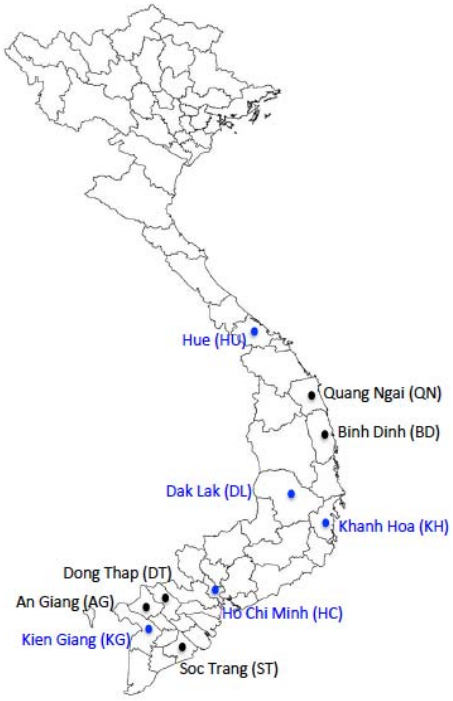

Figure 2.1 Geographic locations of ten collection sites. Blue dots represent collection sites that are analyzed in Chapter 3, 4, and 5.

Table 2.1 List of hospital laboratories where samples were collected

Hospital Wards	Ward Code
Outpatients (not admitted to any wards)	0
General Infectious Diseases Ward	1
HIV Ward	2
Malaria Ward	3
Hepatitis Ward	4
Respiratory/Chest Ward	5
Gastroenterology Ward	6
General Surgical Ward	7
Trauma/Orthopedics	8
Intensive Care Unit	9
Other wards (not listed from 0 to 9)	10
Unknown	11

2.2.2 Serological assays using protein microarray

Human samples were tested for presence of a range of seasonal and pandemic influenza antibodies at serial four-fold dilutions from 1:20 to 1:1280. A commercially international standard (IS) against H1N1 Pandemic 2009 tested at dilutions 1:40 to 1:2560 was included on every slide as a positive control. Commercially available HA1 proteins of the 16 influenza viruses (Table 2.2) were spotted in duplicate on each of the 64-pad nitrocellulose coated slides as described by Koopmans et al. (2012). Each 64-nitrocellulose pad slide tests for 15 human sera and one positive control at four dilutions.

Table 2.2 List of all influenza strains tested on the protein microarrays

Human Antigens		Abbreviations	Avian Antigens		Abbreviations
H1N1	A/South Carolina/1/18	H1-18	**H5N1**	A/Vietnam/1194/2005	H5-05
	A/USSR/92/1977	H1-77		A/Cambodia/R0405050/2007	H5-07
	A/New Caledonia/20/1999	H1-99		A/Hubei/1/2010	H5-10
	A/Brisbane/59/2007	H1-07	**H7N7**	A/Chicken/Netherlands/2003	H7-03
	A/California/6/2009	H1-09	**H9N7**	A/GuineaFowl/HK/1999	H9-99
H3N2	A/Aichi/2/68	H3-68			
	A/Wyoming/3/2003	H3-03			
	A/Wisconsin/67/2005	H3-05			
	A/Brisbane/10/2007	H3-07			
	A/Victoria/210/2009	H3-09			
	A/Victoria/361/2011	H3-11			

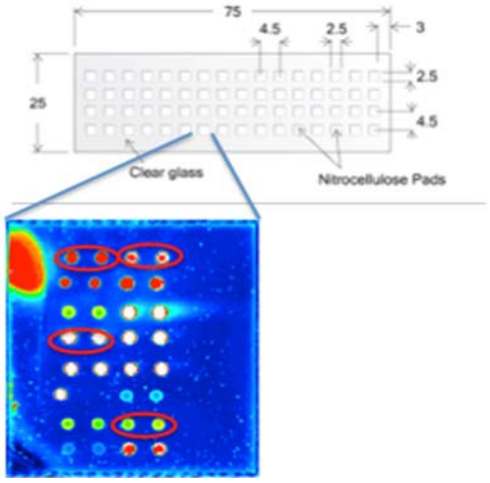

Figure 2.2 An example of the 64-pad protein microarray slide. **Top:** a 64-pad nitrocellulose slide (reproduced from Koopmans et al. (2012)). **Bottom:** a single pad with 16 antigens spotted in duplicate.

2.2.3 Slide preparation and processing

All of the slides used in this study were prepared at the Erasmus Medical Centre (Rotterdam, NL) and the Dutch National Institute for Public Health and Environment (RIVM; Bilthoven, NL) by Erwin de Bruin. The slides were stored in a temperature and humidity controlled settings prior to testing. The samples were processed in a BSL-2 laboratory at the Oxford University Clinical Research Unit (OUCRU) in Ho Chi Minh City by Tran Thi Nhu Thao, Nguyen Ha Thao Vy, and Huynh Thi Phuong. The laboratory procedure has been described in details elsewhere (de Bruin et al. 2014; Koopmans et al. 2012).

2.2.4 Slide scanning and analysis

The processed slides were then dried and sent back to RIVM for scanning. The antigen signals were quantified by a Scanarray Gx Plus microarray scanner (PerkinElmer) with an adaptive circle size of 80–200μm. Digital copies of the scan images were analyzed using ScanArray Express (version 4.0) Software (PerkinElmer)

to determine the median fluorescence intensity. Assessment was performed to compare between using the median and mean fluorescence, and the median values were chosen due to its stable performance. The majority of the slides were scanned by me, and the rest was done by other research assistants in the group – Tran Minh Quan, Ha Minh Lam, and Dang Duy Hoang Giang.

2.3 Mapping luminescence values to titers using luminescence values at four dilutions

The PM titers were fit by four-parameter log-logistic function using fluorescence measured at four dilutions and then standardized to a positive control in order to correct for variation across slides. Titer values falling outside the [20, 1280] range were recorded as 10 and 1810. All data analysis was done in Matlab R2015a. The initial script was written by Janko van Beek.

2.3.1 Four-parameter log-logistic curve

For each human-antigen combination, the eight luminescence scores obtained from serial four-fold dilutions were fitted, using non-linear least-squares regression, to a four-parameter log-logistic curve (Figure 2.3). Errors were defined as absolute luminescence differences between the model and the data point. The log-logistic luminescence curve is sigmoidal in shape. The maximum readout given by the scanner was 65355; thus, 65356 was used as the maximum luminescence in the log-logistic fit. The minimum read out was defined as 3000, below which it was difficult to differentiate between the antigen signals and the background luminescence. Mathematically, the titer value was determined as the x-value of the inflection point

of the fitted log-logistic curve, which is equivalent to the point where the fitted curve achieves a luminescence of 34268. Samples were assigned titer values of NaN if the width of the 95% confidence interval for the fitted titers was greater than one $\log_2$-unit (Figure 2.3). The variables *titer* and *b* were fit with eight luminescence data points using the equation below:

$$\mathrm{Lum_i} = \mathrm{c} + \frac{\mathrm{d} - \mathrm{c}}{1 + \exp\left(\mathrm{b} * \log\left(\frac{\mathrm{dilution_i}}{\mathrm{titer}}\right)\right)}$$

in which: Lum_i : luminescence score at dilution *i; c* = 3000: minimum luminescence*; d* = 65535: maximum luminesce*;* and *titer*: dilution of the inflection point

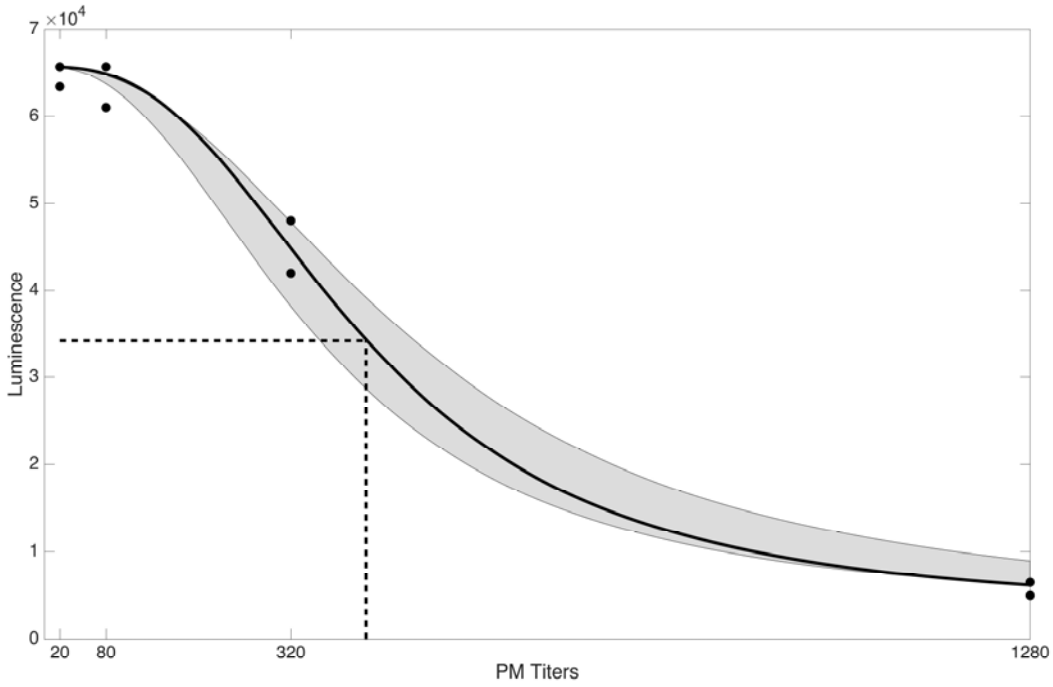

Figure 2.3 Four-parameter log-logistic curve. Luminescence vs. four-dilution titers fitted to four-parameter log-logistic curve in which *c* = 3000, *d* = 65536, *titer* = dilution at the inflection point, and *b* = slope at the inflection point.

2.3.2 Defining maximum error tolerance to identify a monotonic quartet

Theoretically, all luminescence scores within a dilution series should be decreasing monotonically. However, about 3% of the luminescence series had non-monotonic responses leading to inaccurate titer values. Figure 2.4 shows examples of some non-monotonic luminescence series. This problem can be severe if the non-monotonic luminescence signals happen at either the 1:20 or 1:1280 dilution which could lead to wrongful assignment of titer values of 10 or 1810. In addition, the non-monotonic luminescence is not always identifiable if more than one luminescence score is non-monotonic. It is necessary to define a maximum error tolerance and a systematic approach to identify the non-monotonic luminescence score.

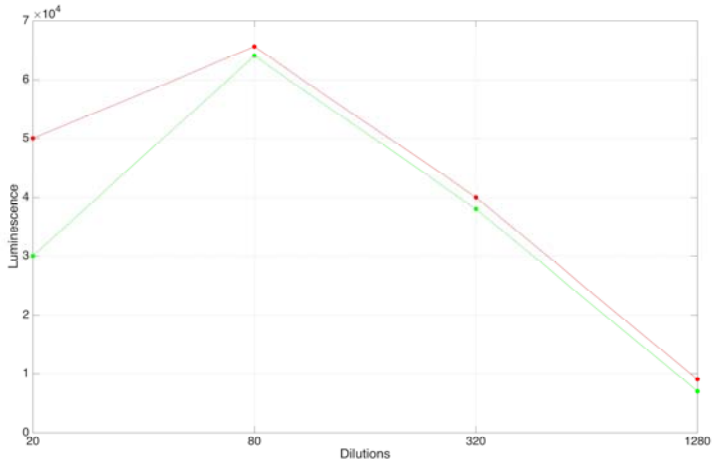

Figure 2.4 Examples of two non-monotonic luminescence quartets. For the green series, it is quite obvious that lum20 (luminescence at dilution 1:20) is the non-monotonic one. However, for the red series it is difficult to tell whether lum20 (luminescence at dilution 1:20) or lum80 (luminescence at dilution 1:80) is the non-monotonic one.

Figure 2.5 shows the luminescence differences, in $\log_{10}$-units, between the luminescence values of duplicate spots, for different luminescence ranges at different dilutions. The pairwise nonparametric Wilcoxon rank-sum test was used to

determine if there is any significant difference between the differences (log_{10} scale) in luminescence values of two duplicate spots in five luminescence ranges (≥50000, 50000>lum≥40000, 40000>lum≥30000, 30000>lum≥20000, <20000) at four given dilutions. When comparing the log_{10}-luminescence difference of a given luminescence range across different dilutions, the difference is not significant (for all pairwise tests within one given luminescence range). However, when comparing the log_{10}-luminescence difference of a given dilution across different luminescence ranges, the test returns near-zero p-values for all pairwise comparisons for the highest luminescence ranges (≥50000, 50000>lum≥40000, 40000>lum≥30000) indicating significant differences between the luminescence differences (between paired spots) across all dilutions. For the lower luminescence range, the differences are not statistically significant. This result suggests that we should define a different relative error tolerance for different luminescence ranges.

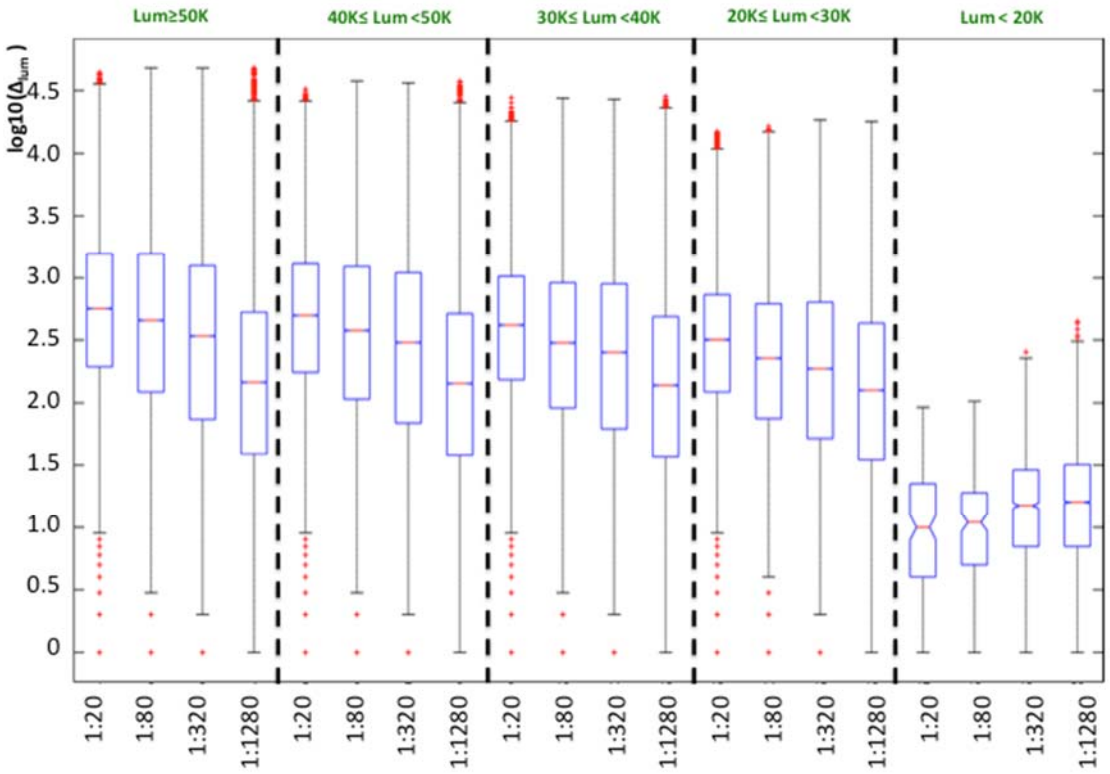

Figure 2.5 Log_{10}-luminescence difference between two duplicate spots grouped by luminescence ranges and dilutions. Results shown at different luminescence ranges and dilutions for N=844,932 luminescence-antigen pairs. The red line is the median difference; and top and bottom edges are 75th and 25th percentile for each box, respectively. The whiskers extend to $q_3 + 1.5*(q_3 - q_1)$ and to $q_1 - 1.5(q_3 - q_1)$, where q_1 and q_3 are the 25th and 75th percentiles. Outliers are plotted in red dots.

2.4 Standardization against H1N1 Pdm 2009 International Standard (IS)

A sample of the WHO Second International Standard (ISH2) for antibody to influenza H1N1 Pdm 2009 virus (H1-09) (National Institute for Biological Standards and Controls (NIBSC), NIBSC code: 10/202) was included on every slide to correct for variation among slides, technicians, slide batches (different printing runs), and slide series (different commercial antigen purchases). Assuming that the positive control gives the same titers values regardless of the time that a given slide was printed and processed (batches) and the quality of the printed antigens (series). In

order to take into account the titer change across series, the standardization procedure was divided into a two-step procedure. First, all samples within the same slide series were corrected to the geometric mean titers for ISH2 samples of a reference antigen within the respective series. This step is meant to correct for slide to slide variations across different printing runs using the antigens purchased at the same time. Second, depending on the difference between the geometric mean of the reference antigen for series *s* compared to its geometric mean in series 1, the titers were deflated/inflated over the geometric-mean titers of series 1. This second step is meant to adjust for differences in commercial antigens' quality across different purchases. In our analysis, the pandemic 2009 H1N1 (H1-09) antigen was chosen as the reference antigen for correcting variance across slides due to its stable performance over time (Table 2.3).

Table 2.3 Summary of geometric means of the ISH2 against all antigens for different antigen purchases (series). P-values refer to comparisons to series 1 (Wilcoxon Rank-Sum Test).

Antigen	Series 1		Series 2				Series 3			
	Mean	Std	Mean	Std	Inflation over Series1	P-value	Mean	Std	Inflation over Series1	P-value
H1-18	144.15	59.04	250.23	91.47	1.74	0	149.35	48.56	1.04	0.76675
H1-77	762.14	388.88	1091	514.66	1.43	0	905.99	312.2	1.19	0.00031
H1-99	287	156.21	307.74	121.12	1.07	0.01314	190.88	39.08	0.67	0.00491
H1-07	247	110.69	325.42	119.93	1.32	0	483.18	179.65	1.96	0
H1-09	158.91	44.76	154.15	89.66	0.97	0.48132	201.72	54.78	1.27	0
H3-68	348.95	145.17	542.08	103.93	1.55	0	458.56	87.03	1.31	0.00064
H3-03	392.81	119.55	550.42	275.15	1.40	0	448.03	94.08	1.14	0
H3-05	679.28	336.05	631.39	277.52	0.93	0.00109	777.45	209.43	1.14	0.01081
H3-07	126.14	37.55	189.85	75.41	1.51	0	158.85	93.98	1.26	0
H3-09	108.86	40.07	159.54	56.99	1.47	0	171	65.97	1.57	0
H3-11	146.08	61.06	214.03	82.15	1.47	0	174.75	64.58	1.20	0
H5-04	40.01	0.23	40.27	12.36	1.01	0.21794	NaN	NaN	NaN	NaN
H5-07	40.03	0.52	41.14	19.01	1.03	0.02606	NaN	NaN	NaN	NaN
H5-10	40.01	0.18	40.34	5.34	1.01	0.03549	40.33	24.04	1.01	0.21348
H7-03	40.23	14.71	40.96	48.39	1.02	0.36462	40.22	2.85	1.00	0.83947
H9-99	47.28	27.6	89.58	35.03	1.89	0	69.7	25.59	1.47	0

2.4.1 Standard procedure

Assuming that the commercial antigens (within the same series) behave identically in the laboratory, the ISH2's titers against all antigens should be the same regardless of the time that the slide was printed or processed in the laboratory. The standard correction procedure is meant to correct for slide to slide variation due to natural laboratory variation (e.g. pipetting volume, temperature changes, wash cycle differences), rather than assuming that the antigen quality is not the same within the one purchase. The within-series correction factor or normalization factor for sample *s* on slide *i* and series *k* is calculated as:

$$CF_{ik} = \frac{GMT_{ISH1,H109,k}}{T_{ISH1,i,H109,k}}$$

in which $T_{ISH1,i,H109}$ is the H1-09 titer of the positive control on slide *i* (assuming it is in series *k*); and $GMT_{ISH1,H109,k}$ is the geometric mean of ISH2 titers for the H1-09 antigen in series *k*. Hence, the normalization factor is the same for all antigens *a* and all samples *s* on the same slide; and it serves as the rejection criterion to discard slides whose H1-09 titers of the positive control differ by more than 1.2 dilutions ($\log_2$-units) away from $GMT_{ISH1,H109,k}$. It is considered normal for HI or MN titers of the same samples measured on different days to be one dilution different. The rejection criterion was initially chosen at one dilution; however, that gave a rejection rate of more than 20% with many slides with borderline correction factors. When increasing the rejection criterion to 1.2, the rejection rate dropped to 3%. In section 2.6, it is shown that even when the rejection criterion is relaxed to 1.2, the PM method still has a much higher titer reproducibility compared to the HI and MN assays.

2.4.2 Advanced correction procedure

This step is meant to correct for slide to slide variation when using a new antigen purchase. The correction is done per antigen, in order to account for the fact that the variation when switching between different purchases is different for different antigens. For example, the GMT of H1-18 antigen (Table 2.3) in series 2 is 74% higher than that of series 1 while the GMT of H1-09 antigen in series 2 is 7% lower than that of series 1. To correct for the inter-series variation, the mean titer of antigen *a* in series *k* is inflated/deflated over its corresponding mean from series 1:

$$CF'_{ak} = \frac{GMT_{ISH1,a,1}}{GMT_{ISH1,a,k}}$$

The individual titer of antigen a for all samples s on slide i in series k is then corrected as:

$$Titer_{saik} = CF_{ik} * CF'_{ak} * Fitted_Titer_{saik}$$

2.5 Mapping luminescence to titers for two testing dilutions

After analyzing about 19,000 human sera at four-fold dilutions (~300,000 sample-antigen combinations), we began a process of mapping luminescence series to titers to determine if fewer luminescence points could be used for titer inference. This was done to reduce the number of dilutions done per sample in order to reduce cost. Figure 2.6 shows the relationship between luminescence scores at single dilutions and the four-dilution titers.

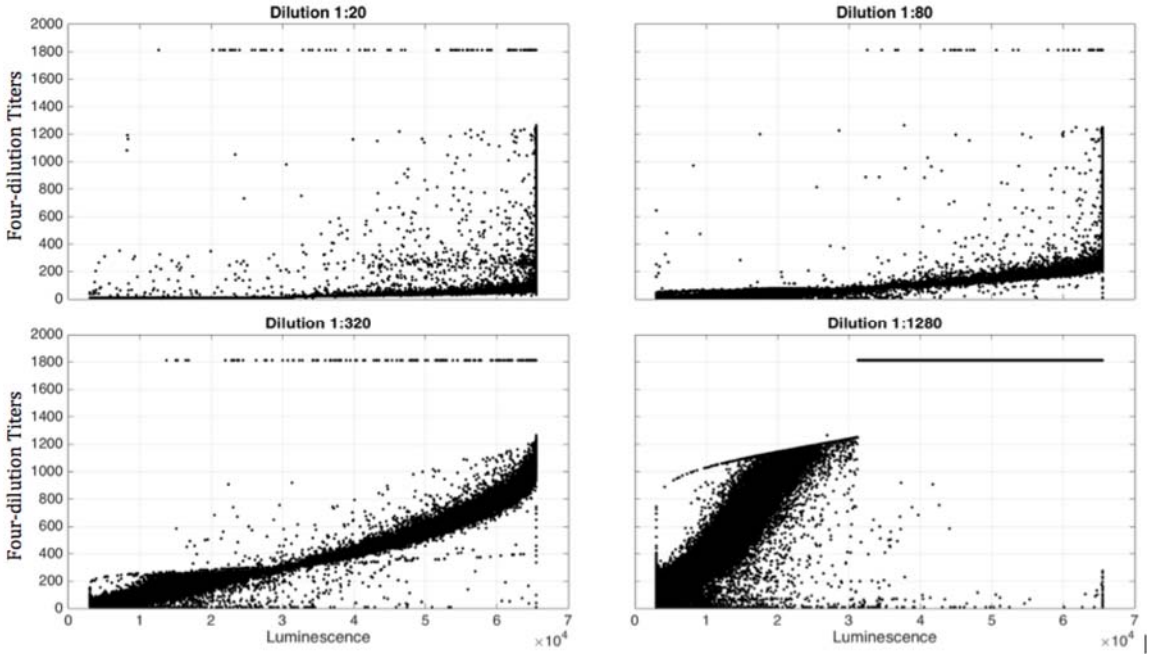

Figure 2.6 Four-dilution titers vs. luminescence at each dilution from 1:20 to 1:1280

2.5.1 Possible dilution pairs

Clearly, a single dilution is not sufficient to be used as a proxy for a four-fold titer, as the majority of mappings from single dilutions to titers would result in mapped titers that are one or two log units distant from the true titer. The single dilution at 20 is especially uninformative, as 80% of the luminescence scores at dilution 1:20 are saturated at 65535 (Figure 2.6, top-left panel). Thus, we considered three dilution pairs as the best candidates for mapping luminescence pairs to true titers. The three pairs considered were 1:80 and 1:320, 1:80 and 1:1280, and 1:320 and 1:1280.

2.5.2 Comparing mapping models

The objective was to define a mapping function $f(L_1, L_2) = T$, where T is the true titer obtained from four-fold dilutions and L_1 and L_2 are luminescence scores at two different dilutions. Four different functional forms of f were investigated:

i. a simple grid approach where the $L_1 \times L_2$ space was divided into grid squares of size $n \times n$ luminescence points on each side. Values of n = 100, 200, 500, and 1000 were tried. The exact $L_1 \times L_2$ space used was [3000, 65536] × [3000, 65536]. The median titer was used as the mapped titer point in each grid square. This function gave poor mapping power at the two ends, titers below 200 and above 1000. The quality of the mapping did not improve with smaller grid size.

ii. a piecewise linear function $f(L_1, L_2) = \begin{cases} aL_1 + bL_2 & for L_1 < 65355 \; and \; L_2 \leq L_1 \\ c + dL_2 & for L_1 = 65355 \; and \; L_2 \leq L_1 \end{cases}$ with the breaks occurring at the luminescence points where the titers achieve their boundary values; i.e. titer of 1810 was assigned for $L_2 > 34268$.

iii. a linear spline surface plot of $f(L_1, L_2)$ using a linear interpolation method with the MATLAB family of functions fitobject.

iv. a cubic spline surface plot of $f(L_1, L_2)$ using cubic spline interpolation method with the MATLAB family of functions fitobject.

Figure 2.7 shows the mapped two-dilution titers using functional form (*iv*) against the true four-dilution titers. Three different dilution pairs for the two-dilution titers are shown in the three panels. The 1:80 and 1:320 dilution pair lost discriminatory power for titer values above 700. The 1:80 and 1:1280 dilution pair, on the other hand, failed to map titers in the intermediate range [400, 1000]. Even though the 1:320 and 1:1280 dilution pair did not map titers below 200 accurately, this should not affect the seroprevalence estimates because the titer ranges for recently infected individuals (as interpreted in Chapter 3) are higher than 200 for all age-groups (Table 3.3 and 3.5). In other words, losing discriminatory power among the seronegative groups should not affect seroprevalence estimates. After the initial 19,000 sera were processed using four-dilution titers, subsequent sera were processed at dilutions 1:320 and 1:1280 only (with the exception of Ho Chi Minh City samples, which were always processed at four dilutions). To ensure accurate standardization across slides, the positive control samples (ISH2) were always processed at four dilutions; and the standardization procedure presented in Section 2.4 was unchanged.

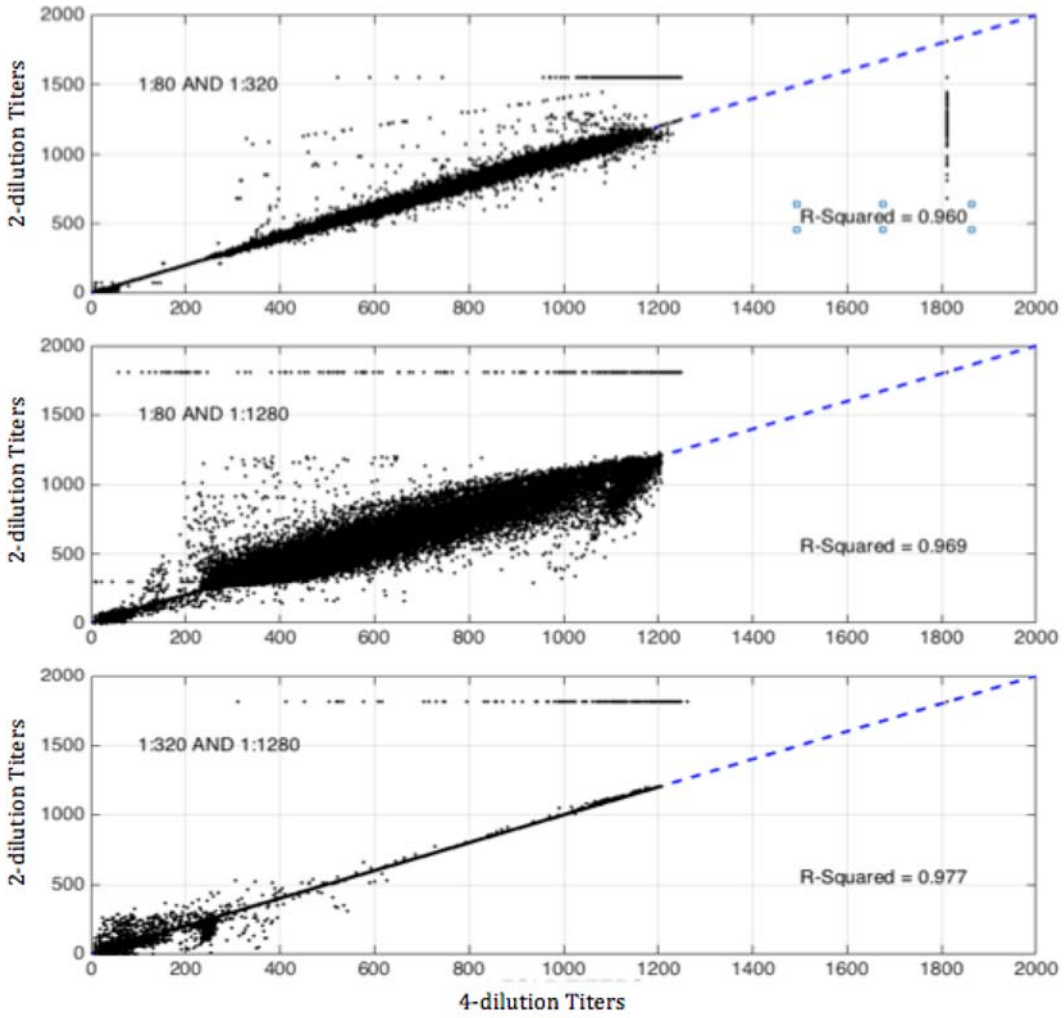

Figure 2.7 Two-dilution titers obtained from cubic spline surface map vs. four-dilution titers for different pairs of dilutions. The three dilution pairs shown are 1:80 and 1:320, 1:80 and 1:1280, and 1:320 and 1:1280.

2.6 Titer reproducibility

Thirty-two samples collected from Khanh Hoa were tested eleven times by different lab technicians on different days to assess titer reproducibility. Across all sixteen antigens on the array, 98.6% of the sample-antigen combinations and 98.3% of the sample-human antigen combinations had a standard deviation of $\log_2$-titer less

than one when performing replicate experiments (Figure 2.8, top panel), making PM titers more reproducible compared to standard HI assays.

We also looked at the reproducibility of the positive control (ISH2); see Figure 2.8, bottom panel. The median difference between an individual ISH2 titer and the geometric mean of all (n = 1457) ISH2 titers was below 0.5.

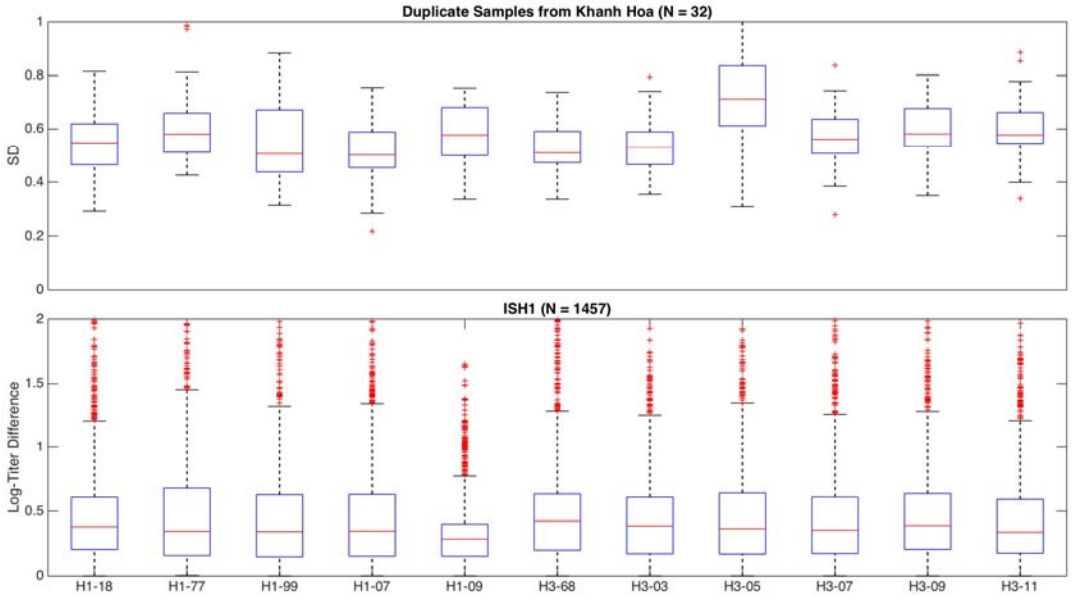

Figure 2.8 Titer reproducibility ($\log_2$-titer scale) for human and ISH2 sera from eleven duplicates. **Top:** Box plots of standard deviations of $\log_2$-titers for eleven human antigens (x-axis) for eleven replicates of 32 different samples from Khanh Hoa. In other words, each box plot summarizes 32 standard deviations. **Bottom:** Differences between individual ISH2 $\log_2$-titers and the $\log_2$-geometric mean of the ISH2 for 1457 replicates on 11 human antigens ($\log_2$-titer scale). In both plots, the red line is the median difference; and top and bottom edges are 75th and 25th percentile for each box, respectively. The whiskers extend to $q_3 + 1.5*(q_3 - q_1)$ and to $q_1 - 1.5(q_3 - q_1)$, where q_1 and q_3 are the 25th and 75th percentiles. Outliers are plotted in red dots.

2.7 Age-dependent titer cut-offs to define positivity

A pre-pandemic dataset of 829 samples (N=829) collected before September 1st, 2009 (from Hue, Khanh Hoa, Dak Lak, and Kien Giang) combined with a post-

pandemic data set (n=850 from Khanh Hoa, HCMC, Kien Giang, and Hue) collected between Mar 1st and Apr 30th, 2010 were used to define age-dependent titer cut-offs for seropositivity to the H1-09 virus. The results were then adjusted according to the age and sex distribution for rural area using the Vietnam Population and Housing Census 2009. These adjusted values allowed direct comparison with the seroprevalence estimates for the 2009 H1N1 pandemic influenza from the Ha Nam cohort study as measured in April 2010 (Horby et al. 2012). The age groups were chosen to match exactly those in Horby et al. 2012.

Table 2.4 The age-specific 95th, 90th, and 80th percentile titers for pre-pandemic dataset against H1-09

Age Group	0-4	5-9	10-19	20-29	30-39	40-49	50-59	60-69	70+
95th percentile	242.80	202.87	121.94	257.01	359.04	334.76	540.16	463.77	699.90
90th percentile	137.52	108.51	83.60	123.02	193.25	276.37	260.26	323.92	361.38
85th percentile	68.36	81.59	68.70	82.00	132.58	220.85	203.44	267.89	328.29

The pre-pandemic 95th percentile titers for different age groups were chosen as the cut-off values for seropositivity (Table 2.4). The age-dependent cut-offs correlated positively with the age of the individuals, which was consistent with previous studies looking at baseline response among different age groups for H1N1 Pdm 2009 virus (Steens et al. 2011; Baas et al. 2013).

The age-specific seroprevalence of the post-pandemic sample was then adjusted to the Vietnam housing and population census 2009 for Ha Nam province, in order to compare with the Ha Nam cohort study. Overall, the age-specific seroprevalence of the post-pandemic sample showed good agreement with the Ha Nam cohort data for all age groups between 10 and 69 years of age (Figure 2.9). After

adjusting for age and sex distributions, the post-pandemic seropositive rate in our four sites was 0.16 (95% CI: 0.13–0.22) compared to 0.17 (95% CI: 0.14–0.20) seroprevalence for Ha Nam. The difference in underlying demography as well as the high proportion of infant and young adult groups could be the reasons that our estimate of the seroprevalence is higher than what was observed in Hong Kong (Wu et al. 2010) and England (Baguelin et al. 2011).

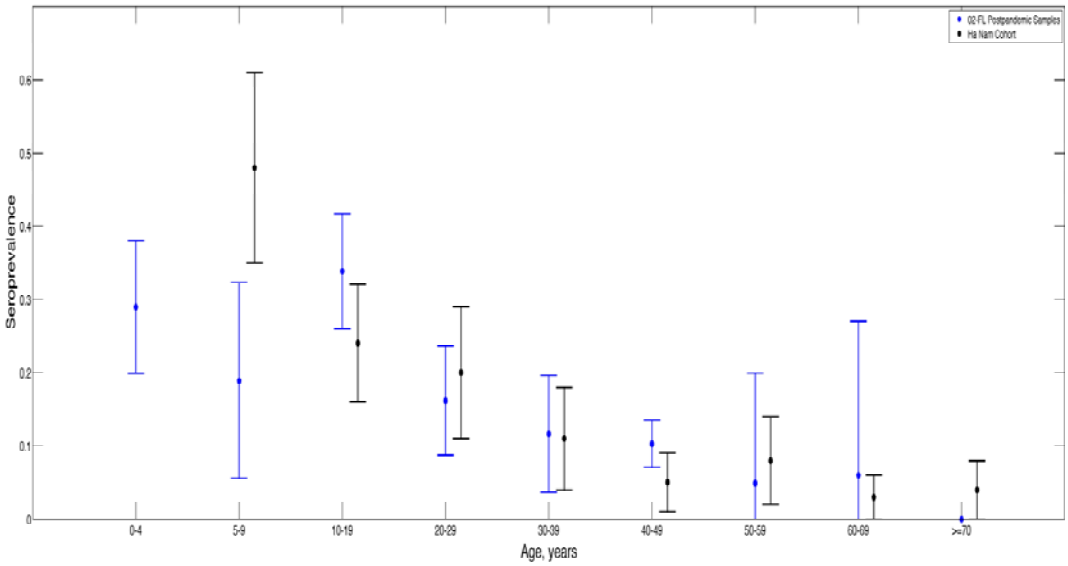

Figure 2.9 Age-specific seroprevalence for post-pandemic data (blue) and the Ha Nam cohort (Horby et al. 2012) (black) using age-specific cut-offs estimated from the pre-pandemic dataset.

Unfortunately, this approach of using the pre-pandemic data collected from Jul 1, 2009 to Aug 31, 2009 to define titer cut-offs was not an appropriate method for defining seropositivity for older individuals (≥ 50 years-old) (Figure 2.10). Because the 2009 pandemic strain was a descendent of the swine virus that circulated during and after the Spanish Flu Pandemic 1918, individuals who were older than 60 in 2009 possibly possessed pre-existing immunity due to previous exposure (Huijskens et al. 2013; Wu et al. 2010; Shek and Lee 2003, Hancock et al. 2009). If the patient

profiles of Pdm H1N1 2009 and its attack rate patterns are similar to what was observed in Hong Kong and other countries (Baguelin et al. 2011; Wu et al. 2010; Miller et al. 2010; Van Kerkhove et al. 2013; Deng et al. 2011), the post-pandemic time reference point to compare the seroprevalence estimates had to be modified to late 2010 in order to capture the titer increases for the older individuals.

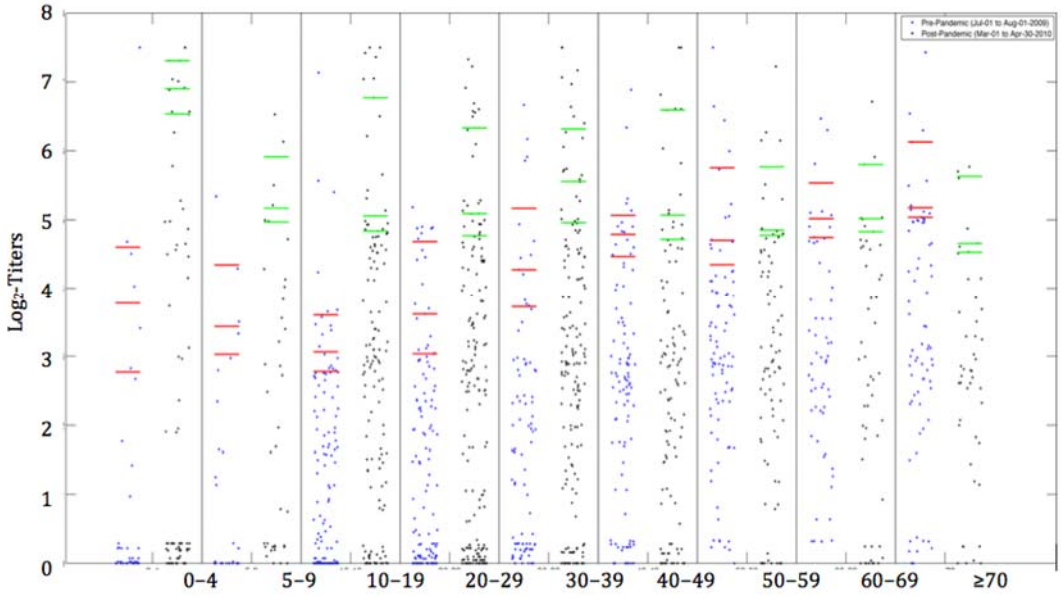

Figure 2.10 Pre-pandemic log_2-titers (blue dots) and post-pandemic log_2-titers (black dots) by age groups. Red horizontal bars indicate the 95th, 90th, and 85th percentile titers for the pre-pandemic dataset of 829 samples (n = 829) collected between Jul 1st and Aug 31st, 2009. Green horizontal bars indicate the 95th, 90th, and 85th percentile titers for the post-pandemic dataset of 850 samples (n = 850) collected between Mar 1st and Apr 30th, 2010.

2.8 Discussion

In this chapter, I presented an analytical advance of the methods used to analyze protein microarray titers originally developed by Koopmans et al. 2012. This new standardization allows correcting for spotting variations of the antigens, e.g. when switching between different antigen manufacturers, in addition to the basic

standardization across slides that corrects for laboratory variations. The inclusion of the ISH2 made the PM titers more reproducible compared to the traditional HI and MN essays. A new mapping method presented in this chapter helped us halving the cost of testing without sacrificing a lot of titer precision by using luminescence at only two dilutions. Early results during the development and testing phase of the PM assay showed that PM titers were subtype-specific to all testing antigens and more sensitive than the HI titers; nevertheless, heterosubtypic cross-reaction was observed in older individuals. Analyses of the quantitative nature of both homosubtypic and heterosubtypic responses to human influenza viruses H1N1 and H3N2 were presented in detail by two former PhD Students from our group (Vinh 2015; Todd 2016). Even though we were not able to define an age-specific cut-off for seropositivity for individuals older than 60 years old using the pre-pandemic dataset, this was not a problem with the PM assay itself, as it has been demonstrated that about 20-30% of individuals in this age group had prior-immunity against the pandemic virus due to early exposure in life (Hancock et al. 2009; Miller et al. 2010; Rizzo et al. 2010).

Koopmans et al. (2012) suggested that using a PM titer cut-off of 40 as an equivalent to HI titers 40 gave this assay a better sensitivity compared to the HI assay. However, results from population-level and cohort studies suggested a cut-off value of around 100 as an approximate of HI titer 40 (te Beest et al. 2014a; Todd 2016, unpublished results). It is one of the limitations that we were not able to quantitatively correlate HI and PM titers to estimate the range of PM titers that is considered equivalent to HI titers of 40 due to failure to obtain the same printed

antigens to use in HI assays at our laboratory. Nevertheless, HI tests on a subset of samples with similar H1N1 strains correlated positively with the PM titers (unpublished results). While the HI assay targets the complete HA proteins, the PM assays only measures HA1-specific antibody epitopes. Therefore, the two quantities might not correlate quantitatively. For the rest of this work, the PM titers were referred to as an independent quantity and we did not try to further correlate the two titers.

Another limitation is the low response of the ISH2 to the avian antigens which calls into question the usefulness of the standardization procedure on these antigens. The ISH2 sample was produced from a pool of human sera that was meant to serve as a reference values for the H1-09 antigen. Thus, its response against the avian antigens was measured at the lower limit of detection (titers below 40) for all avian antigens except H9-99. Analyses looking to use the avian titers have to account for the ineffective standardization across slides.

CHAPTER 3

3 Stationary Structure of General-Population Antibody Titer Distributions to Influenza A Virus

This chapter makes up the main article text and part of the supplementary materials of the publication titled "Structure of the general-population antibody titers distributions in influenza virus" published in *Nature Scientific Reports* (7:6060, 2017).

3.1 Background

The distribution of antibodies in a human population reveals a fossil imprint of the population's past exposure to infectious disease. If individuals' antibody concentrations can be measured accurately, they can be used to infer both the size and timing of past epidemics. The two key post-epidemic processes that need to be measured to make this inference possible are the rate of antibody acquisition and the rate of antibody waning. The rate of antibody acquisition post-infection is rapid (weeks) for most viral pathogens, but more difficult to measure for more complex pathogens that present the immune system with a diverse set of antigens. The rate of

antibody waning, however, is rarely measured even for viral pathogens. To correctly translate a population's antibody titer distribution to its epidemic history, accurate measures of both these rates are necessary. To validate that this reconstruction has been done correctly, a large cohort with long-term follow-up and precise antibody measurements would be required. Studies like these are difficult to run and difficult to find in the scientific literature – both in methodological development and field implementation. Further complicating the issue is that antibody measurements are rarely 100% specific, and that low-level cross-reactive antibodies often are ignored by setting a cut-off for positivity.

To begin investigating what an antibody distribution can tell us about a population's epidemic history, the Boni lab initiated a large-scale time-structured serological survey (Boni et al. 2013; Todd et al. 2014) and an observational clinical study that included repeat patient follow-ups to measure rates of antibody waning (Todd 2016); the results of the serological survey are presented here. The first aim of this chapter was to move away from the binary approach to serology – which classifies individuals as seropositive or seronegative – and to describe the underlying structure of a general-population antibody-titer distribution by assuming that an individual can belong to any number of serological states.

The rationale for a detailed descriptive analysis of antibody titer distributions is that titer groups or titer ranges may be able to provide differentiating information on the type of infection, e.g. recent versus non-recent infections, or primary versus non-primary. The binary approach of classifying individuals as seropositive and seronegative is not as informative as it could be given the richness of some

serological datasets, and it is already known to have two practical drawbacks. First, the cutoff value for seropositivity is typically calibrated from a group of patients with confirmed acute infection, by collecting convalescent serum samples a few weeks or a few months after symptoms onset. This means that the correct application of the cut-off value is the identification of recent symptomatic infections rather than any past infections. Thus, applying this threshold to a population-wide serological cross-section will likely result in an underestimate of the seroprevalence. Second, binary classification in serology results in incorrect or inconclusive classifications for samples with borderline measurements (Cauchemez et al. 2012; Broberg, Nicoll, and Amato-gauci 2011; Baughman et al. 2006). Non-binary analyses of serological data are present in the literature for a range of pathogens (Baughman et al. 2006; Gay et al. 2003; Neuenschwander et al. 2002; Hardelid et al. 2008a; Greiner et al. 1994; Rota et al. 2008; Vyse et al. 2004; Y. Liu et al. 2011; Fujii et al. 2014) including influenza virus (te Beest et al. 2014a; 2014b) but very few of these studies are able to look at non-vaccinated populations and none have the scale and precision presented here.

In general, the advantage of analyzing continuous serological measurements is that this results in better classification for borderline samples and more accurate estimation of the seroprevalence (Baughman et al. 2006; Bollaerts et al. 2012; Gay 1996; 2003; Kafatos et al. 2015). Statistical approaches using mixture distributions have proven successful in describing the uncertainty of individuals' past infection status (Gay 1996; 2003; Vink et al. 2015; Nielsen et al. 2007; Neuenschwander et al. 2000; Pai et al. 2008; Vyse et al. 2004). In some instances, mixture distribution approaches have shown that the population is best classified into three or more

subgroups, and these subgroups are normally interpreted as having a different status of protection, past infection, and/or vaccination (Baughman et al. 2006; Gay et al. 2003; Neuenschwander et al. 2000; Vyse et al. 2004; Greiner et al. 1994; Hardelid et al. 2008a; Rota et al. 2008; te Beest et al. 2014a; Fujii et al. 2014; Liu et al. 2011). Note that in some of these past studies there was statistical evidence – using either Bayesian Information Criterion (BIC) or Akaike Information Criterion (AIC) – that the multimodal distribution fit better than unimodal and bimodal ones, but none of these studies took into account the epidemiological interpretations of the underlying process or performed visual inspection when choosing the best-fit model (see Rota et al. 2008 or Gay et al. 1996 for a typical analysis).

Recently, mixture distribution approaches have been extended to influenza serology by Steens et al. (2011) and te Beest et al. (2014a; 2014b), in which post-pandemic data were collected right after the first wave of the H1N1 Pandemic 2009 in the Netherlands and analyzed by protein microarray. In these studies, mixture analysis was meant to measure the proportion of recent infection of a novel virus in the population.

In the present study, I analyze a large set of general-population serum samples collected as residual serum from biochemistry and haemotology labs in four hospitals in southern Vietnam, from 2009 to 2013. Using a zero-inflated mixture modeling approach, I allow for up to seven serological states. To account for the large sample size in our model selection procedure, I use the Bayesian Information Criterion, and to avoid inference of spurious serological states we set additional criteria to ensure that inferred titer groups are epidemiologically meaningful. I

hypothesized that serological classification of influenza antibody titers would be non-binary and that age and lineage exposure (H1N1 only) would be associated with certain titer groups. The main findings are that H1N1 antibody titer distribution is best classified into four titer groups, that H3N2 is best classified into three groups, and that censoring may have prevented a complete classification of H3N2 titers.

3.2 Data

Residual serum samples were collected from four hospital laboratories in southern Vietnam: the Hospital for Tropical Diseases in Ho Chi Minh City (urban, densely populated), Khanh Hoa Provincial Hospital in Nha Trang city (small urban, central coast), Dak Lak Provincial Hospital in Buon Ma Thuot city (central highlands, rural), and Hue Central hospital in Hue City (small urban, central coast). Samples were collected from July 2009 to December 2013 on a bimonthly basis; 200 were included in each collection from all age groups as described in Section 2.2. Two early analyses (unpublished results; and Berto et al. 2017) suggest that when looking at hospital presentation with hepatitis, the younger age range (<20) in the sample set may represent a sub-population more vulnerable to infectious disease exposure than the general population.

The sample collection described here is part of a large ongoing study in serial seroepidemiology (Boni et al. 2013; Todd et al. 2014; Todd 2016) aimed at describing the dynamics of influenza circulation in southern Vietnam (Section 2.2). Samples were tested for presence of influenza antibodies using a protein-microarray (PM) method (Koopmans et al. 2012), at serial four-fold dilutions from 20 to 1280, to

test for IgG antibody to the HA1 component of 16 different influenza viruses (Boni et al. 2013). The standardization procedure was described in detail in Section 2.3 & 2.4. In this analysis, titers to the 2009 H1N1 virus (A/California/6/2009) and recently circulating H3N2 viruses (geometric mean titer to A/Victoria/210/2009 and A/Victoria/361/2011) were analyzed.

Data on influenza vaccine imports in Vietnam were obtained from Vietnam's Customs and Imports Department via IMS Health Vietnam. Annual influenza vaccine imports for 2014–2016 are sufficient to cover approximately 0.8% of the Vietnamese population. As wealth and access to medicines are growing in Vietnam, the coverage level for 2009 to 2013 was likely to be lower than 0.8% (data obtained privately, IMS Health, Vietnam).

3.3 Methods

3.3.1 Maximum likelihood framework

To describe the distribution of influenza antibody titers in the Vietnamese population, titer values were separated by site, adjusted to their province's age and gender distribution (Vietnam Housing and Population Census 2009) (Section 3.4.1), and plotted as a simple weighted histogram (Figure 3.4). A series of mixture models was used to fit this distribution, with the assumption being that individual samples have one of several immune statuses which are represented by the different components in the mixture model. Our hypothesis was that the sample population consists of different subpopulations with different antibody levels depending on

their infection history and that each of these components could be represented by a single parametric distribution.

Titers were log-transformed and assumed to come from a C-component mixture distribution with the corresponding likelihood:

$$\mathcal{L}(\mathrm{x} \mid \boldsymbol{\theta}) = \prod_{i=1}^{n} \sum_{j=1}^{C} w_j \cdot f_j(\mathrm{x}_i \mid \theta_j) \qquad (3.1)$$

where f is the probability density function of a normal distribution with parameters θ_j and $\mathbf{w} = (w_1, w_2, \ldots, w_C)$ is the vector of component weights in the mixture. The log-likelihood was defined as:

$$\ell(\mathrm{x} \mid \boldsymbol{\theta}) = \sum_{i=1}^{n} s_i \cdot log\left[\sum_{j=1}^{C} w_j \cdot f_j(\mathrm{x}_i \mid \theta_j)\right] \qquad (3.2)$$

in which the s_i parameters are sampling corrections to adjust the sample age and sex distribution to the population's true demographic distribution; $f_j(x_i \mid \theta_j)$, j = 1, 2, .. , C is the probability density function that a given sample x_i belongs to the jth-component in the mixture. C is the number of mixture components (McLachlan and Peel 2000; Hens et al. 2012).

The microarray assay produces continuous log-titer results between 1.0 (titer of 20) and 7.0 (titer of 1280). To account for these detection limits, an extra probability weight w_0 was added at 20 to account for samples that had antibody concentrations at or below the detection limit of 20. This can be considered a zero-inflated mixture model, where titers of 20 are the "zeroes". Because of this added probability mass, I discretized the probability mass functions to make the entire distribution discrete; hence the distributions f formally represents discretized

versions of continuous density functions (Section 3.4.3). At the upper detection limit of 7.0, the mixture distribution was censored assuming that individuals with titers of 7.0 represented a class of seropositive individuals with a real titer value if the assays had been continued to be diluted until the real titer was found. Hence, the mixture model distributions censored on the right and truncated on the left was adopted in this analysis to properly account for the two limits of assay detection. Thus, the likelihood in (3.1) was modified as:

$$\ell^{interval}(\,\mathrm{x}\mid \boldsymbol{\theta}\,) = \begin{cases} \sum_{i=1}^{\boldsymbol{n_{>20}}} s_i \cdot log\left[\sum_{j=1}^{C} w_j \cdot f_j(\,\mathrm{x}_i \mid \theta_j\,)\right] & \text{for} \quad \mathrm{x}_i > 20 \\ \sum_{i=1}^{\boldsymbol{n_{\leq 20}}} s_i \cdot \log(\,w_0) & \text{for} \quad \mathrm{x}_i \leq 20 \end{cases} \tag{3.3}$$

in which $n_{\leq 20}$ is the number of samples whose titers are at least 20, $n_{>20}$ is the number of samples whose titers are above 20, and $n_{\leq 20} + n_{>20} = n$. Maximum likelihood estimation was carried out using the Nelder-Meade algorithm implemented in Java 8.0 (Apache Commons Math 3.3). Global optima and convergence were assessed by starting searches from different sets of the initial conditions. Weibull, Gamma, and normal distributional forms were tested for the mixture components, and as there was little difference in the fits (Section 3.4.4), normal distributions were chosen for the analysis. Confidence intervals for means, variances, and weight parameters w_j were computed using likelihood profiles (McLachlan and Peel 2000).

3.3.2 Model selection

For multi-component mixture models, the likelihood ratio test between a specific model and its immediate predecessor (e.g. *n* components versus *n*-1 components) is not a valid statistical comparison. Since interchanging the components' identity gives the same mixture likelihood, the regularity conditions do not hold for the likelihood ratio test to have its usual χ^2 distribution (McLachlan and Peel 2000). Thus, the most appropriate number of mixture components was chosen (*1*) by Bayesian Information Criterion to take into account the number of samples, and (*2*) by a qualitative inspection of the means and variances of the components to ensure that (*a*) multiple means did not overlap and (*b*) variances and weights were not too small, which would make them not epidemiologically meaningful.

3.4 Results

3.4.1 Representativeness of sample collection versus census data

The 0-4 yrs-old age group was clearly over sampled for Ho Chi Minh City, and undersampled for Dak Lak, which might have been caused by different health care systems in these two regions causing pediatric admissions to be over/under-represented in certain hospitals. Ho Chi Minh City is a densely populated city with easy access to many levels of healthcare, whereas Dak Lak Provincial Hospital is in a small city in a rural region of the Vietnamese highlands, with a lower socioeconomic level and less access to healthcare. For some of the age groups, the sample population was very close to that of the real data (older than 40, both genders, Hue; older than 50, both genders, Ho Chi Minh City and Khanh Hoa; older than 60, both

genders, Dak Lak). For the 5-20 age group, all of the sites are undersampled for both genders, which is to be expected as these individuals are the least likely to report to hospitals. Overall, the serum sample set had an age structure similar to the true demography; thus, the sample weights included in the likelihood function introduced only minor adjustments.

The sample weights s_i in the likelihood (3.2) and (3.3) were calculated from these data. For example, the fraction of males in the 0-5 year-old age range in the census data for HCMC is 0.0364 while this fraction is 0.1241 for the sample set. Thus, every sample that was male and belonged to the 0-5 age category in the sample should be down-weighted by a factor of s_i = 0.0364 / 0.1241= 0.2933.

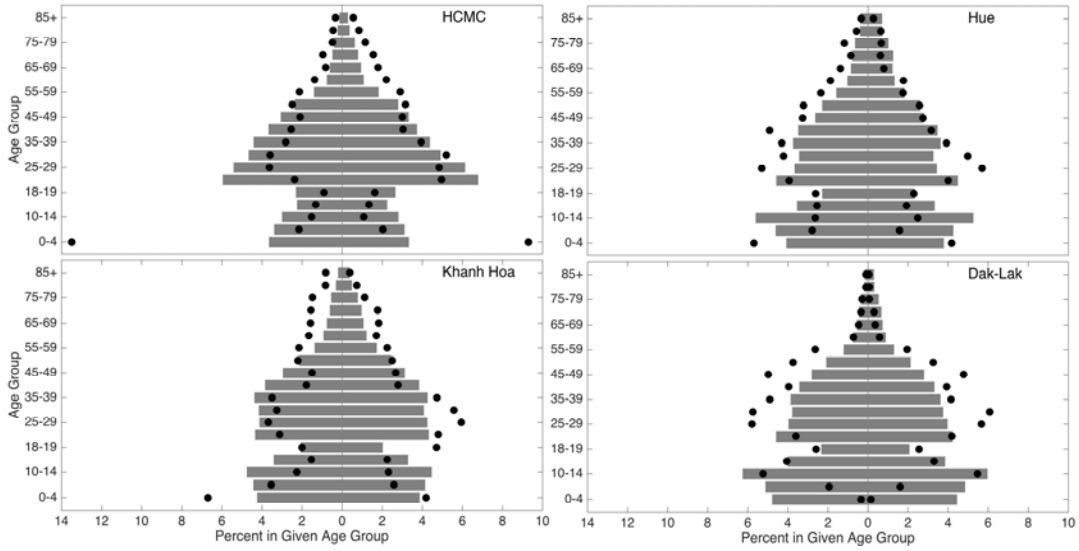

Figure 3.1 Collected sample population (black dots) versus Vietnam national housing census in 2009 (gray bars) for different sites. The *y*-axis shows different age groups and *x*-axis is the percentage of the population or sample in that age group. Left columns are data for males and right columns for females.

3.4.2 Choosing bin width to discretize the normal distribution

When computing the likelihood function, the normal distribution needed to be discretized so that a 'zero-inflated' normal distribution could be constructed ($\log_2$-titer = 1 was the inflated probability mass). A probability mass and continuous probability function cannot be combined into a single likelihood function. The normal mixture was defined on the $\log_2$-titer range [1, 7], and seven different bin widths of 1.000, 0.500, 0.100, 0.050, 0.010. 0.005, and 0.001 (in $\log_2$-units) were tested in this range to investigate the behavior of the seven different probability mass functions in the likelihood optimization algorithm (Table 3.1). For a single normal distribution fit, the optimum was the same for all bin widths. In the case of two and three components in a mixture distribution, there were few changes in the fitting results, unless the bin width was less than or equal to 0.100. It also was important to avoid using too small of a bin width to avoid the problem of having "a spike" in the fitted distribution that had no epidemiological meaning. A bin width of 0.100 (in $\log_2$-units) was used in the analysis.

Table 3.1 LLH optimization results for different bin widths

Interval Width	w_0	w_1	μ_1	σ_1	w_2	μ_2	σ_2	w_3	μ_3	σ_3	SumNegLLH
1.000	0.228	0.772	3.945	1.551							38357.07
0.500	0.228	0.772	3.946	1.551							48240.31
0.100	0.228	0.772	3.950	1.551							71504.04
0.050	0.228	0.772	3.950	1.551							81535.65
0.010	0.228	0.772	3.949	1.551							104838.69
0.005	0.228	0.772	3.949	1.551							114876.59
0.001	0.228	0.772	3.949	1.551							138181.93
1.000	0.228	0.150	2.063	0.234	0.622	4.387	1.386				37870.75
0.500	0.228	0.211	2.443	0.686	0.561	4.509	1.398				47830.31
0.100	0.228	0.218	2.462	0.698	0.555	4.532	1.393				71076.04
0.050	0.228	0.218	2.462	0.697	0.555	4.532	1.392				81105.93
0.010	0.228	0.218	2.462	0.697	0.555	4.531	1.393				104410.41
0.005	0.228	0.218	2.462	0.697	0.555	4.532	1.393				114448.07
0.001	0.228	0.218	2.462	0.697	0.555	4.532	1.393				137753.27
1.000	0.228	0.205	2.017	0.059	0.377	4.026	0.794	0.190	5.765	1.207	37634.10
0.500	0.228	0.379	2.735	0.812	0.151	4.640	0.426	0.242	5.422	1.352	47639.60
0.100	0.228	0.396	2.771	0.830	0.159	4.684	0.434	0.217	5.571	1.298	70856.20
0.050	0.228	0.398	2.774	0.830	0.161	4.685	0.433	0.214	5.594	1.288	80881.55
0.010	0.228	0.398	2.774	0.830	0.161	4.684	0.434	0.214	5.591	1.290	104186.77
0.005	0.228	0.398	2.774	0.830	0.161	4.684	0.435	0.213	5.597	1.287	114224.69
0.001	0.228	0.398	2.774	0.830	0.161	4.684	0.435	0.213	5.596	1.288	137529.83

3.4.3 Comparisons of Gamma, Weibull, and Normal distribution

Normal distributions were chosen for the form of the mixture components, as this is the traditional distributional form chosen for mixture distribution fits of continuous quantities when no other information is known or assumed about the data points. Comparisons were done with mixtures of Weibull and gamma distributions, although note that both Weibull and gamma distributions allow for symmetry and right skew, but not for left skew. In choosing a distributional form, when all other considerations are equal, a normal distribution form should be chosen

over Weibull or gamma forms to prevent fits where rights skews are "discovered" by the fitting process but left skews remain undiscovered.

In the Figures 3.2 and 3.3, the four-component fits for H1N1 have the lowest BIC value when normal distributions are used as components. For three-component fits for H3N2, the gamma-fits have a somewhat lower BIC value than the normal fits ($\Delta BIC \approx 19$), but it is also clear that the component structure in this fit does not distinguish titer groups. Normal components had better BIC than Weibull components for both H1N1 and H3N2.

Based on (1) our initial considerations of skewness in the fits, (2) the BIC values when comparing the fits for both subtypes, and (3) our visual inspection of the fits, we concluded that we did not have any evidential support for using gamma distributions or Weibull distributions in the mixture analysis.

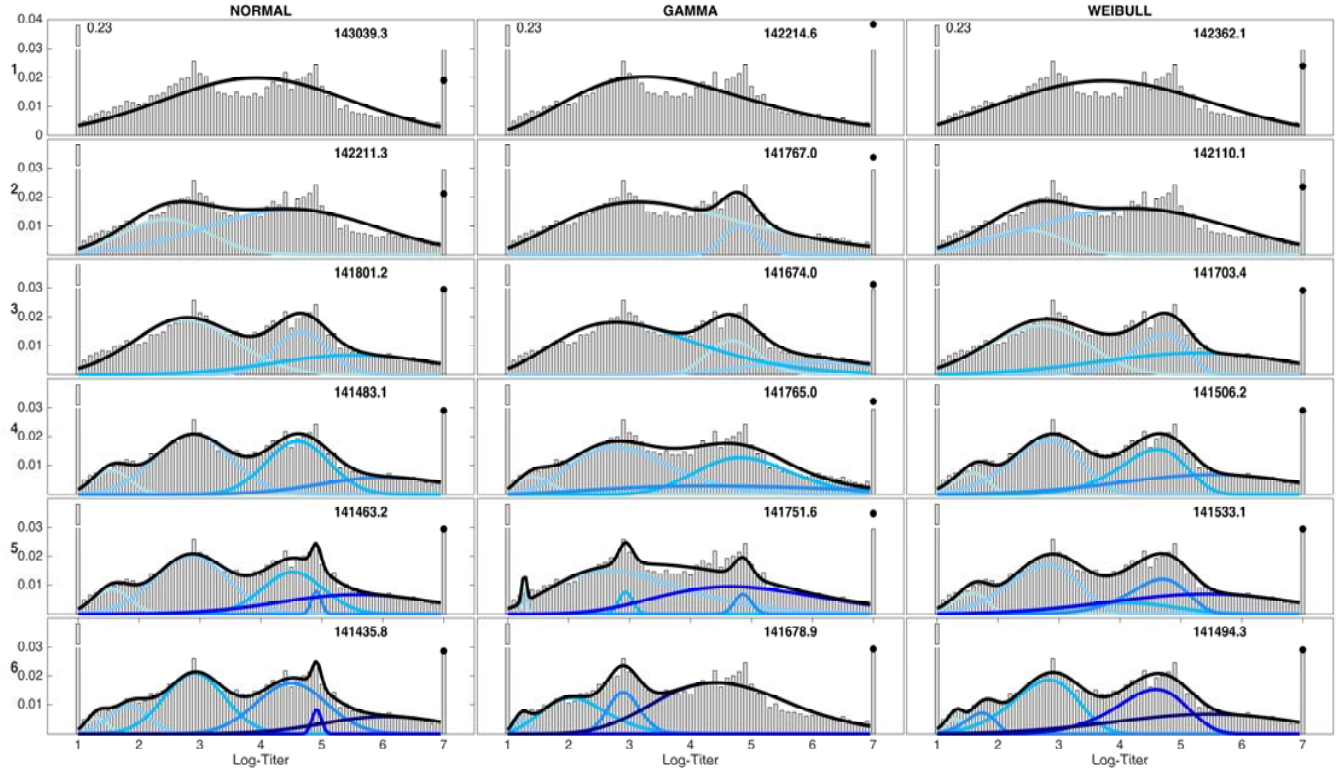

Figure 3.2 Comparing model fits between Normal, Gamma, and Weibull distributions for aggregated titers against H1-09 (N=19785). Showing fit results for mixture models with different numbers of normal components (top to bottom; the label to the left of the y-axis is the number of mixture components) and performed with three different distributional forms (shown in columns). Histograms are weighted to adjust for age and gender according to the Vietnam national housing census in 2009 for each of the four collection sites. The blue lines in each panel are the normalized probability density functions of the component distributions with darker colors used for increasing μ. The black lines show the full mixture distribution density, and the black dots are the estimated cumulative distribution of the mixture models at 7.0 (titer of 1280). The numbers in the upper right corner of each panel are the BIC scores of the model fits. The fractions of individuals with titers below the detection limit of 20 and above 1280 that were out of the plotting ranges were given next to their respective bars.

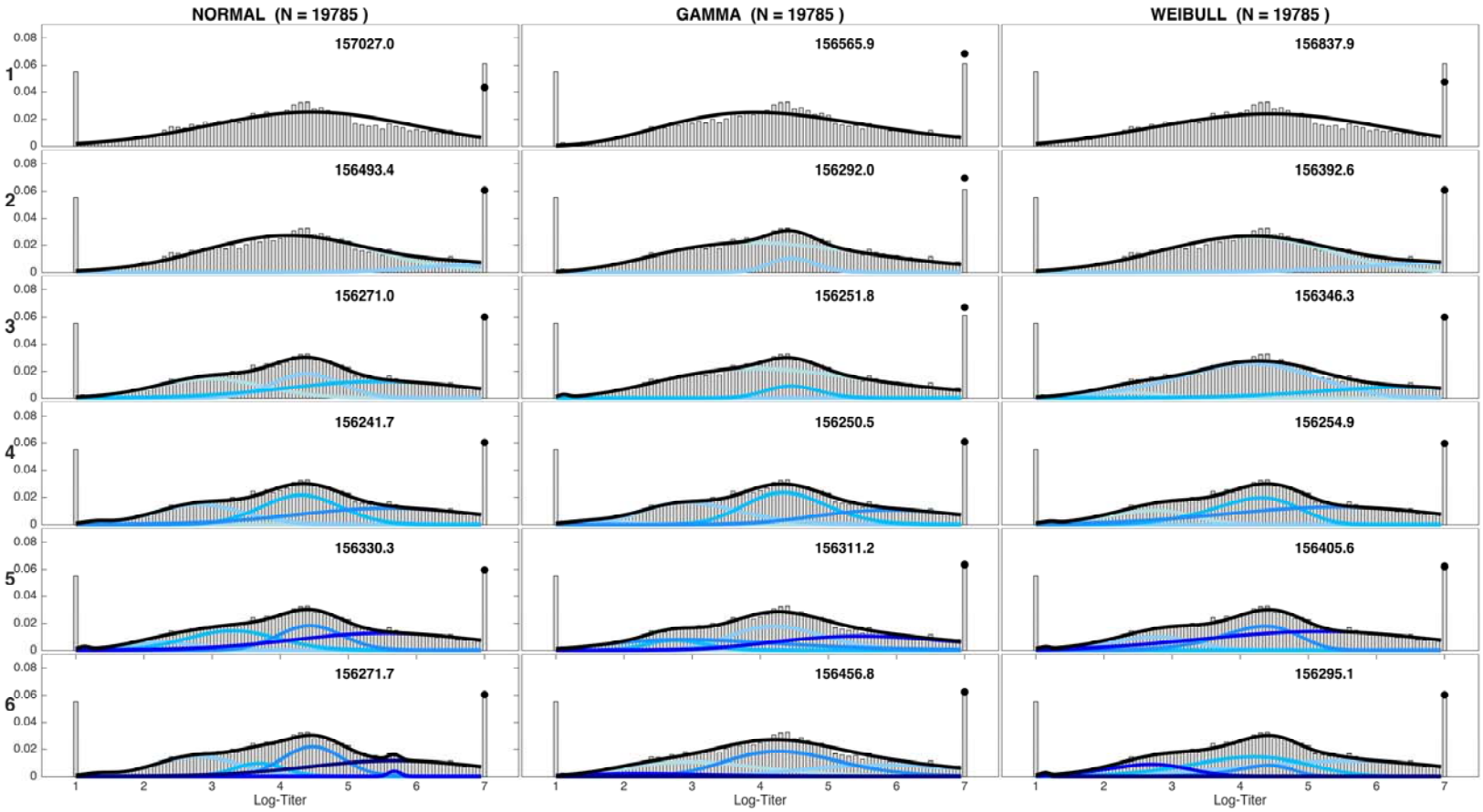

Figure 3.3 Comparing model fits between Normal, Gamma, and Weibull distributions for aggregated titers against seasonal H3N2 strains. Mixture fits were performed with three different distributional forms, shown in the three columns. For more details, see caption Figure 3.2.

Table 3.2 Change in BIC scores for aggregated data against H1-09

Change in BIC as the number of normal distributions in the mixture increases from one to six for 2009 H1N1, for the aggregated data for different forms of the component density (the corresponding estimated parameters were plotted in Figure 3.2). The values of the negative sum of the log likelihood were weighted to adjust for age and gender according to the Vietnam national housing census in 2009. The first row shows the exact values of sum of negative log-likelihood (SumNegLLH). Bold numbers represent the mixtures with the best BIC (Figure 3.2).

		Normal Components	Gamma Components	Weibull Components
SumNegLLH (C=1)		71504.04	71092.51	71166.23
ΔBIC	1 to 2	-828	-448	-252
	2 to 3	-410	**-93**	-407
	3 to 4	-318	91	-197
	4 to 5	-20	-13	27
	5 to 6	**-27**	-73	**-39**

Table 3.3 Change in BIC scores for aggregated data against H3N2

Change in BIC as the number of normal distributions in the mixture increases from one to six for H3N2, for the aggregated data for different forms of the component density (the corresponding estimated parameters were plotted in Figure 3.3). The values of the negative sum of the log likelihood were weighted to adjust for age and gender according to the Vietnam national housing census in 2009. The first row shows the exact values of sum of negative log-likelihood (SumNegLLH). Bold numbers represent the mixtures with the best BIC (Figure 3.3) (BIC change of less than 6 is considered negligible).

		Normal Components	Gamma Components	Weibull Components
SumNegLLH (C=1)		78498.68	78268.11	78404.12
ΔBIC	1 to 2	-534	-274	-445
	2 to 3	-222	**-40**	-46
	3 to 4	**-29**	-1	**-91**
	4 to 5	15	91	26
	5 to 6	15	115	14

3.4.4 Multimodal patterns of the general population antibody titers distribution against H1N1 and H3N2

A total of 20,152 sera were collected and tested for antibody concentrations by protein microarray. The samples represent patients attending hospitals in four cities – Ho Chi Minh City (n=5788), Nha Trang (n=5630), Buon Ma Thuot (n=4144), and Hue (n=4590) in central and southern Vietnam. Titer distributions varied by age, as expected (Figure 3.4) but did not vary by site (Figure 3.5 and 3.6). Figure 3.4 shows the age-stratified titer distributions to the HA1 component of the 2009 H1N1 virus and the most recently circulating H3N2 variants. If individuals truly represented seropositive (exposed) and seronegative (unexposed or naïve) categories, a mixture model of two components would classify samples into two subgroups. Visually, this does not appear to be the case as a broad range of titers was observed for both subtypes across all age groups. Thus, a mixture distribution fitting approach was employed to determine the appropriate number of components necessary to accurately describe the titer data.

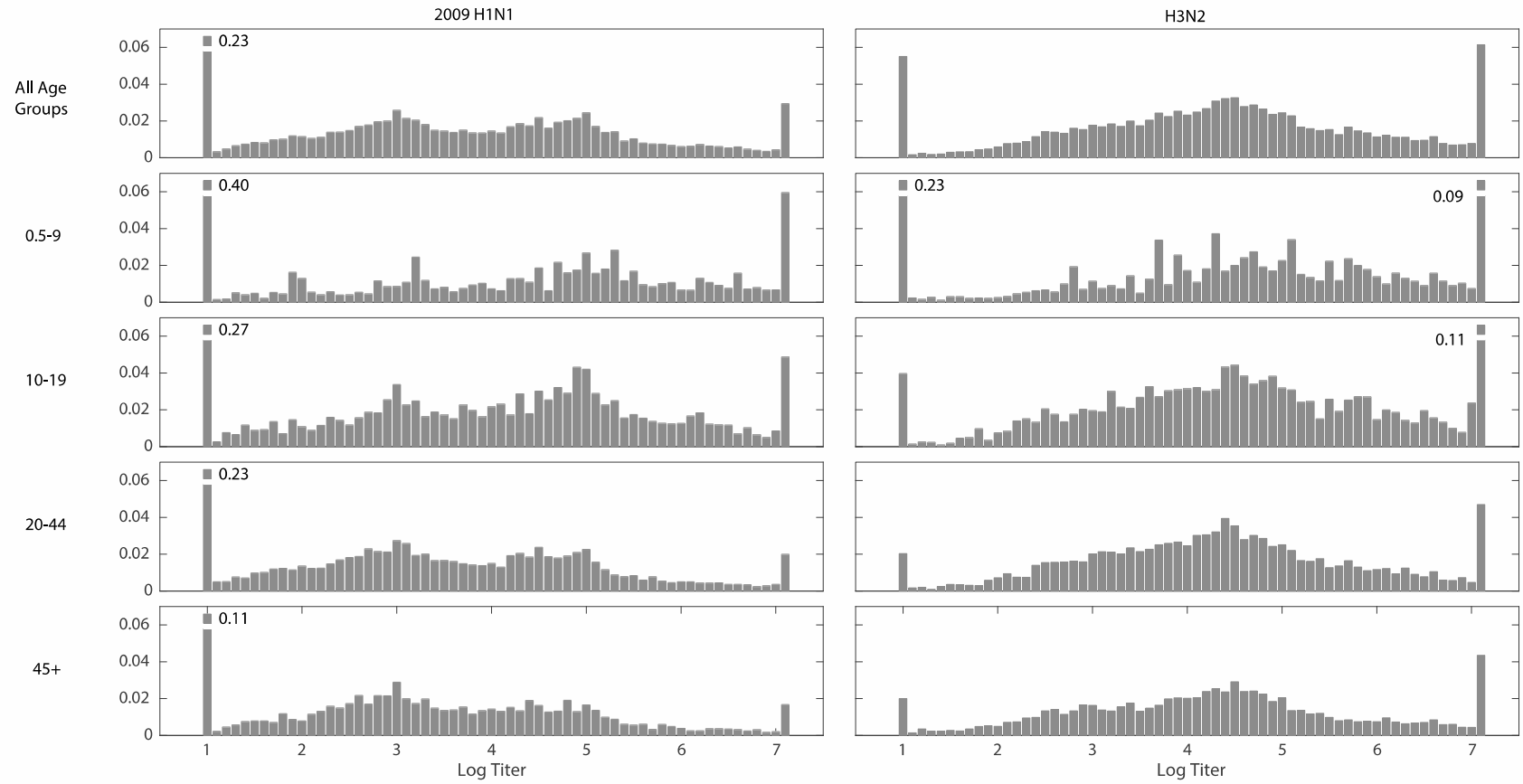

Figure 3.4 Population-level antibody titer histograms H1-09 and H3N2 grouped by age groups. Showing titer histograms for n=20,152 individuals, plotted for all ages (top panels) and by age group (bottom four panels). Titers shown are to the HA1 components of the 2009 H1N1 pandemic influenza virus (left column) and to recently circulating H3N2 viruses (right column). The fractions of individuals with titers below the detection limit of 20 and above 1280 that were out of the plotting ranges are given next to the respective bar. Histograms were weighted to adjust for age and gender according to the Vietnam national housing census in 2009 for the four collection sites.

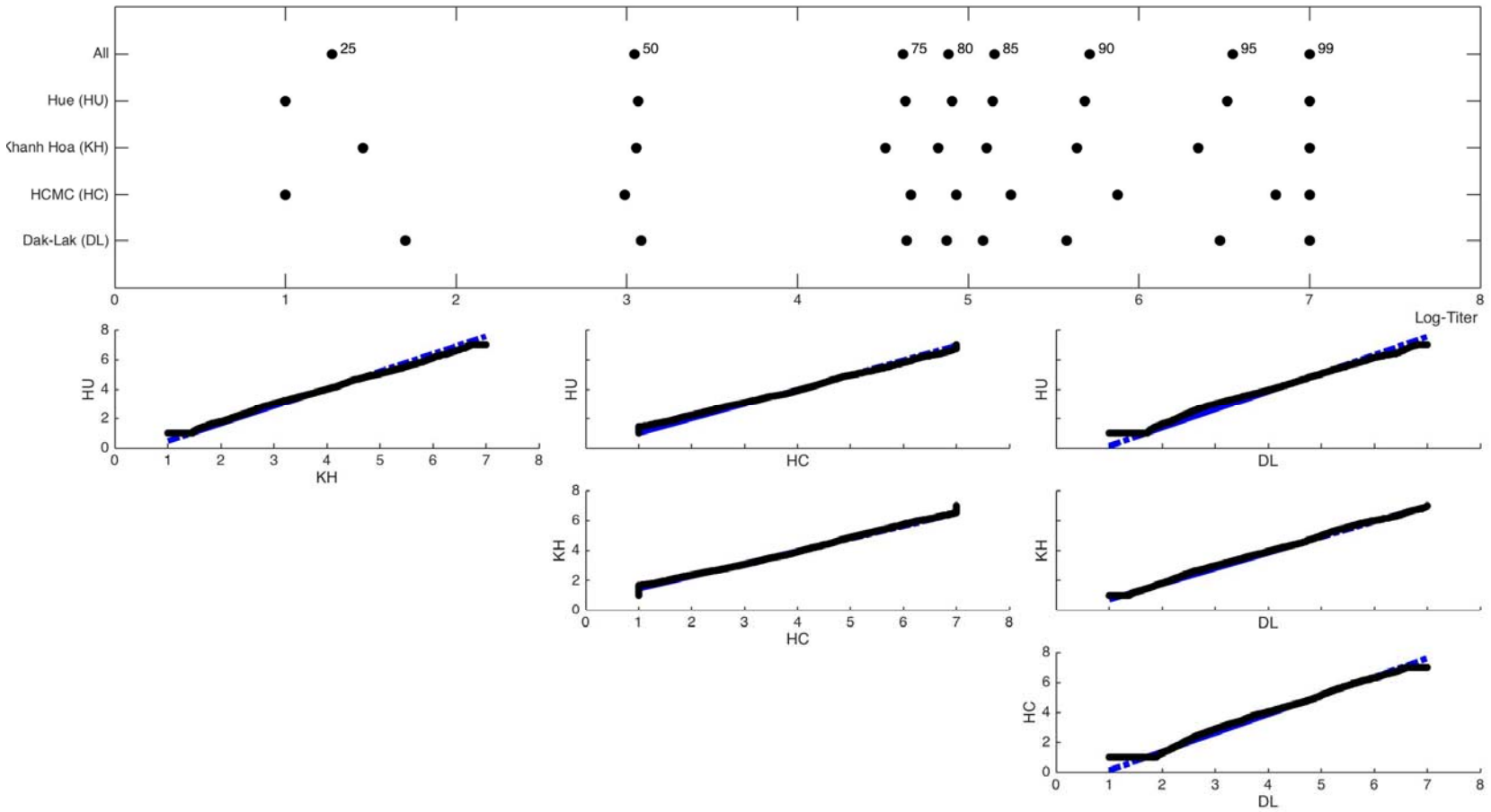

Figure 3.5 QQ-plot comparisons among different collection sites for H1-09 titers. **Top:** Quantile plot showing the 25th, 50th, 75th, 80th, 85th, 90th, 95th, and 99th percentiles of log-titer for 2009 H1N1 (log-titer on *x*-axis) for the aggregated data and the individual collection sites (*y*-axis). **Bottom:** quantile-quantile plots for pairwise comparison among the four collection sites (all age groups included; not re-weighted by province population). When the two datasets contain different numbers of samples, the plotting quantiles were calculated based on the smaller dataset. Blue lines are the extrapolated straight line connecting the first and third quartiles of the smaller dataset.

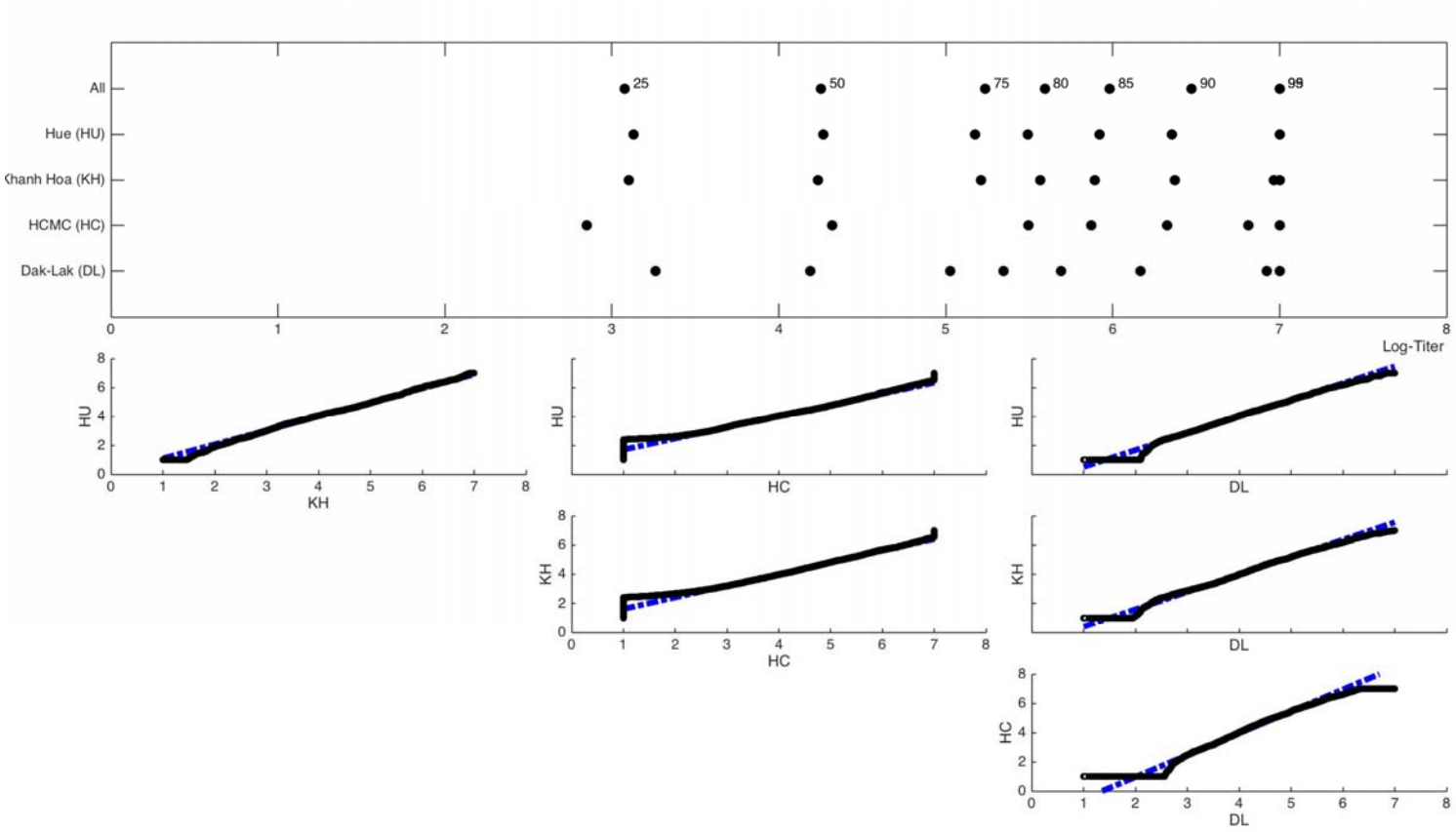

Figure 3.6 QQ-plot comparisons among different collection sites for H3N2 titers. **Top:** Quantile plot showing the 25th, 50th, 75th, 80th, 85th, 90th, 95th, and 99th percentiles of log-titer for H3N2 (log-titer on *x*-axis) for the aggregated data and the individual collection sites (*y*-axis). **Bottom:** quantile-quantile plots for pairwise comparison among the four collection sites (all age groups included; not re-weighted by province population). When the two datasets contain different numbers of samples, the plotting quantiles were calculated based on the smaller dataset. Blue lines are the extrapolated straight line connecting the first and third quartiles of the smaller dataset.

3.4.5 Four-component mixture models for H1N1 Pdm 2009 strain

Mixture distribution fits for up to six components, with an additional weight at a log-titer of one ("zero inflation"), are shown in Figure 3.7 for H1N1. For both subtypes, it is clear that a binary classification of titer is not the most informative interpretation of the titer distribution, as both the one- and two-component models (top two rows) did not capture the underlying structure of the dataset adequately. When stratifying the data by site (sample size > 4,000), the Bayesian Information Criterion (BIC) selected four components as the best model for the H1N1 data (five for Hue, but the ΔBIC=18 here was relatively small compared to other changes between nested models). The five- and six-component models either overfit the data (according to the BIC) or included low-variance/low-weight components, which would correspond to an implausible population subgroup with a very specific antibody titer (Figures 3.7 and 3.8). This was readily seen in the aggregate data which is why the BIC-selected models of the by-site data are likely to be better explanations of the structure of these titer distributions. BIC improvement from n mixture components to $n + 1$ components varied is shown in Table 3.4 for 2009 H1N1. The means and variances were allowed to be free in these analyses, and the confidence intervals for the inferred parameters (Table 3.5) suggest that the structure of the distributions and the inferred values were robust across the four sites in our analysis.

The four-component mixtures indicate that these data can be used to develop a more informative serological classification for influenza. Using known results for this microarray assay (Todd 2016; Huijskens et al. 2013; te Beest et al. 2014), titers

below 100 would be classified as negative or `not previously exposed to this particular influenza strain'. For H1N1, this means that titers in the first component $\mu_1 = 29.8$ (95% CI 29.1–30.5) and in the second component $\mu_2 = 75.0$ (95% CI 73.4–76.7) would both correspond to seronegative individuals. The second-highest titer component has mean μ_3=247.2 (95% CI 240.0–253.7) and the highest titer component has mean μ_4=671.1 (95% CI 484.7–818.6). Confidence intervals were computed using likelihood profiles (McLachlan and Peel 2000). The natural interpretation of these high-titer subgroups – based on antibody titers measured as a function of time since infection (Todd 2016) – is that they represent more recent infections. As it is known that the influenza antibody decay rate is fast enough to be observed in the first six to twelve months after an acute infection (Ng et al. 2013; Horsfall and Richard 1941), for H1N1 the highest titer subgroup may be an approximate designation for recently infected individuals, and the second highest titer subgroup may correspond to 'historically infected' individuals, i.e. individuals infected at some point in the non-recent past.

Table 3.4 Change in BIC scores for H1-09 data grouped by collection site
BIC scores for the number of normal distributions in the mixture increases from one to six for 2009 H1N1, for the aggregated data as well as the individual collection sites (the corresponding estimated parameters were plotted in Figure 3.7 and 3.8). The values of the negative sum of the log likelihood were weighted to adjust for age and gender according to the Vietnam national housing census in 2009. The first row shows the exact values of sum of negative log-likelihood (SumNegLLH). Bold numbers represent the mixtures with the best BIC.

		ALL SITES (N = 19335)	HUE (N = 4390)	KHANH HOA (N = 5053)	HCMC (N = 5753)	DAK-LAK (N = 4139)
SumNegLLH (C=1)		71504.04	15812.88	18726.69	21496.01	15432.06
ΔBIC	1 to 2	-826	-171	-182	-215	-209
	2 to 3	-410	-75	-80	-138	-131
	3 to 4	-318	-67	**-56**	**-77**	**-33**
	4 to 5	-20	**-18**	9	17	6
	5 to 6	**-27**	2	24	10	-3

Table 3.5 Estimates with 95% confidence intervals in parentheses, for means, variances, and weight parameters, for one-component to four-component mixture models of H1N1 titers plotted in Figure 3.7 and 3.8.

Number of normal components		ALL SITES (N = 19335)	HUE (N = 4390)	KHANH HOA (N = 5053)	HCMC (N = 5753)	DAK-LAK (N = 4139)
1	w_0	0.228	0.254	0.225	0.224	0.209
	w_1	0.772	0.746	0.775	0.776	0.791
	μ_1	3.950 (3.925 – 3.975)	4.014 (3.962 – 4.065)	3.910 (3.865 – 3.956)	4.018 (3.974 – 4.062)	3.840 (3.790 – 3.890)
	σ_1	1.551 (1.533 - 1.570)	1.576 (1.520 - 1.615)	1.513 (1.480 - 1.547)	1.589 (1.558 - 1.622)	1.515 (1.478 - 1.553)
2	w_0	0.228	0.254	0.225	0.224	0.209
	w_1	0.218 (0.205 - 0.230)	0.242 (0.218 - 0.272)	0.230 (0.208 - 0.256)	0.184 (0.169 - 0.200)	0.251 (0.229 - 0.275)
	μ_1	2.462 (2.445 - 2.500)	2.646 (2.550 - 2.750)	2.502 (2.420 - 2.590)	2.236 (2.285 - 2.440)	2.403 (2.330 - 2.470)
	σ_1	0.698 (0.686 - 0.715)	0.763 (0.723 - 0.816)	0.717 (0.684 - 0.760)	0.659 (0.632 - 0.693)	0.673 (0.645 - 0.705)
	w_2	0.555 (0.542 - 0.568)	0.504 (0.475 - 0.530)	0.545 (0.520 - 0.567)	0.592 (0.577 - 0.608)	0.540 (0.517 - 0.565)
	μ_2	4.532 (4.480 - 4.580	4.671 (4.605 - 4.745)	4.504 (4.450 - 4.570)	4.530 (4.492 - 4.567)	4.506 (4.440 - 4.570)
	σ_2	1.393 (1.377 - 1.410)	1.438 (1.435 - 1.442)	1.356 (1.347 - 1.365)	1.428 (1.425 - 1.433)	1.317 (1.297 - 1.335)
3	w_0	0.228	0.254	0.225	0.224	0.209
	w_1	0.396 (0.365 - 0.420)	0.332 (0.282 - 0.400)	0.066 (0.053 - 0.078)	0.348 (0.320 - 0.382)	0.449 (0.340 - 0.482)
	μ_1	2.771 (2.730 - 2.815)	2.857 (2.720 - 3.020)	1.594 (1.500 - 1.690)	2.668 (2.590 - 2.760)	2.766 (2.700 - 2.835)
	σ_1	0.803 (0.815 - 0.843)	0.870 (0.805 - 0.920)	0.297 (0.255 - 0.345)	0.796 (0.761 - 0.837)	0.830 (0.800 - 0.866)
	w_2	0.159 (0.140 - 0.200)	0.042 (0.035 - 0.062)	0.157 (0.148 - 0.167)	0.184 (0.178 - 0.201)	0.254 (0.227 - 0.272)
	μ_2	4.684 (4.658 - 4.710)	4.922 (4.780 - 5.190)	2.753 (2.680 - 2.810)	4.613 (4.586 - 4.643)	4.794 (4.740 - 4.845)
	σ_2	0.434 (0.413 - 0.472)	0.100 (0.075 - 0.170)	0.402 (0.375 - 0.445)	0.467 (0.465 - 0.468)	0.465 (0.432 - 0.505)
	w_3	0.217 (0.155 - 0.270)	0.372 (0.295 - 0.430)	0.552 (0.528 - 0.572)	0.467 (0.456 - 0.477)	0.088 (0.077 - 0.112)
	μ_3	5.571 (5.250- 6.100)	4.948 (4.820 - 5.280)	4.514 (4.420 - 4.610)	5.510 (5.290 - 5.870)	6.520 (6.250 - 6.680)
	σ_3	1.298 (1.065 - 1.430)	1.482 (1.170 - 1.795)	1.325 (1.292 - 1.357)	1.415 (1.230 - 1.500)	0.683 (0.587 - 0.862)
4	w_0	0.228	0.254	0.225	0.224	0.209
	w_1	0.062 (0.056 - 0.069)	0.057 (0.046 - 0.072)	0.060 (0.046 - 0.079)	0.054 (0.044 - 0.068)	0.089 (0.063 - 0.122)
	μ_1	1.576 (1.540 - 1.610)	1.601 (1.530 - 1.680)	1.525 (1.450 - 1.610)	1.522 (1.460 - 1.600)	1.692 (1.580 - 1.810)
	σ_1	0.296 (0.280 - 0.313)	0.274 (0.237 - 0.316)	0.270 (0.233 - 0.318)	0.266 (0.238 - 0.308)	0.370 (0.328 - 0.418)
	w_2	0.322 (0.317 - 0.328)	0.347 (0.317 - 0.370)	0.306 (0.285 - 0.328)	0.290 (0.279 - 0.303)	0.338 (0.300 - 0.358)
	μ_2	2.907 (2.875 - 2.940)	3.052 (2.960 - 3.140)	2.850 (2.780 - 2.920)	2.809 (2.740 - 2.880)	2.952 (3.040 - 2.870)
	σ_2	0.619 (0.609 - 0.630)	0.668 (0.642 - 0.708)	0.565 (0.540 - 0.610)	0.615 (0.602 - 0.639)	0.616 (0.550 - 0.650)
	w_3	0.235 (0.226 - 0.239)	0.166 (0.122 - 0.192)	0.202 (0.179 - 0.225)	0.231 (0.218 - 0.246)	0.278 (0.266 - 0.292)
	μ_3	4.628 (4.590 - 4.660)	4.752 (4.660 - 4.840)	4.483 (4.380 - 4.570)	4.568 (4.500 - 4.630)	4.760 (4.700 - 4.820)
	σ_3	0.512 (0.503 - 0.525)	0.435 (0.360 - 0.500)	0.512 (0.485 - 0.565)	0.516 (0.492 - 0.553)	0.491 (0.474 - 0.517)
	w_4	0.153 (0.128 - 0.191)	0.176 (0.128 - 0.260)	0.207 (0.115 - 0.290)	0.201 (0.141 - 0.260)	0.086 (0.075 - 0.106)
	μ_4	6.068 (5.700 - 6.300)	5.993 (5.410 - 6.320)	5.610 (5.000 - 6.290)	5.806 (5.395 - 6.320)	6.546 (5.395 - 6.700)
	σ_4	1.058 (0.925 - 1.220)	1.162 (0.940 - 1.450)	1.134 (0.820 - 1.350)	1.287 (1.020 - 1.450)	0.665 (0.565 - 0.850)

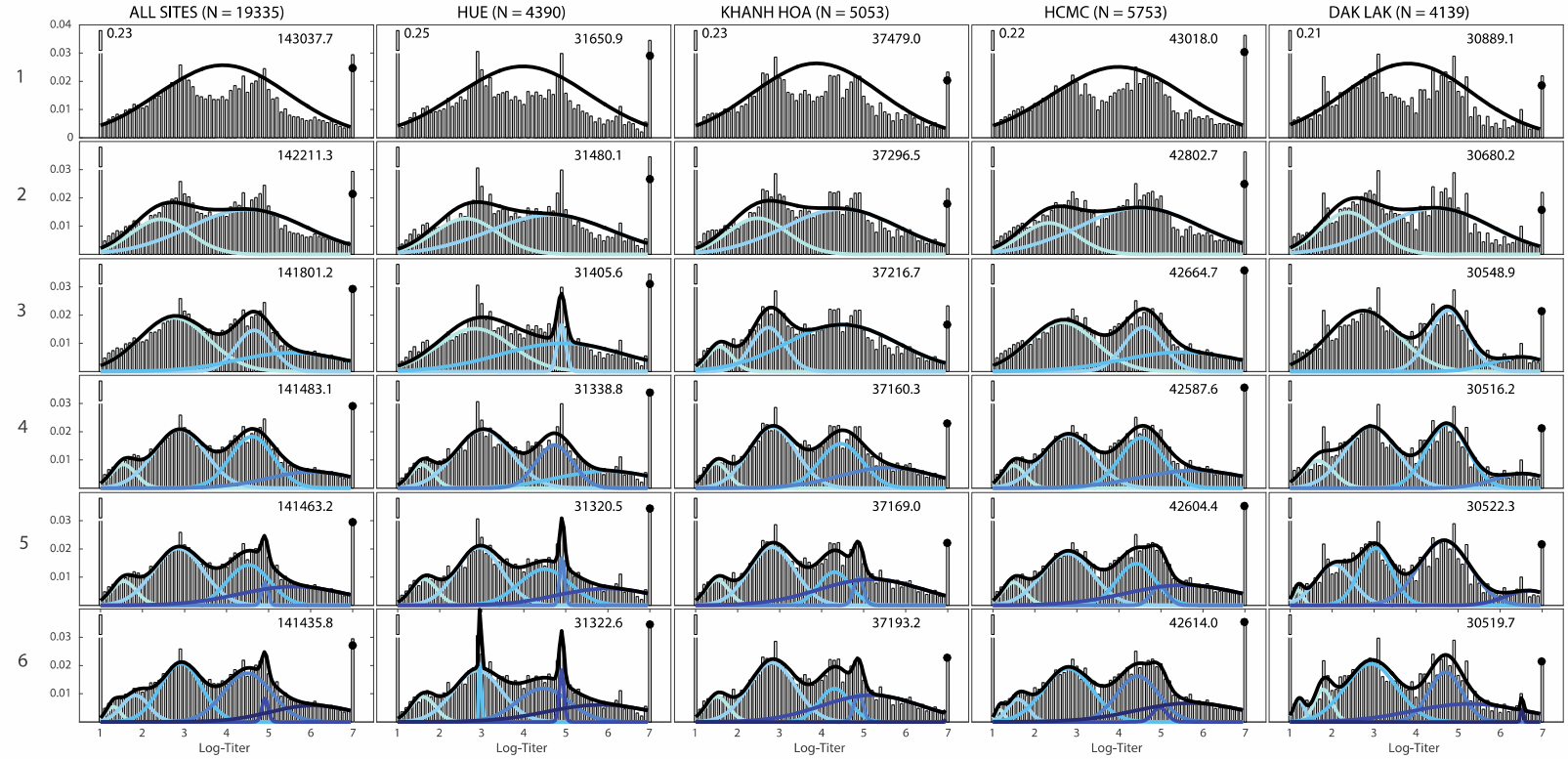

Figure 3.7 Fit results different number of mixture components for H1-09 grouped by collection sites. Titer histograms for 2009 H1N1, showing fit results for mixture models with different numbers of normal components (top to bottom; the label to the left of the y-axis is the number of mixture components) and grouped by collection sites. Histograms are weighted to adjust for age and gender according to the Vietnam national housing census in 2009 for each of the four collection sites. The blue lines in each panel are the normalized probability density functions of the component distributions with darker colors used for increasing μ. The black lines show the full mixture distribution density, and the black dots are the estimated cumulative distribution of the mixture models at 7.0 (titer of 1280). The numbers in the upper right corner of each panel are the BIC scores of the model fits. The fractions of individuals with titers below the detection limit of 20 and above 1280 that were out of the plotting ranges were given next to their respective bars.

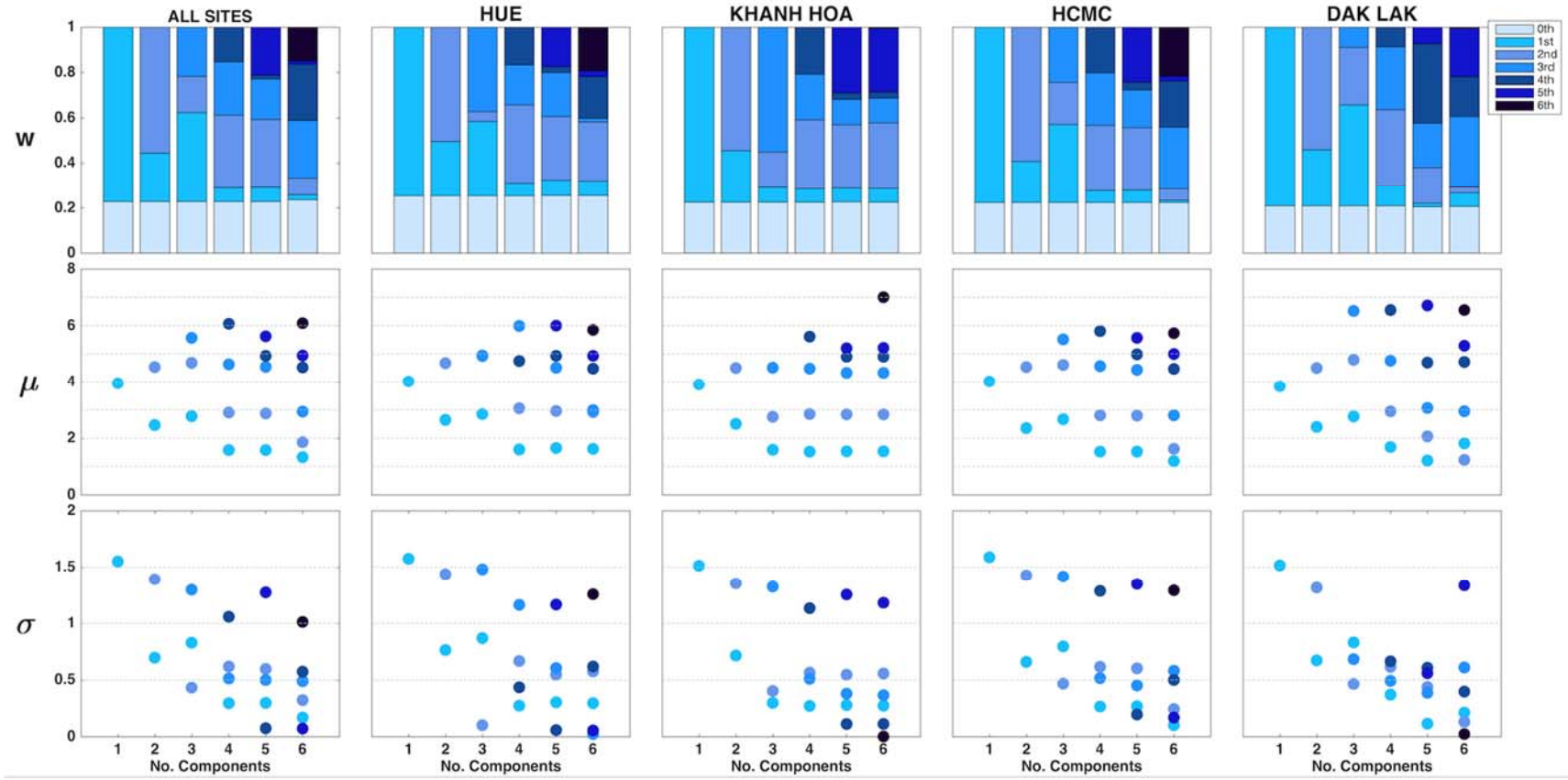

Figure 3.8 Visualization of model selection process for 2009 H1N1 titer-distribution models from Figure 3.7. The *y*-axes show the fitted values of w_i (mixture weights), μ_i (means), and σ_i (standard deviations). Components' shades were ranked from lightest to darkest in the order of increasing μ. In the top panel, the "0th component" represents the point mass w_0 placed at 20 for titers below the lower detection limit of 20. Note that in many cases for five or six components, the weights or standard deviation parameters are close to zero; for some cases, two of the inferred mean parameters are very close to each other.

3.4.5.1 Sub-sampling data according to the age-group proportions and age bands in the general population

In order to test the robustness of our analysis and to make sure that the four-component mixture model fit was not a result of stratifying data by collection site, four random sub-samples (N= 5000) were drawn to match with the age and gender structure from the aggregated data set. This is essentially a bootstrap-like uncertainty analysis, but the number of bootstrap samples that can be analyzed is limited by our ability to fit them. The results of this analysis point to the same conclusion: that four-component mixture is chosen as the best fit for three out of four sub-samples (Table 3.6). Even though one of the sub-samples favors five-component mixture over four, the difference in BIC score was only 4, which could be considered negligible in this case.

Table 3.6 Change in BIC scores for model fits to H1-09 titers for four random subsamples. Showing the BIC changes as the number of normal distributions in the mixture increases from one to six for 2009 H1N1, for four random sub-samples (with replacement N = 5000) according to the age-group proportions and age bands in the general population (tcorresponding estimated parameters were plotted in Figure 3.9). The values of the negative sum of the log likelihood were weighted to adjust for age and gender according to the Vietnam national housing census in 2009. The first row shows the exact values of sum of negative log-likelihood (SumNegLLH). Bold numbers represent the mixtures with the best BIC.

		SUBSAMPLE 1 (N = 5000)	SUBSAMPLE 2 (N = 5000)	SUBSAMPLE 3 (N = 5000)	SUBSAMPLE 4 (N = 5000)
SumNegLLH (C=1)		9461.54	9341.28	9184.87	9367.61
ΔBIC	1 to 2	-102	-126	-123	-113
	2 to 3	-43	-16	-28	-37
	3 to 4	-37	**-20**	**-5**	**-31**
	4 to 5	**-4**	8	14	7
	5 to 6	28	22	8	25

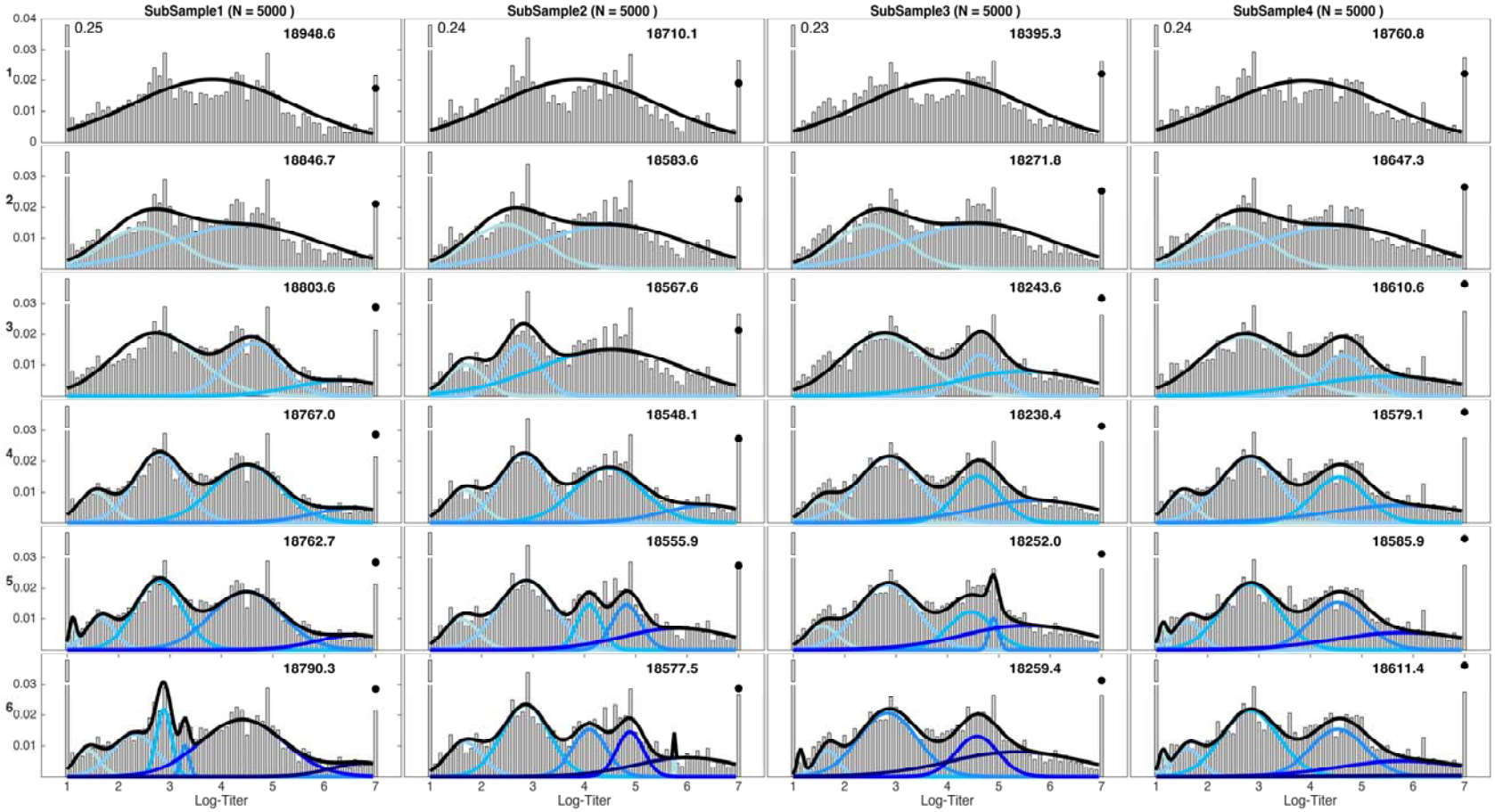

Figure 3.9 Model fits for H1-09 titers for four random sub-samples. As Figure 3.7, but here four random sub-samples were drawn (with replacement) according to the age-group and gender proportions of the general population. Four or five components are the best explanatory models, according to BIC. However, the component means, variances, and weights are not the same across sub-samples when five components are used.

3.4.5.2 Stratifying data by collection years

Stratifying the data by collection year (Figure 3.10) revealed the four-component mixture as the best fit with the exception of the aggregated data. The overall distributional shape did not change through time and the components' means and standard deviations did not vary significantly from year to year (except in 2013). This observation gave us confidence about the stationary nature of the four-component mixture observed in the aggregated data. No obvious pattern was observed and the component means and standard deviations stayed almost constant from 2010 to 2012, but the fraction of recently infected and historically infected individuals did decrease from 2012 to 2013.

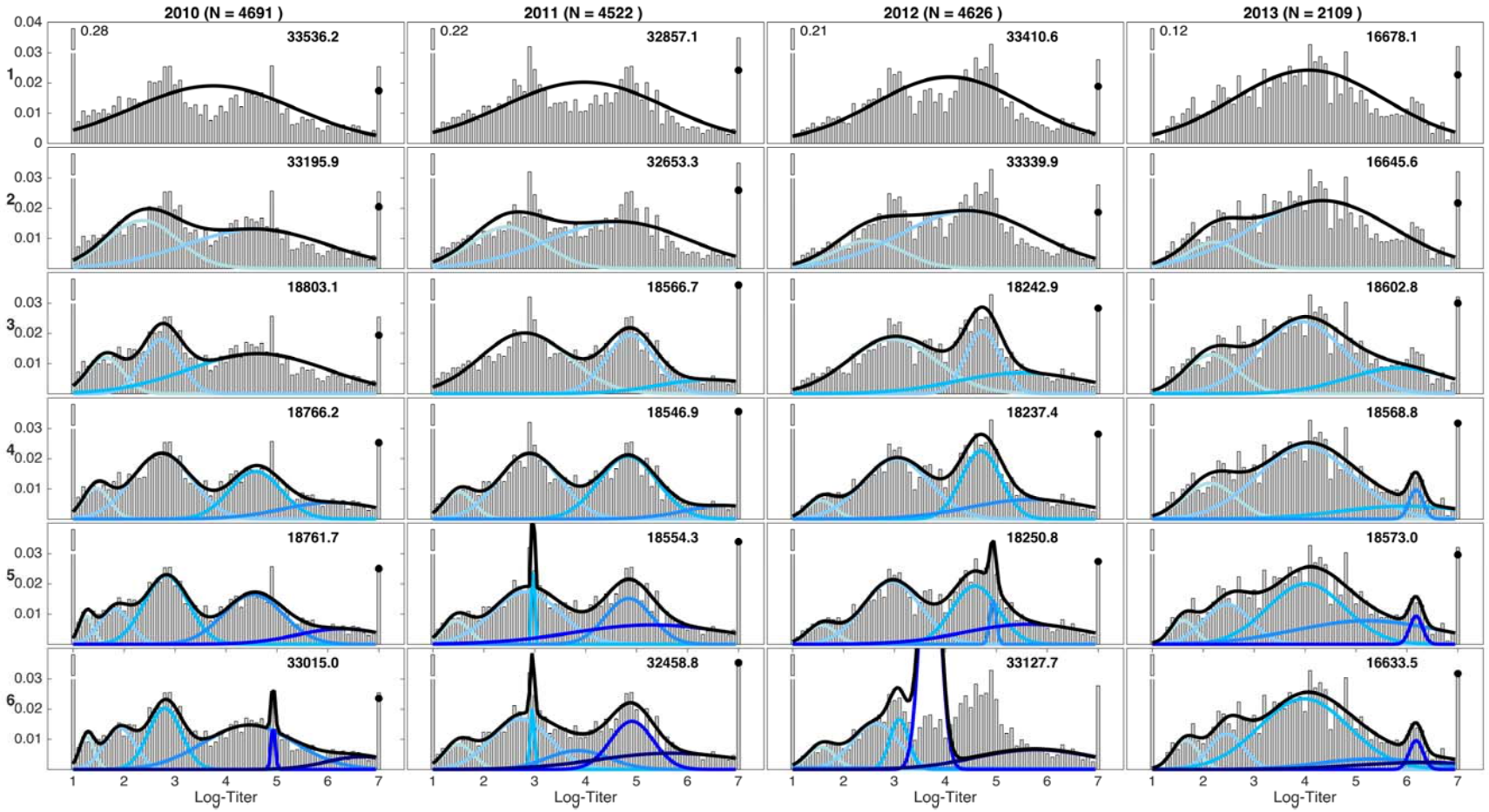

Figure 3.10 Model fits for H1-09 titers for aggregated data stratified by collection years. As Figure 3.7, but data were grouped by collection years for the 4 collection sites, Hue (HU), Khanh Hoa (KH), Dak Lak (DL), and Ho Chi Minh city (HC).

3.4.5.3 Stratifying data by samples' ages

As it is known that the influenza antibody decay rate is fast enough to be observed in the first six to twelve months after an acute infection (Ng et al. 2013; Horsfall and Richard 1941), for H1N1 the highest titer subgroup may be an approximate designation for recently infected individuals, and the second highest titer subgroup may correspond to 'historically infected' individuals, i.e. individuals infected at some point in the non-recent past.

For H1N1, assuming that the highest-titer component (w_4) of the mixture distribution corresponds to recently infected individuals and the second highest-titer component (w_3) corresponds to historic infection, one would expect to be able to validate these interpretations using post-pandemic sera. Looking at samples collected from January 2010 to June 2010 – i.e. after the first wave of the 2009 influenza pandemic in Vietnam (Hien et al. 2010; Horby et al. 2012) – the proportions of individuals that were recently infected with 2009 H1N1 were highest among younger individuals (0.14, 0.23, 0.08, and 0.16, for the 0.5–9, 10–19, 20–44, and ≥45 age groups, respectively), while the proportions of historically-infected individuals were approximately equal among age groups (0.16, 0.22, 0.23, and 0.20; same age groups); see Table 3.7 for confidence intervals.

The estimates of 14% of children aged 0.5–9 and 23% of children aged 10–19 falling into the recently infected category are likely to be slight underestimates (Chen 2010; Horby et al. 2012; Wu et al. 2011) of pandemic attack rate as the post-pandemic sample here includes samples collected through June 2010. Nevertheless, these are within the expected ranges of the attack rate of the first year of the 2009

pandemic. For older individuals, pandemic attack rates are more difficult to validate but it is important to remember that older individuals had measurable antibody titers to 2009 H1N1 prior to the arrival of the new pandemic virus (Broberg, Nicoll, and Amato-Gauci 2011). The pattern of attack rates observed in our samples is consistent with the two highest titer categories representing recent and historical infections with the H1N1 subtype. The individual components in the mixture models did not correspond to any specific age groups (Figure 3.11), and stratifying the samples by age did not explain any particular component of the mixture (Figure 3.12). All age groups included individuals with high, medium, and low titer levels.

Table 3.7 Estimates and confidence intervals for weight parameters in post-pandemic (January to June 2010) analysis for four-component models

Age group	Number of samples	w_3(95% CI)	w_4(95% CI)
0–9	161	0.160 (0.146 - 0.174)	0.138 (0.117 - 0.169)
10–19	355	0.216 (0.182 - 0.234)	0.226 (0.200 - 0.268)
20–44	871	0.230 (0.227 - 0.393)	0.085 (0.070 - 0.108)
45+	439	0.196 (0.169 - 0.221)	0.157 (0.135 - 0.205)

Table 3.8 Change in BIC scores for H1-09 data grouped by age groups
Showing BIC changes as the number of normal distributions in the mixture increase from one to six for **H1N1**, for different age groups as recommended by CONCISE (the corresponding estimated parameters were plotted in Figure 3.12 and 3.13). The values of the negative log-likelihood were weighted to adjust for age and gender according to the Vietnam national housing census in 2009. The first row shows the exact values of the negative log-likelihood. Bold numbers represent the best fit models (BIC and visual inspection).

		ALL AGES (N = 19335)	0-9 Yrs-Old (N = 2988)	10-19 Yrs-Old (N = 2876)	20-44 Yrs-Old (N = 8116)	45+ Yrs-Old (N = 5355)	0-49 Yrs-Old (N = 15168)	60+ Yrs-Old (N = 2152)
SumNegLLH (C=1)		71504.04	9951.65	14564.33	30125.89	16100.72	49844.40	5757.17
ΔBIC	1 to 2	-1670	-86	-78	-346	-238	-547	-101
	2 to 3	-838	-47	-58	-207	-91	-277	**-38**
	3 to 4	-654	**-25**	**-51**	**-135**	**-58**	**-208**	-4
	4 to 5	-57	-7	5	-7	14	-20	18
	5 to 6	**-72**	11	-1	30	18	-8	21

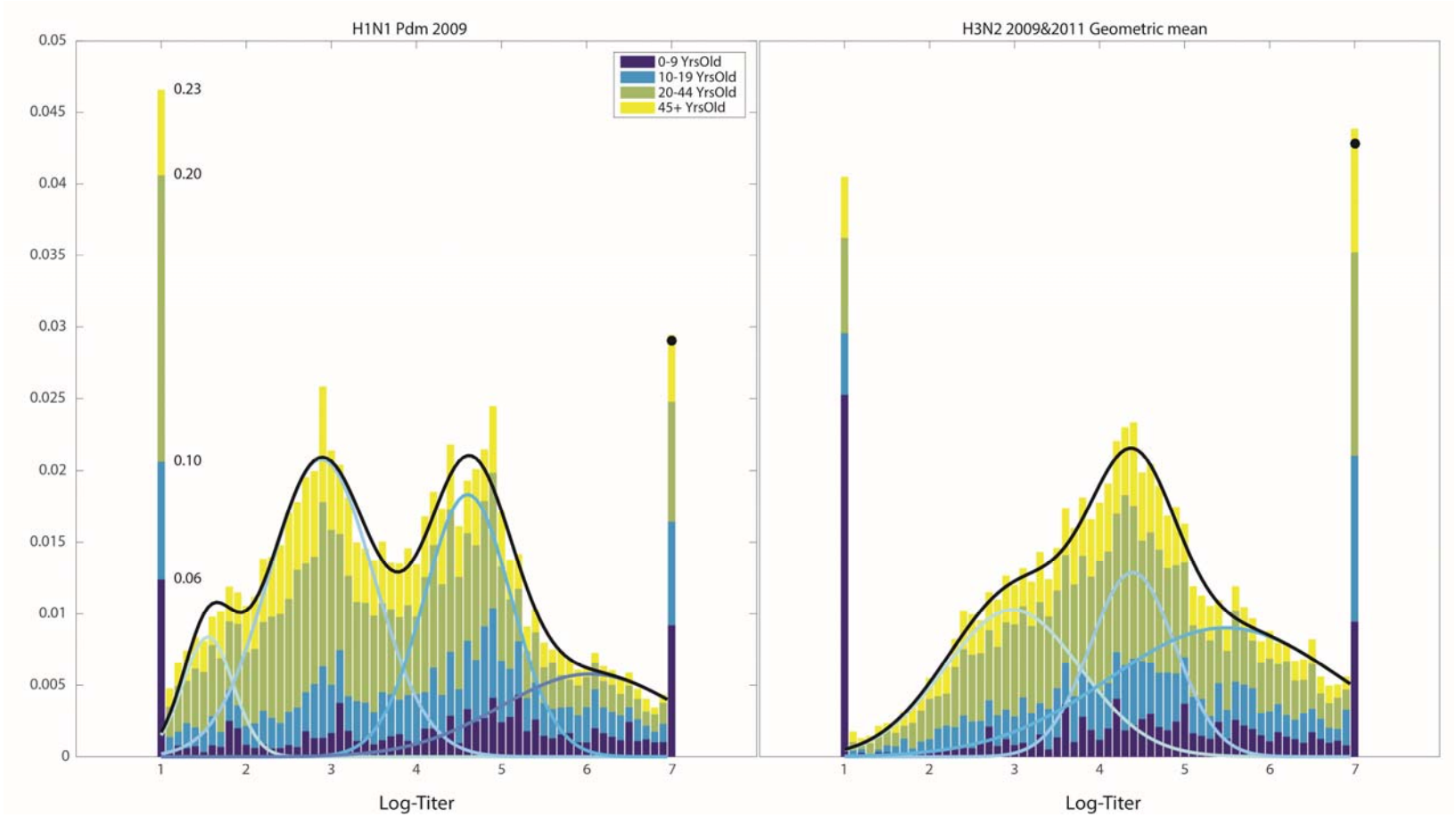

Figure 3.11 Additional visualization of age structure in the titer distributions against H1-09 and H3N2. Here, the four-component model is shown for H1N1 and the three-component model is shown for H3N2. The individual histogram bins (0.1 width on a $\log_2$-scale) are displayed as a stacked bar graph with different age groups corresponding to different colors. Note that for H1N1, the left-hand bar at a log-titer of one is shown on a separate scale. There are no clear age patterns in these titer distributions suggesting that certain mixture components correspond to certain age groups.

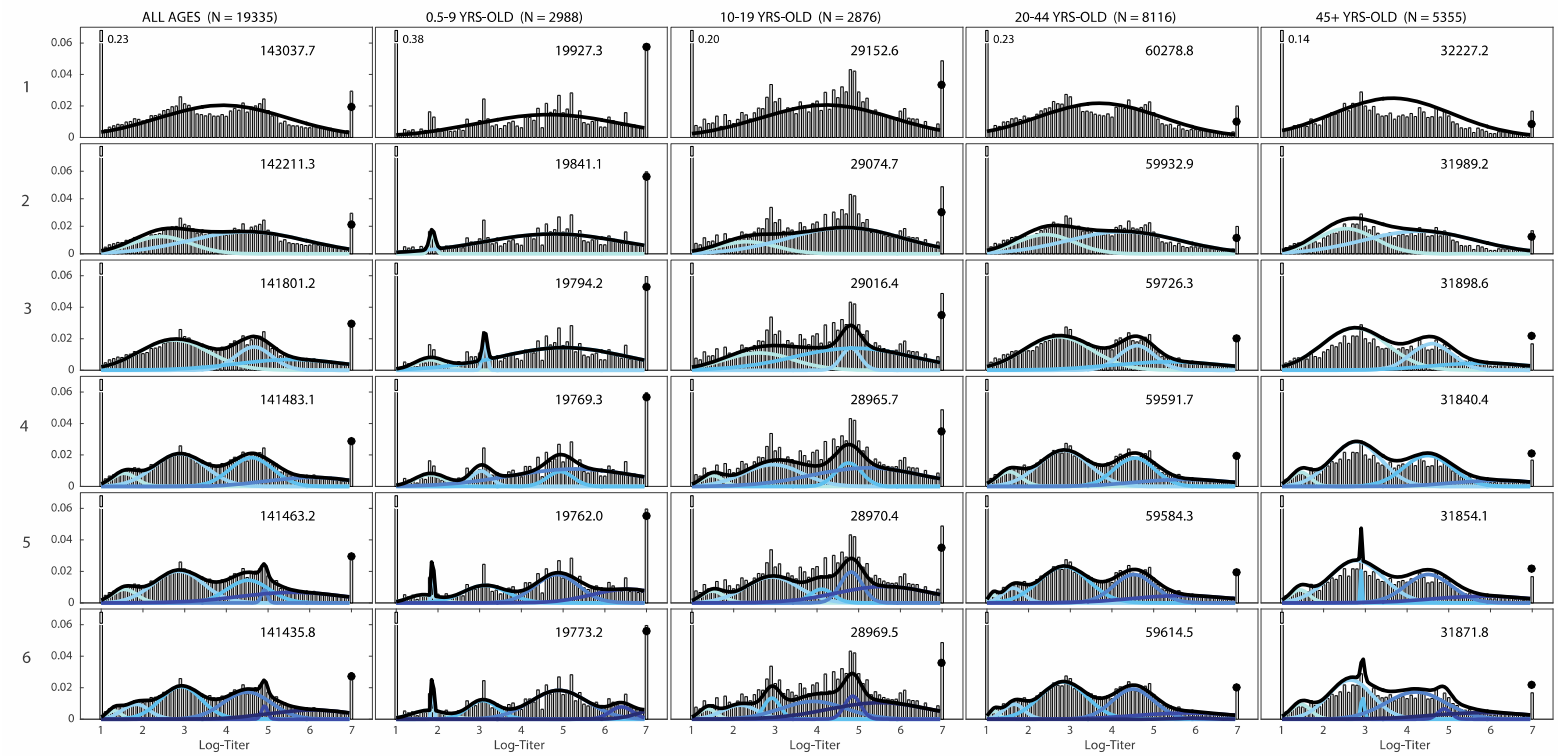

Figure 3.12 Model fits for titer distributions against H1-09 grouped by different age groups. Titer histograms and fit results for mixture models with different numbers of components (label on the left is the number of mixture components) and grouped by different age groups recommended by the CONCISE (http://consise.tghn.org/) for 2009 H1N1 influenza. Histograms are weighted to adjust for age and gender according to the Vietnam national housing census in 2009. The numbers in the upper right corner of each panel are the fitted BIC scores of the respective model. For each panel, the blue lines are the normalized probability density of the component distributions with darker colors used for increasing μ. Black lines are the total mixture distribution density; and the black dots are estimated probability weight of the mixture model for titers ≥ 7.0. The fractions of individuals with titers below the detection limit of 20 and above 1280 that were out of the plotting ranges are shown right next to their respective bars.

3.4.5.4 Multi-lineage hypothesis for H1N1

H1N1 has a more complex lineage history than H3N2, with three different lineages circulating since 1918. This suggests that separating the samples into H1N1 lineage-exposure groups (pre-1957, post-1977, post-2009) may account for certain titer groups or categories. However, separating the samples by birth year – 0.5-50 years-old and ≥60 years-old, to distinguish individuals that could and could not have been infected by the 1918-lineage H1N1 – did not provide any evidence for this effect (Figure 3.13 and Table 3.6).

Individuals in the 60+ age group were born in 1953 or earlier and are likely to have been exposed to three H1N1 lineages: the 1918-1957 lineage, the 1977 lineage, and the 2009 pandemic lineage. The BIC comparisons (see also Table 3.8) show that 3 components is the best fit for 60+ and that 4 components is the best fit for 0.5-49. However, the difference between the 3-component fits and 4-component fits here – as in all other groupings that have been looked at – is that the 4-component fit includes an extra small peak in the seronegative titer range, covering titers between 20 and 30. There does not appear to be a reason why the different lineage-exposure history would produce this extra peak for seronegative individuals.

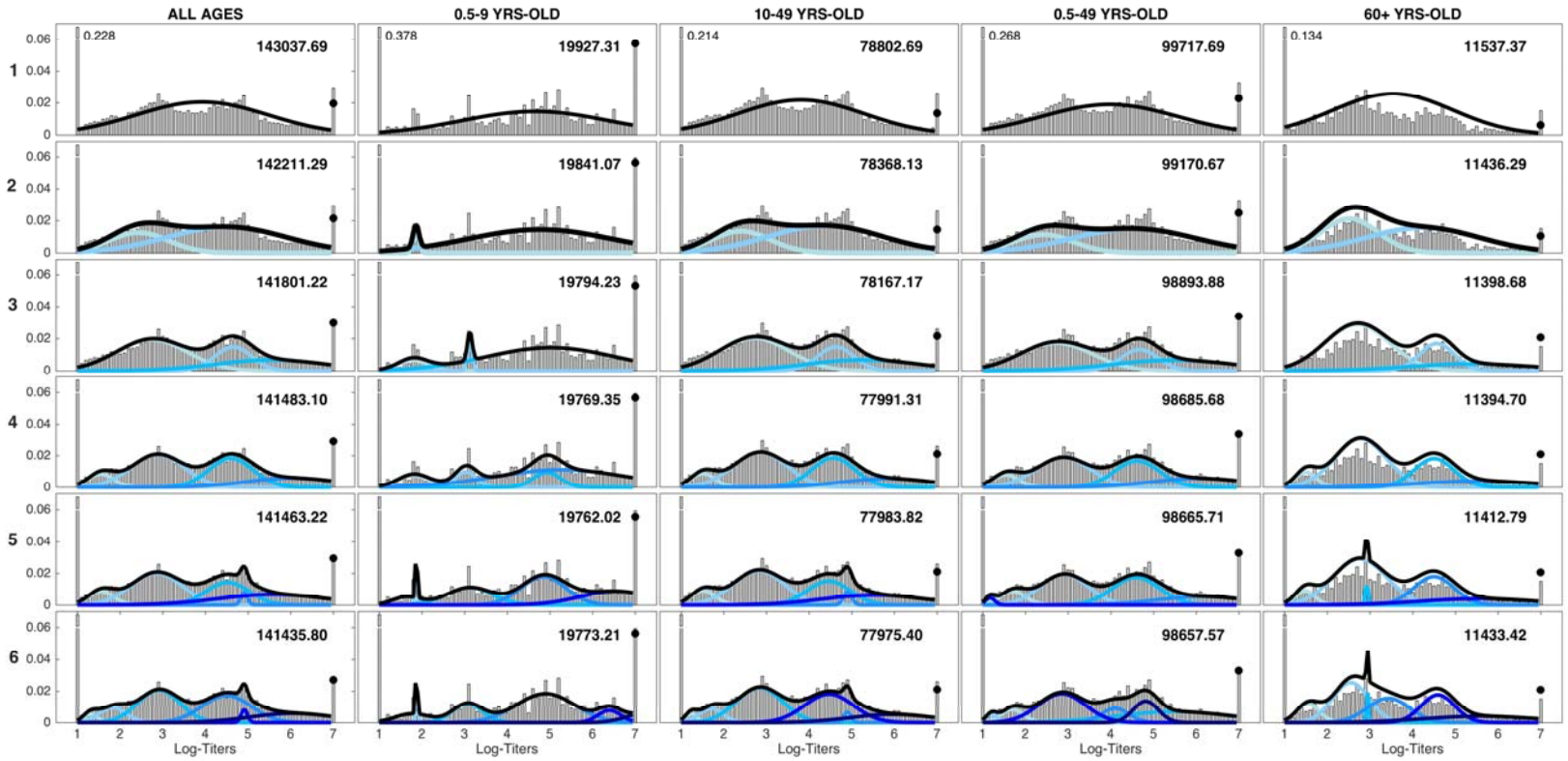

Figure 3.13 Model fits to validate multi-lineage hypothesis for H1-09. Similar to Figure 3.12, but age groupings are different. Individuals in the 0.5-49 age group were born in 1960 or later and would have been exposed to two lineages of H1N1: the 1977 lineage and the 2009 pandemic lineage.

3.4.6 Three-component mixture models for geometric mean titers of H3N2 2009 and 2011 strains

When stratifying the data by site (sample size ~4,000), the Bayesian Information Criterion (BIC) selected three components as the best model for H3N2. The five- and six-component models either overfit the data (according to the BIC) or included low-variance/low-weight components, which would correspond to an implausible population subgroup with a very specific antibody titer (Figure 3.14 and 3.15). This was readily seen in the aggregate data which is why the BIC-selected models of the by-site data (~4000 data points each) are likely to be better explanations of the structure of these titer distributions. BIC improvement from n mixture components to $n + 1$ components is shown in Table 3.9 for H3N2. For H3N2, this means that seronegative individuals would be represented by the lowest titer component ($\mu_1 = 80$). The second-highest titer component has mean μ_2=213.3 (95% CI 204.8–221.5) and the highest titer component has mean μ_3=455.0 (95% CI 401.4–536.7. Confidence intervals were computed using likelihood profiles (McLachlan and Peel 2000). Similar to H1N1, the natural interpretation of these high titer subgroups is that they represent different times since last infection.

The epidemiological interpretation of the H3N2 mixture components cannot be validated at present. The best-fit mixture models for H3N2 had larger variances than those for H1N1. The log-titer ranges (±2σ) for the three H3N2 titer groups were 26–240, 114–456, and 68–3045. Thus, the discriminatory power between the last two components was not as good as for H1N1 (Figure 3.7). The large standard deviations of the last component for H3N2 may have been the result of the high

fraction of right-censored samples with titers ≥1280. In addition, the proportions of individuals in the highest titer group (third component) are 0.46 (ages 0.5–9), 0.49 (ages 10–19), 0.43 (ages 20–44), and 0.34 (≥45). These are unlikely to represent recent attack rates of H3N2 epidemics and are more likely to represent historical infection, i.e. individuals who have been exposed to the currently circulating H3N2 strain at some point in the past. One plausible explanation for these observations is the existence of an additional fourth peak for the H3N2 titers describing individuals with titers above the upper limit of detection (≥1280). In our sample set, the proportions of individuals with H3 titers equal to 1280 were two to three times higher than those for H1N1 in the same age category. This is consistent with the existence of a fourth titer group with mean titer >1280, but we cannot confirm this with the current data as the samples were not diluted past 1:1280.

Similar to H1N1, the individual components in the mixture models did not correspond to any specific age groups, and stratifying the samples by age did not explain any particular component of the mixture (Figure 3.16). All age groups included individuals with high, medium, and low titer levels.

Table 3.9 Change in BIC scores for H3N2 models fits grouped by collection site.
Showing BIC changes as the number of normal distributions in the mixture increase from one to six for **H3N2**, for the aggregated data as well as the individual collection sites (the corresponding estimated parameters were plotted in Figure 3.14 and 3.15). The values of the negative log-likelihood were weighted to adjust for age and gender according to the Vietnam national housing census in 2009. The first row shows the exact values of the negative log-likelihood. Bold numbers represent the mixtures with the best BIC (BIC change of less than 6 is considered negligible). **NB:** Even though the BIC is designed to take sample size into account in selecting the best fitted models, the large number of data points in the aggregate data (~20,000) still caused the BIC to select six components as the best model for H1N1 (Figure 3.7) and four components as the best model for H3N2 (Figure 3.14). Thus, BIC is imperfect and cannot be used as the sole criterion for model selection.

		ALL SITES (N = 19785)	HUE (N = 4519)	KHANH HOA (N = 5384)	HCMC (N = 5784)	DAK-LAK (N = 4134)
SumNegLLH (C=1)		78498.68	17790.08	21515.90	22757.09	16264.15
ΔBIC	1 to 2	-534	-111	-77	-120	-154
	2 to 3	-222	**-104**	**-39**	**-34**	**-55**
	3 to 4	**-29**	5	2	-1	8
	4 to 5	15	16	18	13	-3
	5 to 6	15	16	6	21	24

Table 3.10 Change in BIC scores for H3N2 models grouped by age group.
Showing BIC changes as the number of normal distributions in the mixture increase from one to six for H3N2, for different age groups as recommended by CONCISE (The corresponding estimated parameters were plotted in Figure 3.16). The values of the negative log-likelihood were weighted to adjust for age and gender according to the Vietnam national housing census in 2009. The first row shows the exact values of the negative log-likelihood. Bold numbers represent the mixtures with the best BIC (BIC change of less than 6 is considered negligible).

		ALL AGES (N = 19785)	0-9 Yrs-Old (N = 3031)	10-19 Yrs-Old (N = 2922)	20-44 Yrs-Old (N = 8353)	45+ Yrs-Old (N = 5479)
SumNegLLH (C=1)		78498.68	11518.25	15750.62	33377.53	16966.21
ΔBIC	1 to 2	-534	**-26**	-81	-223	-146
	2 to 3	-222	7	-23	**-83**	**-82**
	3 to 4	**-29**	17	**-10**	9	-6
	4 to 5	15	-7	11	21	23
	5 to 6	15	-1	24	23	26

Table 3.11 Estimates with 95% confidence intervals in parentheses, for mean, variance, and weight parameters, for one-component to four-component mixture models of H3N2 titers plotted in Figure 3.14 and 3.15.

Number of normal components		ALL SITES (N = 19785)	HUE (N = 4519)	KHANH HOA (N = 5384)	HCMC (N = 5784)	DAK-LAK (N = 4134)
1	w_0	0.055	0.066	0.054	0.065	0.028
	w_1	0.945	0.934	0.946	0.935	0.972
	μ_1	4.483 (4.472 – 4.495)	4.459 (4.415 – 4.500)	4.434 (4.398 – 4.468)	4.693 (4.655 – 4.600)	4.292 (4.250 – 4.335)
	σ_1	1.491 (1.483 - 1.499)	1.476 (1.445 - 1.507)	1.467 (1.441 - 1.493)	1.587 (1.560 - 1.615)	1.378 (1.347 - 1.410)
2	w_0	0.055	0.066	0.054	0.065	0.028
	w_1	0.827 (0.817 - 0.837)	0.814 (0.615 - 0.840)	0.485 (0.340 - 0.785)	0.813 (0.762 - 0.833)	0.888 (0.778 - 0.910)
	μ_1	4.140 (4.115 - 4.167)	4.110 (3.880 - 4.190)	3.604 (3.400 - 4.100)	4.315 (4.200 - 4.385)	4.050 (3.910 - 4.120)
	σ_1	1.219 (1.207 - 1.230)	1.198 (1.120 - 1.235)	1.056 (0.980 - 1.190)	1.301 (1.250 - 1.337)	1.150 (1.095 - 1.180)
	w_2	0.118 (0.110 - 0.128)	0.120 (0.095 - 0.320)	0.461 (0.180 - 0.595)	0.122 (0.104 - 0.170)	0.083 (0.065 - 0.195)
	μ_2	6.890 (6.820 - 6.940)	6.841 (5.600 - 7.020)	5.310 (4.950 - 6.240)	7.137 (6.800 - 7.220)	7.016 (5.800 - 7.420)
	σ_2	0.845 (0.810 - 0.905)	0.884 (0.795 - 1.470)	1.334 (1.030 - 1.420)	0.729 (0.640 - 1.040)	1.009 (0.082 - 1.550)
3	w_0	0.055	0.066	0.054	0.065	0.028
	w_1	0.287 (0.270 - 0.303)	0.279 (0.235 - 0.333)	0.405 (0.330 - 0.475)	0.332 (0.278 - 0.410)	0.186 (0.152 - 0.230)
	μ_1	3.003 (2.940 - 3.060)	2.983 (2.800 - 3.185)	3.226 (3.070 - 3.390)	3.267 (3.070 - 3.480)	2.581 (2.420 - 2.770)
	σ_1	0.795 (0.770 - 0.820)	0.775 (0.690 - 0.870)	0.873 (0.810 - 0.945)	0.909 (0.833 - 1.000)	0.613 (0.555 - 0.700)
	w_2	0.225 (0.208 - 0.243)	0.211 (0.160 - 0.263)	0.136 (0.117 - 0.148)	0.153 (0.117 - 0.148)	0.412 (0.357 - 0.480)
	μ_2	4.415 (4.390 - 4.437)	4.400 (4.335 - 4.437)	4.540 (4.490 - 4.585)	4.657 (4.570 - 4.705)	4.168 (4.120 - 4.225)
	σ_2	0.497 (0.478 - 0.520)	0.386 (0.318 - 0.465)	0.386 (0.355 - 0.413)	0.447 (0.390 - 0.530)	0.592 (0.539 - 0.672)
	w_3	0.434 (0.410 - 0.458)	0.443 (0.525 - 0.458)	0.404 (0.350 - 0.480)	0.450 (0.412 - 0.488)	0.374 (0.340 - 0.482)
	μ_3	5.508 (5.420 - 5.596)	5.428 (5.100 - 5.466)	5.607 (5.350 - 5.780)	5.768 (5.430 - 5.913)	5.301 (4.990 - 5.400)
	σ_3	1.371 (1.332 - 1.410)	1.381 (1.482 - 1.410)	1.166 (1.085 - 1.280)	1.409 (1.340 - 1.520)	1.426 (1.410 - 1.500)
4	w_0	0.055	0.066	0.054	0.065	0.028
	w_1	0.008 (0.007 - 0.010)	0.231 (0.378 - 0.295)	0.004 (0.004 - 0.009)	0.018 (0.010 - 0.030)	0.020 (0.001 - 0.042)
	μ_1	1.311 (1.263 - 1.370)	2.803 (2.640 - 3.060)	1.100 (1.082 - 1.300)	1.524 (1.370 - 1.690)	1.505 (1.050 - 1.850)
	σ_1	0.181 (0.215 - 1.158)	0.693 (0.610 - 0.820)	0.001 (0.001 - 0.170)	0.283 (0.207 - 0.370)	0.277 (0.110 - 0.430)
	w_2	0.233 (0.215 - 0.252)	0.042 (0.012 - 0.053)	0.313 (0.305 - 0.405)	0.256 (0.010 - 0.030)	0.186 (0.110 - 0.220)
	μ_2	2.844 (2.780 - 2.910)	3.618 (3.540 - 3.740)	3.118 (2.990 - 3.320)	3.081(2.880 - 3.280)	2.504 (2.240 - 2.650)
	σ_2	0.646 (0.614 - 0.700)	0.158 (0.015 - 0.230)	0.793 (0.695 - 0.850)	0.671 (0.560 - 0.790)	0.593 (0.540 - 0.665)
	w_3	0.308 (0.287 - 0.320)	0.225 (0.160 - 0.305)	0.114 (0.107 - 0.265)	0.274 (0.195 - 0.340)	0.453 (0.370 - 0.630)
	μ_3	4.332 (4.298 - 4.367)	4.418 (4.332 - 4.438)	4.515 (4.445 - 4.600)	4.563 (4.448 - 4.660)	4.141 (4.030 - 4.412)
	σ_3	0.572 (0.543 - 0.610)	0.341 (0.320 - 0.373)	0.359 (0.330 - 0.540)	0.563 (0.477 - 0.765)	0.682 (0.580 - 0.860)
	w_4	0.397 (0.378 - 0.402)	0.436 (0.410 - 0.505)	0.514 (0.370 - 0.560)	0.387 (0.280 - 0.480)	0.333 (0.265 - 0.460)
	μ_4	5.634 (5.615 - 5.700)	5.484 (5.250 - 5.535)	5.256 (5.120 - 5.680)	6.006 (5.448 - 6.530)	5.422 (5.120 - 5.780
	σ_4	1.328 (1.303 - 1.321)	1.361 (1.285 - 1.440)	1.324 (0.890 - 1.420)	1.300 (1.020 - 1.510)	1.422 (1.210 - 1.580)

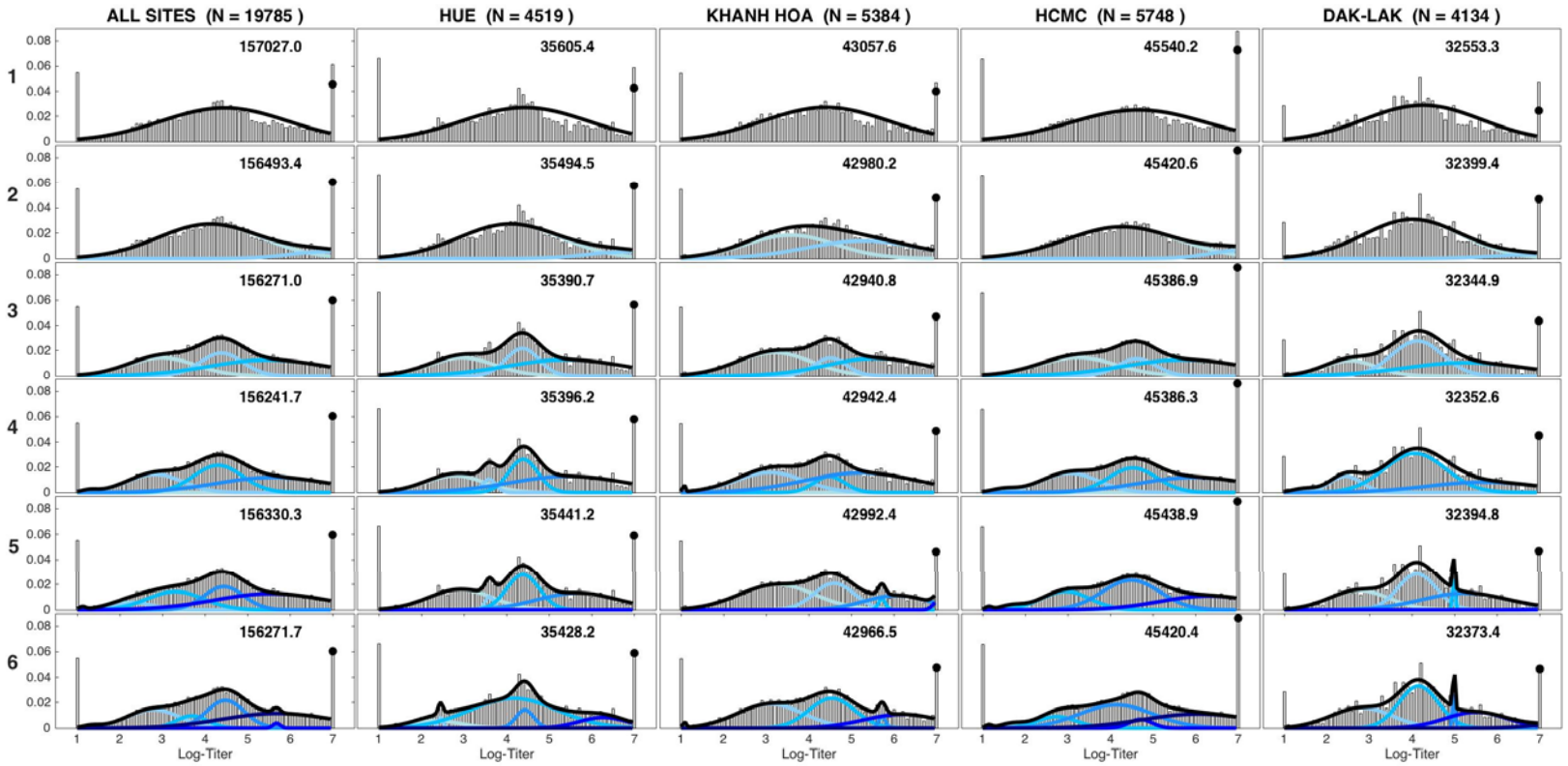

Figure 3.14 Model fits for titer distributions against H3N2 grouped by different collection sites. Histograms of antibody titers to H3N2 (GMT of 2009 and 2011 strains), showing fit results for mixture models with different number of normal components (top to bottom, the label to the left of the *y*-axis is the number of mixture components) and grouped by collection sites (left to right). Histograms are weighted to adjust for age and gender according to the Vietnam national housing census in 2009 for each of the four collection sites. The blue lines in each panel are the normalized probability density functions of the component distributions whose intensity was ranked in order of increasing μ. The black lines show the full mixture distribution density, and the black dots are the estimated cumulative distribution of the mixture models at 7.0 (titer of 1280). The numbers in the upper right corner of each panel are the BIC scores of the model fits.

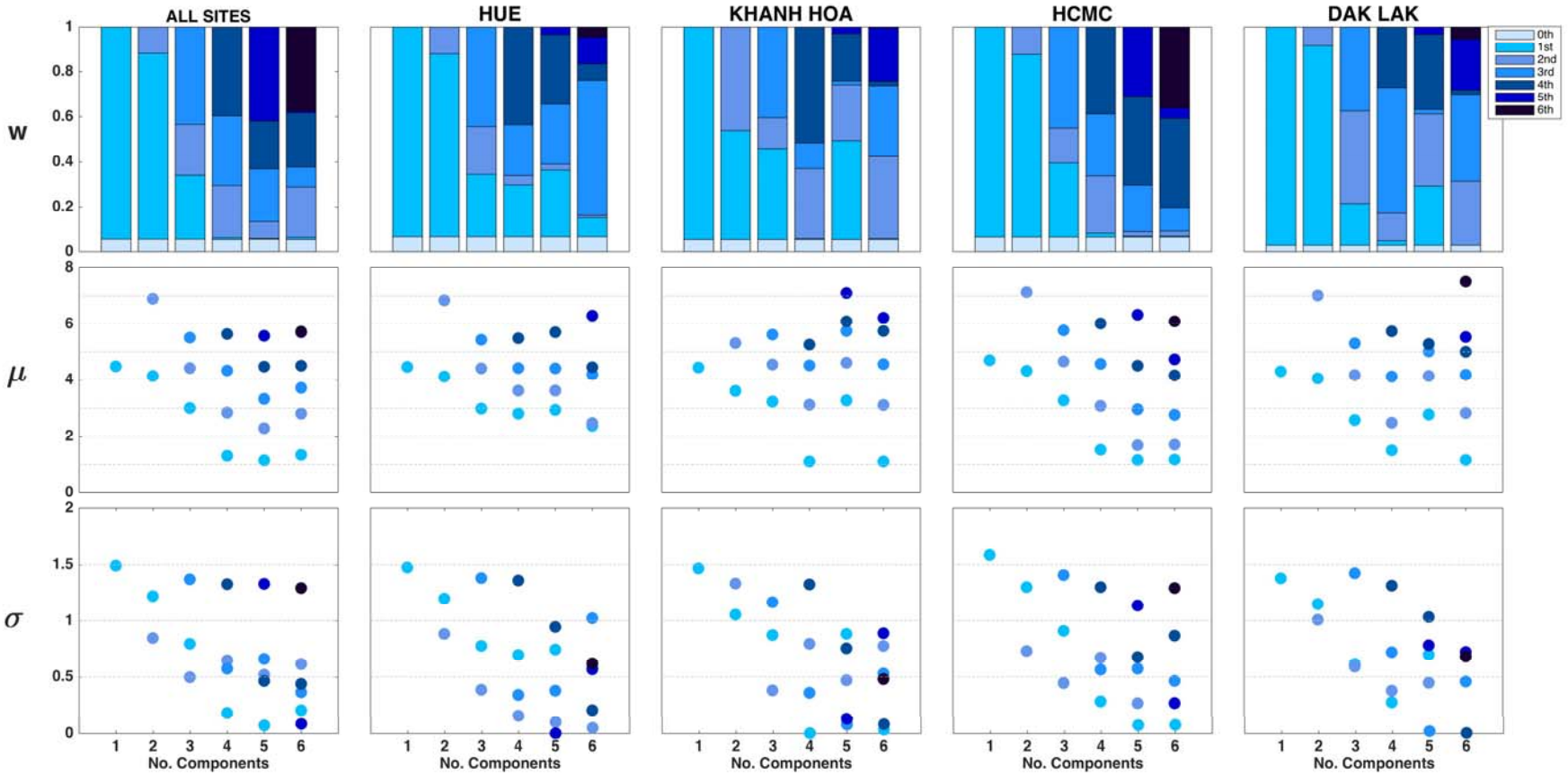

Figure 3.15 Visualization of model selection process for H3N2 titer distributions from Figure 3.14. The *y*-axes show the fitted values of w_i (mixture weights), μ_i(means), and σ_i (standard deviations). Components' shades were ranked from lightest to darkest in increasing order of μ. In the top panel, the "0th component" represents the point mass w_0 placed at 20 for titers below the lower detection limit of 20. Note that for five or six components, in many cases, the weights or standard deviation parameters are close to zero; for some cases, two of the inferred mean parameters are very close to each other.

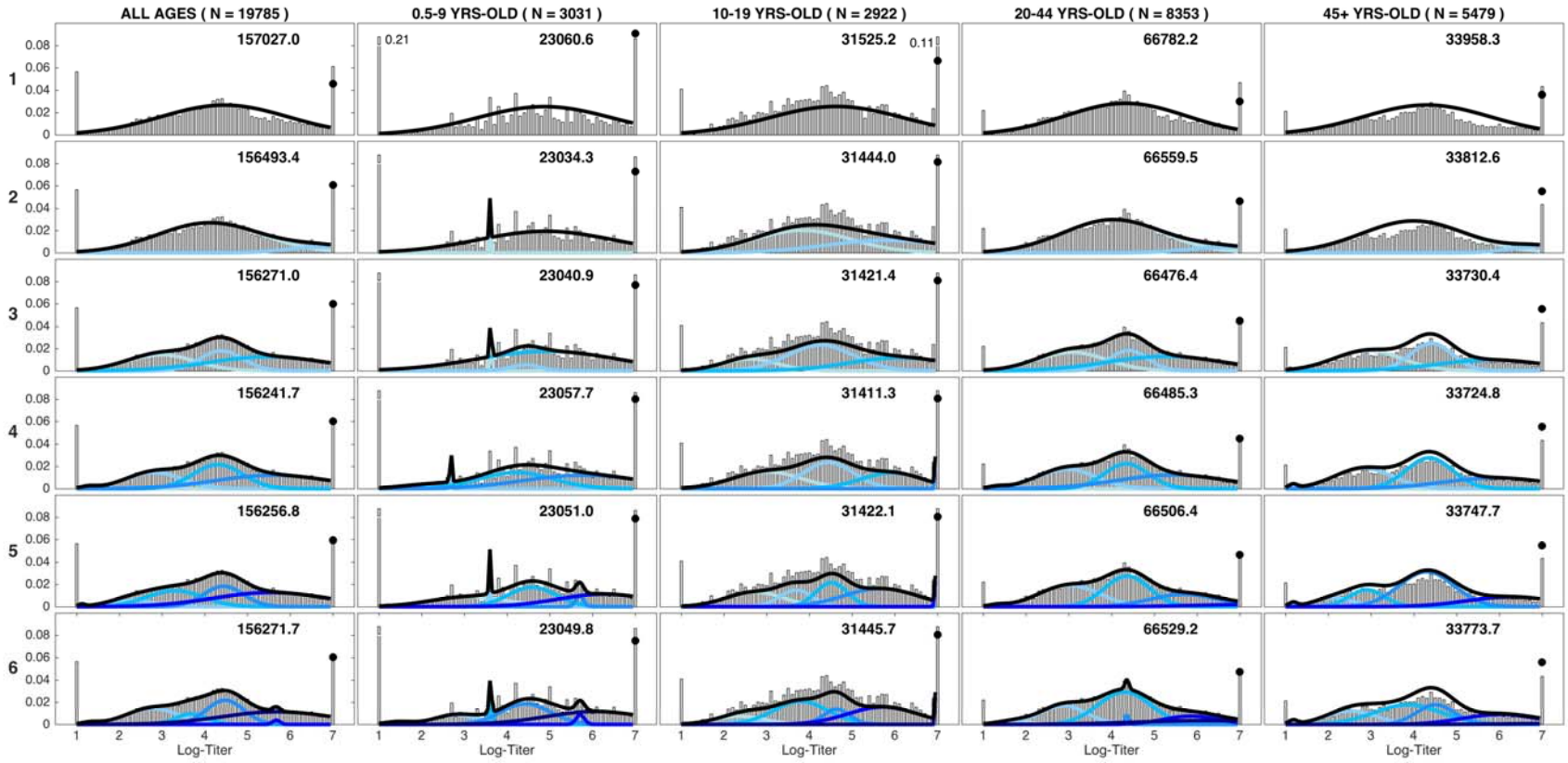

Figure 3.16 Model fits for titer distributions against H3N2 grouped by different age groups. Titer histograms for H3N2 and fit results for mixture models with different number of components (label on the left is the number of mixture components) and grouped by different age groups. Histograms are weighted to adjust for age and gender according to the Vietnam national housing census in 2009. The numbers in the upper right corner of each panel are the fitted BIC scores of the respective model. For each panel, the blue lines are the normalized probability density of the component distributions whose intensity from lightest to darkest was ranked in order of increasing μ. Black lines are the total mixture distribution density; and the black dots are estimated probability weight of the mixture model for titers ≥ 7.0.

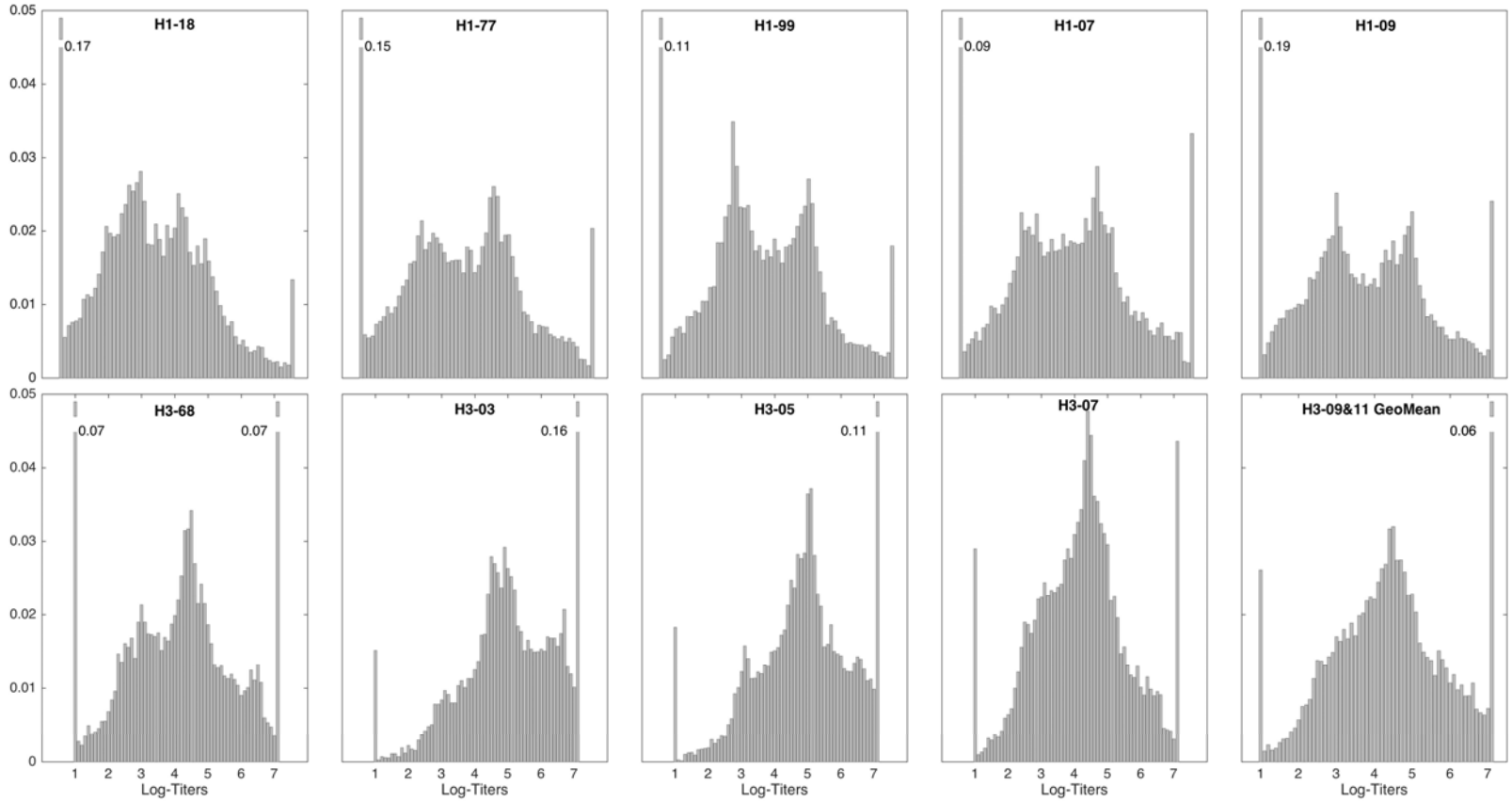

Figure 3.17 Antibody titer histograms against all H1N1 and H3N2 strains on the protein microarrays. Showing results for n = 20,152 individuals, plotted for H1N1 strains (top panels) and H3N2 strains (bottom panels). The fractions of individuals with titers below the detection limit of 20 and above 1280 that were out of the plotting ranges are given next to the respective bar. Histograms were weighted to adjust for age and gender according to the Vietnam national housing census in 2009 for the four collection sites.

3.4.7 ROC for the four-component mixture model for H1-09

An ROC curve constructed using the methods in te Beest et al. (2014a) (Figure 3.18) shows that the model-assigned titer groups provide a high degree of discrimination for identifying recently infected individuals. A titer cut-off is determined to have a particular sensitivity and specificity based on how well it sorts individuals into the different mixture components, with the fourth component representing positivity. In the left panel, the mixture distribution for all sites is used. The titers indicated on the curve show, from left to right, 99% specificity, 95% specificity, 90% sensitivity, 95% sensitivity, and 99% sensitivity. In the right panel, mixture distributions for individual sites are used. The indicated titers show 90% sensitivity and 95% sensitivity. The performance of each titer cut-off in this ROC curve entirely depends on the location of that cut-off in the overlapping regions between the third and fourth components. Even though this ROC was computed using the same approach as te Beest et al. (2014a), it is not an appropriate approach without knowing the true infection status of each individual.

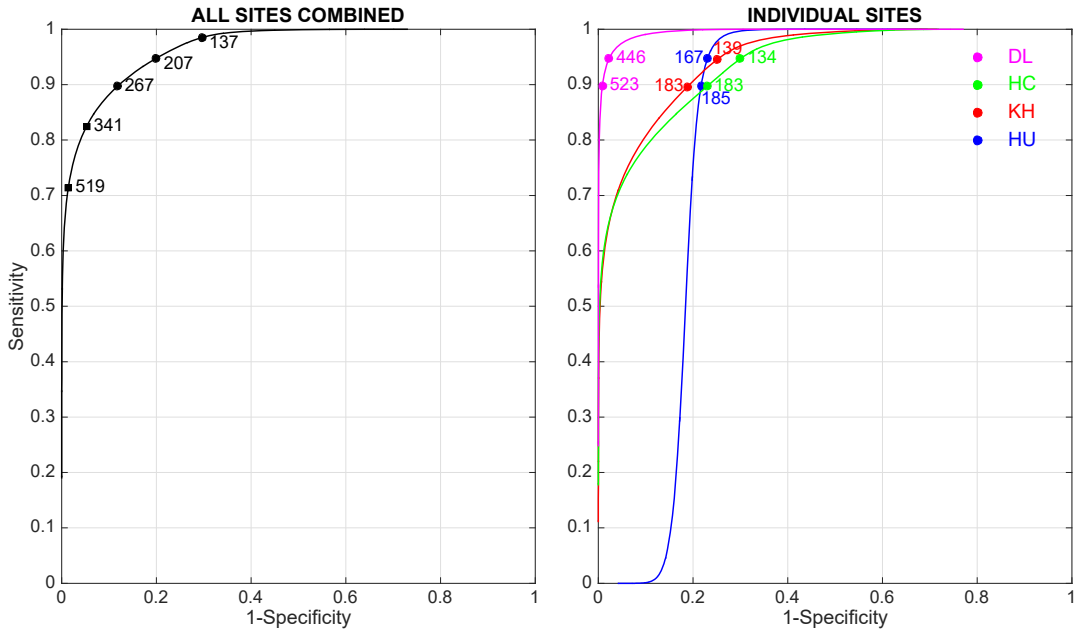

Figure 3.18 ROC curves for H1N1 using four mixture components for aggregated data (left) and individual sites (right). Different colors are for different collection sites. **Left:** Numbers show titer cut-offs corresponding to 99% and 95% specificity, and 90%, 95%, and 99% sensitivity (left to right). **Right:** Numbers show titer cut-offs corresponding to 90% and 95% sensitivity for each collection site.

3.5 Discussion

Using a large collection of serum samples and continuous measurements of antibody titers, we were able to describe the natural distribution of antibody titers to the 2009 H1N1 and H3N2 subtypes of influenza virus. As there is almost no influenza vaccination in Vietnam and as influenza in Vietnam is characterized by a combination of local persistence and annual/biannual outbreaks (Nguyen et al. 2013; Le et al. 2013, Lam et al. 2017), characterization of titer distribution in this context is a useful general approach for looking at the immune status of a population at quasi-equilibrium with an endemic infectious disease. With a mixture model approach, we were able to identify the presence of multiple exposure groups in the population according to their titers. Our interpretation of these multiple exposure groups –

according to titers measured for confirmed cases (Todd 2016; Huijskens et al. 2013) and past measurements of the rate of antibody waning (Ng et al. 2013; Horsfall and Richard 1941) – is that they represent recently infected individuals, historically (i.e. non-recently) infected individuals, and naïve individuals. Note that for influenza, a naïve individual is one who has not been exposed to the currently circulating strain, which means that there will be naïve individuals in all age groups.

This study used an atypical seroepidemiological design as the samples were collected continuously, and not specifically in a post-epidemic or post-pandemic scenario. In addition, the serum samples were collected in the tropics where continuous circulation of influenza virus is believed to occur (Le et al. 2013; Viboud, Alonso, and Simonsen 2006; Alonso et al. 2007; Nelson et al. 2014; Cheng et al. 2013) and where populations are much less likely to be vaccinated for influenza (less than 0.8% annual coverage for Vietnam). Therefore, the present data set is the first to show the natural distribution of influenza antibody titers in a human population.

One useful application of these results in future serological studies is to encourage, by default, the inclusion of multiple serological states in the data analysis phase, which may result in a more informative classification of antibody titer than a separation into seropositive and seronegative. The classification proposed here uses antibody levels as proxies for recency of infection, and if correct, this should allow for a more informative reconstruction of the population's epidemic history. In general, knowing the IgG antibody waning rate is essential for interpreting the titers measured in serological cross-sections (Vinh and Boni 2015; Wu et al. 2014), and using waning rates to estimate the time of past infection has already been attempted

for some infectious diseases (de Melker et al. 2006; Simonsen et al. 2009; Teunis et al. 2012; Borremans et al. 2016), but not for influenza virus. Longitudinal follow-up studies that are able to provide accurate estimates of antibody waning rates are crucial for this type of analysis, but they are rare (Todd 2016; Horsfall and Richard 1941; Versteegh et al. 2005; Strid et al. 2001).

Two major limitations of serological classification systems will need to be better understood. First, a mixture distribution approach does not guarantee that individuals can be easily classified into one of several titer subgroups. With substantial overlap in some mixture components, individuals can have approximately equal probabilities of belonging to two or three different titer categories. In addition, individual variation will have a large effect on titer interpretations. A high-titer sample could represent a recent infection, but individuals can maintain high titers longer than the mean duration observed in clinical studies. This would normally, but not exclusively, be observed in children. Likewise, lower antibody titers (in the 200–250 range) could indicate historical past infection, a low response to a recent infection (Strid et al. 2001), or a recent but mild infection. With serological data alone, these scenarios cannot be distinguished. For subtype H3N2 specifically, low titer levels could indicate cross-reactions between antibodies generated to an older influenza variant than the recent H3N2 HA1 proteins spotted on the protein microarray.

Second, a major challenge in influenza seroepidemiology is that it is difficult to take into account the effects of original antigen sin (Lessler et al. 2012; de St.Groth and Webster 1966) or age-dependent seroconversion (ADS) (Versteegh et al. 2005).

Age-dependent seroconversion is distinct from original antigenic sin in that ADS assumes that individuals of different ages seroconvert to different titer levels irrespective of the individual's infection history. In principle, the effect of ADS should be detectable for 2009 H1N1 infections in individuals younger than 50, as for these individuals an exposure to the 2009 virus would have been a first exposure. However, the mixture component means (μ_i parameters) and the component weights (w_i) are not separately identifiable in the mixture model. Thus, I cannot state that the 'recently infected' titer subgroups are comparable across age groups, as the inferential process will make the exact definition of recency different for the 10-19 age group than for the 20-44 age group. Even if I were to assume that the fourth mixture components should be comparable across age groups, the titer means denoted by μ_4 in Figure 3.12 do differ but are within one standard deviation of one another. Thus, there is a lack of evidence for ADS in this titer data. As I only considered recent antigens in this analysis, effects of original antigenic sin were not able to be investigated.

The next critical step in this analysis will be using titer data from follow-up on confirmed cases to determine if the natural distribution of antibody titers should conform to the recent, historical, and naïve categories as presented here. If antibody waning rates can be measured with a high degree of precision, these may allow for a detailed description of individuals' recency of infection and possibly a reconstruction of past epidemic history in human populations. Large-scale serological studies like the one presented here are labor-intensive and slow to generate results. Nevertheless, the long follow-up, the large sample size, and the diligence put in to

obtain precision in titer measurements will be worth it if seroepidemiology can be pushed forward to maximize the amount of biological information that can be extracted from population-level serology studies.

CHAPTER 4

4 Serological Dynamics For 2009 H1N1 Using Mixture Components

4.1 Background

The analysis of the population-level antibody titer distributions in Chapter 3 allows for the defining of categories for individuals' serological states. If the observed categories do indeed correspond to the population's true stationary structure, I can describe and analyze the dynamics of various serological states in the population by looking at the stationary structure at different points in time. In this chapter, I use the mixture model techniques from Chapter 3 to determine if the dynamics of serological states can be used in a meaningful way to describe the population epidemic history. Two reconstruction methods were tried, one using a time series of mixture components' weight, and another using a dynamical model with free incidence parameters and likelihood inference (Chapter 5).

In general, epidemic histories of a given population can be described if the population in question operates an infectious disease surveillance system. All of the world's current influenza surveillance relies on weekly or monthly reports of symptomatic influenza-like illness (ILI) cases, a fraction of which are confirmed as

positive or negative for influenza virus, resulting in a time series of confirmed influenza cases in a particular country or region. Two shortcomings of this surveillance design are that (*i*) two locations cannot be compared if it is not known what proportion of the population would report to the surveillance network for a standard case of ILI, and (*ii*) it fails to capture sub-clinical and asymptomatic cases of influenza, which means the system is poor at distinguishing between epidemics that differ in severity (mild and severe cases).

One solution to these two shortcomings of traditional surveillance is to use serological rather than syndromic surveillance to describe a seasonal influenza epidemic. Serological data use antibody measurements as a proxy to determine recent infection of a given virus regardless of presence/absence of symptoms. An antibody titer does not tell us how long ago an individual was infected, unless we apply the knowledge from antibody waning dynamics or the interpretations from Chapter 3 that higher titers correspond to more recent infections. Even though cross-sectional seroepidemiology was designed to reconstruct the disease dynamics of a population of interest, a single population cross-section can be only used to estimate an epidemic attack rate that depends heavily on the identification of the baseline activity before the epidemic. Multiple cross-sections are frequently taken in cohort studies (for several influenza seasons) but this is very rarely done for general-population samples. Some of the cohort designs available in the literature normally take one cross-sectional sample per year, meaning that the analysis of these data simply results in multiple attack rates for multiple influenza epidemics. As a practical matter, it would be expensive and potentially intrusive to take frequent blood

samples from a cohort during an influenza epidemic. When using general-population sampling, this becomes less expensive and more ethical, but still very few studies have presented analyses of multiple serological cross-sections taken from the general population.

Using the interpretations of recent infection and non-recent infection proposed in Chapter 3, I present here the dynamics, though time, of the weights of these mixture components. The number of free parameters in the mixture time series is reduced by fixing various components' means and standard deviations. If the w_4 parameters represent recent infections (as hypothesized in Chapter 3), then we should be able to use them as a proxy to reconstruct influenza epidemics in southern Vietnam. These results are presented in this chapter and compared to the known epidemic timings of influenza activity obtained from Vietnam's National Influenza Surveillance System (Nguyen et al. 2009; Nguyen et al. 2013). Do the w_4 parameters form a smooth or a noisy time series? Does this time series appear to have an 'epidemic shape' or a shape that looks like waves of post-epidemic immunity? All of these questions will be answered descriptively, with basic graphical and statistical methods in this chapter.

Two of the best comparisons with this work using influenza serological time series are the ones by te Beest et al. (2014a) and Zhao et al. (2017), which applied mixture models to estimate the infection attack rate (IAR) during the first wave of H1N1 Pdm 2009 in the Netherlands and Singapore, respectively. With cross-sectional serological data at only two time points, the work by te Beest et al. (2014a) did not look beyond three categorical states and relied heavily on the pre-pandemic samples

to estimate the amount of prior-immunity in the 45+ year-old group. Recently, Zhao et al. (2017) applied a two-component mixture distribution model to a relatively small number of serological data collected from adult cohort and challenged the traditional application of a single titer threshold.

4.2 Data

4.2.1 Serological data

The serum samples used in this chapter are the same as those from Chapter 3, and they are stratified by the same collection sites as before (Section 3.2). Bimonthly time windows were chosen as the study design specified 200 samples every two months from each of the hospitals. The sites' compliance with this sampling protocol was not ideal; and most of the samples were collected within one or two weeks before the cut-off time (Figure 5.1). Stratifying data into time windows of less than two months yielded insufficient sample size for the mixture models. With sample collection starting in July 2009 for Hue (n = 4390), Khanh Hoa (n = 5053), and Dak Lak (n = 5753), and January 2010 for Ho Chi Minh City (n = 4139), and ending in December 2013 for all sites, each site had between 24 and 28 time windows. Again, serological data were adjusted to the age and gender distribution of their respective provinces using the Vietnam Population and Housing Census 2009 (Section 3.4.1).

4.2.2 Sentinel data

Vietnam sentinel data on influenza are collected at 15 sentinel hospitals that participate in the national influenza surveillance network (Nguyen et al. 2009; Nguyen et al. 2013). The most recent visualization of these data can be seen in Thai

(2014) (reproduced in Figure 1.1). These sentinel data will be used as an independent comparator to the sero-dynamics inferred in this chapter and Chapter 5. Each hospital reports weekly counts of influenza-like illness (ILI) – defined as a combination of body temperature ≥38°C and cough/sore throat within three days of symptom onsets. The first ten ILI cases were swabbed every week for further molecular analysis against influenza A and B to determine positivity. Influenza A positive specimens were then subtyped for H1, H3, and H5. For each hospital or region, an "ILI positive" (ILI+) measure was computed by multiplying a detrended version of the number of ILI cases by the percent positive for influenza virus (see Thai (2014) for full details). The sentinel data were presented in the form of monthly or bimonthly ILI+ cases. ILI+ data from Da Nang (used to compared against Hue), Dak Lak, and Khanh Hoa from July 2009 until December 2013 were used to compare against their respective cities from our SSE data. An evenly weighted sum of four hospitals in southern Vietnam was used as the ILI+ signal for comparisons with Ho Chi Minh City (this chapter) and Kien Giang (Chapter 5). A geographically weighted sum (6 hospitals) was used as the aggregate ILI+ signal for all of southern and central Vietnam.

4.3 Methods

4.3.1 Fixing parameters in mixture fits

Every two months starting from July 2009 to December 2013, a mixture fit with four components was performed to determine the proportion of individuals falling into the third and fourth mixture categories – w_3 and w_4 – (the second highest

and highest titer groups, respectively). In Chapter 3, these quantities were interpreted as the proportion of historically and recently infected individuals. Since it is impossible at this stage to verify the hypothesis that there was an unobserved fourth peak for the H3N2 model fit, only H1N1 titers were analyzed in this chapter.

In Chapter 3, the mean and variance parameters of the mixture components were allowed to be completely free (Figure 3.7). I started the analysis with the four-component model for H1N1 Pdm 2009 from the aggregated data (n = 20,152) to obtain the component's means μ_1 to μ_4, standard deviations σ_1 to σ_4, and weights w_0 to w_4, for the site-aggregated data and each of the four collection sites individually. The reasons for keeping some parameters fixed and allowing others to vary was to avoid time series patterns that fluctuate too much (scenario *iv* below) while also avoiding imposing too much underlying structure onto the time series (scenario *iii* below). Four fitting scenarios were attempted:

i. Keeping the components' means (μ_1 to μ_4) for individual sites at each time window the same as the respective components' means from the aggregated data. Assumption: If the four titer categories are really associated with the four proposed exposure statuses, the titer means of each sub-group should stay the same over time as in the population-level distribution. Allowing the variances to vary from time to time allowed us to account for the sampling variations between different collections.

ii. Keeping the components' standard deviations (σ_1 to σ_4) for individual sites at each time window the same as the respective components' standard deviations from the aggregated data. Assumption: The components' variation representing observation errors associated with each titer groups should be the same over time as in the population-level distribution; any time-to-time variation should be captured by the flexible components' means.

iii. Keeping the components' standard deviations and means (μ_1 to μ_4 and σ_1 to σ_4) for individual sites at each time windows the same as the respective components' standard deviations and means from the aggregated data. Assumption: if there exists such a general population structure to the titer distribution, that distribution should be the same across sites and over time.

iv. Optimizing all parameters for each collection site and time window without restriction. Assumption: the time-to-time titer distributions retain the four-component structure, but all parameters are allowed to vary freely.

I studied all four scenarios and computed the BIC for each of them (Figure 4.1).

4.3.2 Comparison of w_4 and $w_4 + w_3$ time series to monthly ILI+ cases from sentinel data

There are two quantities of interests: w_4 and $w_3 + w_4$. With the proposed interpretations, we want to validate the time series of w_4 against the number of ILI+ cases and the $w_3 + w_4$ time series against cumulative ILI+ cases from the sentinel data. Pertaining to the interpretations from Chapter 3, time series w_4 represents the seroincidence, and time series w_3+w_4 represents the cumulative seroincidence – or seroprevalence.

First, the time series of $w_3 + w_4$ and w_4 were studied for bimonthly periods from July 1, 2009 until Dec 31, 2013 for the four-fitting scenarios presented in Section 4.3.1. Before comparing these to the dynamics of influenza virus as seen in Vietnam's national influenza sentinel program, the w_4 time series needs to be transformed into a time series that more closely resembles a seroincidence time series. An individual who has an influenza antibody titer in the highest titer subgroup

(μ_4=671.1 (95% CI 484.7–818.6)) is likely to have been infected in the past m months, where m probably ranges between 3 and 12. The data in Todd (2016) only extend out to seven months, but the data in Horsfall, Hahn, and Rickard (1940), and Horsfall and Richard (1941) showed a predictable decline of antibody titer over 12 months. In this analysis, different values of m from 3, 6, 9, and 12 months were studied.

The bimonthly w_4 time series was first broken down into monthly time series by assuming equal monthly contributions. The period from July 1, 2009 to Dec 31, 2013 generated 54-monthly data points of $w_{4,i}$ with $7 \leq i \leq 60$ (for convenience, the time index starts from 7 denoting July 1st, 2009). I then "back-mapped" these time series by m months to transform monthly w_4 (proportion of recently infected individuals) into m monthly seroincidences y_t distributed evenly over the past m months. This mapping did not go back any further than Jun 1, 2009 as the first case of H1N1 Pdm 2009 was reported on May 31, 2009 in Vietnam (Hien et al. 2010). In order to handle the case at the boundary appropriately, every seroincidence y_t can be written as

$$y_t = \begin{cases} \sum_{i=t+1}^{5+m} \frac{w_{4,i}}{i-6} + \sum_{i=6+m}^{t+m} \frac{w_{4,i}}{m} & for \;\; 6 \leq t < 5+m \\ \sum_{i=t+1}^{t+m} \frac{w_{4,i}}{m} & for \;\; 5+m \leq t < 61-m \\ \sum_{i=t+1}^{59} \frac{w_{4,i}}{m} & for \;\; 61-m \leq t \leq 59 \end{cases}$$

in which $6 \leq t \leq 59$ represents the period from July 1, 2009 until December 31, 2013. The time series y_t was then comparable to the sentinel incidence time series.

In order to further explore the data, a second picture of seroincidence was drawn with the $w_3 + w_4$ time series assuming that $w_3 + w_4$ should represent all individuals that were infected with the 2009 H1N1 pandemic virus. Adding together these two weight parameters should give a summary statistic for seropositivity, and the resulting time series should look like a seroprevalence curve. In this analysis the seroprevalence time series z_t was made by (*1*) redistributing each weight $w_{4,t}$ back over the past m months (m ranging between 3 and 12 months), and (*2*) redistributing each weight $w_{3,t}$ back over the past k months (k ranging between 12-18 months).

4.3.3 Comparison of $w_3 + w_4$ time series to the cumulative ILI+ cases from sentinel data

In this analysis, there is no back-mapping. The bimonthly time series of $w_4 + w_3$ was simply plotted against the cumulative ILI+ incidence. The Spearman's correlations and p-values were computed.

4.4 Results

4.4.1 BIC comparison among the four fitting scenarios

When re-performing the mixture fits from Chapter 3, fixing either the means or variances or both, the general patterns on titer distribution structure remain relatively unchanged. Figure 4.1 shows results of the four fitting scenarios (*i*) fixing μ_1 to μ_4 (*ii*) fixing σ_1 to σ_4 (*iii*) fixing μ_1 to μ_4 and σ_1 to σ_4 (*iv*) optimizing all parameters. All of the fits are very close to each other (regardless of what we fix) and this gives us confidence that the means and variances of the four titer groups are robust to a variety of assumptions. The mean log-titer of the highest titer group is

μ_4=671.1 (95% CI 484.7–818.6), and the mean log-titer of the second-highest titer group is μ_3=247.2 (95% CI 240.0–253.7) (For a complete table of all components' means, standard deviations, and weights and their confidence intervals, see Table 3.5).

Table 4.1 Change in BIC scores for four-component mixture model for four fitting scenarios. The corresponding estimated parameters were plotted in Figure 4.1. The values of the negative log-likelihood were weighted to adjust for age and gender according to the Vietnam national housing census in 2009. The first row shows the exact values of the negative log-likelihood for the free parameter fits. Bold numbers represent the mixtures with the best BIC.

		ALL SITES (N = 19335)	HUE (N = 4390)	KHANH HOA (N = 5053)	HCMC (N = 5753)	DAK-LAK (N = 4139)
SumNegLLH (Free Params)		70682.33	15619.08	18529.00	21241.85	15208.14
ΔBIC	Fixed μ_1 to μ_4		-21	-18	-27	-5
	Fixed σ_1 to σ_4		-31	-28	-30	-11
	Fixed μ_1 to μ_4 and σ_1 to σ_4		**-45**	**-43**	**-55**	**-29**

Table 4.1 shows that if the BIC again was used as the sole criterion for model selection, fixing both standard deviations and means (scenario *iii*) gave the best BIC. Among fixing only standard deviations and means, fixing standard deviations (scenario *ii*) was consistently better than fixing means (scenario *i*). My initial hypothesis was that fixing the components' means (scenario *i*) would make the most sense since the mean titer of a recently infected group should be a fixed quantity on biological grounds. In principle, the variance of each sub-component could vary from time window to time window due to sampling, but the mean titer of the recently infected group should stay the same. Previously published papers using the mixture distribution approach believed that fixing the standard deviation was the correct approach (Zhao et al. 2017) or that fixing both means and standard deviation was the

best approach (te Beest et al. 2014a). Some studies chose to assume equal variances for all components (McLachlan and Peel 2000). However, none of these studies provided statistical justification for their choice of models.

Figure 4.2 shows the fit results for time series w_4 from the four-component mixture fit broken up by collection site and bimonthly time window. This figure was assembled as a diagnostic to help determine which mixture components should be fixed during the fitting process. Visually, none of these gave a clear indication that fixing one set of parameters creates a "stable" or "expected" w_4 time series. In particular, the one-step auto-correlations should be positive, but this was not the case for all sub-analyses. The main noticeable feature in Figure 4.2 was an increase in w_4 from mid-2009 to early-2010 as a result of the first wave of H1N1 Pdm 2009 influenza (not able to be seen in Ho Chi Minh City, as sample collection started in Jan 2010). The year 2011 saw a low level of continuous transmission of 2009 H1N1 from sentinel data (Figure 1.1), but this was barely reflected (or not at all) in the late-2011 or early-2012 time series of w_4.

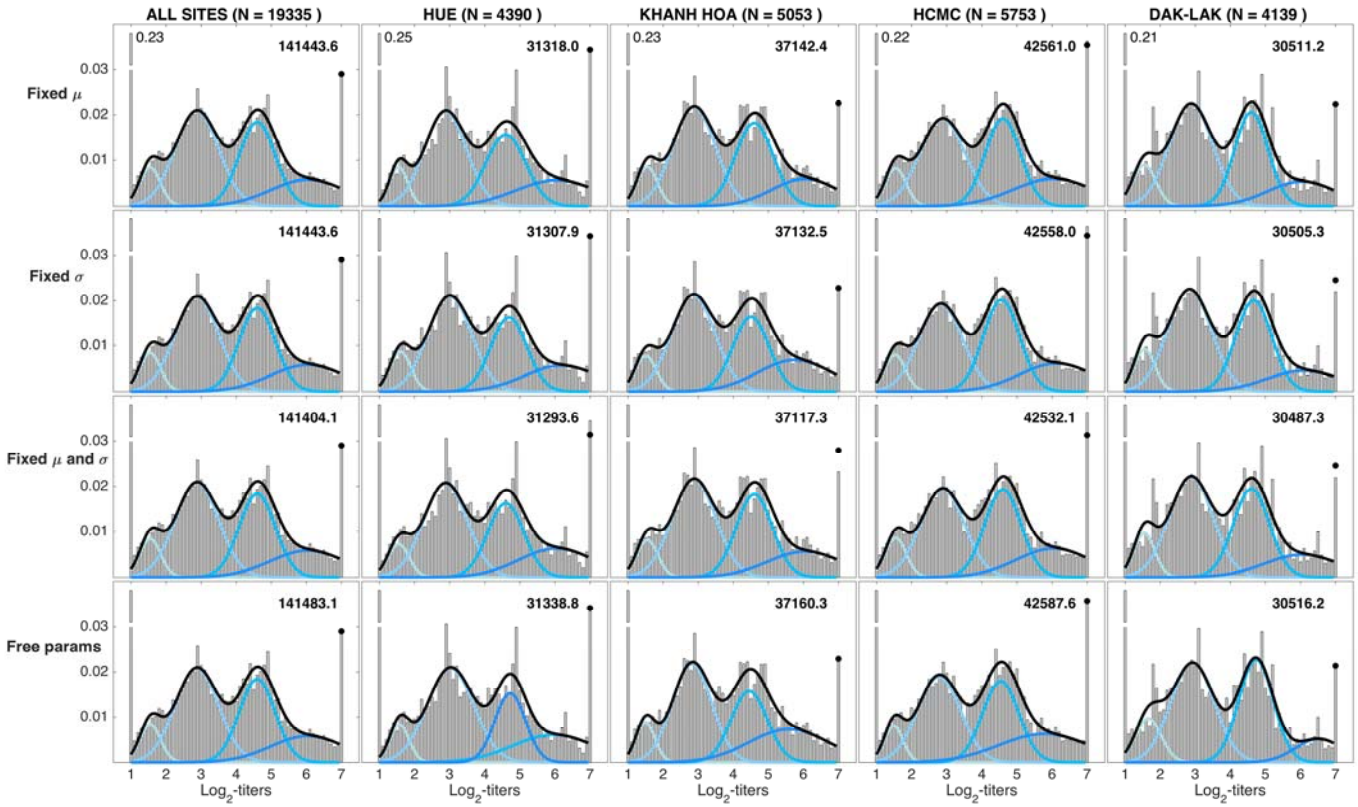

Figure 4.1 Model fits different fitting scenarios grouped by collection site. Titer histograms for H1-09, showing fit results for four-component mixture models for different fitting scenarios *i* to *iv* (in rows) grouped by collection sites (in columns). Histograms are weighted to adjust for age and gender according to the Vietnam national housing census in 2009 for each of the four collection sites. The blue lines in each panel are the normalized probability density functions of the component distributions with darker colors used for increasing μ. The black lines show the full mixture distribution density, and the black dots are the estimated cumulative distribution of the mixture models at 7.0 (titer of 1280). The numbers in the upper right corner of each panel are the BIC scores of the model fits. The fractions of individuals with titers below the detection limit of 20 and above 1280 that were out of the plotting ranges were given next to their respective bars.

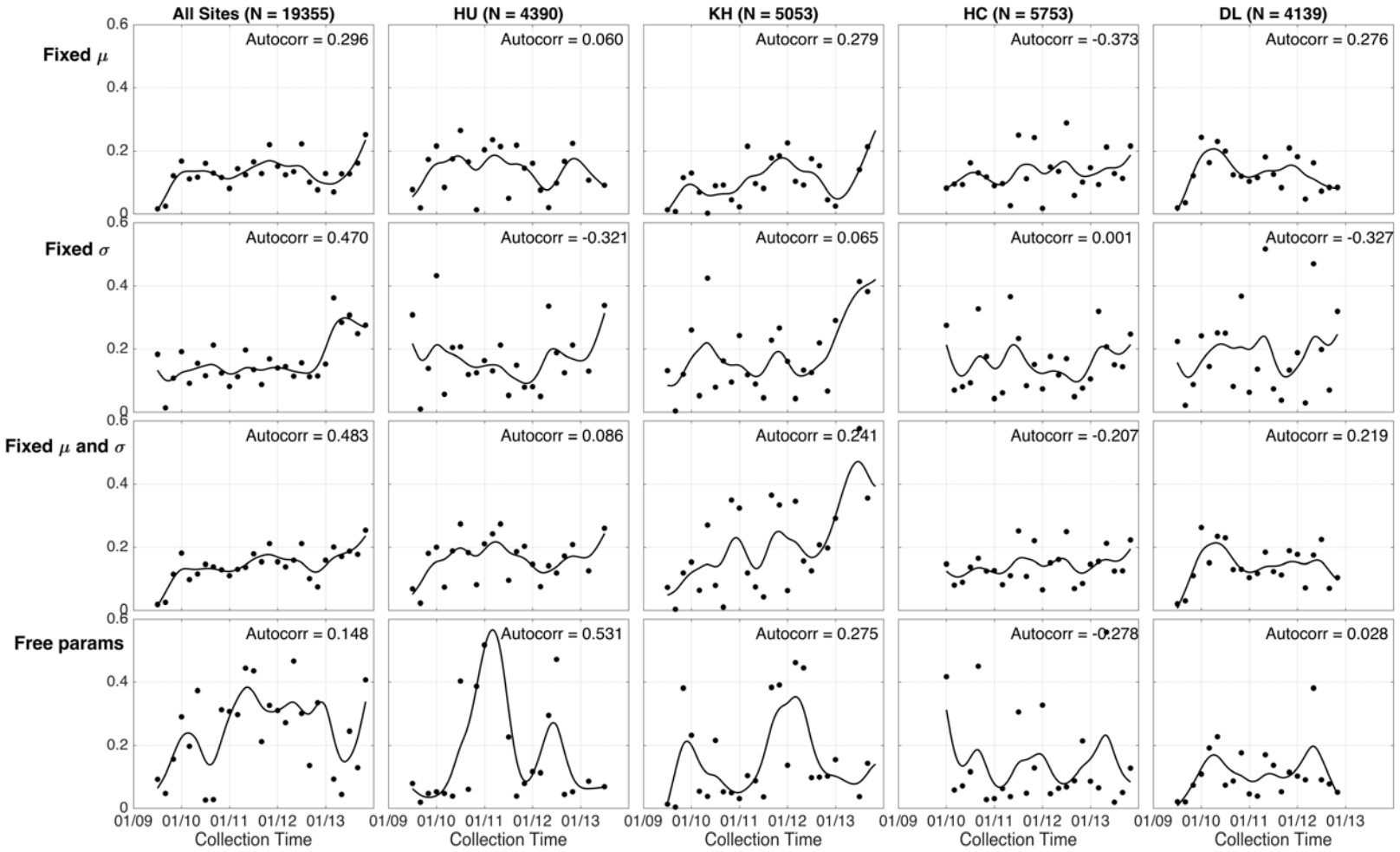

Figure 4.2 Bimonthly time series of w_4 for different fitting scenarios. Showing fit results for data grouped by collection site (in columns) for four different fitting scenarios (in rows). One-step temporal autocorrelation were shown in each panel. The smoothing parameter for the spline was 0.5.

4.4.2 Back-mapped time series of w_4 vs. monthly ILI+ cases from sentinel data

The results of mapping back time series w_4 by 3, 6, 9, and 12 months are shown in Figures 4.3 to 4.6, respectively. The Spearman's correlations (ρ) between the sentinel data and the back-mapped seroincidence are presented in Table 4.2. Visually, the seroincidence curves (black dots) did not line up with the hospital-reported incidence patterns (gray bars) in any sub-analyses. The fixed-means (scenario *i*) reconstruction gave the best correlation between the hospital-reported data and the back-mapped time series w_4 time series for most of the collection sites (except in HCMC). This result suggested that the initial hypothesis for fixing means might have been correct even though this approach did not give the best BIC. As discussed in Chapter 3, the application of BIC as the only criterion for model selection was imperfect as it failed to account for overfitting; therefore, the visual inspection of the components' means and standard deviations was introduced as additional an criterion. In this case, the fixed-means model seemed to be a better choice. Another noteworthy feature of these seroincidence reconstructions was the high seroincidence in all provinces during 2010 (and some of 2011) that was not reported in the sentinel data. As *m* increases, the seroincidence plots (black dots) appear more smoothed (Figures 4.3 to 4.6). Increasing values of *m* from 3 to 12 months increased the association between ILI+ incidence and seroincidence; nevertheless, none of the positive correlations was significant.

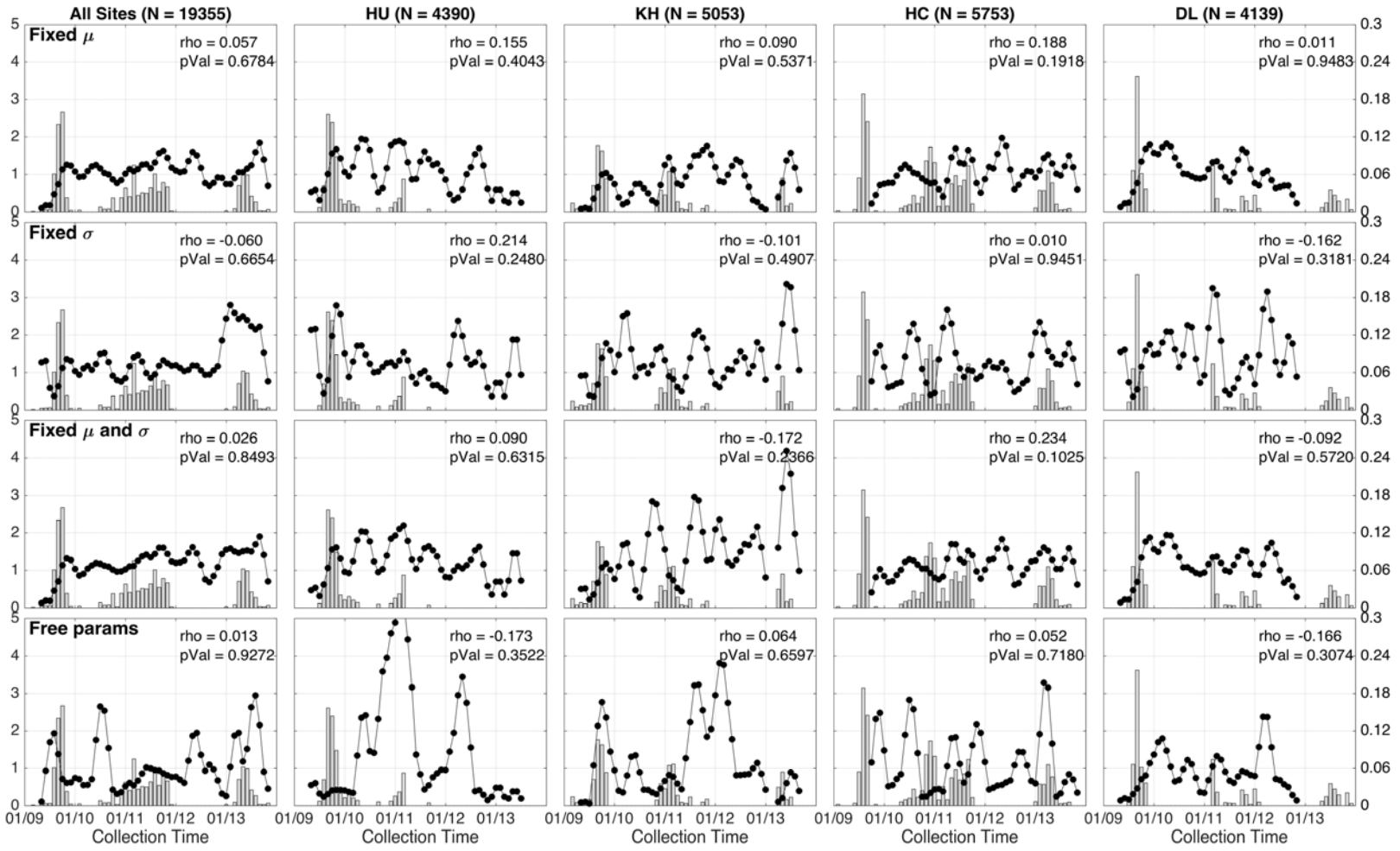

Figure 4.3 Monthly time series of w_4 (right y-axes) back-distributed by **3 months**. Data were grouped by collection site (in columns) for different fitting scenarios (in rows). Gray bars are monthly ILI+ cases (left y-axes) from sentinel data. Spearman's rho and p-values between the sentinel and serological time series are shown in each panel.

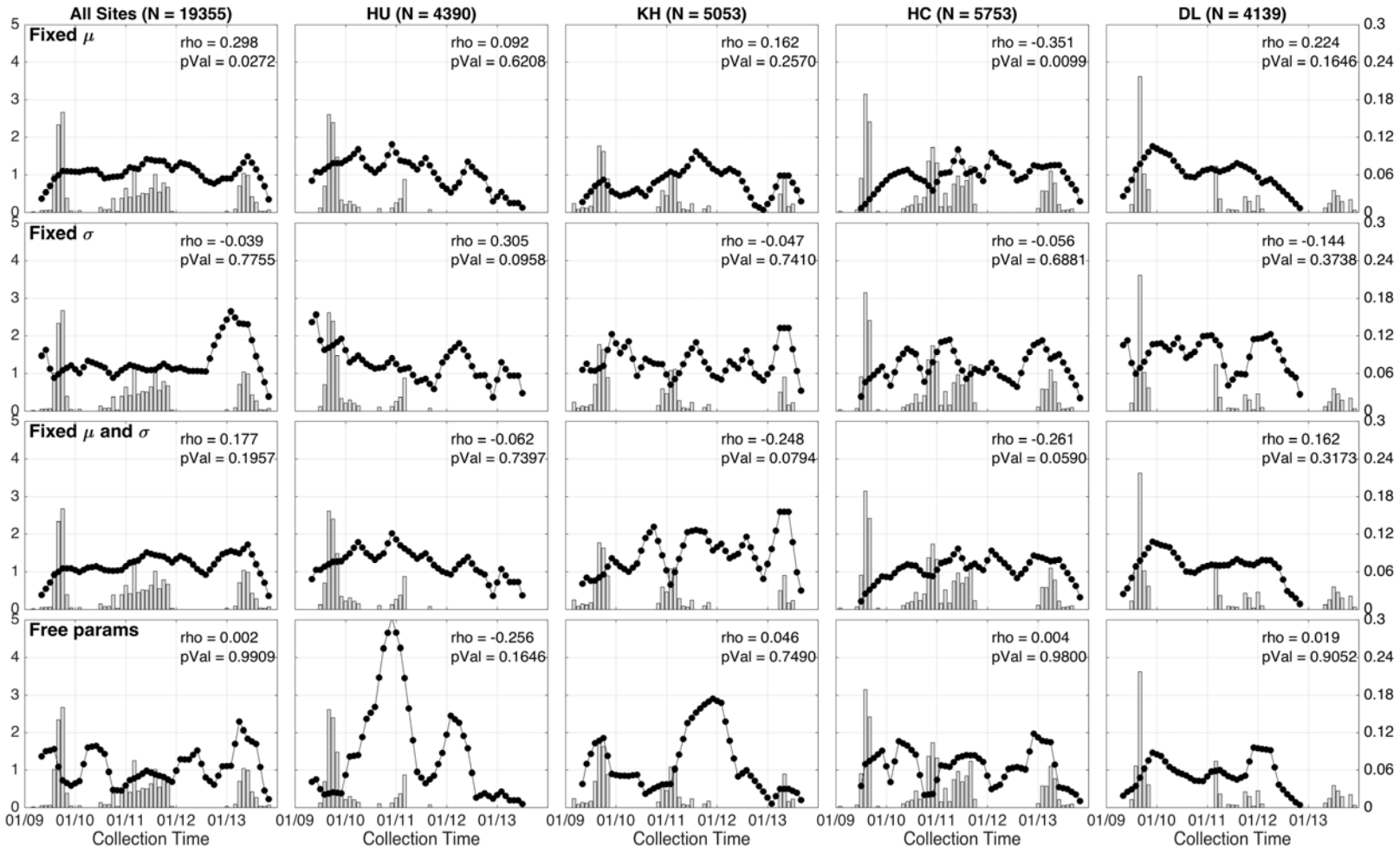

Figure 4.4 Monthly time series of w_4 (right y-axes) back-distributed by **6 months**. Data were grouped by collection site (in columns) for different fitting scenarios (in rows). Gray bars are monthly ILI+ cases (left y-axes) from sentinel data. Spearman's rho and p-values between the sentinel and serological time series are shown in each panel.

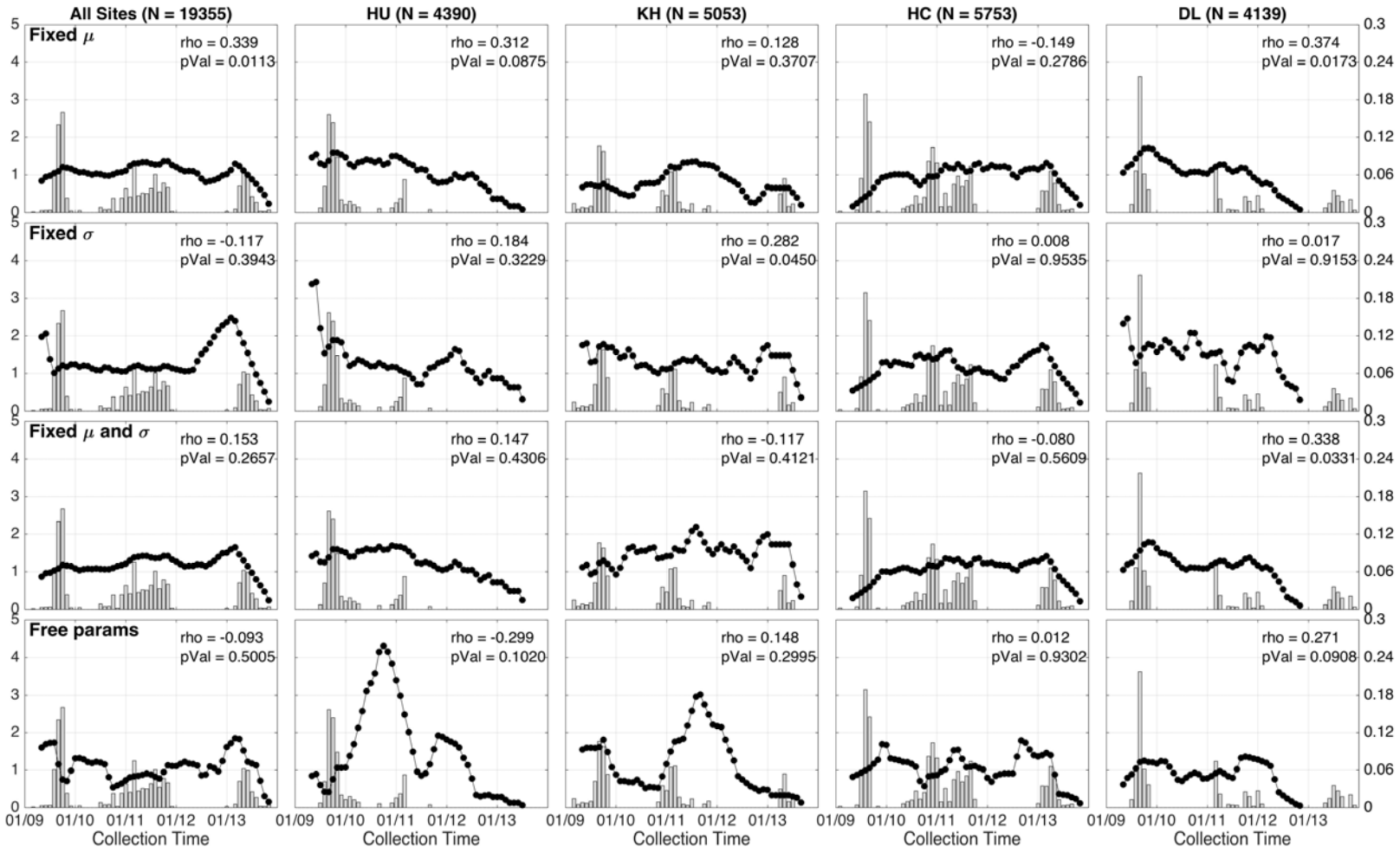

Figure 4.5 Monthly time series of w_4 (right y-axes) back-distributed by **9 months**. Data were grouped by collection site (in columns) for different fitting scenarios (in rows). Gray bars are monthly ILI+ cases (left y-axes) from sentinel data. Spearman's rho and p-values between the sentinel and serological time series are shown in each panel.

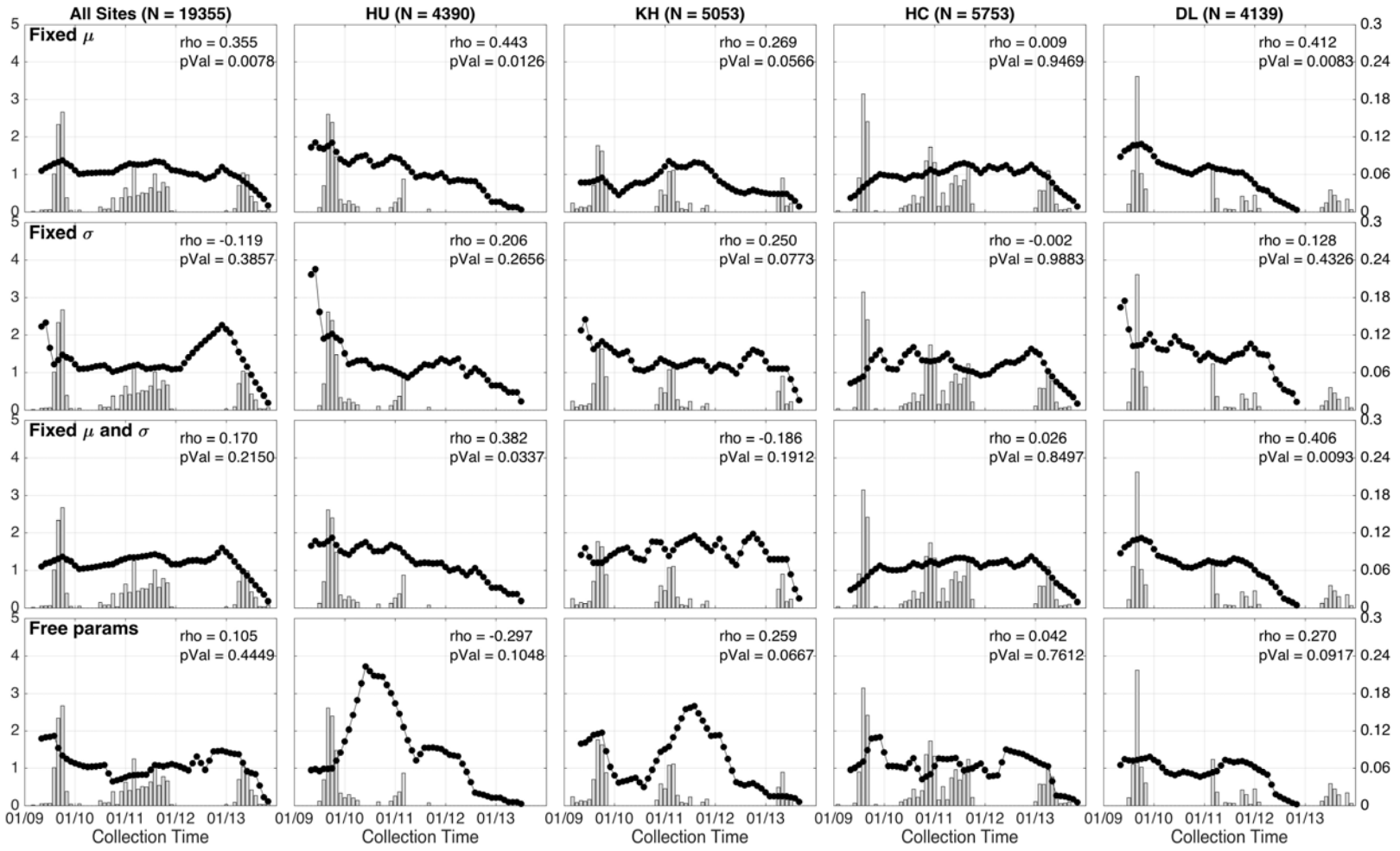

Figure 4.6 Monthly time series of w_4 (right y-axes) back-distributed by **12 months**. Data were grouped by collection site (in columns) for different fitting scenarios (in rows). Gray bars are monthly ILI+ cases (left y-axes) from sentinel data. Spearman's rho and p-values between the sentinel and serological time series are shown in each panel.

Table 4.2 Spearman's correlations and p-values for different fitting scenarios grouped by collection site for different values of *m* ranging from 2 to 12 months. These are the numbers in the top right corners of each panel in in Figures 4.3 to 4.6.

		2 months		3 months		4 months		6 months		9 months		12 months	
		rho	pVal	rho	pVal	rho	pVal	rho	pVal	rho	pVal	rho	pVal
Fixed μ_1 to μ_4	All Sites	-0.054	0.695	0.057	0.678	0.173	0.206	**0.298**	0.027	**0.339**	0.011	**0.355**	0.008
	HU	0.023	0.905	0.155	0.404	0.187	0.314	0.092	0.621	**0.312**	0.087	**0.443**	0.013
	KH	0.014	0.923	0.090	0.537	0.159	0.269	0.162	0.257	0.128	0.371	**0.269**	0.057
	HC	0.119	0.417	0.188	0.192	-0.103	0.473	-0.351	0.010	-0.149	0.279	0.009	0.947
	DL	-0.079	0.629	0.011	0.948	0.131	0.420	0.224	0.165	0.374	0.017	**0.412**	0.008
Fixed σ_1 to σ_4	All Sites	-0.129	0.347	-0.060	0.665	-0.010	0.943	-0.039	0.776	-0.117	0.394	-0.119	0.386
	HU	-0.070	0.713	**0.214**	0.248	**0.431**	0.015	**0.305**	0.096	0.184	0.323	**0.206**	0.266
	KH	-0.179	0.223	-0.101	0.491	-0.024	0.868	-0.047	0.741	**0.282**	0.045	**0.250**	0.077
	HC	0.047	0.749	0.010	0.945	-0.107	0.453	-0.056	0.688	0.008	0.953	-0.002	0.988
	DL	-0.178	0.272	-0.162	0.318	-0.148	0.363	-0.144	0.374	0.017	0.915	0.128	0.433
Fixed μ_1 to μ_4 and σ_1 to σ_4	All Sites	-0.073	0.596	0.026	0.849	0.125	0.364	0.177	0.196	0.153	0.266	0.170	0.215
	HU	-0.025	0.894	0.090	0.632	0.084	0.655	-0.062	0.740	0.147	0.431	**0.382**	0.034
	KH	-0.188	0.201	-0.172	0.237	-0.179	0.214	-0.248	0.079	-0.117	0.412	-0.186	0.191
	HC	0.211	0.145	**0.234**	0.103	-0.081	0.574	-0.261	0.059	-0.080	0.561	0.026	0.850
	DL	-0.180	0.266	-0.092	0.572	0.042	0.796	0.162	0.317	**0.338**	0.033	**0.406**	0.009
Free params	All Sites	0.064	0.641	0.013	0.927	0.001	0.996	0.002	0.991	-0.093	0.501	0.105	0.445
	HU	-0.196	0.299	-0.173	0.352	-0.197	0.288	-0.256	0.165	-0.299	0.102	-0.297	0.105
	KH	0.029	0.844	0.064	0.660	0.077	0.593	0.046	0.749	0.148	0.299	0.259	0.067
	HC	0.084	0.566	0.052	0.718	-0.006	0.965	0.004	0.980	0.012	0.930	0.042	0.761
	DL	-0.192	0.235	-0.166	0.307	-0.109	0.505	0.019	0.905	0.271	0.091	0.270	0.092

4.4.3 Time series of $w_3 + w_4$ vs. monthly ILI+ cases from sentinel data

Since the time series w_4 unsuccessfully reflect the seroincidence dynamics, in order to gain a more complete reconstruction of the time series seroincidence, it is important to account for intermediate titer subgroups resulted from either low-level titer conversion post-infection or antibody waning. In this analysis, I attempted to back-map the w_4 by 6 and 9 months (the ones with the best correlations from Section 4.4.2), and w_3 by 12 and 18 months, to determine if any of these combination corresponded closely to the pattern observed in the Vietnam sentinel data. The results are shown in Figures 4.7 to 4.10. My goal was to determine if adding the weight w_3 into the analysis would allow for a more complete analysis of infected individuals (both recently infected and non-recently infected) whose back-mapping would then more closely correspond to the sentinel data. Despite the addition of this additional class of individuals, none of the combinations of back-mapping showed any promising or consistent results. The correlations between the seroincidence data and the sentinel data were not always positive, and visual inspections of these two time series indicated that the seroincidence data did not have the same epidemic timings as the sentinel data.

As an exercise, another analysis was done when time series w_3 was evenly distributed to all months starting Jun 1, 2009; nevertheless, no insight was gained (results not presented here). In Section 4.5, I discussed some possible reasons why these analyses did not work as expected.

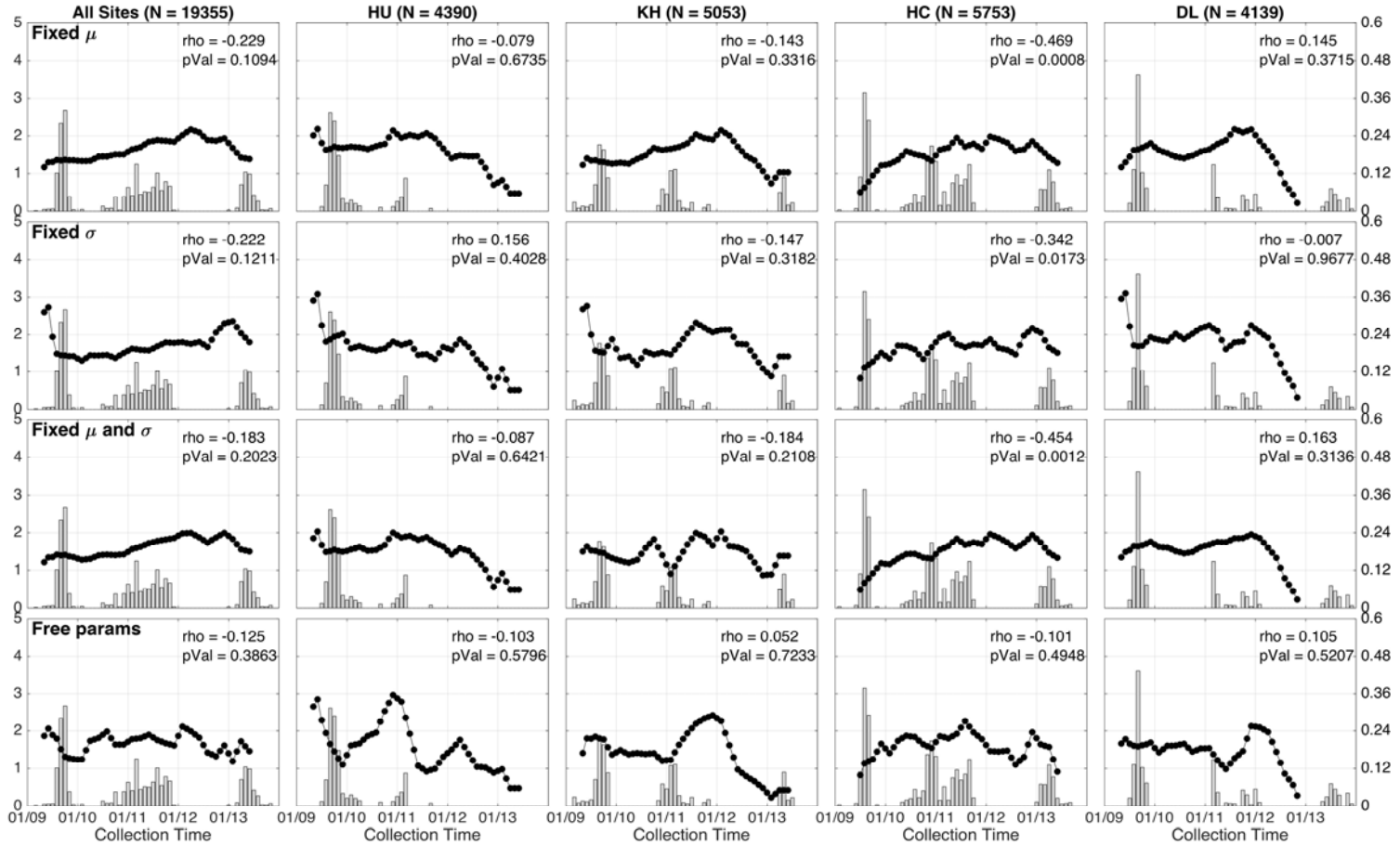

Figure 4.7 Monthly time series of w_3+w_4 for data grouped by collection site in which w_4 was back-distributed by **6 months,** and w_3 was back-distributed by **12 months.** Showing monthly time series of w_3+w_4 – sum of the weight of the two highest mean components (right y-axes) – grouped by collection site (in columns) for different fitting scenarios (in rows). Gray bars are monthly ILI+ cases (left y-axes) from sentinel data. Spearman's rho and p-values between the sentinel and serological time series are shown in each panel.

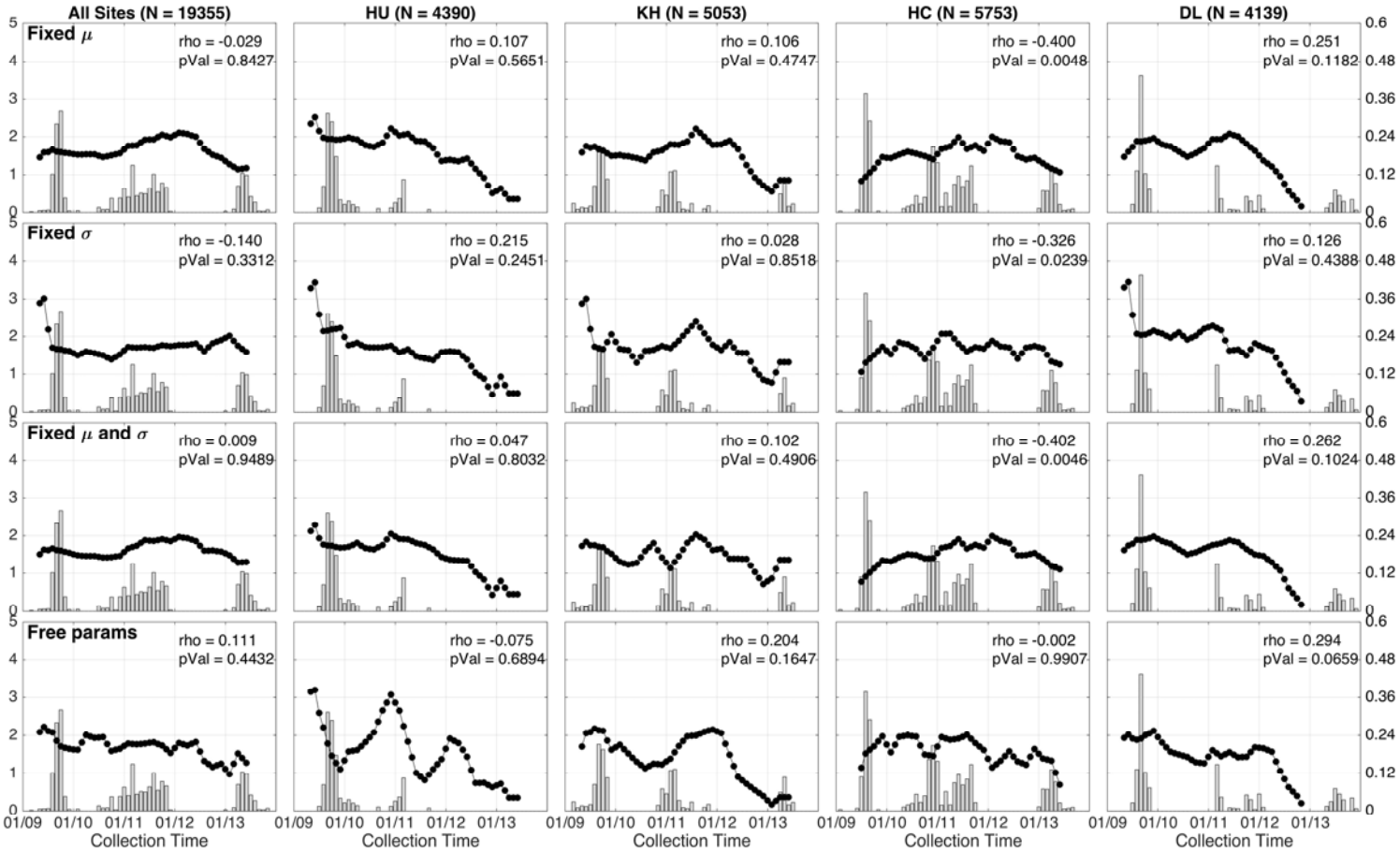

Figure 4.8 Monthly time series of w_3+w_4 for data grouped by collection site in which w_4 was back-distributed by **6 months,** and w_3 was back-distributed by **18 months.** Showing monthly time series of w_3+w_4 – sum of the weight of the two highest mean components (right y-axes) – grouped by collection site (in columns) for different fitting scenarios (in rows). Gray bars are monthly ILI+ cases (left y-axes) from sentinel data. Spearman's rho and p-values between the sentinel and serological time series are shown in each panel.

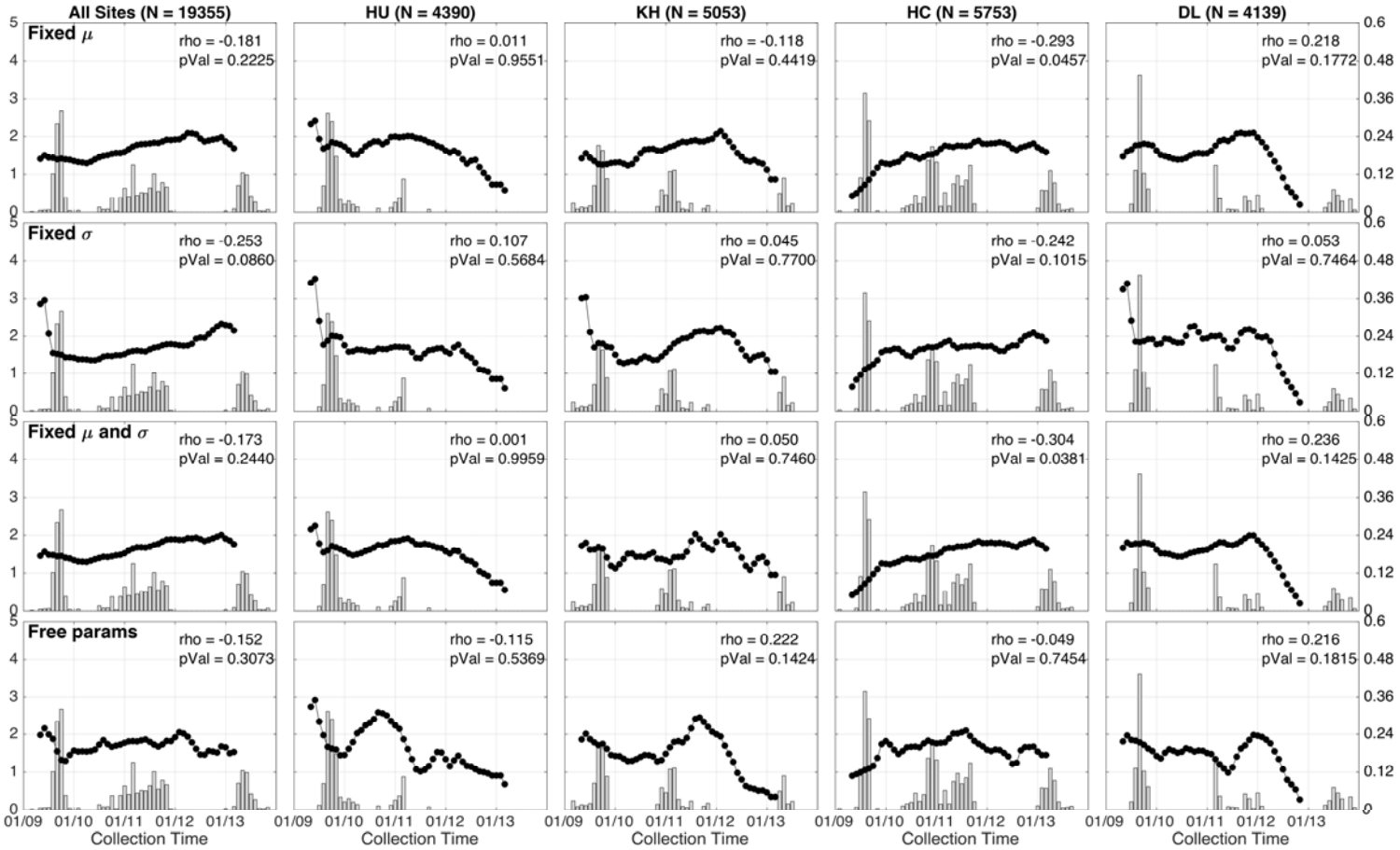

Figure 4.9 Monthly time series of w_3+w_4 for data grouped by collection site in which w_4 was back-distributed by **9 months,** and w_3 was back-distributed by **12 months.** Showing monthly time series of w_3+w_4 – sum of the weight of the two highest mean components (right y-axes) – grouped by collection site (in columns) for different fitting scenarios (in rows). Gray bars are monthly ILI+ cases (left y-axes) from sentinel data. Spearman's rho and p-values between the sentinel and serological time series are shown in each panel.

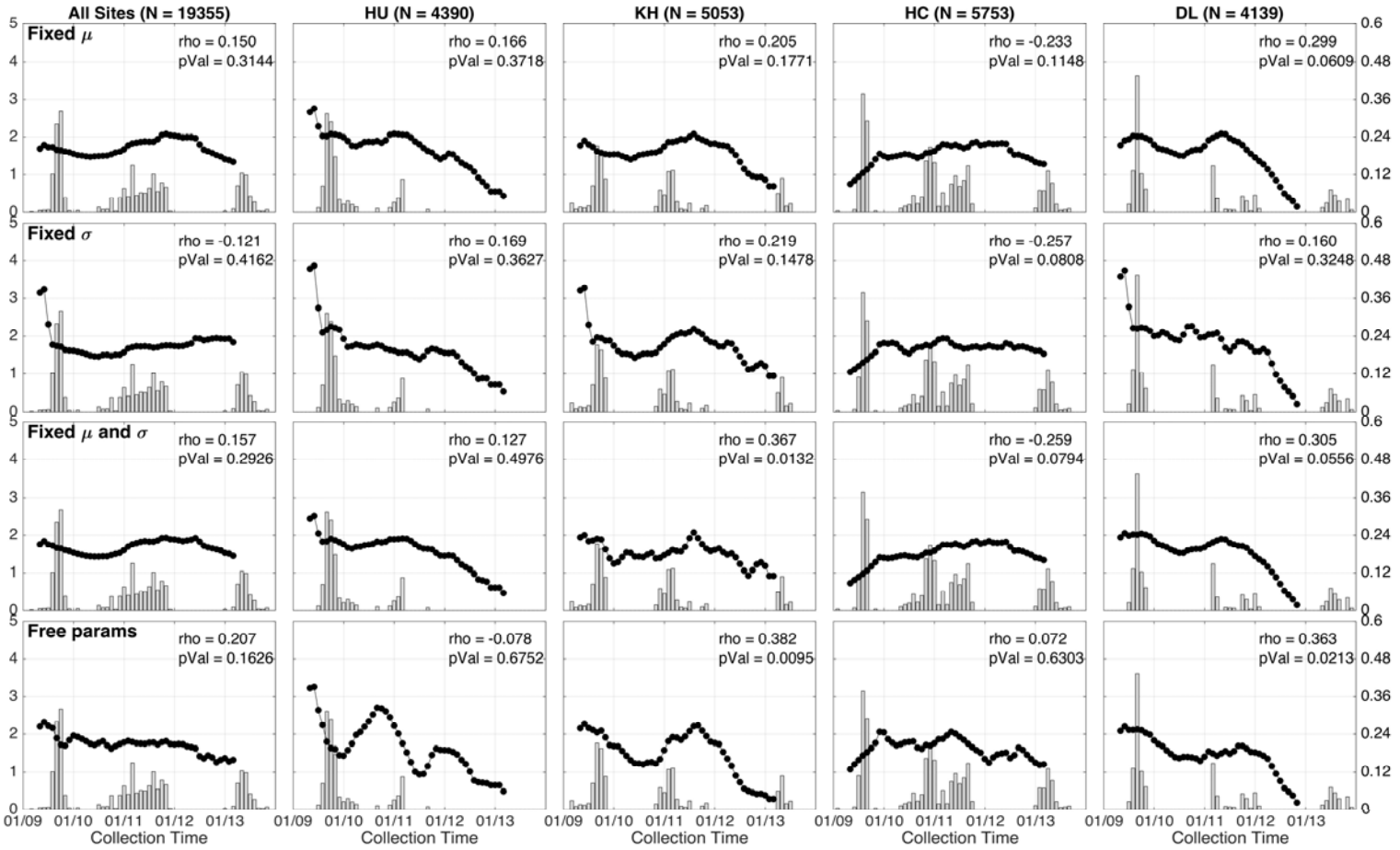

Figure 4.10 Monthly time series of w_3+w_4 for data grouped by collection site in which w_4 was back-distributed by **9 months,** and w_3 was back-distributed by **18 months.** Showing monthly time series of w_3+w_4 – sum of the weight of the two highest mean components (right y-axes) – grouped by collection site (in columns) for different fitting scenarios (in rows). Gray bars are monthly ILI+ cases (left y-axes) from sentinel data. Spearman's rho and p-values between the sentinel and serological time series are shown in each panel.

4.4.4 Time series $w_3 + w_4$ vs. cumulative ILI+ cases from sentinel data

Figure 4.11 shows the bimonthly time series $w_3 + w_4$, with a spline drawn through the points (smoothing parameter=0.5), and as expected the majority of these curves increase in time. The cumulative incidence (cumulative sum of ILI+) increases in time by definition and these two time series do frequently correlate. The Spearman's correlations and *p*-values are shown in Table 4.3.

Table 4.3 Spearman's correlation and p-values for different fitting scenarios described in Figure 4.11 grouped by collection sites.

	All Sites		HU		KH		HC		DL	
	rho	pVal	rho	pVal	rho	pVal	rho	pVal	rho	pVal
Fixed μ_1 to μ_4	0.816	2.14E-07	0.631	0.001	0.828	6.08E-07	0.639	0.001	0.780	3.01E-05
Fixed σ_1 to σ_4	0.658	1.89E-04	-0.002	0.991	0.504	0.012	0.368	0.077	0.185	0.421
Fixed μ_1 to μ_4 and σ_1 to σ_4	0.844	3.08E-08	0.663	0.001	0.458	0.024	0.665	3.89E-04	0.816	6.64E-06
Free params	0.450	0.019	0.100	0.650	0.302	0.152	0.084	0.698	0.418	0.060

The fixed μ models (scenario i) showed significant correlations across the board, both for the aggregated data and the individual-site data. When the means were not fixed, the upward trends in the seroprevalence data were more difficult to observe. One possible explanation is that the means and weights in the mixture analyses are not separately identifiable. In other words, when the means are allowed to be fit freely, a higher mean can be offset by a lower weight and a lower mean can be offset by a higher weight, suggesting that small variations in the sampling could lead to a non-robust inference of the weight parameter in the highest-titer or second-highest titer category.

A clear jump in seroprevalence occurred in late 2009 and/or early 2010, at all sites except Ho Chi Minh City where the collections started too late to observe this pattern. These jumps in seroprevalence almost certainly corresponded to the initial

wave of the 2009 H1N1 Pdm. Note that the fixed variance analysis (second row) fails to capture the dynamics of the 2009 H1N1 pandemic wave in the second half of 2009. The observations in this section lend some support to the biological justification for fixing means in a mixture model analysis with titer groups.

If we were to interpret the time series $w_3 + w_4$ in Figure 4.11 as an age-adjusted attack rate of 2009 H1N1 pandemic influenza, these splines indicate that the attack rate of the first wave of the pandemic was between 30% and 40%, and that by 2013 between 55% and 60% of the population had been exposed to the pandemic virus. These numbers are slightly higher than the expected ranges for pandemic influenza attack rates and annual influenza attack rates (Dawood et al. 2012), but note that as in all serological analyses of the 2009 pandemic, it is important to keep in mind that these attack rates will include older individuals (>60 years-old) with pre-existing immunity to the 2009 H1N1 virus prior to the pandemic (Hancock et al. 2009). The sentinel data in Vietnam (Nguyen et al. 2009; Nguyen et al. 2013), as well as worldwide, show that the majority of influenza epidemics are H3N2. The Vietnamese sentinel data indicated that 2011 was the only other year after 2009 with substantial H1N1 circulation (Figure 1.1). Thus, the estimated 55% to 60% seroprevalence at the end of 2013 likely represented the attack rates after one pandemic (2009) and one epidemic (2011).

In summary, the w_3+w_4 time series from the fixed-mean model did seem to correspond to a cumulative attack rate. Indeed, the p-values indicated significant correlation for some collection sites, and the cumulative attack rate numbers were in

a credible range for the expected attack rate after several years of circulation of the 2009 H1N1 subtype.

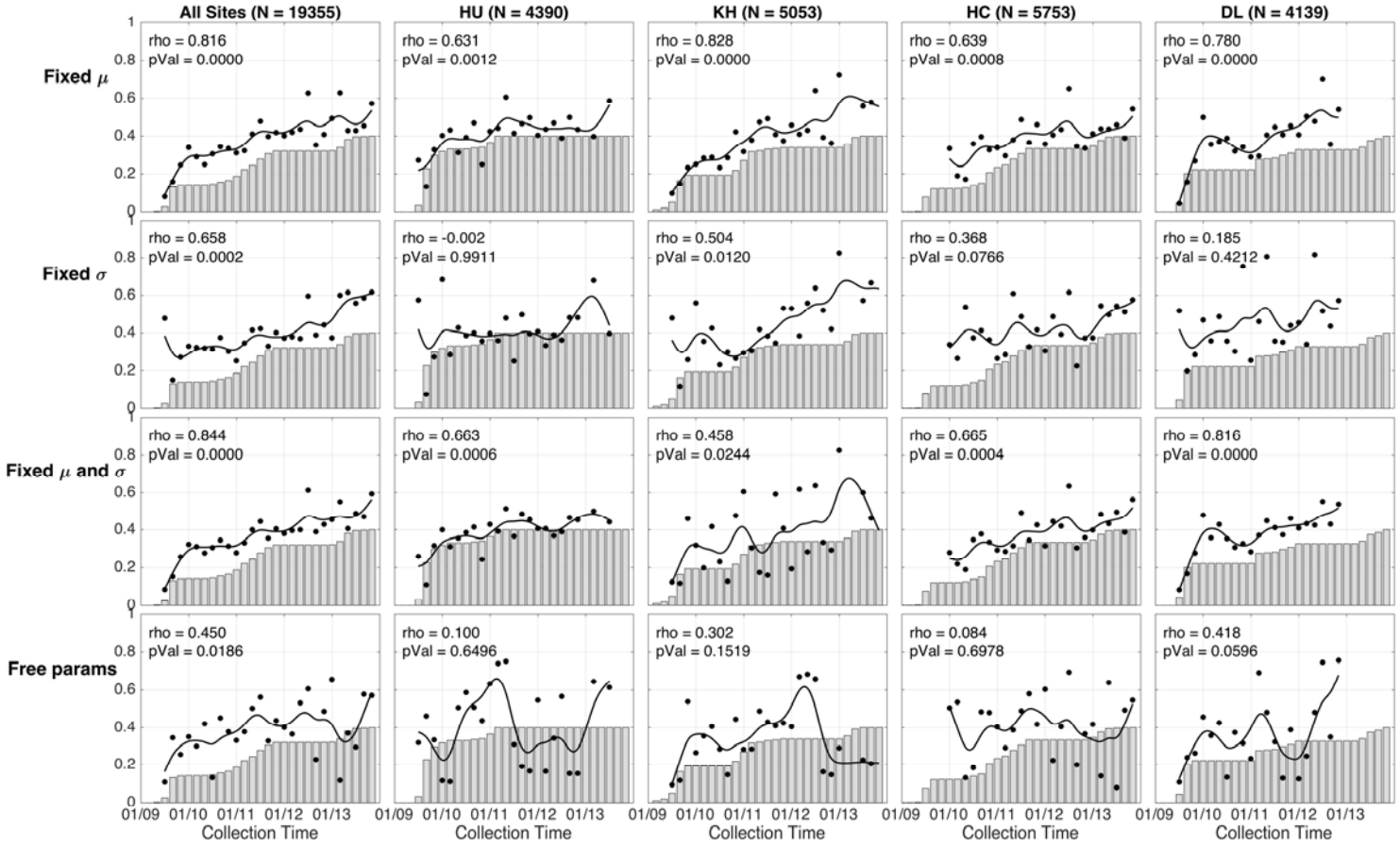

Figure 4.11 Bimonthly time series of w_3+w_4 vs. bimonthly cumulative ILI+ cases from sentinel data. Showing bimonthly time series of w_3+w_4 (right y-axes) – grouped by collection sites (in columns) for different fitting scenarios (in rows). There is no back-mapping in this analysis. Gray bars are bi-monthly cumulative sentinel ILI+ cases (left y-axes) normalized by the total number of cases multiplied by 0.4 (for visualization purposes). The smoothing parameter was 0.5, and Spearman's rho and p-values between the sentinel and serological time series are shown in each panel.

4.5 Discussion

After the H1N1 Pdm 2009, several serological studies looking at age-specific seroprevalence and influenza attack rates (IAR) during the first wave were published where sera were consecutively collected at two to three different time points (Baguelin et al. 2011; Iwatsuki-Horimoto et al. 2011; McLeish et al. 2011; Soh et al. 2012), or continuously over a short period (Wu et al. 2010; 2011). All of these studies relied on either single HI or MN titer cut-offs or a four-fold increase in paired sera. Advancing from the traditional single titer threshold approach, some estimated IAR using mixture models with two to three components using either cross-sectional data or paired sera (Zhao et al. 2017; te Beest et al. 2014a; 2014b). Due to the small number of serological time points, these studies were not able to reconstruct the dynamics in the same detail as in Wu et al. (2010; 2011). The time series serological data from this thesis bridged the shortcomings of these studies by reconstructing the dynamics of H1-09 with continuous sampling over a period of four and a half years using a mixture model approach.

The aim of this chapter was to use the components' weight parameters obtained from a mixture distribution approach in Chapter 3, interpret these weights as population fractions representing individuals that were infected in the past or recent past, and then use these assumptions to reconstruct the recent infection dynamics of H1N1 influenza in southern Vietnam. None of the correlations between the back-mapped time series w_4 and the monthly sentinel ILI+ cases among four fitting scenario was significant. This result renders the assumption that titer sub-group μ_4=671.1 (95% CI 484.7–818.6) represented recent infections in the last three

to twelve months inconclusive. The time series $w_3 + w_4$ when keeping the means fixed without back-mapping did have an expected shape of a seroprevalence curve and significant correlation with the cumulative sentinel data (except in Hue and Ho Chi Minh City). Nevertheless, the results were not always consistent across different collection sites. The reason might have been due to the smaller overlapping region between the second and third component compared to the overlapping regions between the third and fourth components in the mixture fit (Figure 3.7 and 4.1) that made the sum of the two highest titer components a better indication of past exposure. In short, even though the categorization proposed in Chapter 3 might be useful, it was not precise enough to perform temporal epidemic curve reconstructions.

There are some possible explanations as to why neither back-mapped time series of w_4 nor $w_3 + w_4$ could consistently reproduce the observed epidemic dynamics of the 2009 H1N1 influenza activities in southern Vietnam:

i. High titers are not strongly associated with recent infections at a population-level. Some individuals seroconverted to intermediate titers or failed to developed protective antibody titers following infections (Miller et al. 2010; Cox, Brokstad, and Ogra 2004; Chen et al. 2010; Chan et al. 2011) while others were able to maintain high titers for a long period of time (Lessler et al. 2012; Kucharski et al. 2015).

ii. No age dependency was included in the analysis causing young high-titer individuals to be classified as recent, despite the fact that children can maintain high titers for a long time (Francis 1960; Davenport, Hennessy, and Francis 1953). The same reason applies to a fraction of individuals born before 1953 with prior-immunity against H1-09 as a result of childhood infection (Hancock et al. 2009).

iii. The fourth component was defined over too broad of a titer range. Thus, some borderline cases (in the overlapping regions with neighboring components) might be a result of waning. This was a major concern especially after the first wave of the H1N1 2009 Pdm when a significant proportion of the population had been exposed to the Pdm virus, and their titers started to wane.

iv. The coarse bimonthly time series of the weight parameters made it difficult to obtain a precise (fine-scale) reconstruction of past epidemic dynamics.

v. The imperfect implementation of the sampling protocol caused a lot of sampling variation between different time points especially during the second half of 2009.

The first three reasons are the most obvious as breaking the link between titer and recency would render the majority of the analysis in this chapter as invalid. Failure to use w_4 as a meaningful epidemiological classification could have been a simple outcome of the fact that only ~50-70% of individuals classified as w_4 truly had recent infections. Indeed, this is a concern in most serological studies using cross-sectional or anonymized samples without knowledge about individuals' infection history. This analysis relies heavily on the components' means and standard deviations from data aggregated over a period of four and a half years; these quantities could have changed slightly over time (Figure 3.10). Even though a single titer value cannot be used as precisely as a molecular clock to date an event in the past, the qualitative relationship between titers and time since last infections is based on evidence from clinical data (Todd 2016). One way to improve the model's performance is to introduce age dependency. Perhaps looking at both H1-09 and H1-77 titers for high-titer older individuals (≥60) would have changed the seroincidence reconstruction shown in Figures 4.2 to 4.6. At no point in the analysis did we

introduce any age-dependency either to antibody waning or post-infection seroconversion titers. Even though antibody waning could be safely ignored during the first wave of the pandemic as in other studies (te Beest et al. 2014a; Zhao et al. 2017; Wu et al. 2010) due to the novel antigenicity of H1-09, it could affect the later results in the time series. In addition, a short-lived heterosubtypic boosting of one $\log_2$-unit PM titers to H1N1 strains for confirmed H3N2 infected patients was observed in the absence of subsequent infections (Todd 2016).

Vaccination was not a considerable concern as the influenza vaccine coverage in Vietnam was negligible. Cross-reaction caused by the assay is likely another contributor as the PM assay is known to be more sensitive than HI (Koopmans et al. 2012). Individuals from this SSE data were also found to show substantial titers against antigens that circulated before their birth (Vinh 2015). A combination of titer boosting, absence of waning, and cross-reaction might be a plausible explanation to the high proportion of individuals in the two highest mean component in 2010 and 2012 who were neither children nor older than 60 years old (Figure 3.10), if it were true that H1-09 was absent from the population in 2010 and 2012 as observed in the sentinel data (Figure 1.1).

Finally, the last possibility for the discordance between the sentinel ILI+ time series and the seroincidence may simply be that these two time series are truly weakly associated, and that the true dynamics of H1N1 and the hospital-reported dynamics are different. The sentinel data and the serological data represent two different populations as explained in Section 4.1. The dynamics of symptomatic disease do not have to match the dynamics of asymptomatic disease. For malaria, it

is known that different fractions of the population are asymptomatic at different transmission levels (Lindblade et al. 2013). In dengue epidemiology, it is known that one dengue serotype can be identified as the cause of hospitalized cases while a different one can be identified through serology as the primary circulating serotype that season (Sangkawibha et al. 1984). In *Salmonella*, a trend of inverse correlations between seroincidence and case report data was observed in a number of European countries (Falkenhorst et al. 2012). Nothing like this has been demonstrated for influenza virus, but it is certainly possible that some epidemic years are milder than others, with greater fractions of subclinical or asymptomatic cases.

Whether an influenza epidemic reconstruction is being done through a cohort design, a surveillance system, or a general-population serological time series, one must be able to account for the representativeness of the samples. It is not clear if any particular study design has an advantage over the other. Cohort studies are biased by anything that correlates with the given location (e.g. socio-economic status, population density, household size). Surveillance systems are biased by the reporting patterns to those participating hospitals and clinics as they may attract patients from a particular socio-economic group or it may filter in/out certain sets of symptoms depending on whether the surveillance points are locations in primary/tertiary care facilities. Population-level cross sectional data from convenience samples will contain different sources of bias depending on the study design. Serum samples from blood donors will likely show results for a healthier-than-average component of the population, while residual serum samples from hospital labs may bias the sample set to a less healthy or more vulnerable part of the population. Although none of these

potential biases could be accounted for in this thesis, in Chapter 6 I present a discussion of this bias with some additional data on non-influenza assays performed on serum samples collected in this study.

CHAPTER 5

5 Sero-Dynamics Using Individual Weekly Incidence Parameters

5.1 Background

In Chapter 4, even though time periods of above-average influenza incidence were identified using reconstructions of the population's serological dynamics on a coarse bimonthly scale, these results were largely unsuccessful. In this chapter I aim to present a more fine-scale reconstruction of the population's past infection dynamics by using a dynamical model and maximum likelihood inference. If this SSE dataset consists of sufficient age-stratified and time-stratified samples from a representative population following an epidemic, the seroincidence will be able to be back-calculated using knowledge on post-infection seroconversion and antibody waning.

Seroincidence is different from the sentinel system's incidence estimated from case report data, as seroincidence is meant to capture symptomatic, asymptomatic, and mild cases. The seroincidence estimates can be compared qualitatively to the sentinel incidence if they were collected from the same population during the same period. If successful, this seroincidence description will reveal influenza activity in

the population that was not captured in the sentinel data. This approach of using population wide serological data to reconstruct disease incidence using knowledge of antibody waning rates has been presented previously in the literature for a number of diseases (Simonsen et al. 2009; Falkenhorst et al. 2012; Heisterkamp et al. 2008; de Melker et al. 2006; Versteegh et al. 2005; de Angelis, Gilks, and Day 1998) including influenza (Wu et al. 2010; 2011). In order to reconstruct an epidemic, a time scale must be chosen with which the epidemic dynamics are to be described. In my epidemic reconstructions, every two-week window will be represented by an independent parameter – defined as the number of influenza cases that occurred during that two-week period – to be inferred from the SSE data. At some of our participating hospitals, the sample collections started as early as July 2009; which provided an invaluable opportunity to reconstruct the first wave of the H1N1 Pandemic 2009 (H1-09) in southern Vietnam. Thus, the analysis presented in this chapter was restricted to the period from June 2009 to March 2010, which encompasses the first epidemic period of H1-09 in Vietnam.

The best comparisons of this work are the analyses presented in Wu et al. (2011; 2014) and Baguelin et al. (2011) for influenza, and Simonsen et al. (2009) and Falkenhorst et al. (2012) for *Salmonella*. Wu et al. (2011; 2014) gathered convenience samples from different sources to generate multiple cross-sectional time points to reconstruct the weekly incidence during the first wave of the H1N1 Pdm 2009 in Hong Kong. Nevertheless, their study and Baguelin et al. (2012) both used discrete titer measurements with pre-defined titer cut-offs to define seropositivity. Simonsen et al. (2008) and Falkenhorst et al. (2012) used a

longitudinal dataset of confirmed *Salmonella enterica* infection as a proxy to compute time since last infection for a cross-sectional dataset allowing for individual variation. Due to uncertainty in disease status, i.e. mild vs. severe, and different post-infection seroconversion profile, and age, just like our results in Chapter 3, the model worked well at population level but not at individual level. What sets the present analysis apart from all of the above is the longer time series, a more informative serological assay, and a more complete model including antibody waning and individual variation in post-infection seroconversion.

Multiple challenges are involved this reconstruction of the time series seroincidence, including sensitivity and specificity of the serological assay, age effects, uniformity of sampling, and the fact that an antibody signal can wane from positive to negative during the ten-month time period in which incidence parameters are being inferred. Rather than focus on these issues individually, I will present a dynamical model that includes all of these features (except age). The fact that the microarray assay, like a quantitative ELISA, produces more reproducible titers on a continuous scale, allows these data points to be analyzed with a more detailed statistical model. Specifically, the clinical study run by Dr. Stacy Todd (Todd 2016) allowed better model parameterization because it used the same assay to measure antibody waning over a seven-month period at an individual level.

The inferred seroincidence was then compared to the sentinel dataset from NIHE to see if the SSE data captured the same influenza activity in southern Vietnam. However, there are several factors complicating this comparison. First of all, previously published clinical studies conducted just for the H1N1 Pdm 2009 strain

demonstrated that only about 80-90% of the symptomatic flu cases developed a protective level of antibody response either by HI or MN tests in 21-28 days following acute infection (Cox, Brokstad, and Ogra 2004; Baguelin et al. 2011; Chen et al. 2010; Miller et al. 2010; Cowling et al. 2010; Hung et al. 2010; Chan et al. 2011) while other studies suggested that the seroconversion rates are much lower for mild and asymptomatic cases (Wu et al. 2014). Also the definition for influenza-like-illness (ILI) symptoms could overlap with other respiratory diseases circulating in the population. Therefore, it is important to keep in mind that the sentinel incidence could be used to validate seroincidence inference presented in this chapter only in a qualitative sense.

5.2 Data

5.2.1 Serological data

Ten collection sites in southern Vietnam have serum sample collection extending back to 2009, as described in Chapter 2 (Section 2.2). Only collection sites whose sample collection started from early July 2009 and for which a substantial number of samples were processed during 2009-2010 were included in this subset of the data. The samples represented patients attending hospitals in four cities: Nha Trang (small urban, central coast n=970), Dak Lak (central highlands, rural n=1074), Hue (small urban, central coast n=1023), and Kien Giang (small urban, Mekong Delta, n=560) in central and southern Vietnam (Figure 2.1). The samples were analyzed either at four-dilutions or two-dilutions by protein microarray. Only samples whose positive control titers of H1-09 was within 1.2 dilutions from the series mean was

used in this analysis. For details on sample processing and titer calculations refer to Section 2.2 to 2.5.

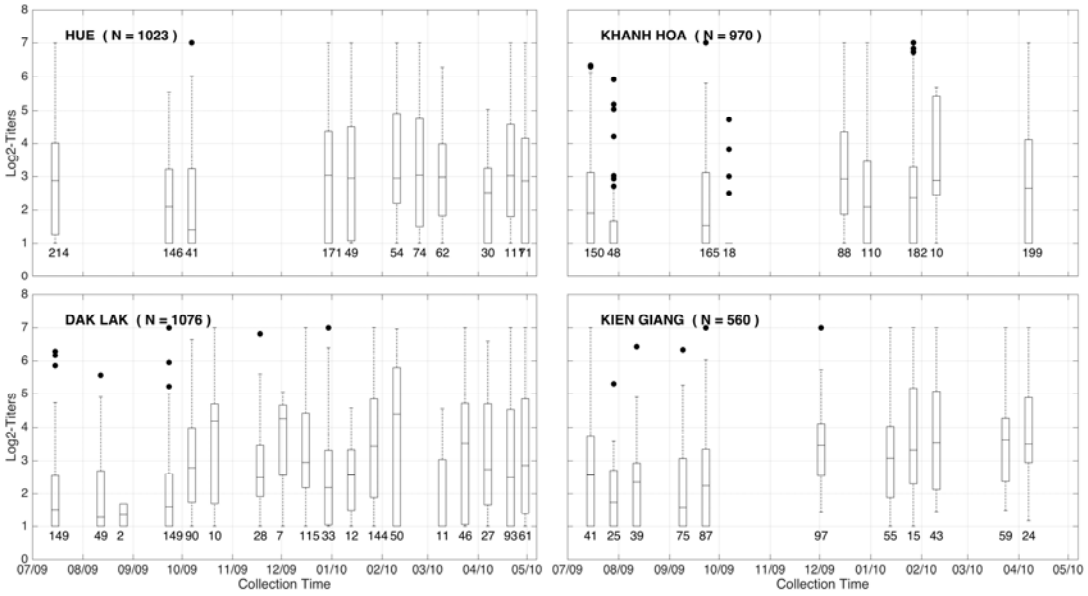

Figure 5.1 Time series (MM/YY) of antibody titers against H1N1 Pdm 2009.
Showing data for four collection sites from July 1st 2009 to April 30th 2010. Samples were adjusted for age and gender differences of the corresponding collection sites according to the Vietnamese Housing Census 2009 and grouped by two-week periods. The numbers below the boxes represent the number of samples collected in that period. On each box, the middle mark represents the median of the log2-titers while the lower and upper edges represent the 25th and 75th percentiles. The whiskers extend to the most extreme data that are not considered outliers. In this plot, points are considered outliers (black dots) if they are outside the ±2.7σ range which covers approximately 99.3% of the range of a normal distribution.

In order to capture the initial dynamics of the H1N1 Pdm 2009 in Vietnam, we only looked at samples collected from July 1, 2009 until Apr 30, 2010. Preliminary examination of the data revealed an increase in geometric mean titers around October and November 2009 for Khanh Hoa, Kien Giang, and Dak Lak. One of the challenges is that when breaking up the data by collection site and collection time, there seems to be a lot of missing data (time period with no samples). The reason for this is that those samples were collected in clustered periods of one to two weeks

before the collection cut-off time. Thus, analyses were only performed for Dak Lak (17/22 bi-weekly time windows with data), Kien Giang (11/22 bi-weekly time windows with data) and Hue (11/22 bi-weekly time windows with data).

5.2.2 Sentinel data

The sentinel data used in this chapter were described in detail in Section 4.2.2. For comparison purposes, only data collected from July 1, 2009 to April 30, 2010 from Dak Lak, Hue (sentinel comparison is Da Nang), and Kien Giang (sentinel comparison is all of southern Vietnam: two hospitals in Ho Chi Minh City, one in Dong Nai, and one in Cai Be) were included. Again, the sentinel data were presented in the form of dentrended monthly "ILI confirmed flu-positive" (ILI+) cases for H1N1 Pdm 2009 as the product of the monthly "% positive" and monthly ILI counts that were described elsewhere (Thai 2014).

5.3 Methods

5.3.1 Model description

This model is an extension from the model for influenza by Vinh and Boni (Vinh and Boni 2015), for reconstructing a seroincidence curve using a serological time series or a "serial seroepidemiology" study design (SSE). One of the novel aspects of this analysis is that the entire inference was driven by the serological data without using any presumed seasonal force of infection. The main model compartments are exposed individuals (E), infectious individuals (I), recovered individuals awaiting seroconversion (P), and recovered individuals with post-infection titer i in $\log_2$-units (R_i). In this model, the seven R-classes corresponds to $\log_2$-titers of 1.0 to 7.0. Recovered individuals are distributed into six R-classes from R_2 to R_7 according to their $\log_2$-titers. The antibody waning process describes movements of individuals from the higher R-classes to the lower ones but not to R_1.

R_1 represents individuals whose titers are equal to or less than 20.0 (1.0 in $\log_2$-units).

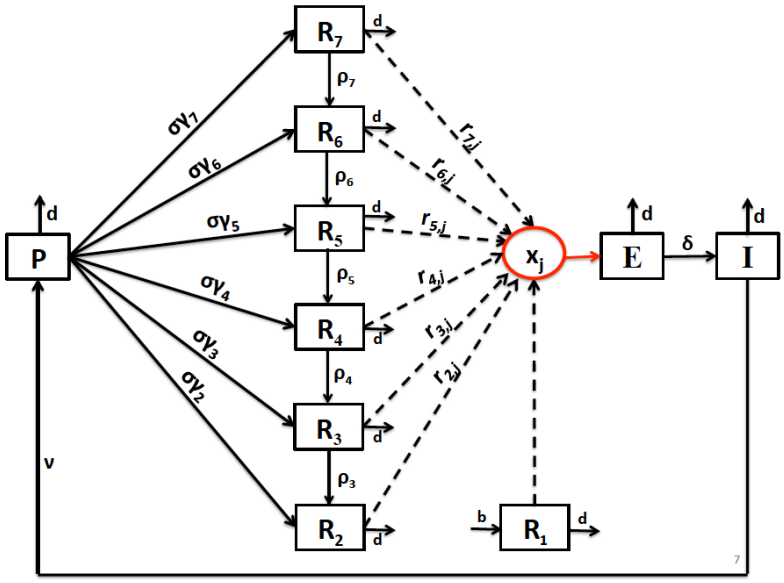

Figure 5.2 Compartmental models for equations (5.1) – (5.6). In this model, E represents exposed individuals, I for infectious individuals, P for recovered individuals awaiting seroconversion, and R_i for recovered individuals with post-infection titer i in $\log_2$-units.

From previous analysis (te Beest et al. 2017; Koopmans et al. 2012) and clinical data (Todd 2016), titers of 20 are believed to represent negative individuals with no historical infection. Thus, R_1 represents individuals who have never been infected before; naïve individuals are born into this class (b term). The dynamical system described in Figure 5.2 is a hybrid system, in which the continuous part was first integrated for time t_0 to $t_0 + \varepsilon$ according to:

$$\frac{dP}{dt} = \nu I - \sigma\left(\sum_{i=1}^{7}\gamma_i\right)P - dP = \nu I - (\sigma + d)P \tag{5.1}$$

$$\frac{dR_1}{dt} = b - dR_1 \tag{5.2}$$

$$\frac{dR_i}{dt} = \sigma\gamma_i P - (\rho_i + d)R_i + \rho_{i+1}R_{i+1} \qquad for\ 2 \le i \le 6 \tag{5.3}$$

$$\frac{dR_7}{dt} = \sigma\gamma_7 P - (\rho_7 + d)R_7 \tag{5.4}$$

$$\frac{dE}{dt} = -(\delta + d)E \tag{5.5}$$

$$\frac{dI}{dt} = \delta E - (\nu + d)I \tag{5.6}$$

This integration results in a mapping of $\overrightarrow{X_{t_0}} \xrightarrow{F} \overrightarrow{X_{t_0+\mathcal{E}}}$. The discrete part of the system is then defined as $\overrightarrow{X_{t_0+\mathcal{E}}} \xrightarrow{G} \overrightarrow{X'_{t_0+\mathcal{E}}}$ where G moves individuals from the R-classes to the E-class to mimic the process of infection, as a discrete-time infection process (DTIP). We can write $G(\vec{x}) = \overrightarrow{X_{t_0+\mathcal{E}}} + \overrightarrow{[DTIP]}$

$$\text{in which } DTIP = \begin{cases} -r_{i,j} \ for\ R_{1\to 7} \\ +x_j\ for\ E \\ 0\ for\ P\ and\ I \end{cases}.$$

Thus, the final mapping from time t_0 to time $t_0 + \varepsilon$ is defined as $H(\vec{x}) = G(F(\vec{x}))$. The critical difference between this model and other dynamical models used for this type of inferences is that instead of having a typical non-linear term (usually $S{\cdot}I$) determining the instantaneous incidence at time t entering the E class (equation 5.6), every two weeks there is an infection pulse, and x_j individuals are removed from the R_i classes and placed into the E class. The x_j are free parameters and the inference in this chapter is aimed at estimating these parameters. At each bi-weekly time point j, the number of individuals removed from class R_i is:

$$r_{i,j} = \frac{(1-\varepsilon_i)R_i}{\sum_{k=1}^{7}(1-\varepsilon_k)R_k}x_j \tag{5.7}$$

Table 5.1 Model parameters

Parameter	Description	Values/ranges
δ^{-1}	incubation period (days)	1.4 (1.3 – 1.5) (Lessler et al. 2009)
ν^{-1}	infection period (days)	5.0 (3.0 – 7.0) (Yang et al. 2009)
σ^{-1}	number of days post-infection before seroconversion (days)	21.0 (15.0 – 28.0) (Miller et al. 2010; Baguelin et al. 2011; Chen et al. 2010; Chan et al. 2011; Hung et al. 2010; Todd 2016)
γ_i	fraction of recovered individuals seroconvert to R_i post-infection	determined by (5.9)
λ	seroconversion rate of the truncated Poisson distribution	fitted
C	normalization constant of the truncated Poisson distribution	determined by (5.9)
ρ_i^{-1}	antibody waning rate from R_i to R_{i-1} ($days^{-1}$)	determined by (5.8)
ω	antibody waning duration for individuals to wane one $\log_2$-titer without inflation (days)	90.0
c	inflation parameter to slow down the waning as increasing i (c>0 to observe fast-then-slow pattern)	fitted
ε_i	susceptibility reduction of individuals in R_i	determined by (5.10)
$T50$	susceptibility or titer value corresponds to 50% susceptibility reduction	80.0 & 160.0
β	slope of the tangent line to the reduced susceptibility log-logistic curve at the inflection point	b>0: decreasing sigmoidal curve
d	daily death rate ($days^{-1}$)	[4.0×10^5, 3.0×10^4]
b	number of birth ($days^{-1}$)	d^*N
N	provincial population size	Vietnam Housing and Population Census 2009
		1.73×10^6 for Dak Lak
		1.68×10^6 for Kien Giang
		1.08×10^6 for Hue
x_j	weekly incidence at time j-th	fitted
n_j	number of valid H1-09 titers at time j-th	[0, 200]

5.3.2 Antibody waning

The short-term dynamics of antibody have been studied in various publications. Antibody waning appears to be a fast-then-slow process (rapid during the first 3 months) starting as early as day 11-25 following acute infection with various rates depending on the influenza strains (Horsfall and Richard 1941, Chan et al. 2011, Wang et al. 2016, Todd 2016).

The antibody waning process describes movement between the high-index R-classes to the lower ones by a piecewise function:

$$\rho_i^{-1} = \begin{cases} 30.0 + \omega(1+c)^{(7-i)} = 30.0 + \omega & for\ i = 7 \\ \omega(1+c)^{(7-i)} & for\ 3 \le i \le 6 \end{cases} \quad (5.8)$$

where ρ_i^{-1} is the expected number of days an individual spends in class R_i. In this analysis, individuals whose post-infection titers were at least 1280 were assumed to stay in the first (highest) R-class for 30 days before any waning was observed. Clinical data assembled by Todd (2016) shows that there was no loss in antibody titers for at least 90 days post-infection for individuals of titers 1280 for seasonal H3N2 strains. The R_7 class is not a single titer category, but it represents individuals whose titers were measured at 1280 or higher due to the upper limit of detection of the serological assay. Thus, individuals might seem to stay longer in this class according to (5.8). The truth is that it just takes longer to observe waning for these individuals. In this analysis, ω was fixed at 90 days and c was optimized.

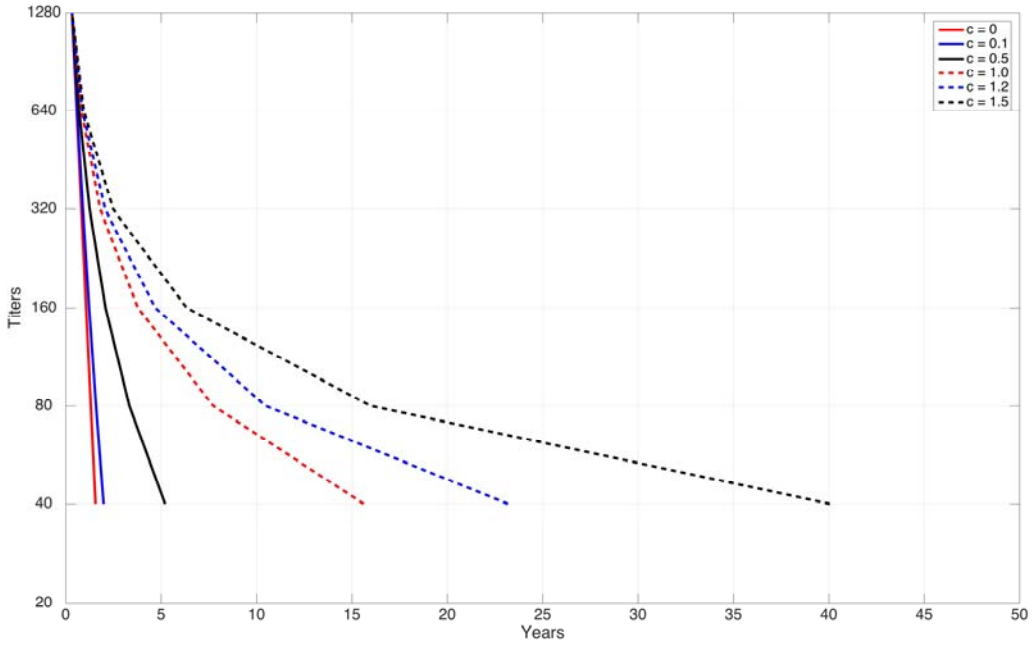

Figure 5.3 Antibody waning function as a function of time in which ω = 90.0 (days) and a 30-day delay in R_7 for different values of c.

5.3.3 Post-infection seroconversion

The underlying mechanism governing post-infection seroconversion has not been well understood despite a number of studies that were conducted after the H1N1 Pdm 2009. Most of these studies looked at post-infection seroconversion as a binary variable (Chen 2010; Miller et al. 2010; Wu et al. 2014), so the exact proportions of individuals converting to various titer levels were not presented. Even though some studies reported the proportion of seroconversion to different titer values, the results were almost always discretized (Steens et al. 2011, te Beest et al. 2014a).

About 10-20% of infected individuals fail to seroconvert to a protective antibody titer (Cox, Brokstad, and Ogra 2004; Baguelin et al. 2011; Miller et al. 2010; Chen et al. 2010; Cowling et al. 2010; Hung et al. 2010; Chan et al. 2011). About 20% of the PCR-confirmed cases reached the upper limit of detection (1:1280) against H1N1 Pdm 2009 using identical PA method (Todd 2016). Assuming that individuals seroconverted to titer levels anywhere between the protective level and the upper limit of detection following a truncated Poisson distribution. The function below was parameterized to incorporate all of the above knowledge:

$$\gamma_i = \begin{cases} C\frac{\lambda^{(i-3)}e^{-\lambda}}{(i-3)!} & for\ 3 \le i \le 7 \\ 0.2 & for\ i = 2 \end{cases} \qquad (5.9)$$

in which: γ_i describes the proportion of post-infection cases seroconverted to class R_i; λ determines the seroconversion rate to the R_3 to R_7 classes, and C is the normalization constant of the truncated Poisson distribution.

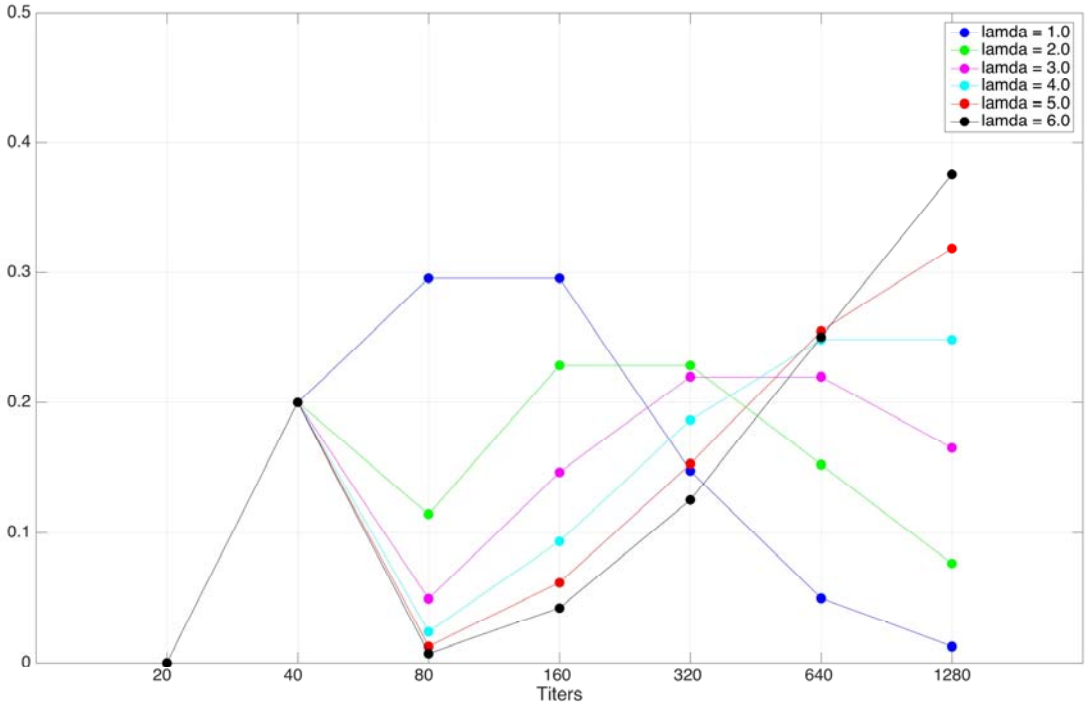

Figure 5.4 Proportion of post-infection titers seroconverted into different R-Classes for different values of λ

5.3.4 Reduced susceptibility

Reduced susceptibility was modeled using a log-logistic function to accurately capture the titer value corresponding to 50% protection, which has important clinical implications:

$$\varepsilon_i = 1 - \frac{1}{1 + \exp\left(\beta * log2\left(\frac{titer_i}{T50}\right)\right)} \qquad for\ 1 \le i \le 7 \quad (5.10)$$

The *T50* parameter corresponds to 50% susceptibility reduction while β is the slope of the tangent line around the inflection point. According to Todd (2016), this *T50* value is around 160.0 for H3N2 subtype for recent infection. Nevertheless, H1N1 infection was known to be less immunogenic compared to H3N2. Titers against H1N1 Pdm 2009 to influenza negative patients were in the range of [80, 160] up to seven

months following ILI onset while geometric means baseline titers for positive and negative influenza cases against H1-09 were around 3.5 (in $\log_2$-units) (Todd 2016). Thus, we used a *T50* value of 80.0 in this analysis. A positive value of β describes the rate at which individuals become susceptible as a function of titer. Parameter β was fixed at 0.5, 1.0, and 1.5 in this analysis.

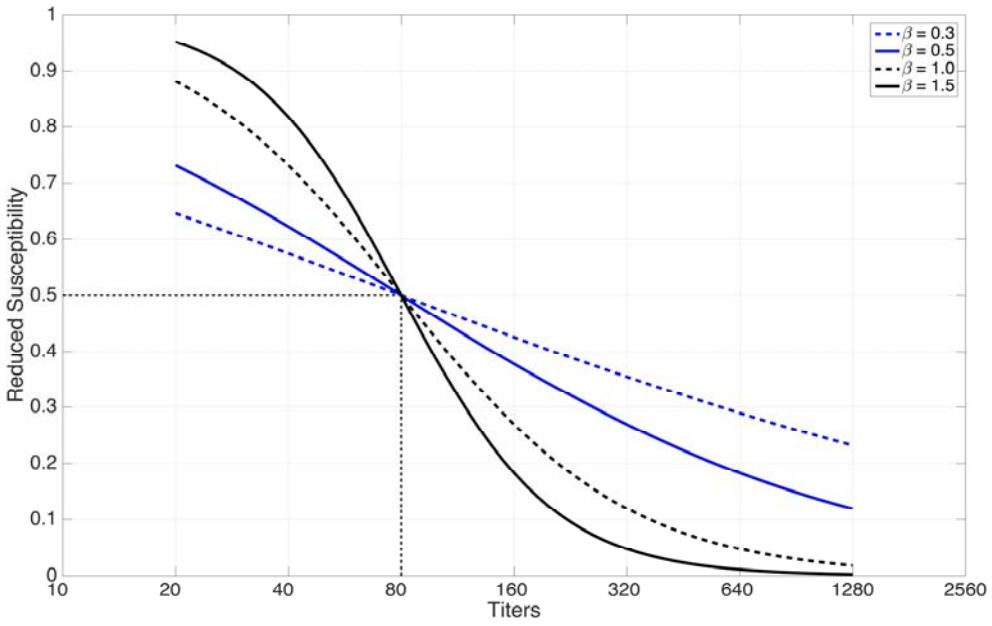

Figure 5.5 Reduced susceptibility as a function of titer values with *T50* = 80.0 and β varies from 0.3 to 1.5

5.3.5 Likelihood framework

Three different functions were used in the likelihood framework. First, I used a simple multinomial framework on the seven titer categories R_1 to R_7 to compare the true and observed distribution of these seven categories in each two-week window. Second, I used a framework where each titer was assumed to be a normally-distributed observation from the model geometric-mean seroprevalence. Between 500 and 1000 titers were evaluated with a likelihood in this procedure.

Third, I used a framework where each titer was assumed to be a gamma-distributed draw from the full-model titer distribution defined by R_1, R_2, ... R_7. All three of these likelihood functions are introduced below. As usual, data were adjusted for age and gender according to the Vietnam Population and Housing Census 2009.

5.3.5.1 Multinomial distribution of discrete titer values

In this analysis, assuming that at a given time point, a sample was drawn from a multinomial distribution with parameters described by the *R*-class populations in (5.1)–(5.6). The likelihood is computed as:

$$\mathcal{L}_1(\boldsymbol{y}|\boldsymbol{\theta},\boldsymbol{x}) = \prod_{j=1}^{n} f_j(\boldsymbol{y}_j|\boldsymbol{p}_j, n_j, x_j)^{\boldsymbol{s}_j} \qquad (5.11)$$

in which: n is the number of time points; n_j is the number of samples at time j; f_j is the probability mass function of a multinomial distribution with parameter $\boldsymbol{p}_j = p_{1,j}, p_{2,j}, .., p_{7,j}$ describing the proportion of each of the seven R-classes at time j from equations (5.1)–(5.6); $\boldsymbol{x} = (x_1, x_2, .., x_n)$ is the bi-weekly incidences vector; $\boldsymbol{y}_j = (y_{1j}, y_{2j}, .., y_{7j})$ is the number of samples in each discrete titer categories at time j, $\boldsymbol{s}_j = s_{1,j}, s_{2,j}, .., s_{7,j}$ is the sample weight vectors to adjust for the age and gender difference between the samples and the housing census data. The log-likelihood was defined according to:

$$-\log\big(\mathcal{L}_1(\boldsymbol{y}|\boldsymbol{\theta},\boldsymbol{x})\big) = -\sum_{j=1}^{n} \boldsymbol{s}_j * log\big(f_j(y_j|\boldsymbol{p}_j, n_j, x_j)\big) \qquad (5.12)$$

Maximum likelihood estimation was carried out using the Nelder-Mead algorithm implemented in Java 8.0 (Apache Commons Math 3.3). Global optima and convergence were accessed by starting at different initial search conditions. About

50 to 100 initial conditions were performed for each search, convergence was assessed by counting the number of times the same minimum was attained with different sets of starting conditions.

5.3.5.2 Normal likelihood of individual titer observations

At a given time point *j*, the weekly incidence vector $\boldsymbol{x}$ are determined by the geometric mean titer GMT_j – computed from the *R*-classes described by equations (5.1) – (5.6). The likelihood is computed as:

$$\mathcal{L}_2(\boldsymbol{y}|\boldsymbol{\theta},\boldsymbol{x}) = \prod_{j=1}^{n}\prod_{k=1}^{n_j} f_j(y_{jk}|\mu_j,\boldsymbol{\theta},\boldsymbol{x})^{s_{ij}} \qquad (5.13)$$

where n is the number of time windows, n_j is the number of samples in time window j, k is the index of an individual sample in time window j, and f_j is the probability density function of a normal distribution:

$$f_j(y_{jk}|\mu_j,\boldsymbol{\theta},\boldsymbol{x}) = \begin{cases} k_j & for\ y_{jk} \le 20 \\ A * N(y_{jk}|\mu_j,\boldsymbol{\theta},\boldsymbol{x}) & otherwise \end{cases} \qquad (5.14)$$

in which: k_j is the proportion of titers 20 at time j; A is the normalization constant; the parameter vector $\boldsymbol{\theta}$ again includes σ, c, and λ, and $\boldsymbol{x} = (x_1, x_2, \ldots, x_n)$ – the bi-weekly incidence vector; and s_{jk} is the sample weight to adjust for the age and gender difference between the sample population and the target population. The log-likelihood was weighted according to:

$$-\log\left(\mathcal{L}_2(\boldsymbol{y}|\boldsymbol{\theta},\boldsymbol{x})\right) = -\sum_{j=1}^{n}\sum_{k=1}^{n_j} s_{jk} * log\left(f_{jk}\left(y_{jk}|\mu_j,\boldsymbol{\theta},\boldsymbol{x}\right)\right) \qquad (5.15)$$

5.3.5.3 Gamma likelihood of individual titer observations

Similar to (5.11) and (5.13), but (5.14) describes f_j as a gamma probability density function instead of a normal distribution.

5.4 Results

Each result will be an inference on $\boldsymbol{x}$, the incidence vector of 22 bi-weekly incidences x_1 to x_{22}, the parameter c determining antibody waning rate, the parameter λ that describes the post-infection titer distribution, and the variance/scale parameter for normal/gamma likelihood function. Note that rather than interpreting the exact numerical values of the maximum likelihood estimates (MLE) of $\hat{c}$ and $\hat{\lambda}$, we will try to understand these inferences in a more intuitive epidemiological form. The parameter c determines how quickly antibodies wane, and it will be presented as the number of months it takes for the first two, three, and four $\log_2$-titer drop. For example, a $\hat{c}$ value of 0.60 corresponds to a waning time of 8.8 months for the first two $\log_2$-titer drops (you could call this the second half-life), 16.5 months for the third $\log_2$-titer drops, and 28.8 months for the fourth $\log_2$-titer drops. In other words, it takes about 2.4 years for a given individual to become 50% susceptible. The parameter λ will be presented using the total fraction of individuals that convert to a titer of at least 160.

Each maximum-likelihood inference on these 24 parameters (for multinomial likelihood function) and 25 parameters (when including the standard deviation/scale parameter for normal/gamma likelihood function) was done for the following scenarios:

- For three different locations (Dak Lak, Kien Giang, and Hue)
- Using three different likelihood functions (multinomial, normal, gamma)
- Assuming four different "birth/death rates" in the population (b)
- Assuming three different susceptibility parameters (β) of 0.5, 1.0, and 1.5

This makes for a total of 324 likelihood inferences. All of them will be presented graphically, some in this section and others at the end of this chapter in Section 5.6.

The birth rate b and the death rate d are adjusted together to keep the population size fixed (N = 1.73 million for Dak Lak, 1.68 million for Kien Giang, and 1.08 million for Hue). However, note that these two parameters describe the rate at which individuals enter and exit the R_1 class. When b and d are both doubled, the population size stays the same but individuals enter the R_1 class twice as quickly. This corresponds to a more rapid immune loss that could be explained by immigration of susceptibles, antigenic drift (in longer-term studies), or some other immunological process. As b and d are adjusted, we are really adjusting the rate at which individuals regain full susceptibility to influenza infection.

The reason that the parameter β was not included in the likelihood search was due to statistical identifiability problem in conjunction with the waning parameter c (Vinh and Boni 2015). When the value of β is high (individuals with high titers are more immune and individuals with lower titers are more susceptible), the post-infection titer distribution (λ) can be shifted to have individuals recover to higher titers, and the waning rates would be quickened as a result. In contrast, when the value of β decreases, the post-infection titer distribution (λ) can be shifted to have

individuals recover to intermediate titers resulting in slower waning rates. All of these parameter manipulation could be done while keeping the likelihood relatively unchanged. For these reasons, β was fixed at 0.5, 1.0, and 1.5, which is within a reasonable range. The optimization was much less sensitive toward changes in values of β compared to changes in c (Table 5.2, 5.4, and 5.6).

Of the three likelihood functions investigated, gamma-distributed titers had higher likelihoods than normally-distributed titers (for all three sites). Only the gamma and normal AICs are comparable because the multinomial likelihood was computed from a probability mass function for an aggregated data set. In other words, the multinomial likelihood is of a different dataset compared to the normal/gamma likelihoods. In the main part of the chapter, the gamma-results are presented since the likelihood was higher than the normal distribution analysis, and no information was lost in data aggregation (as opposed to the case for the multinomial likelihood).

5.4.1 Dak Lak

Dak Lak has the richest dataset (N = 1076) with samples collected from July 1, 2009 to Apr 30, 2010, in which 17 of the 22 two-week windows have at least three samples. Table 5.2 shows the maximum log-likelihoods (as AICs), optimized over 24 parameters – 22 bi-weekly incidences $\mathbf{x}$, 1 waning parameter c, and 1 post-infection seroconversion rate λ – for twelve different scenarios, using three likelihood functions. The titers are better fit by a gamma distribution than a normal distribution, and the gamma/normal fits are not sensitive to the birth/death rates or the shape of the susceptibility curve (β). If we look at the likelihoods in the

multinomial column, we see that a steep susceptibility function (higher β) and higher birth/death rates are more likely (Table 5.2).

Table 5.2 AIC values for the Dak Lak data. Showing Akaike Information Criterion (AIC) for three different functional forms and twelve assumptions about birth/death and susceptibility. The gamma-model in the top row has the lowest AIC, corresponding to a waning inflation rate $\hat{c} = 0.60$ and a post-infection titer conversion rate of $\hat{\lambda} = 4.65$.

d	β	$AIC_{Multinomial}$	AIC_{Normal}	AIC_{Gamma}	AIC_{Gamma}-AIC_{Normal}
0.00004	0.5	558	4180	4144	-36
0.00004	1.0	555	4180	4144	-36
0.00004	1.5	552	4180	4144	-36
0.0001	0.5	555	4180	4144	-36
0.0001	1.0	551	4180	4144	-36
0.0001	1.5	550	4180	4144	-36
0.0002	0.5	553	4180	4144	-35
0.0002	1.0	547	4180	4144	-36
0.0002	1.5	543	4180	4144	-36
0.0003	0.5	551	4180	4144	-36
0.0003	1.0	545	4180	4144	-36
0.0003	1.5	543	4180	4144	-36

5.4.1.1 Inferred antibody waning and post-infection seroconversion rates

Using the gamma distributional form of the likelihood function, the visual fits for the maximum-likelihood estimates of $\mathbf{x}$, c, and λ are shown graphically in Figure 5.6 (refer to Figures 5.13 and 5.14 for the multinomial and normal distribution fits). Table 5.3 shows the waning (parameter c) and post-infection seroconversion estimates (parameter λ) from Figure 5.6.

The inference on the waning pattern was largely unaffected by the value of β or the birth/death rate. The time to drop the first two $\log_2$-titer units was less than 9 months, which is consistent with the few estimates of antibody waning rates looking at the short term antibody dynamics against H1-09 strains following natural

infections (Angkasekwinai et al. 2013; Hung et al. 2010; Ng et al. 2013; Todd 2016). The time for a titer to drop to almost naïve status (PM titers of 80 corresponds to 50% susceptibility) was less than 3 years, which is consistent with estimates of how often individuals become re-infected with influenza (Kucharski et al. 2015; Grilli, Davies, and Smith 1986).

Inferred post-infection seroconversion rates indicate that about 80% of individuals seroconverted to titers of at least 160 which corresponds to a susceptibility range of [18%, 38%] depending on values of β, and about 30-45% of cases seroconverted to a titer values of 1280. These results are consistent with results from an independent cohort study of H1N1 infections which showed that 86% of individuals seroconverted to titers of at least 160 and 30% seroconverted to titers of 1280 following natural infections (Todd 2016).

Table 5.3 Inferred antibody waning and post-infection seroconversion patterns for Dak Lak using gamma likelihood function

d (day^{-1})	β	c	Ab waning time (months)		λ	Post-infection seroconversion proportion	
			two $\log_2$-units	50% susceptible		titers ≥160	titers ≥1280
0.00004	0.5	0.60	8.8	28.8	4.65	0.78	0.30
0.00004	1.0	0.52	8.6	26.1	7.33	0.80	0.44
0.00004	1.5	0.54	8.6	26.8	4.82	0.79	0.31
0.0001	0.5	0.59	8.8	28.6	6.80	0.80	0.41
0.0001	1.0	0.55	8.6	26.9	7.74	0.80	0.45
0.0001	1.5	0.52	8.6	26.1	4.87	0.79	0.31
0.0002	0.5	0.53	8.6	26.3	7.17	0.80	0.43
0.0002	1.0	0.53	8.6	26.2	7.23	0.80	0.43
0.0002	1.5	0.54	8.6	26.8	4.70	0.79	0.30
0.0003	0.5	0.67	9.0	31.3	3.88	0.77	0.24
0.0003	1.0	0.54	8.6	26.5	6.74	0.80	0.41
0.0003	1.5	0.55	8.6	26.9	4.78	0.79	0.30

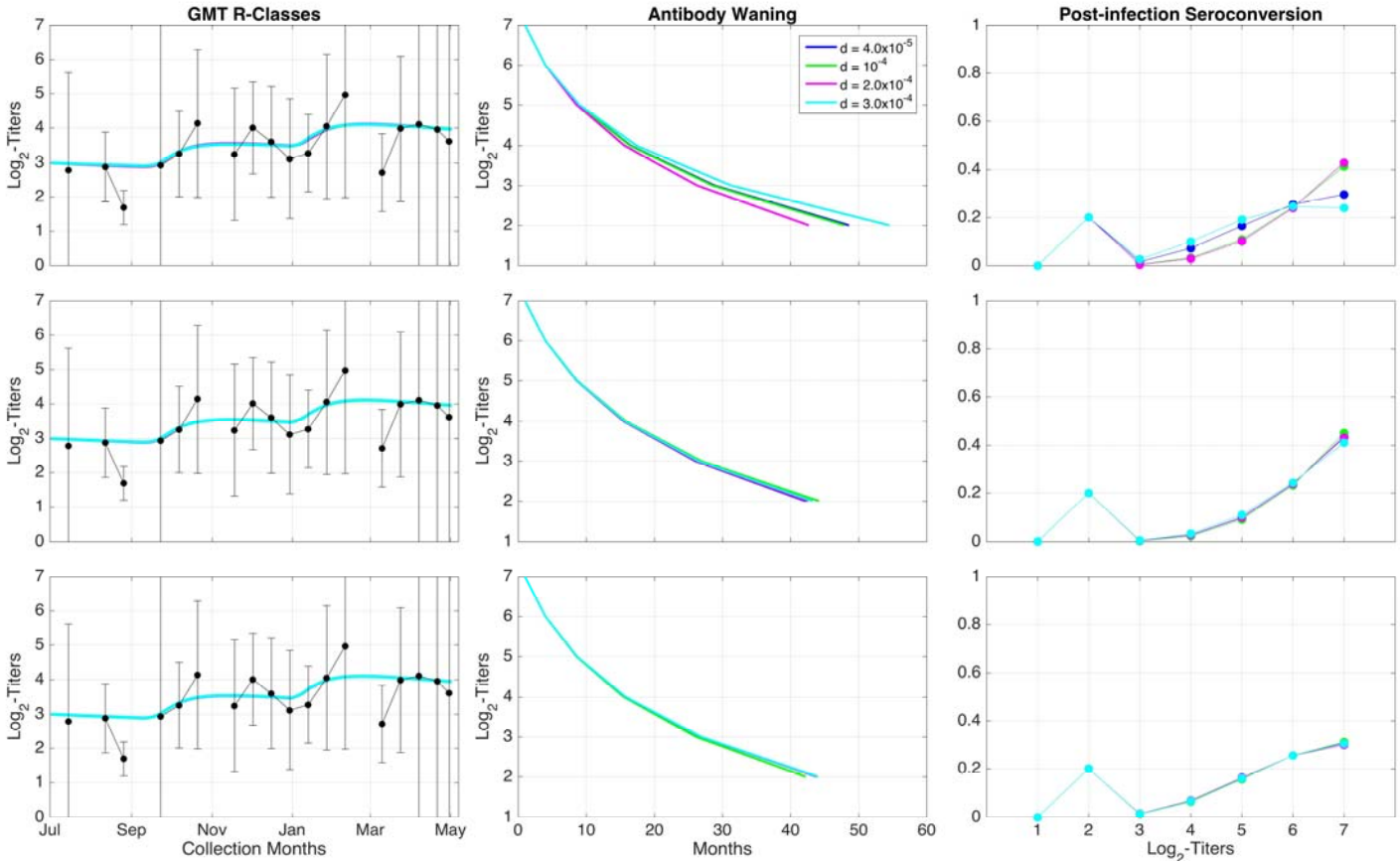

Figure 5.6 Optimization results for **Dak Lak** using the gamma likelihood function. Showing results for different birth/death rates (four colors) d = 4×10^{-5} to 3×10^{-4} (days^{-1}) and three different reduced susceptibility curves β=0.5 (top row), β=1.0 (middle row), and β=1.5 (bottom row) from July 2009 to May 2010. In the first column, black dots are time series GMT from the data and lines are GMT of the seven R-classes from the model. In the third column, y-axis shows fraction seroconverted to a given log$_2$-titer post-infection. Optimization results for normal and multinomial distributions are shown in Figure 5.13 and 5.14.

5.4.1.2 Inferred biweekly incidence vs. sentinel data

Figure 5.7 shows the inferred seroincidence plotted against the sentinel data using the gamma likelihood for different birth/death rates and β. The blue color dots show the corresponding bi-weekly seroincidence estimates, i.e. the number of individuals that were infected in each two-week window from July 2009 to April 2010. Clearly, the likelihood optimization has pulled the estimates into a region of parameter space where all the infections took place during two short time periods. The MLEs for x_6 (period between September 9 and 22, 2009) and x_{14} (period between Dec 30, 2009 and Jan 12, 2010) are much higher than for the other weekly incidence parameters, giving a picture of an epidemic that arrived and caused massive infection in two short two-week bursts. While the general timing of these peaks makes sense (media reports showed the pandemic spreading nationwide in September 2009 (Hien et al. 2010)), it is of course unlikely that all infection took place during a single two-week period. The fact that this is represented a single short-wave of seroconversion (300,000 cases in two weeks) is likely an artefact of an incompletely constructed likelihood function which currently does not take the temporal correlation of seroincidence into account. If a temporal auto-correlation parameter were to be introduced (see discussion), this picture would likely be "smoothed out". The occurrence of these two peaks is consistent between different choices of likelihood functions (Figure 5.15 and 5.16). When comparing the inferred seroincidence $\boldsymbol{x}$ to influenza data collected through Vietnam's sentinel surveillance system, the biggest difference is the two-peak pattern present in the seroincidence and the one-peak pattern observed in the sentinel data.

Both the sentinel data and the inferred seroincidence supported a late-August to early-October wave of influenza infections. The seroincidence estimates corresponded to about 300,000 infections during this first wave, which for Dak Lak would be approximately a 18.4% attack rate. The sentinel data showed no further influenza 2009 H1N1 activity after November 2009, but the seroincidence showed a second wave of infection in January 2010, corresponding to about 540,000 infections, or a 31.2% attack rate. The fact that sentinel and seroincidence peaks of the first wave line up in the exact same two-week windows lends credence to the belief that the first seroincidence peak corresponds to a true wave of seroconversion that occurred after the September-October wave of 2009 H1N1 passed through Dak Lak province in Vietnam. The second seroincidence peak, if real, suggests that the pandemic moved through Vietnam in two distinct waves: one that was recorded in the sentinel surveillance system and one that was not. This second, silent wave of infection may correspond to a wave of asymptomatic or subclinical infections that – either due to low severity or a perceived lower importance ascribed to the pandemic by 2010 – did not cause a wave of influenza reporting to Dak Lak provincial hospital in January 2010. Using a normal (Figure 5.14) or multinomial (Figure 5.13) likelihood function, we also observe two seroincidence waves, although the multinomial inference points to two peaks with much smaller magnitudes.

If true, this would be a major finding in influenza epidemiology: that influenza virus can cause completely asymptomatic waves of infection. I will use the data assembled at two other sites, Hue and Kien Giang, as further support for this hypothesis.

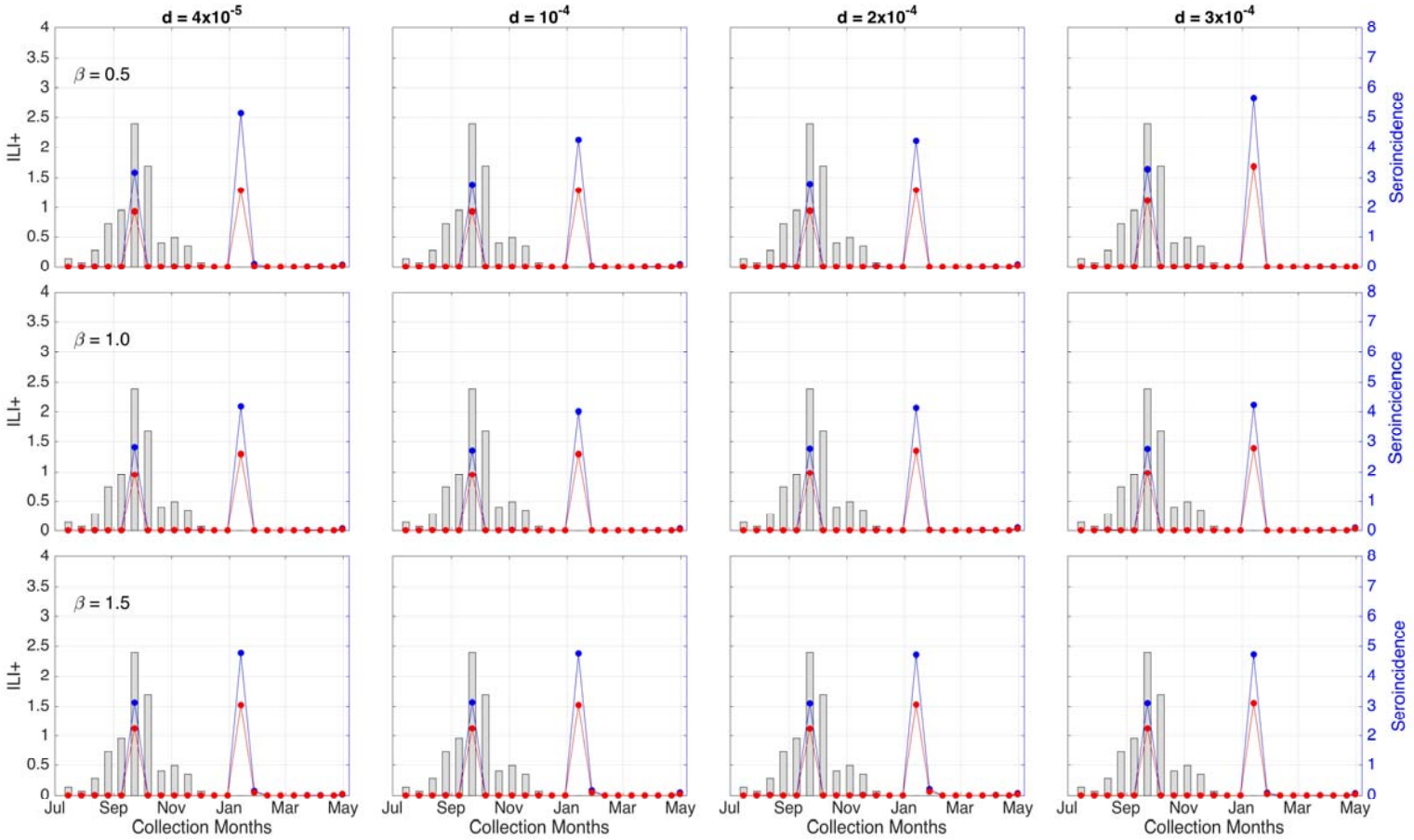

Figure 5.7 Comparing biweekly seroincidence from **Dak Lak** using gamma likelihood function to sentinel data. Showing results for different birth/death rates (four columns) and different reduced susceptibility curves (three rows of figures). Blue dots represent bi-weekly incidence $\times 10^5$ (right y-axis), red dots represent first infections only $\times 10^5$ (right y-axis); and grey bars show number of bi-weekly ILI+ cases from sentinel data (left y-axis). Bi-weekly incidences for normal and multinomial distributions are shown in Figure 5.15 and 5.16.

5.4.2 Kien Giang

The Kien Giang dataset has 560 samples (N=560) collected from Jul 1, 2009 to Apr 30, 2010 in which only 11 of the 22 bi-weekly windows have at least 3 samples. Similar to Dak Lak, the gamma likelihood has a lower AIC than the normal likelihood (Table 5.4); the gamma/normal fits are not sensitive to the birth/death rates or the shape of the susceptibility curve (β), and the multinomial is sensitive to both. Even though the minimum LLH was achieved at death rate = 0.0003 or 0.0001 and β = 1.5, the change in AIC is not significant across different death rates and different β.

Table 5.4 AIC values for Kien Giang data. Showing Akaike Information Criterion (AIC) value for 36 models (three different functional forms and twelve assumptions about birth/death and susceptibility). AIC for multinomial is not comparable to the AICs for normal/gamma models. The gamma-model in the last row has the lowest AIC corresponding to a waning inflation rate of $\hat{c} = 1.495$ and a post-infection titer distribution rate of $\hat{\lambda} = 1.304$.

d	β	$AIC_{Multinomial}$	AIC_{Normal}	AIC_{Gamma}	AIC_{Gamma}-AIC_{Normal}
0.00004	0.5	624	1288	1246	-43
0.00004	1.0	612	1288	1245	-43
0.00004	1.5	604	1289	1245	-44
0.0001	0.5	623	1290	1246	-44
0.0001	1.0	613	1288	1245	-43
0.0001	1.5	606	1288	1244	-44
0.0002	0.5	623	1292	1246	-46
0.0002	1.0	612	1290	1245	-44
0.0002	1.5	605	1290	1245	-45
0.0003	0.5	624	1288	1246	-42
0.0003	1.0	612	1291	1245	-46
0.0003	1.5	604	1290	1244	-46

5.4.2.1 Inferred antibody waning and post-infection seroconversion rates

The waning and seroconversion estimates for the gamma likelihood are presented in Table 5.5. Consistent with the results from Dak Lak, the short term antibody dynamics, i.e. the time it takes to lose two $\log_2$-titer units, was less than one year. Nevertheless, the time it takes to become 50% susceptible was about 6.5–7 years, which is about 50% longer than the waning estimates from Dak Lak. Again, given the duration of the SSE dataset as well as the number of missing data points for Kien Giang, the estimate for the complete waning dynamics should be interpreted with caution.

Table 5.5 Inferred antibody waning and post-infection seroconversion patterns for Kien Giang using gamma distribution

d (day^{-1})	β	c	Ab waning time (months)		λ	Post-infection seroconversion proportion	
			two $\log_2$-units	50% susceptible		titers ≥160	titers ≥1280
0.00004	0.5	1.49	11.47	76.46	1.28	0.58	0.03
0.00004	1.0	1.50	11.50	77.12	1.34	0.59	0.03
0.00004	1.5	1.49	11.47	76.50	1.24	0.57	0.02
0.0001	0.5	1.50	11.50	77.10	1.27	0.57	0.02
0.0001	1.0	1.50	11.49	76.83	1.24	0.57	0.02
0.0001	1.5	1.50	11.50	77.12	1.26	0.57	0.02
0.0002	0.5	1.50	11.50	77.11	1.29	0.58	0.03
0.0002	1.0	1.50	11.49	76.82	1.25	0.57	0.02
0.0002	1.5	1.50	11.49	76.93	1.22	0.56	0.02
0.0003	0.5	1.50	11.50	77.12	1.28	0.58	0.03
0.0003	1.0	1.50	11.49	76.80	1.27	0.57	0.02
0.0003	1.5	1.49	11.48	76.74	1.30	0.58	0.03

Comparing to the estimates from Dak Lak, the proportion of seroconversions to titers 1280 was significantly lower. Unlike Dak Lak, both the waning and seroconversion estimates for Kien Giang vary with the choice of the likelihood function. We will further discuss this in Section 5.5.

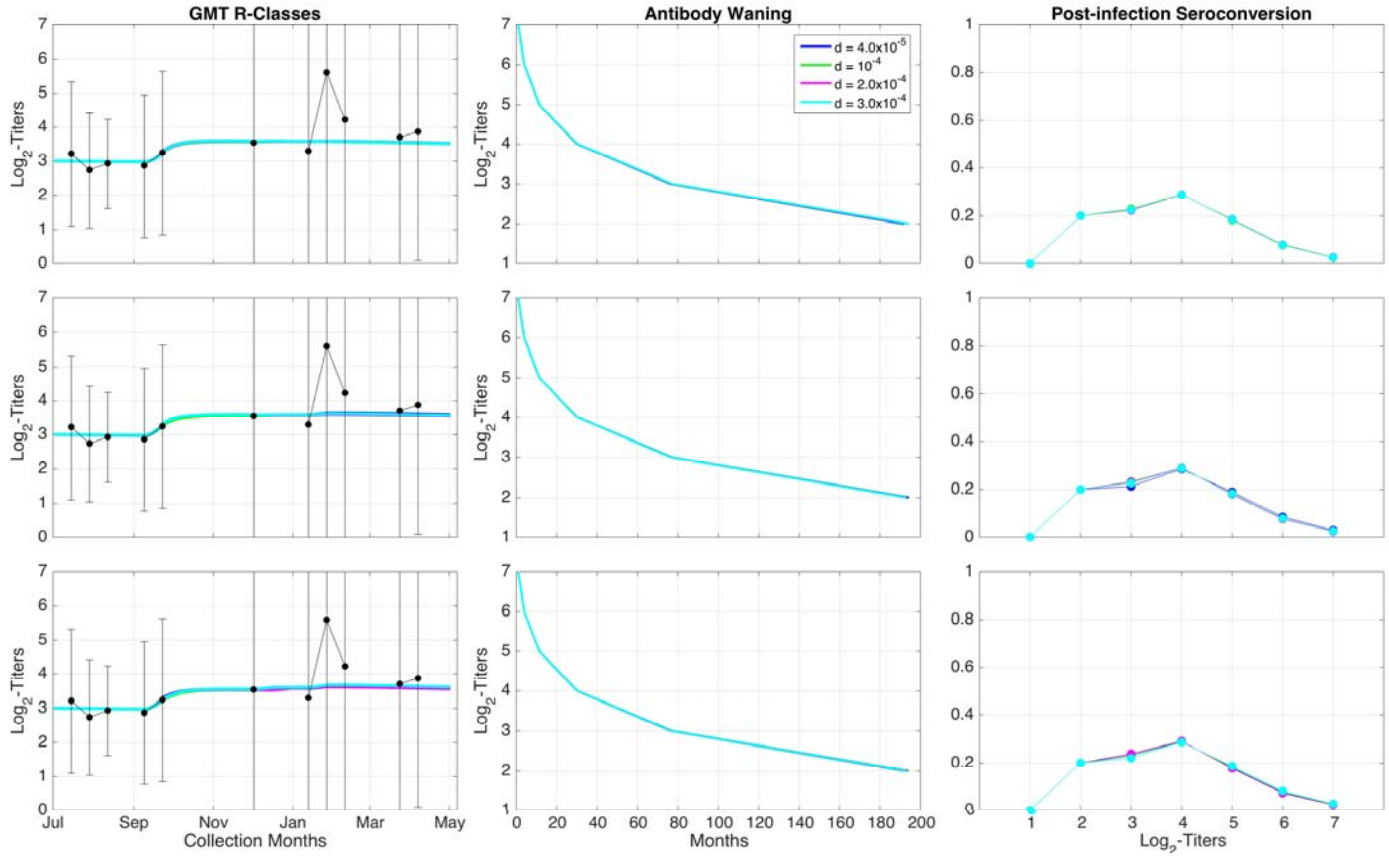

Figure 5.8 Optimization results for **Kien Giang** using gamma likelihood function. Showing results for different birth/death rates (four colors) d = 4×10^{-5} to 3×10^{-4} (days^{-1}) and three different reduced susceptibility curves β=0.5 (top row), β=1.0 (middle row), and β=1.5 (bottom row) from July 2009 to May 2010. In the first column, black dots are time series GMT from the data and lines are GMT of the seven R-classes from the model. In the third column, y-axis shows fraction seroconverted to a given log$_2$-titer post-infection. Optimization results for normal and multinomial distributions are shown in Figure 5.17 and 5.18

5.4.2.2 Inferred biweekly incidence vs. sentinel data

Similar to the Dak Lak results, Figure 5.9 shows two sharp incidence peaks for Kien Giang when all the infections took place (September and December/January). Nevertheless, the existence of the second peak in December/January is not certain and its magnitude is sensitive to the assumed death rates. The reason for this is that during the three-month period from October to January, there was only one two-week time-window containing data; a high degree of missingness in October and November created uncertainty as to the bi-weekly incidence inferences in September and October. However, the timing of the peak in September again gave us confidence that this is the right approach as the SSE peak was estimated independently of the sentinel data, yet this peak coincided with the peak from sentinel data (Figure 5.9). In the period from late-August to early-October, an estimated seroincidence of 800,000 cases occurred, which corresponded to an attack rate of 47.6% during the first wave. The second wave was broken down into smaller peaks, with a total estimate of about 370,000 cases occurring from early December to late February which amounted to an attack rate of 22.0%.

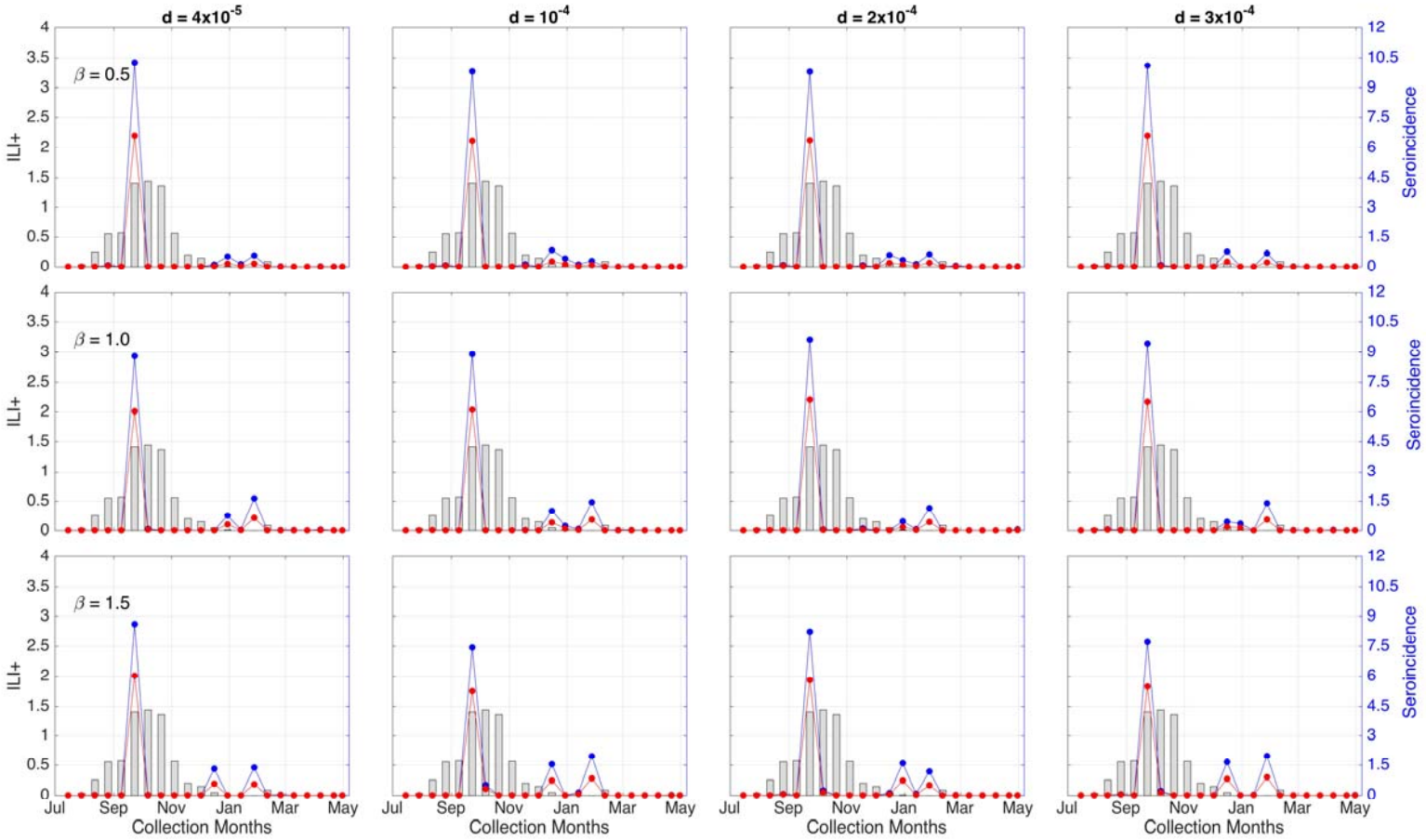

Figure 5.9 Comparing biweekly seroincidence from **Kien Giang** using gamma likelihood function to sentinel data. Showing results for different birth/death rates (four columns) and different reduced susceptibility curves (three rows of figures). Blue dots represent bi-weekly incidence $\times 10^5$ (right y-axis), red dots represent first infections only $\times 10^5$ (right y-axis); and grey bars show number of bi-weekly ILI+ cases from sentinel data (left y-axis). Bi-weekly incidences for normal and multinomial distributions are shown in Figure 5.19 and 5.20.

5.4.3 Hue

The dataset for Hue also had its drawbacks, even though there were a total of 1023 samples (N = 1023), only 11 of the 22 bi-weekly windows have at least three samples from July 1, 2009 to April 30, 2010. Maximum likelihood of gamma, normal, and multinomial distribution fits are shown in Figure 5.10, 5.21 and 5.22, respectively. Consistent with the behavior observed from Dak Lak and Kien Giang, the gamma distribution had lower AIC than the normal (Table 5.6), and the gamma/normal fits were not sensitive to the birth/death rates or the shape of the susceptibility curve (β) as the multinomial was.

Table 5.6 AIC values for Hue data. Showing Akaike Information Criterion (AIC) value for 36 models (three different likelihood functional forms and twelve assumptions about birth/death and susceptibility). AIC for multinomial is not comparable to the AICs for normal/gamma models. The gamma-model in with death rate = 0.0001 (day^{-1}) and β = 1.0 has the lowest AIC corresponding to a waning inflation rate of $\hat{c} = 0.35187$ and a post-infection titer distribution rate of $\hat{\lambda} = 2.7015$.

d	β	$AIC_{Multinomial}$	AIC_{Normal}	AIC_{Gamma}	AIC_{Gamma}-AIC_{Normal}
0.00004	0.5	-8270	4010	3970	-40
0.00004	1.0	-8277	4010	3969	-41
0.00004	1.5	-8280	4010	3969	-41
0.0001	0.5	-8269	4010	3971	-39
0.0001	1.0	-8276	4010	3969	-41
0.0001	1.5	-8280	4010	3969	-40
0.0002	0.5	-8268	4010	3970	-40
0.0002	1.0	-8276	4010	3969	-41
0.0002	1.5	-8280	4010	3970	-40
0.0003	0.5	-8267	4010	3970	-40
0.0003	1.0	-8275	4010	3970	-40
0.0003	1.5	-8280	4010	3969	-41

5.4.3.1 Inferred antibody waning and post-infection seroconversion rates

Quite consistent to the estimates for Dak Lak, the time it takes to lose the first two $\log_2$-titer units was about 9 months and the proportion of recovered cases seroconverting to titers of at least 160 and 1280 was about 70-80% and 10-40%, respectively.

Table 5.7 Inferred antibody waning and post-infection seroconversion patterns for Hue using gamma likelihood function

d (day^{-1})	β	c	Ab waning time (months)		λ	Post-infection seroconversion proportion	
			two $\log_2$-unit	50% susceptible		titers ≥160	titers ≥1280
0.00004	0.5	0.54	8.62	26.65	5.06	0.79	0.32
0.00004	1.0	0.40	8.20	22.30	2.37	0.72	0.11
0.00004	1.5	0.37	8.12	21.55	3.28	0.76	0.19
0.0001	0.5	0.24	7.71	17.99	6.04	0.79	0.38
0.0001	1.0	0.35	8.06	20.95	2.70	0.74	0.14
0.0001	1.5	0.21	7.62	17.23	3.59	0.77	0.22
0.0002	0.5	0.39	8.16	21.93	3.41	0.76	0.20
0.0002	1.0	0.41	8.24	22.67	2.41	0.72	0.11
0.0002	1.5	0.21	7.64	17.45	3.97	0.78	0.25
0.0003	0.5	0.39	8.16	21.94	7.60	0.80	0.45
0.0003	1.0	0.23	7.68	17.73	3.42	0.76	0.20
0.0003	1.5	0.42	8.26	22.90	2.99	0.75	0.16

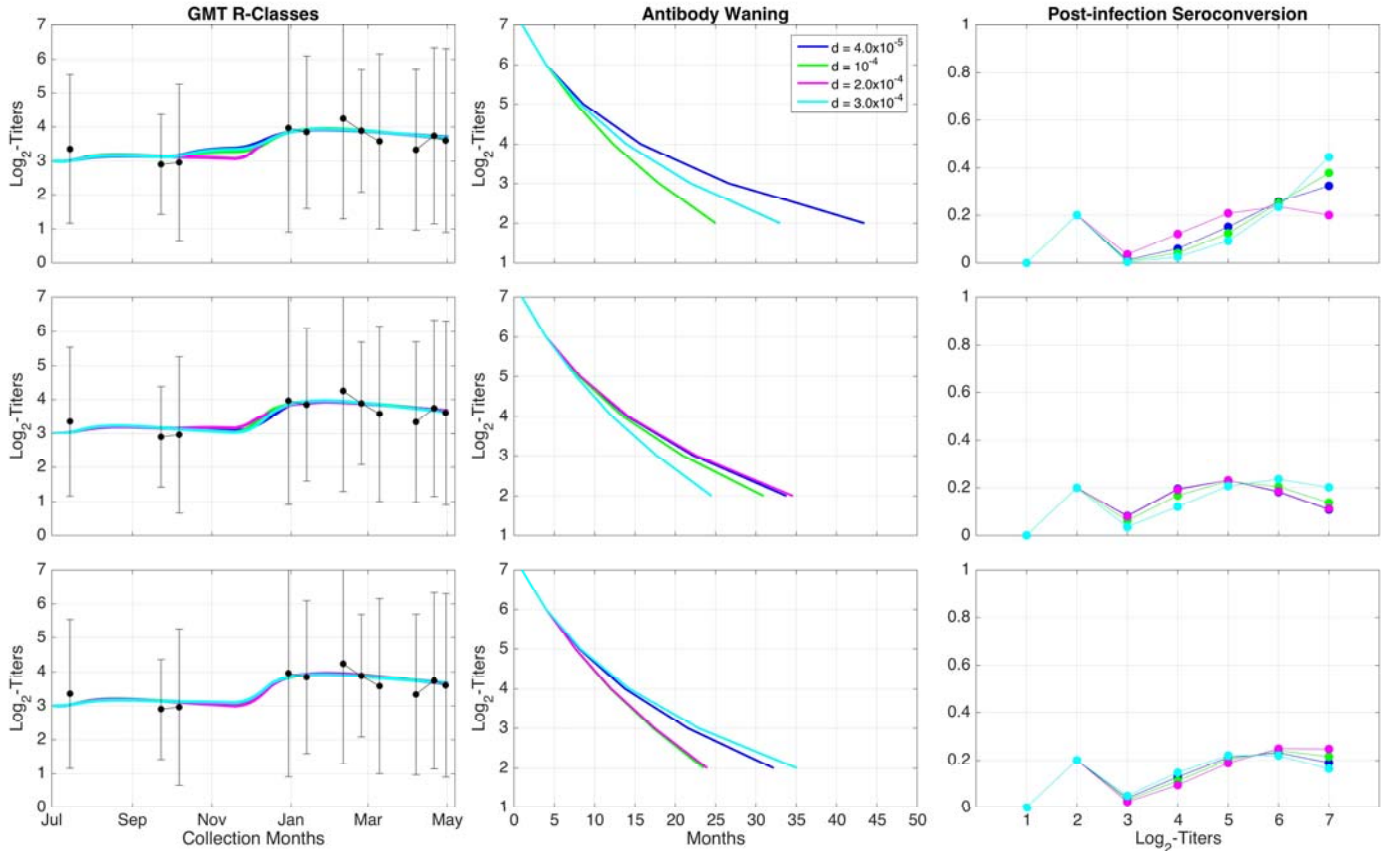

Figure 5.10 Optimization results for **Hue** using gamma likelihood function. Showing results for different birth/death rates (four colors) d = 4×10^{-5} to 3×10^{-4} (days^{-1}) and three different reduced susceptibility curves β=0.5 (top row), β=1.0 (middle row), and β=1.5 (bottom row) from July 2009 to May 2010. In the first column, black dots are time series GMT from the data and lines are GMT of the seven R-classes from the model. In the third column, y-axis shows fraction seroconverted to a given $\log_2$-titer post-infection. Optimization results for normal and multinomial distributions are shown in Figure 5.21 and 5.22 in appendix.

5.4.3.2 Inferred biweekly incidence vs. sentinel data

One interesting feature is that even though the change in AIC is not significant across different death rates and stiffness of the reduced susceptibility functions, the timing and magnitudes of the peaks are very different from one another. The gamma fit with the smallest AIC gives an estimated total incidence of about 640,000 cases corresponding to an AR of 59.8% that started in early November and ended in December. Unfortunately, there was too much missingness in the serological data, from late July until December 2009, to get any accurate inference on the seroincidence during this period. This may be the reason that the first peak in Hue is identified as having occurred later than the peaks in Dak Lak or Kien Giang. Interestingly, the sentinel data from Hue did show a little influenza activity in early 2010, even though the Dak Lak and Kien Giang data did not show this.

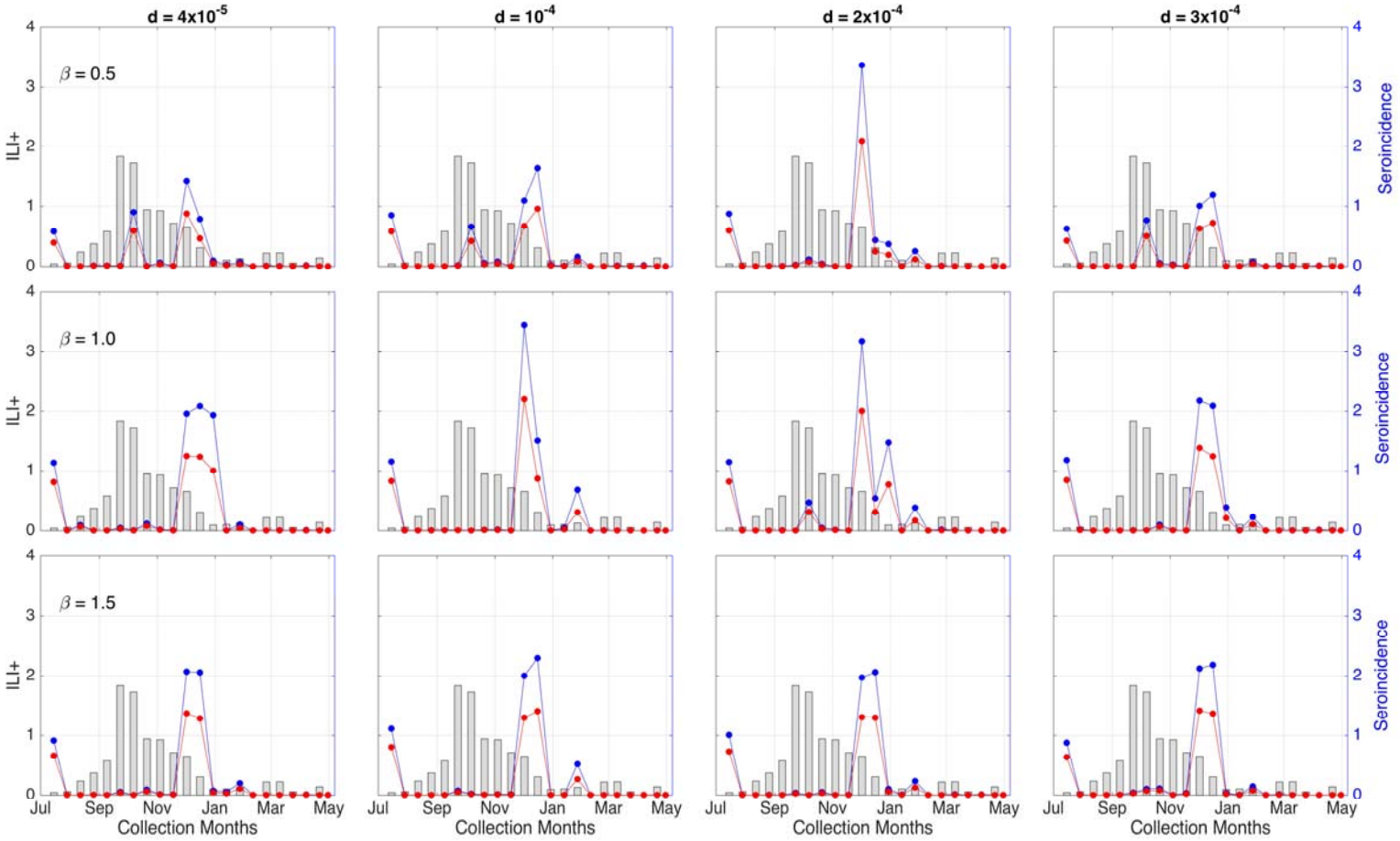

Figure 5.11 Comparing biweekly seroincidence from **Hue** using gamma likelihood function to sentinel data. Showing results for different birth/death rates (four columns) and different reduced susceptibility curves (three rows of figures). Blue dots represent bi-weekly incidence $\times 10^5$ (right y-axis), red dots represent first infections only $\times 10^5$ (right y-axis); and grey bars show number of bi-weekly ILI+ cases from sentinel data (left y-axis). Bi-weekly incidences for normal and multinomial distributions are shown in Figure 5.23 and 5.24.

5.5 Discussion

In most epidemiological analyses, antibody titers are treated as discrete values to signify presence or absence of antibody against an influenza virus of interest, using a predefined titer cut-off for seropositivity. In this analysis, taking advantage of the informative microarray assay results, individual titer values were viewed as continuous quantities coming from different R_i-classes in a dynamical model, with titer values sampled from an R_i-class according to a normal or gamma distribution. The hybrid dynamical model developed in this chapter allowed me to describe a free epidemic pattern of influenza transmission using biweekly incidence parameters for the period from July 1, 2009 to April 30, 2010, for three different provinces in southern Vietnam. The primary motivation of this work was to address the specific shortcoming in Chapter 3 that intermediate titers could be the result of either recent infection or waning.

As a first step to analyze these SSE data, I studied the simultaneous visualization of the biweekly geometric mean titer (GMT) time series from SSE data and the biweekly ILI+ cases from sentinel data either as aggregated data or stratified by age groups to see if changes in reported incidence corresponded to changes in antibody titer (Figure 5.24). This simple visualization showed a peak in sentinel data from September to November 2009 and a corresponding titer increase in Dak Lak and Kien Giang about four weeks later. Unfortunately, this titer increase could not be seen in Hue due to highly non-uniform sample collection at this hospital during the initial phase of the study. One additional notable feature was the presence of another

GMT titer rise from January to March 2010, across all three sites, which was clearly not captured by the sentinel data.

The three crucial processes in reconstructing the dynamics of a given SSE data set are antibody waning rate as a function of time, susceptibility reduction as a function of titer, and the post-infection seroconversion distribution. Since the first two processes are not separately identifiable (Vinh and Boni 2015), and the model was less sensitive to changes in reduced susceptibility (Table 5.2, 5.4, and 5.6), the stiffness of the reduced susceptibility curve (β) was fixed at reasonable values to perform inference on the other two processes and the time series seroincidence.

The waning parameter c was presented in the form of "time to lose the first two $\log_2$-titer units", which includes the fast waning phase shortly following an infection and the time for an individual to become 50% susceptible. Despite differences in numerical values of c, the estimated time for a seroconverted individual to lose the first two $\log_2$-titer units was consistently less than 12 months across all three sites (Table 5.3, 5.5, and 5.7). Numerous clinical studies were conducted to observe the short-term antibody dynamics following natural infection with the H1-09 strain. More than 70% of seroconverted individuals were able to maintain a protective level of antibody for at least six months (Angkasekwinai et al. 2013; Todd 2016; Hung et al. 2010) and possibly up to one year or slightly longer (Sridhar et al. 2015; Waldman et al. 1970; Liu et al. 2012; Delabre et al. 2015). Some studies observed a two-fold titer decrease within four months (Ng et al. 2013; Hung et al. 2010) to one year (Todd 2016). The long-term dynamics are yet to be fully described due to the short durations of follow-up in these studies. The time for an

individual patient to become 50% susceptible varied between 2.5 and 7 years for different sites. Since the SSE dataset was only ten months long, the long-term waning estimates were indeed a mathematical result of the chosen antibody waning function, and were less reliable compared to the short-term dynamics. Nevertheless, these long-term waning dynamics were still in agreement with the literature's results on how often individuals become infected with influenza (Weibel et al. 1970; Kucharski et al. 2015; Grilli, Davies, and Smith 1986).

The proportion of recovered individuals that seroconverted to titers ≥160 varied between 60% and 80% among the three sites, while the proportion seroconverting to titers ≥1280 varied between 2% and 40%. Due to a large number of missing time windows in Hue and Kien Giang, I will only try to interpret results from Dak Lak. These results are quite consistent with results from an independent clinical study that looked at confirmed H1N1 patients using the same PM test (Todd 2016). In this clinical study, the proportion of individuals seroconverting to titers ≥160 was 86% while 30% seroconverted to titers ≥1280. The reason for the difference in waning rates and seroconversion rates observed among the three collection sites may have been caused by differences in demography since waning and seroconversion are known to depend on age and exposure history (Lessler et al. 2012; Kucharski et al. 2015; Fonville et al. 2014; Todd 2016). Indeed, a closer inspection of Figure 5.24 revealed different age-stratified GMT time series patterns across sites suggesting that these different age groups contributed differently to the infection waves. Additional analyses were performed to check the sensitivity of the results to different values of ω – the number of days it takes for an individual to lose

one $\log_2$-titer unit without inflation – and I was able to confirm that the estimates of waning and seroconversion did not depend strongly on ω (Table 5.8).

Seroincidence from the general-population serum collections was estimated independently of any knowledge of the sentinel system's reported incidence, and a correspondence between these two time series was observed. The occurrence of the first wave of the 2009 pandemic from September to October 2009 was easy to see in both the Dak Lak and Kien Giang serological patterns. For Hue, we essentially had no samples collected in this period to infer the incidence during the first wave. For the second wave, the timing was fairly consistent between Dak Lak and Hue, but not in Kien Giang, again due to missing data. The proportion of primary influenza (infections in individuals with no immune memory of H1N1 influenza) during the first wave was higher than that during the second wave, most obviously in Dak Lak (Figure 5.7). Had the sample collection been more uniform in time, the inference for Hue and Kien Giang would have been more conclusive on this topic. Hue has almost the same number of samples as Dak Lak; but the timing of sample collection was really poor during the second half of 2009 (before the official study protocol was correctly implemented). One way to improve the inference for Hue is to look at bi-monthly incidence instead of bi-weekly incidence. This is not guaranteed to help, but perhaps it should be tried.

Even though this hybrid dynamic model was developed to address some of the shortcomings of the *ad hoc* analysis in Chapter 4, there are still some important mechanisms that were not accounted for including differences in waning and seroconversion rates for different age groups, failure to account for original antigenic

sin, and cross-reaction. Since the H1N1 Pdm 2009 virus does not cross react with the 1977-lineage H1N1, and since through 2015 there were no significant antigenic changes between the pandemic strain and the subsequent H1N1 seasonal strains, the main area of concern for cross-reaction would be infections in individuals older than 52 years of age (born before 1957) who would have been exposed to the 1918-lineage of H1N1 influenza which does cross-react, in a predictable way, with the 2009 H1N1 virus.

It is important to keep in mind that even though the seroincidence and the reported sentinel incidence should be correlated quantitatively, it is unrealistic to expect the two datasets to align perfectly with each other. In addition to the unknown age structure of the sentinel data, its sample size was relatively small, and the hospital reporting patterns at the sentinel sites have not been described at length. Nevertheless, the serological results showed that there were likely two waves of the 2009 influenza pandemic in Vietnam, with only one of these identified in the national sentinel surveillance. This is not the first time that serological data showed different results from sentinel data. Falkenhorst et al. 2012 reported a strong disagreement between the seroincidence and the reported incidences for *Salmonella*. If the serological results represent the true epidemic behavior of the 2009 pandemic, a silent wave of influenza passed through the country and was unnoticed by the sentinel surveillance system. This could be a major finding for serological surveillance as this work was set up as a test case to assess whether population-level serological data could be used to monitor influenza activity in the community in southern Vietnam. At the moment, the major question is how believable these types

of results are – i.e. results that rely on serology only – and perhaps the next important area of research will include the development of an independent validation method for this type of inference.

Adding in a temporal auto-correlation parameter for the bi-weekly incidence estimates may be the best way to avoid the appearance of the sharp seroincidence peaks inferred in this chapter. Joint likelihood inference for all three sites would be helpful in order to obtain the same age-dependent waning and seroconversion parameters across the sites, and it would improve the confidence in these estimates since they would depend on three times as many data points. In general, statistical uncertainty will need to be assessed in this inference (either with likelihood profiles or a Bayesian approach). I did not attempt this in the first pass of this analysis as a single inference on 24 parameters was already very computationally expensive. Chapter 6 contains what I believe are the next important directions for this line of seroincidence estimation.

5.6 Additional Figures

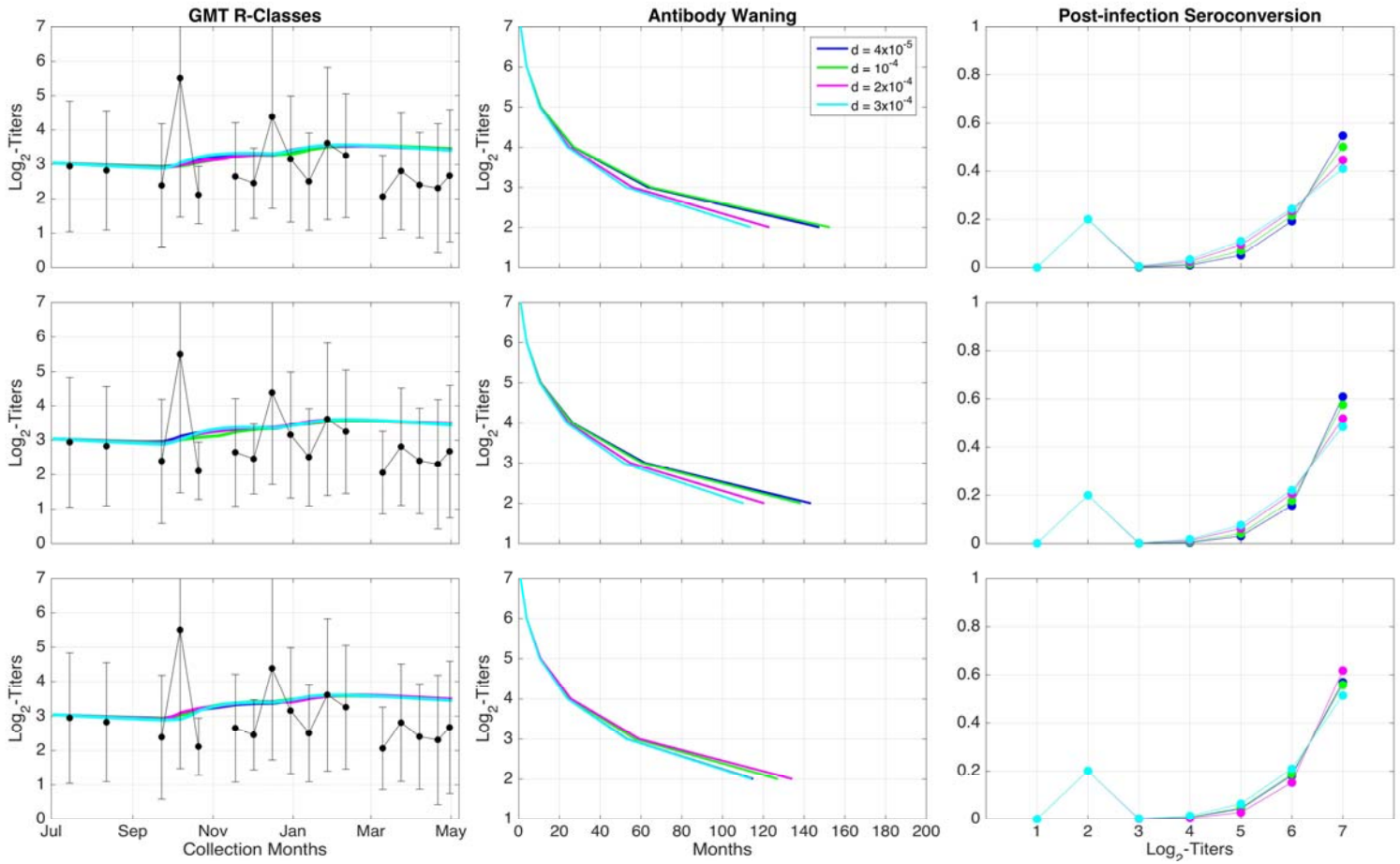

Figure 5.12 Optimization results for **Dak Lak** using multinomial likelihood function. Showing results for different birth/death rates (four colors) d = 4×10^{-5} to 3×10^{-4} (days^{-1}) and three different reduced susceptibility curves β=0.5 (top row), β=1.0 (middle row), and β=1.5 (bottom row) from July 2009 to May 2010. In the first column, black dots are time series GMT from the data and lines are GMT of the seven R-classes from the model. In the third column, y-axis shows fraction seroconverted to a given log$_2$-titer post-infection.

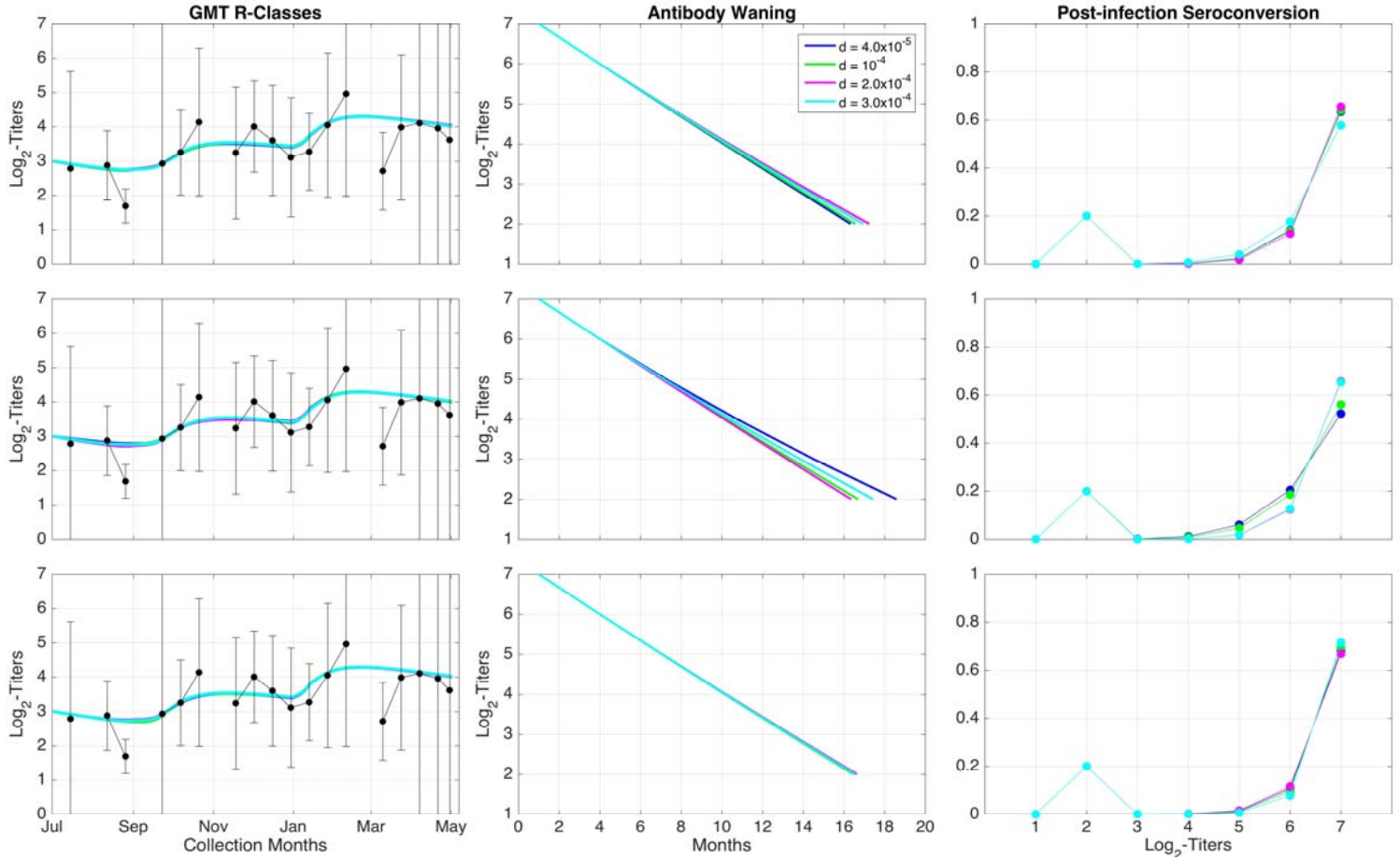

Figure 5.13 Optimization results for **Dak Lak** using normal likelihood function. Showing results for different birth/death rates (four colors) d = 4×10^{-5} to 3×10^{-4} (days^{-1}) and three different reduced susceptibility curves β=0.5 (top row), β=1.0 (middle row), and β=1.5 (bottom row) from July 2009 to May 2010. In the first column, black dots are time series GMT from the data and lines are GMT of the seven R-classes from the model. In the third column, y-axis shows fraction seroconverted to a given log$_2$-titer post-infection.

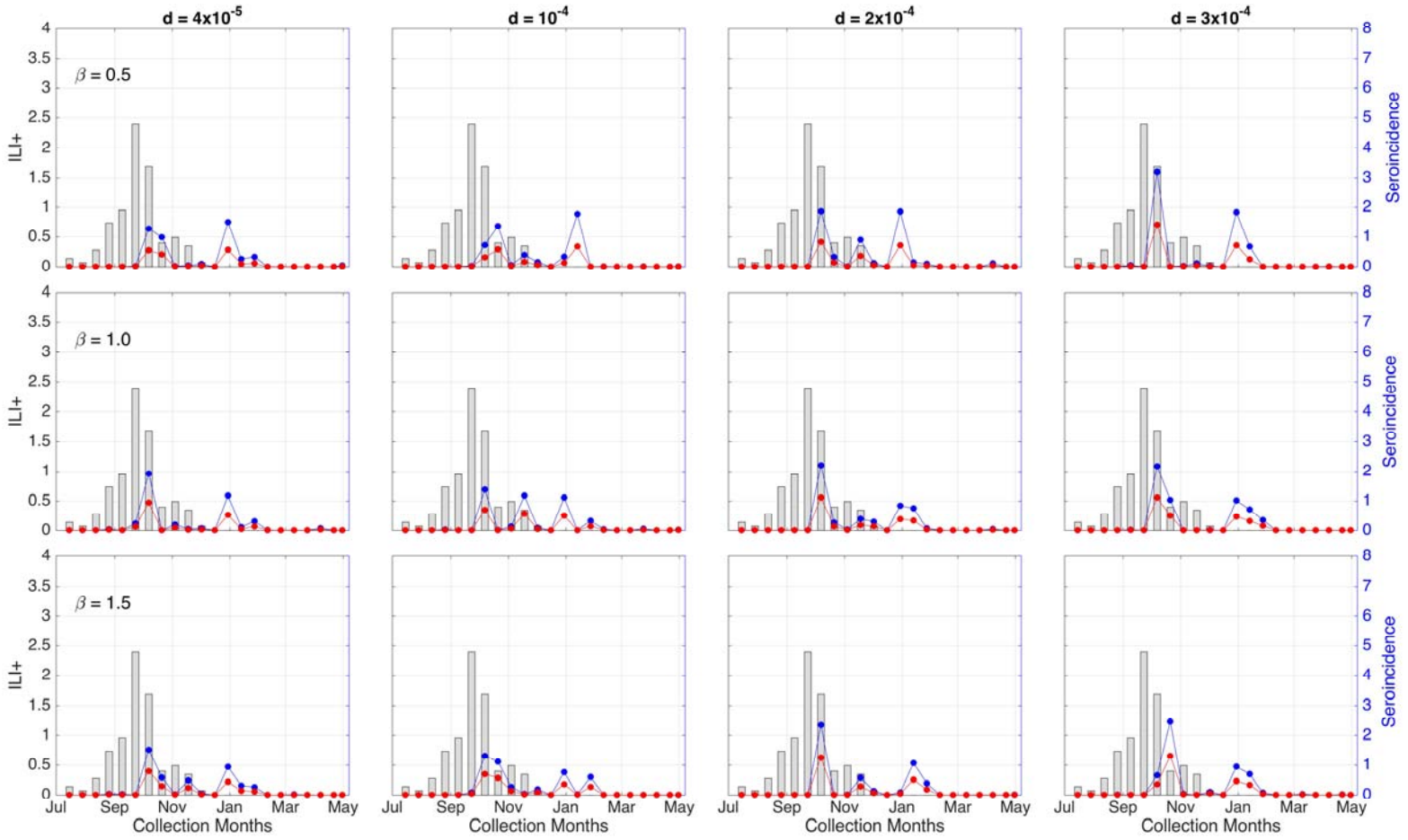

Figure 5.14 Comparing biweekly seroincidence from **Dak Lak** using multinomial likelihood function to sentinel data. Showing results for different birth/death rates (four columns) and different reduced susceptibility curves (three rows of figures). Blue dots represent bi-weekly incidence $\times 10^5$ (right y-axis), red dots represent first infections only $\times 10^5$ (right y-axis); and grey bars show number of bi-weekly ILI+ cases from sentinel data (left y-axis).

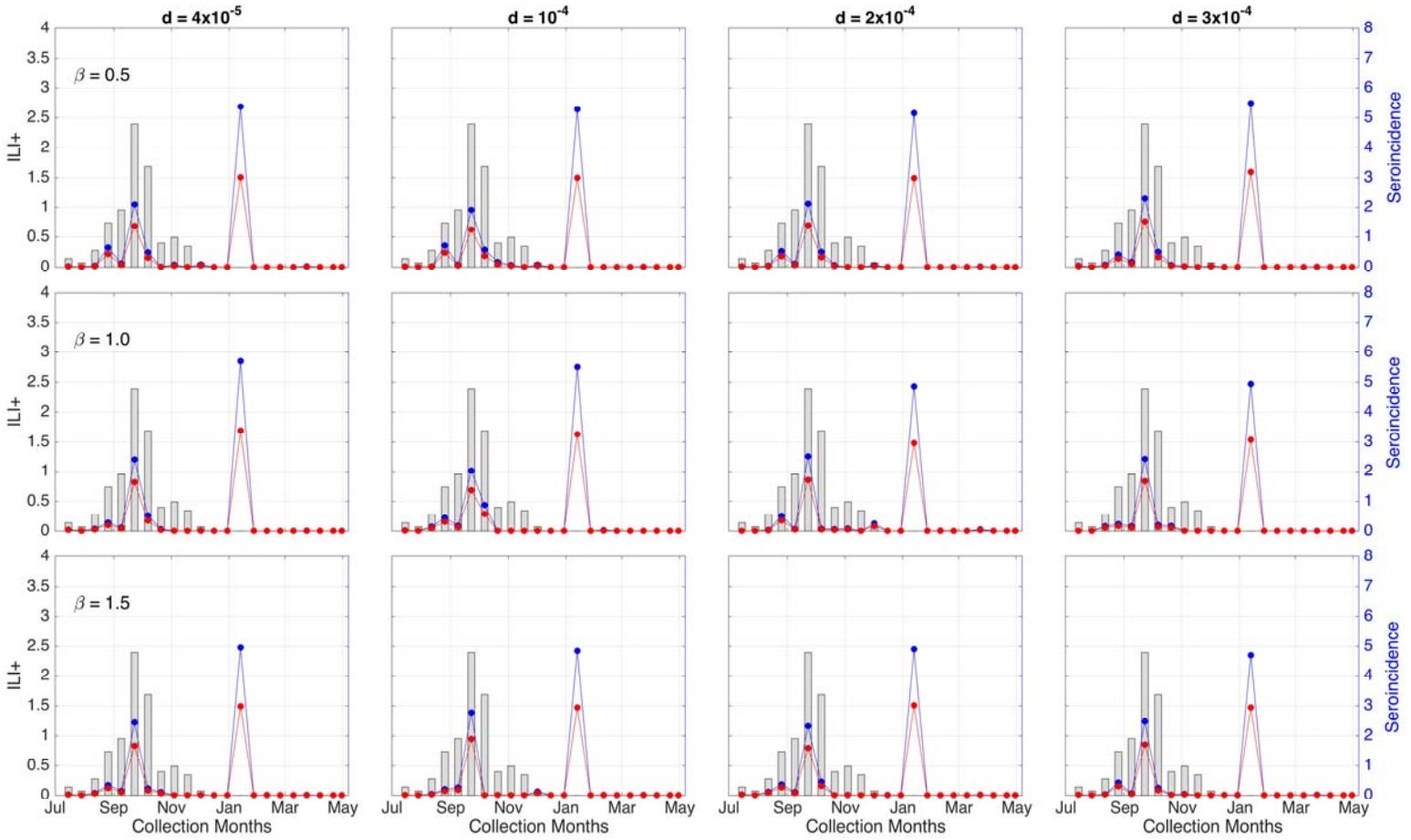

Figure 5.15 Comparing biweekly seroincidence from **Dak Lak** using normal likelihood function to sentinel data. Showing results for different birth/death rates (four columns) and different reduced susceptibility curves (three rows of figures). Blue dots represent bi-weekly incidence $\times 10^5$ (right y-axis), red dots represent first infections only $\times 10^5$ (right y-axis); and grey bars show number of bi-weekly ILI+ cases from sentinel data (left y-axis).

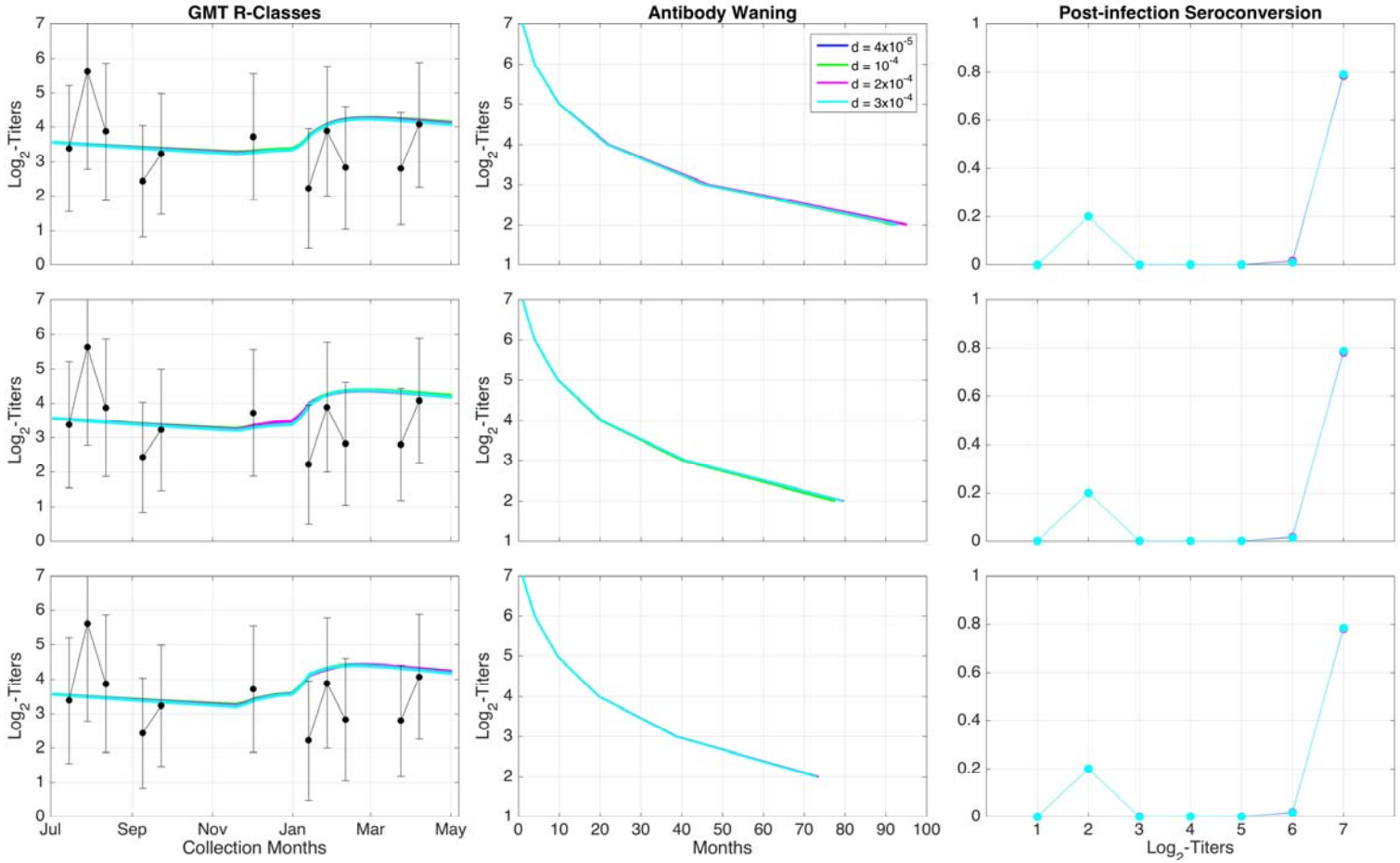

Figure 5.16 Optimization results for **Kien Giang** using multinomial likelihood function. Showing results for different birth/death rates (four colors) d = 4×10^{-5} to 3×10^{-4} (days^{-1}) and three different reduced susceptibility curves β=0.5 (top row), β=1.0 (middle row), and β=1.5 (bottom row) from July 2009 to May 2010. In the first column, black dots are time series GMT from the data and lines are GMT of the seven R-classes from the model. In the third column, y-axis shows fraction seroconverted to a given log$_2$-titer post-infection.

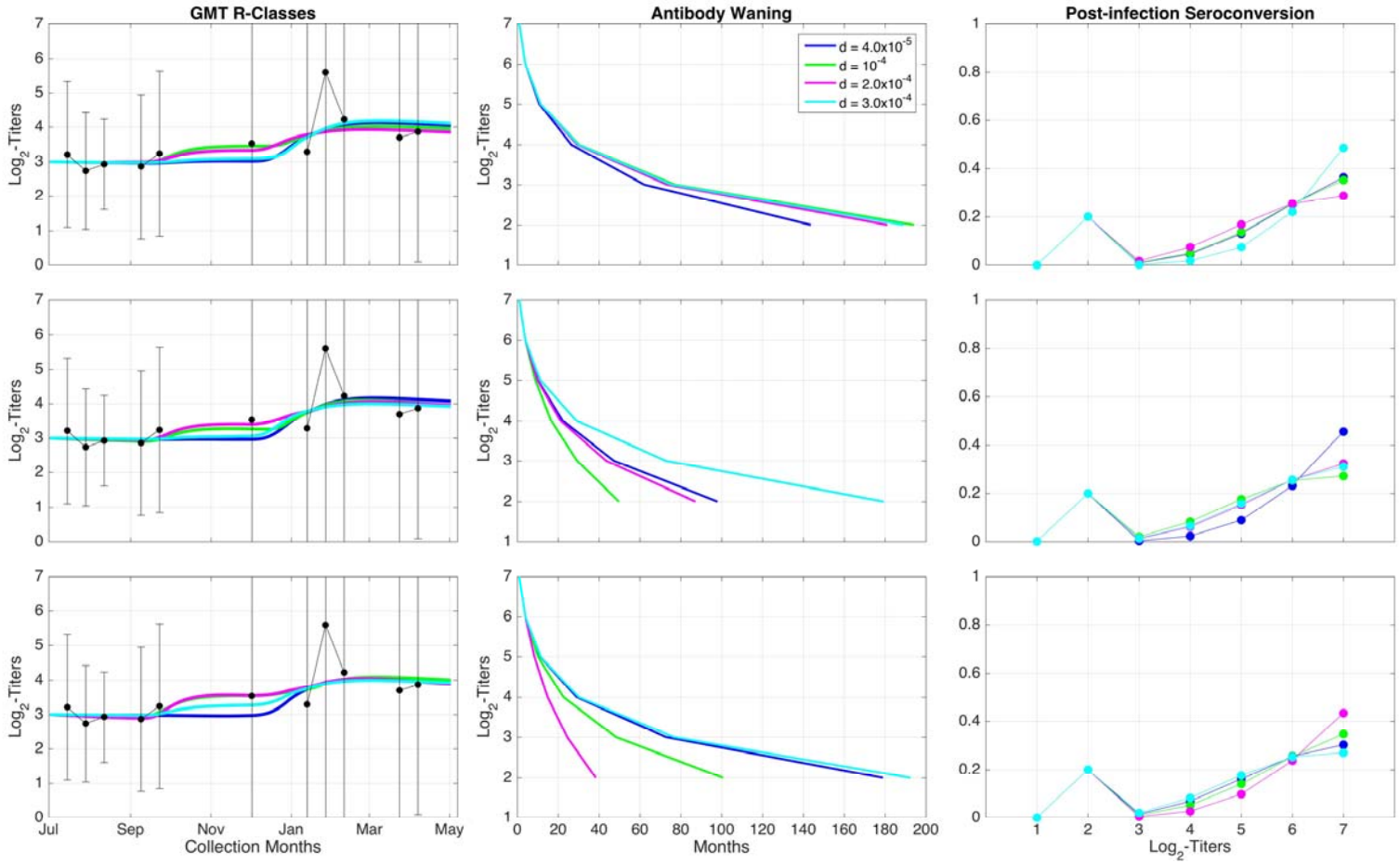

Figure 5.17 Optimization results for **Kien Giang** using normal likelihood function. Showing results for different birth/death rates (four colors) d = 4×10^{-5} to 3×10^{-4} (days^{-1}) and three different reduced susceptibility curves β=0.5 (top row), β=1.0 (middle row), and β=1.5 (bottom row) from July 2009 to May 2010. In the first column, black dots are time series GMT from the data and lines are GMT of the seven R-classes from the model. In the third column, y-axis shows fraction seroconverted to a given log$_2$-titer post-infection.

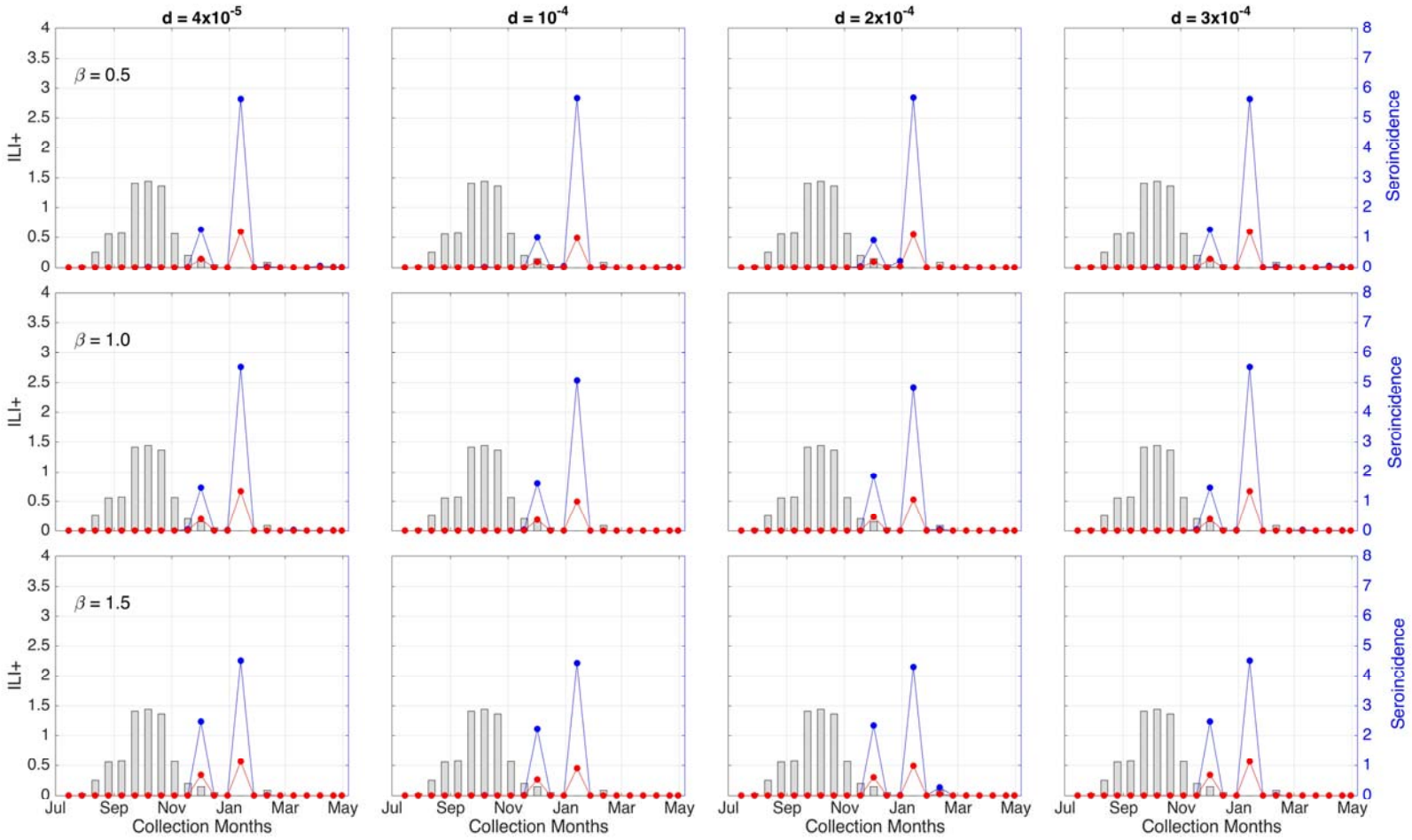

Figure 5.18 Comparing biweekly seroincidence from **Kien Giang** using multinomial likelihood function to sentinel data. Showing results for different birth/death rates (four columns) and different reduced susceptibility curves (three rows of figures). Blue dots represent bi-weekly incidence $\times 10^5$ (right y-axis), red dots represent first infections only $\times 10^5$ (right y-axis); and grey bars show number of bi-weekly ILI+ cases from sentinel data (left y-axis).

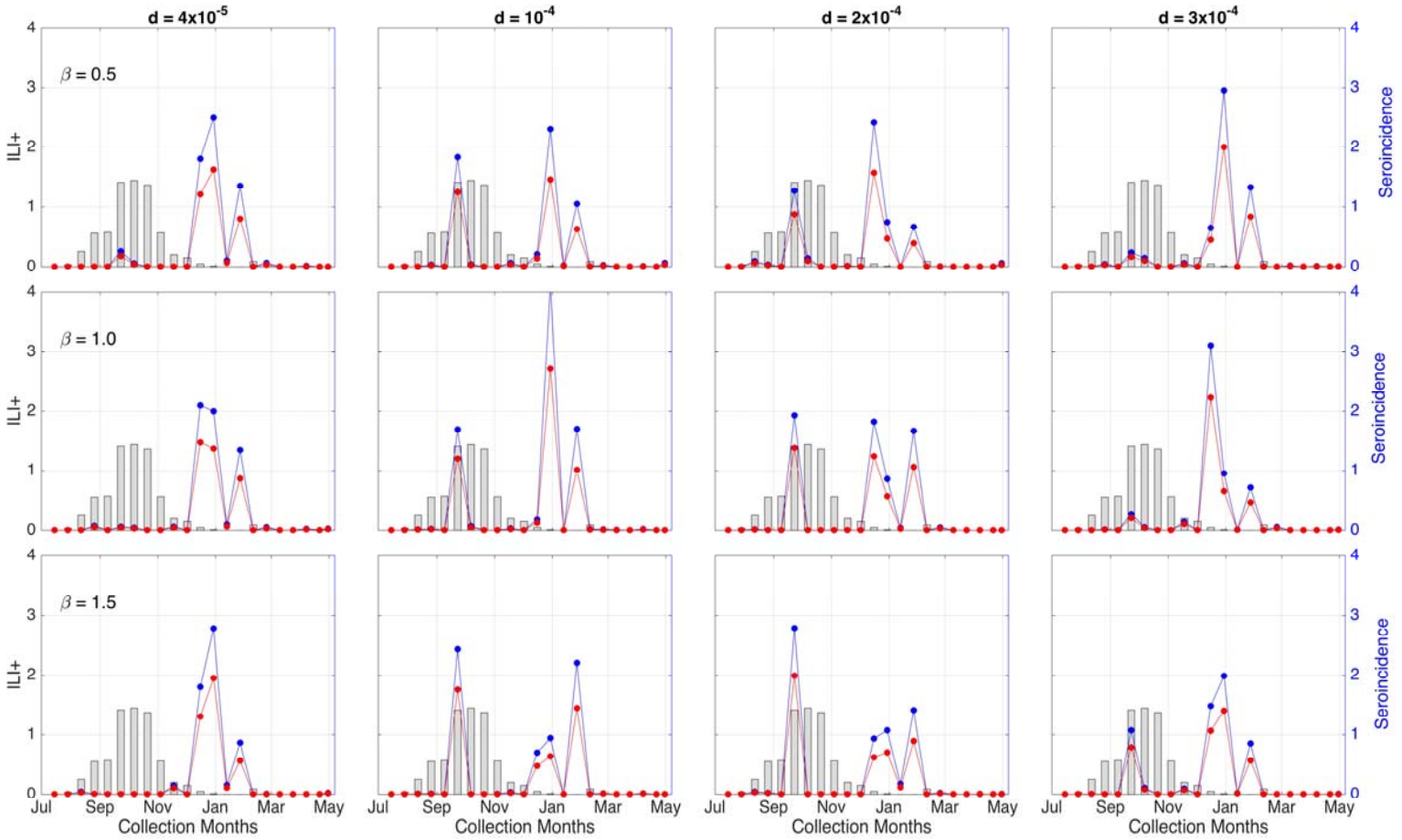

Figure 5.19 Comparing biweekly seroincidence from **Kien Giang** using normal likelihood function to sentinel data. Showing results for different birth/death rates (four columns) and different reduced susceptibility curves (three rows of figures). Blue dots represent bi-weekly incidence $\times 10^5$ (right y-axis), red dots represent first infections only $\times 10^5$ (right y-axis); and grey bars show number of bi-weekly ILI+ cases from sentinel data (left y-axis).

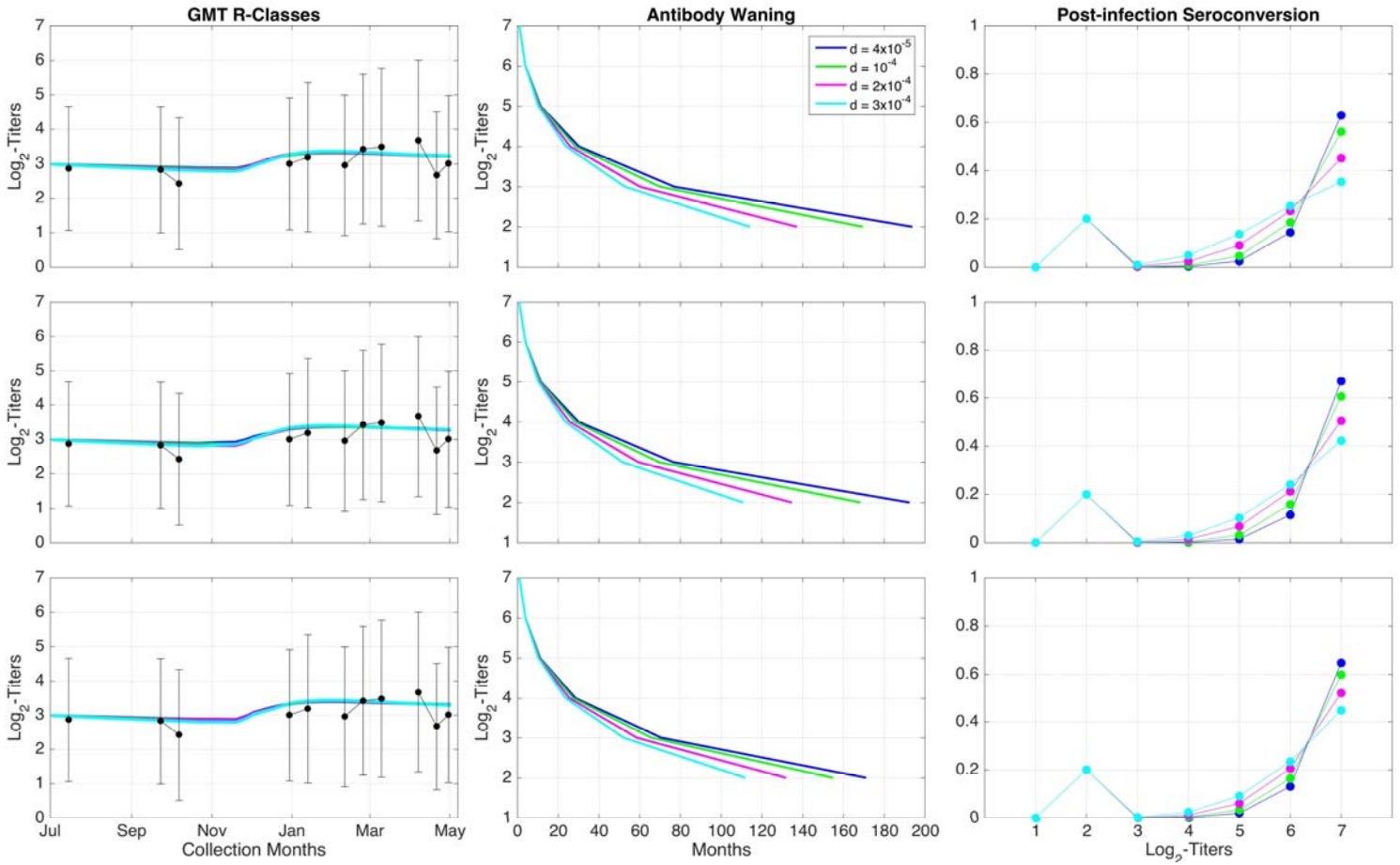

Figure 5.20 Optimization results for **Hue** using multinomial likelihood function. Showing results for different birth/death rates (four colors) d = 4×10^{-5} to 3×10^{-4} (days^{-1}) and three different reduced susceptibility curves β=0.5 (top row), β=1.0 (middle row), and β=1.5 (bottom row) from July 2009 to May 2010. In the first column, black dots are time series GMT from the data and lines are GMT of the seven R-classes from the model. In the third column, y-axis shows fraction seroconverted to a given log$_2$-titer post-infection.

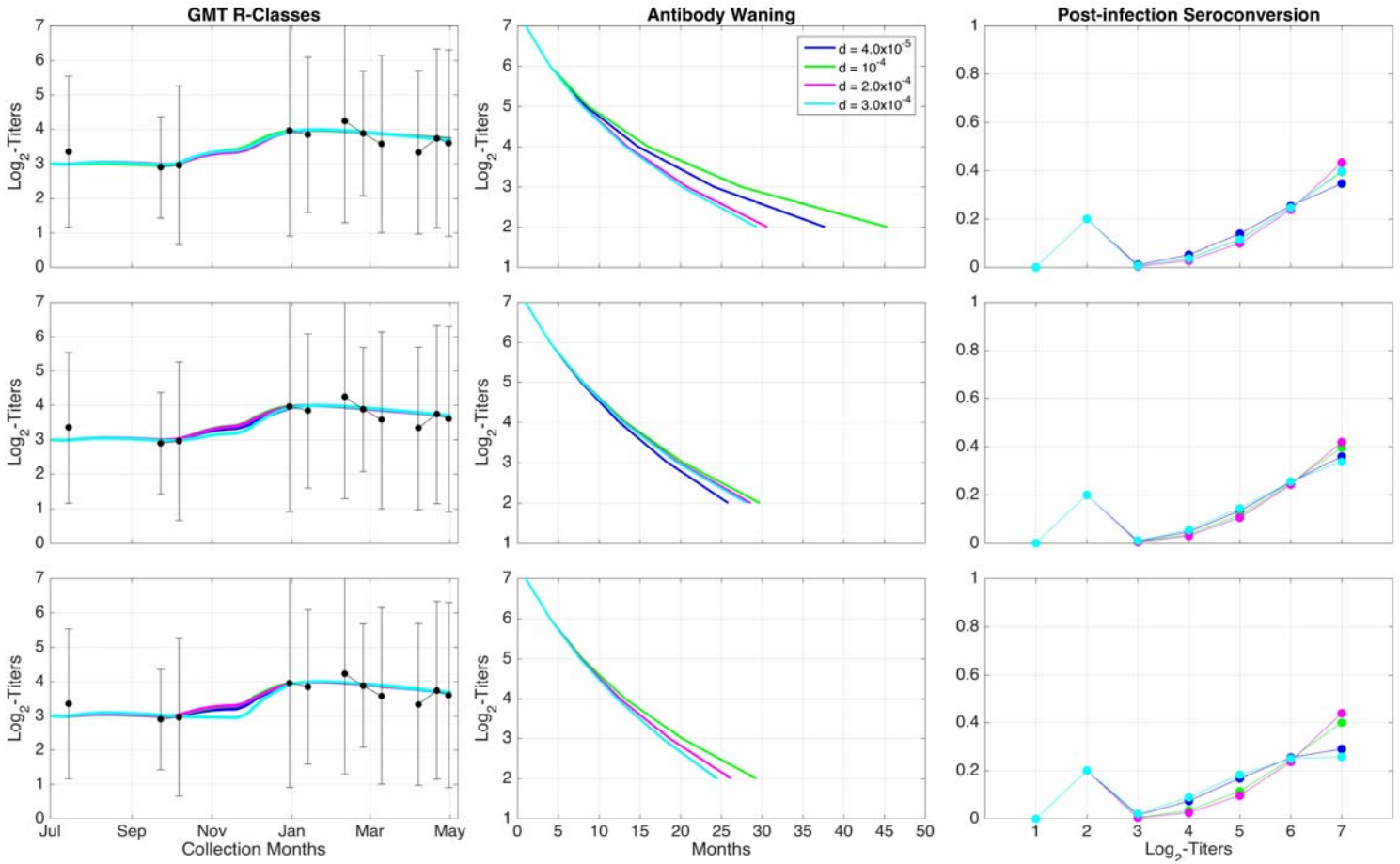

Figure 5.21 Optimization results for **Hue** using normal likelihood function. Showing results for different birth/death rates (four colors) d = 4×10^{-5} to 3×10^{-4} (days^{-1}) and three different reduced susceptibility curves β=0.5 (top row), β=1.0 (middle row), and β=1.5 (bottom row) from July 2009 to May 2010. In the first column, black dots are time series GMT from the data and lines are GMT of the seven R-classes from the model. In the third column, y-axis shows fraction seroconverted to a given log$_2$-titer post-infection.

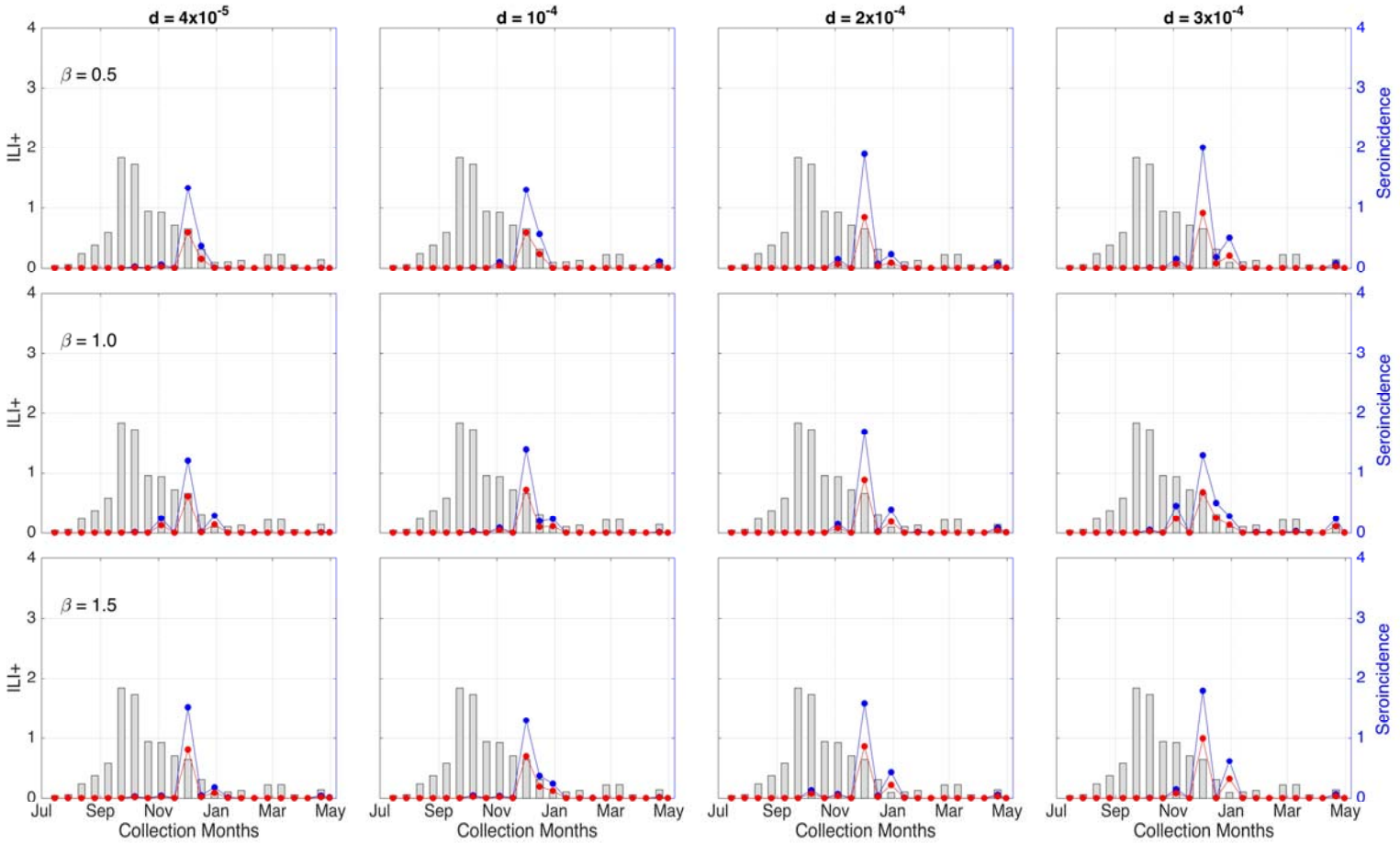

Figure 5.22 Comparing biweekly seroincidence from **Hue** using multinomial likelihood function to sentinel data. Showing results for different birth/death rates (four columns) and different reduced susceptibility curves (three rows of figures). Blue dots represent bi-weekly incidence $\times 10^5$ (right y-axis), red dots represent first infections only $\times 10^5$ (right y-axis); and grey bars show number of bi-weekly ILI+ cases from sentinel data (left y-axis).

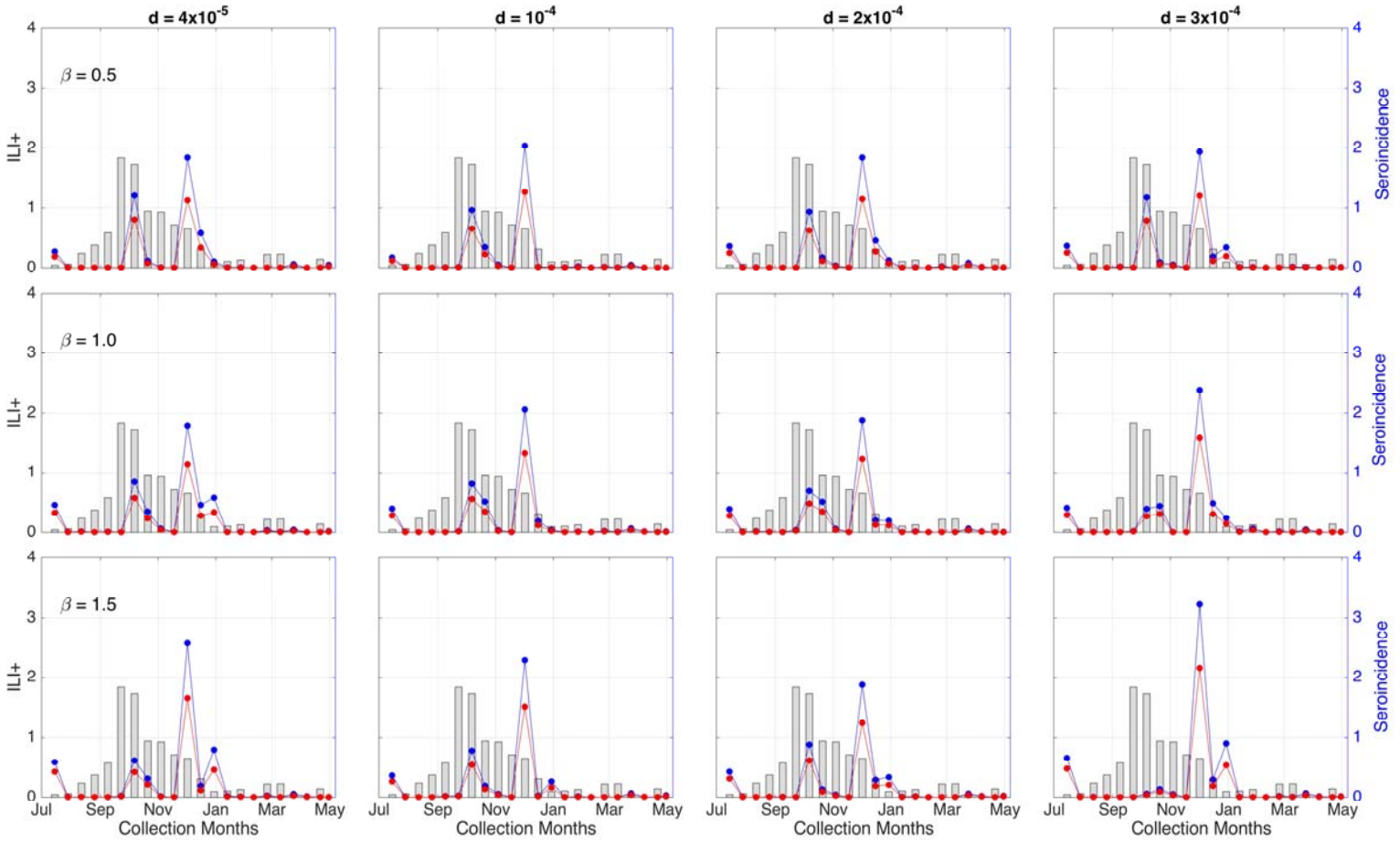

Figure 5.23 Comparing biweekly seroincidence from **Hue** using normal likelihood function to sentinel data. Showing results for different birth/death rates (four columns) and different reduced susceptibility curves (three rows of figures). Blue dots represent bi-weekly incidence $\times 10^5$ (right y-axis), red dots represent first infections only $\times 10^5$ (right y-axis); and grey bars show number of bi-weekly ILI+ cases from sentinel data (left y-axis).

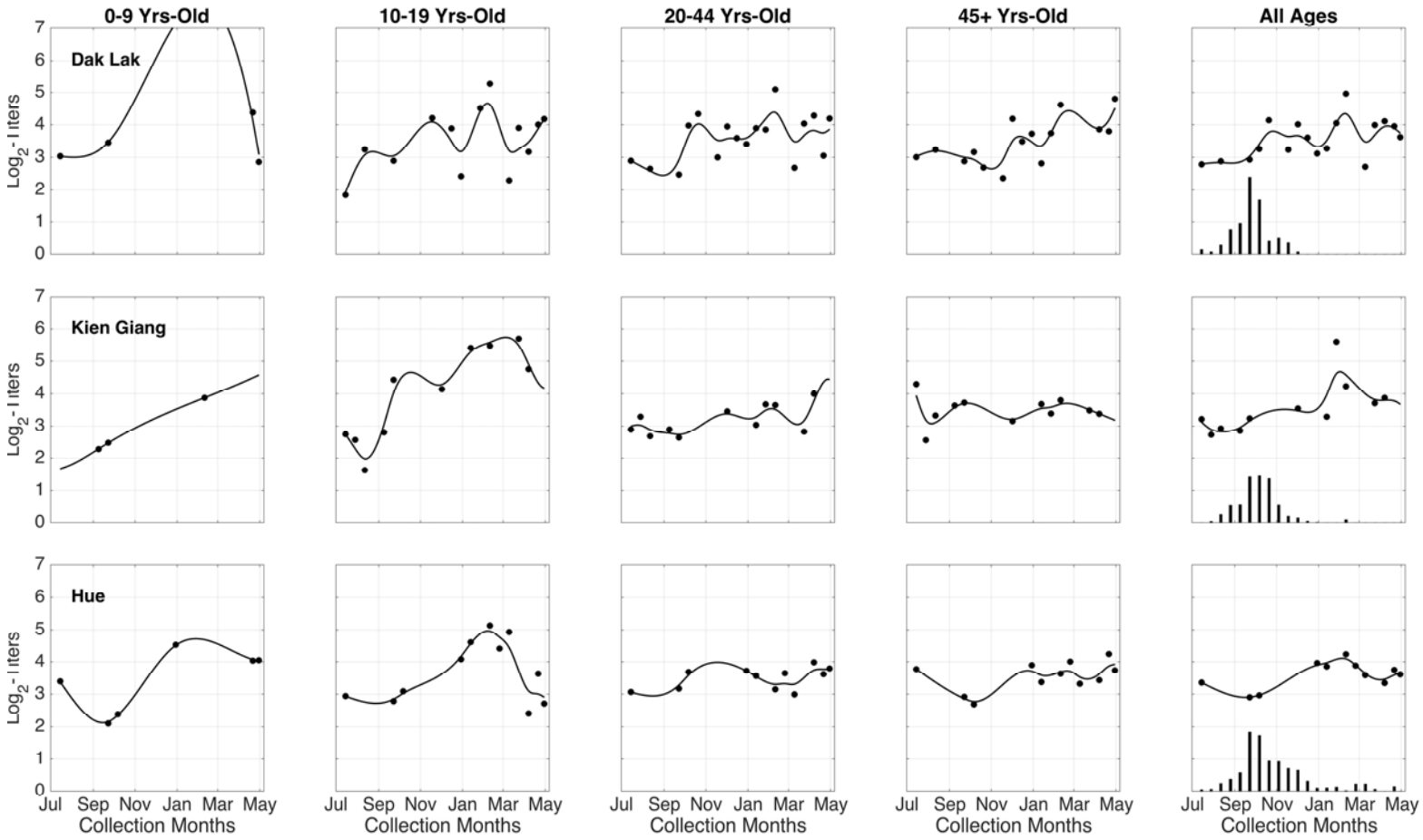

Figure 5.24 Smoothed spline fit to the age-stratified GMT time series against H1-09 by collection site. Showing age-stratified GMT (column 1 to 4) and all age groups (column 5) for different collection site (each row is one site). The black bars in the last column show the bimonthly sentinel ILI+ cases (%PCR positive x number of ILI cases) in the same province.

Table 5.8 Inferred antibody waning and post-infection seroconversion patterns for Dak Lak using gamma likelihood function for different values of ω – the number of days it takes for an individual to lose one $\log_2$-titer unit without inflation

ω (days)	d (day^{-1})	β	c	Ab waning time (months)		λ	Post-infection seroconversion proportion	
				two $\log_2$-unit	50% susceptible		titers ≥160	titers ≥1280
45	0.00004	0.5	1.16	6.5	54.6	6.40	0.79	0.40
	0.00004	1.0	1.26	6.8	61.0	5.39	0.79	0.34
	0.00004	1.5	1.18	6.5	55.7	6.09	0.79	0.38
	0.0001	0.5	1.19	6.6	56.7	7.64	0.80	0.45
	0.0001	1.0	1.11	6.3	52.1	10.47	0.80	0.53
	0.0001	1.5	1.07	6.2	49.9	11.95	0.80	0.56
	0.0002	0.5	1.20	6.6	56.8	11.05	0.80	0.54
	0.0002	1.0	1.13	6.4	52.9	18.12	0.80	0.63
	0.0002	1.5	1.13	6.4	53.0	9.32	0.80	0.50
	0.0003	0.5	1.16	6.5	54.7	5.26	0.79	0.33
	0.0003	1.0	1.40	7.2	70.2	9.99	0.80	0.52
	0.0003	1.5	1.11	6.3	52.0	6.36	0.79	0.39
60	0.00004	0.5	0.88	9.6	40.3	5.71	0.79	0.36
	0.00004	1.0	0.85	9.5	38.6	10.81	0.80	0.54
	0.00004	1.5	0.80	9.4	36.5	8.70	0.80	0.48
	0.0001	0.5	0.89	9.7	40.4	6.60	0.79	0.40
	0.0001	1.0	0.89	9.7	40.7	10.33	0.80	0.52
	0.0001	1.5	0.83	9.5	37.8	8.10	0.80	0.46
	0.0002	0.5	0.85	9.6	38.9	10.46	0.80	0.53
	0.0002	1.0	0.94	9.8	42.8	13.32	0.80	0.58
	0.0002	1.5	0.86	9.6	39.1	11.76	0.80	0.55
	0.0003	0.5	0.83	9.5	38.1	7.41	0.80	0.44
	0.0003	1.0	0.83	9.5	38.0	8.13	0.80	0.46
	0.0003	1.5	0.84	9.5	38.4	9.51	0.80	0.51
90	0.00004	0.5	0.60	8.8	28.8	4.65	0.78	0.30
	0.00004	1.0	0.52	8.6	26.1	7.33	0.80	0.44
	0.00004	1.5	0.54	8.6	26.8	4.82	0.79	0.31
	0.0001	0.5	0.59	8.8	28.6	6.80	0.80	0.41
	0.0001	1.0	0.55	8.6	26.9	7.74	0.80	0.45
	0.0001	1.5	0.52	8.6	26.1	4.87	0.79	0.31
	0.0002	0.5	0.53	8.6	26.3	7.17	0.80	0.43
	0.0002	1.0	0.53	8.6	26.2	7.23	0.80	0.43
	0.0002	1.5	0.54	8.6	26.8	4.70	0.79	0.30
	0.0003	0.5	0.67	9.0	31.3	3.88	0.77	0.24
	0.0003	1.0	0.54	8.6	26.5	6.74	0.80	0.41
	0.0003	1.5	0.55	8.6	26.9	4.78	0.79	0.30

CHAPTER 6

6 Discussion

6.1 Motivation

The main goal of this doctoral thesis was to characterize a large serological time series, collected in southern Vietnam, by the individual sample responses to several influenza antibodies. The first major goal was a characterization into groups, and the second was its characterization as a time series. The public health rationale for this work is that it allows us to make basic assessments about the attack rate of influenza virus in Vietnam – a topic that is understudied as most epidemiological research on influenza takes place in temperate zones. The scientific rationale was to determine if a serological time series – or, a serial seroepidemiology (SSE) study design – would allow us to reconstruct the complete disease dynamics of influenza virus in Vietnam.

Since the 1940s, influenza serology has relied on the haemagglutination inhibition (HI) and microneutralization (MN) assays as the gold standards to correlate influenza antibody levels to immune protection. Recently, a new protein microarray (PM) assay was developed as a high throughput way to profile influenza antibody titers with better standardization to correct for laboratory errors compared to the HI and MN tests (Koopmans et al. 2012). Most of the serological influenza studies using HI or MN assays adopted a 1:40 or 1:32 threshold as a proxy for

'seropositivity' in human serum. Another common practice was to use a four-fold increase in paired acute/convalescent sera as a marker of infection. However, published work on H1N1 Pdm 2009 virus has shown that about 10-20% of the infected subjects fail to develop a protective antibody level following a natural infection, and that the post-infection titer levels depend on age and infection history (Cox, Brokstad, and Ogra 2004; Baguelin et al. 2011; Miller et al. 2010a; Chen et al. 2010; Cowling et al. 2010; Hung et al. 2010; Chan et al. 2011). In addition, since these approaches do not account for the fact that asymptomatic infections were likely to develop a weaker antibody response following infection (Wu et al. 2014), they might have substantially underestimated the number of flu cases at a population level (Simon Cauchemez et al. 2012).

In fact, misclassification of borderline samples into binary categories is not just a problem in influenza serology, and much effort has been dedicated to develop mixture models to categorize individual serological results into more than two different exposure categories, a move away from the single threshold approach, for influenza (te Beest et al. 2014a; Steens et al. 2011; Zhao et al. 2017) and other infectious diseases (Baughman et al. 2006; Neuenschwander et al. 2000; Gay et al. 2003; Hardelid et al. 2008; Greiner et al. 1994; Rota et al. 2008; Vyse et al. 2004; Fujii et al. 2014). Several published studies have aimed to compute influenza attack rates of the H1N1 Pdm 2009 using mixture distributions either with continuous titers (Steens et al. 2011; te Beest et al. 2014a; 2014b) or discrete measurements (Zhao et al. 2017). Nevertheless, these studies relied heavily on the pre-pandemic samples assuming absence of pre-existing immunity in the population, especially in children

and young adults. A pre-pandemic or pre-epidemic dataset might not be readily available in developing countries like Vietnam when routine serological work is usually not carried out. In addition, none of these studies looked beyond three serological states, and the number of samples as well as their representativeness was quite limited. The mixture distribution approach described in this thesis used a statistical framework incorporating both BIC comparison and a visual inspection as model selection criteria to understand the underlying structure of the influenza titer distribution at a population level. To the best of my knowledge, other published studies have not taken this approach.

In temperate zones, influenza burden is usually calculated based on the number of "excess cases" compared to a baseline. The use of a single cross-section or paired data taken right before and after an epidemic to estimate the pandemic/epidemic attack rates/incidence relies heavily on identifying the right collection timing. However, the timing of respiratory disease and influenza epidemics in the tropics is irregular. With many contradicting results being published in the last decade, there is still no convincing evidence linking weather factors and difference in influenza activity moving across different latitudes due to the large year-to-year variations (Tamerius et al. 2013; Deyle et al. 2016; Alonso et al. 2007). Therefore, the syndromic surveillance practices tailored for temperature countries should not be directly implemented in the tropics without reconsideration. In addition, some published studies have shown that the circulation of other respiratory viruses in the population causes the lack of synchrony between the ILI peaks and tropical influenza peaks (Lam et al. 2017). If tropical influenza

transmission really persists year-round, this condition is optimal for generating immune-escape variants. In Vietnam, influenza activity has been monitored primarily by the National Influenza Surveillance System (NISS), it is difficult to assess whether a change in the number of reported cases always corresponds to a real change in influenza activity or is just a result of a change in the reporting practice. This gap highlights the need for independent serological surveillance covering locations other than Ho Chi Minh City, which already has many epidemiological studies on influenza running or complete (Lam et al. 2017; Todd 2016). The data described in this thesis are intended to fill this gap. The serological time series presented here contain sufficient samples per time window (two-month time windows, usually) and age group, that it allowed for better estimates of the attack rate and seroincidence than could be obtained from the sentinel data. At the moment, influenza vaccination coverage in Vietnam is negligible, which makes this dataset especially valuable to understand population-level serological time series results from natural infections only. In the coming decades, given the rapid economical reform that the country is currently undergoing, better access to both public and private healthcare might increase influenza vaccination rate and change the influenza dynamics significantly.

Because serological data account for asymptomatic and mild infections that are missing from sentinel data and case report data, serological data provide a more complete epidemiological picture of transmission. Even though from a disease management perspective, these mild and asymptomatic cases do not contribute much to disease burden, they are still important for obtaining an accurate estimate of influenza incidence in the community and for future vaccination planning, especially

in a developing country like Vietnam which is considering recommending influenza vaccine as a matter of national policy. In comparing the SSE data to the sentinel data, if we had found that the SSE data failed to capture the influenza activity patterns seen in the sentinel data, we may have concluded that either (*i*) there is a flaw in the study design or (*ii*) the serum collection may not be representative of the general population. If we had found that the reconstructed seroincidence always correlated positively with the sentinel influenza data, in this scenario we would be able to compute the number of influenza infections in each epidemic wave, and by extension, for each reported case, i.e. the number of true influenza infections per ILI positive case. However, this result would still rely on the hospital reporting rate and the sensitivity and specificity of the ILI definition used to diagnose flu cases. The pattern that I found was between these two scenarios. The reconstructed seroincidence sometimes correlated with the sentinel data, and other times showed epidemic waves when the sentinel data showed none.

By comparing the sentinel data with the serological data, I hoped to answer one of the two key questions posed at the end of Chapter 1, whether influenza circulation in Vietnam is characterized by long-term persistence or discrete epidemics. The sentinel data seemed to show that both of these epidemiological behaviors were possible, but the SSE data did not add any informative results to this question. Certainly, both the sentinel data and the SSE data indicate that an influenza epidemic is possible at any time of year. However, the SSE data do not have enough temporal precision to prove that influenza virus is present and circulating in the population every month or every week of the year. The sentinel data do have this

precision, and they show that influenza is present in the population >20 weeks of the year during some years and >40 weeks of the year during other years.

I was not able to answer the persistence question, but I was able to uncover a useful result on influenza seasonality or 'seasonal forcing' as it is implemented in mathematical models. Even though the type of back-calculation presented in Chapter 5 to compute seroincidence using multiple serological data points have appeared in a number of publications both for influenza (Wu et al. 2010; 2011) and other infectious diseases (Simonsen et al. 2008; Simonsen et al. 2009; Falkenhorst et al. 2012; de Melker et al. 2006; Heisterkamp et al. 2008; Versteegh et al. 2005), the unique aspect of our work is the ability to reconstruct the seroincidence without a seasonal forcing term and allow the change in population-level titers over time to govern the entire inference. The dynamical model in Chapter 5 could be generalized to any acute infectious diseases for which (*a*) we have a quantitative antibody assay, (*b*) the general antibody dynamics following an infection are known, and (*c*) multiple cross-sectional data points have been taken.

In the early phases of the methodological development for this thesis, I realized that the analysis of population-level dynamics based on antibody titer was a new area of research. Parts of these research goals were experimental and not guaranteed to succeed, and these risks come with their failures. Fortunately, some of these risks led down fruitful and validatable lines of research inquiry, and most of these are presented in the SSE/sentinel data comparisons in Chapter 5. Nevertheless, the work presented in this thesis is meant to serve as an assessment of whether serological surveillance works as an effective tool to monitor influenza

activity in the population. This was the second question I posed at the end of Chapter 1. At present, I think the answer to this question is that serological data can be used successfully for 'past surveillance' purposes but that it would be challenging to use these data for real-time surveillance. The simple reasons are (*i*) that it takes humans two to three weeks to generate an IgG immune response to an influenza infection, and (*ii*) that the sample collection, laboratory assays, and data management will take an additional two to three weeks, even in a highly optimized operation.

This SSE dataset was a one-of-a-kind resource that has allowed tens of thousands of human sera, from ten provincial hospitals spanning the southern and middle regions of Vietnam, to be analyzed for many kinds of antibodies. Though only H1N1 Pdm 2009 and seasonal H3N2 2009 and 2011 were studied here, titers against all antigens in the arrays are readily available for future analyses.

6.2 Key results

The two key advantages that I had in putting together this analysis are the new informative serological assay and the time series serological data from multiple locations. In addition to developing a systematic way to analyze and standardize the PM titers that could be used for all future studies looking to use the PM assay to profile antibody titers, an improvement was made to allow titer mapping using only fluorescence values at two dilutions without sacrificing accuracy. This allowed for processing twice as many samples as using four dilutions.

This SSE dataset is a unique set of about 20,000 samples whose positive influenza titers were likely the result of natural influenza infection (i.e. not

vaccination). The 2009 influenza pandemic gave me a unique and invaluable opportunity to diverge from the conventional epidemiological analysis and analyze the dynamics of a pandemic wave with a more precise serological assay. The traditional single titer cut-off approach was abandoned, and I first used mixture models and then free incidence parameters to assess the attack rate. The mixture model described in Chapter 3 allowed me to go beyond a binary titer classification and revealed a four-component structure for antibody titers to H1N1 Pdm 2009 virus. The highest titer and second-highest titer components were interpreted as recent infection and historical infection (infection in the non-recent past) respectively, and this interpretation was validated by computing the attack rates of pandemic H1N1 during the first 10 months of the pandemic virus' circulation. When looking at samples collected between July 1, 2009 and April 30, 2010, the proportion of individuals who were recently infected was highest among children while the proportion of individuals with historical infection was highest among older individuals, as expected. In addition, the estimated age-specific proportions of recent infection aligned with previous estimates for H1N1 Pdm 2009 attack rates. This gave us some assurance that even though it is impossible look at an individual titer and state with certainty when that given individual might have been infected in the past, when averaging these kinds of SSE dataset over a large population, conclusions about timing could be made at a population level.

For the H3N2 subtype, interpretation of the best-fit mixture distributions was more problematic. The model selection procedure selected three components as the best fit according to the Bayesian Information Criterion (BIC). Thus, if the initial

(validated) explanation of the H1N1 components was negative, negative, historically infected, and recently infected (from lowest to highest), I conjectured that the natural explanation of the H3N2 components should be negative, historically infected, and recently infected. However, this interpretation was not consistent with the 'attack rates' or 'recent attack rates' that we would expect to see for the H3N2 subtype. These terms are obviously subjective. And, of course, an important goal of this work was to measure attack rates rather than confirm attack rates based on our prior beliefs. Nevertheless, I had had enough experience reading through the unpublished clinical data on post-infection antibody titers (Todd 2016), that I felt it justified to question the interpretation of the H3N2 titer groups. The second hypothesis to come to mind was that censoring in these data prevented us from seeing the true titer categories. We already knew from the clinical data that many H3N2-positive patients converted to a titer ≥1280, and thus this category (the censored group of individuals whose titer was higher than 1280) could credibly be called the 'recently infected' group. Under this interpretation, the three components in the H3N2 titer data would be negative, negative, and historically infected. This is consistent with our observations and the known epidemiology of H3N2, but we cannot determine if an uncensored version of the data would have yielded four components in a mixture analysis.

The most surprising result in the mixture analysis was that there were no lineage effects (different lineages of the H1N1 subtype) and essentially no age effects in the mixture distribution. The only obvious age effect was that in the youngest age group (≤9 y.o.) a large proportion of individuals were influenza-naïve (as expected)

and the remainder of the distribution appeared flat. Even in this age group however, the model selection procedure pointed to four groups as the optimal number. None of the four components in the H1N1 analysis corresponded to any particular age group, and breaking the titer data up by age did not lead to any obvious differences among the components. Any potential H1N1-lineage effects should also be seen as age effects. These effects would show that individuals exposed to different H1N1 lineages – the pre-1957 lineage, the post-1977 lineage, and the post-2009 lineage – would be categorized into different mixture components. However, no association between lineage and component was observed.

For H1N1, assuming that the weight of the component with the highest titer mean represents recent infection while the sum of the two components with the highest and second highest means represent individuals who might have been infected at some point in the past, if the stationary distribution observed at a population-level was indeed true, we would be able to reconstruct the H1-09 dynamics by looking at the time series data of the two aforementioned quantities. The question remains how we should incorporate the stationary distribution into the time series data that does not impose too much underlying structure on the data and allows the change in the SSE data over time to be reflected. This resulted in an exploration of which mixture components should be fixed and which should be fitted in the mixture analysis. Unfortunately, there was no definite conclusive answer to this question as a BIC-based selection procedure suggested either fixing both means and variances or fixing variances as the best-fit models, but correlating the time series (the w_4 time series) with the sentinel data suggested that the mixture means

should be fixed. Correlating the cumulative seroprevalence in these analyses (w_3 + w_4) with cumulative incidence from the sentinel data in general *did* show a positive correlation. This worked best for fixed μ, regardless of whether σ was fixed or not. In addition, the w_3 + w_4 quantity reached values upwards of 60% by 2013, which is consistent with the interpretation that w_3 + w_4 corresponds to the traditional seroprevalence (infection at any point in the past).

Setting the mixture-model approach aside, I chose to study the time dimension of the SSE data with a hybrid dynamical SEIR model in which the incidence parameters were completely free. The process was discovered to be very sensitive to (*i*) the type of underlying distribution for the serological observations in each two-week window, (*ii*) the antibody waning process, and (*iii*) the magnitudes and timing of the major peaks. Though the inferred antibody waning rate was not perfectly consistent across sites, it is in agreement with the published data that the time to lose the first two $\log_2$-titer units was less than one year. The waning inference beyond one year was more likely to be a result of the particular functional form used to describe waning rather than a confidence inference from a ten-month long dataset. In two out of the three collection sites – Dak Lak and Kien Giang – the first wave of H1-09 identified in the sentinel data was captured in our time series of inferred biweekly incidences. This first wave was missed out in Hue due to missing data during the initial phase of the study when the sampling protocol was not correctly carried out at all participating sites. The surprising finding was the observation of a second wave of H1N1 infections in early 2010 from all three sites (though not very prominently in Kien Giang) that went silent from the sentinel surveillance. The major

encouraging finding in this analysis was that the inferred seroincidence peaks lined up perfectly with the reported incidence peaks from the sentinel data even though the SSE data were analyzed completely independently of the sentinel data.

A major drawback of the analysis in this chapter was that in most of these inferential exercises, one would find it difficult to believe at how sharp the seroincidence peaks were, e.g. hundreds of thousands cases within 2-4 weeks and almost zero cases in the inter-peak periods. This is likely to be an artefact of the fitting procedure which relies on fitting differences in mean titer from one time window to another. In reality, the incidence in one time window will be correlated to the incidence in the previous and following time windows, but this correlation was not included in my likelihood function.

6.3 Limitations and challenges

First, the general-population study design relied on convenience sampling from a hospital-based population whose health status could not be assessed at time of admission. This is a common problem in many cross-sectional designs. In cohort studies where much more is known about the population, health status can be assessed but we still may not be able to correct for it if the same health variables were not measured in some unbiased population pool. In hospital-based studies like ours, the concern is generally that the hospital-going population represents a sicker or more vulnerable group than the general population, while in a study using blood donors the concern is in the opposite direction, namely, that this sample represents a sub-population with above-average health indicators. In our population, we know

for a fact that in the <20 age group, individuals had higher seroprevalence to hepatitis E virus than was measured in a randomly selected cohort of farmers from the same location (Berto et al. 2017). We also know that hepatitis B vaccination rates in infants are lower in our sample set than reported by the Ministry of Health in Vietnam (unpublished data).

The major methodological limitation in this thesis is that, in Chapters 3 and 4, the mixture distribution approaches did not give any clear visual break-up of the data into distinct groups. Even though I was able to show that the four- and three-component models were the best representations for H1-09 and H3N2 seasonal strains statistically and visually, it was impossible to validate the proposed interpretation associated with each component systematically because the samples were anonymized and did not come with patient history. As a result, I can assess neither sensitivity nor specificity with the mixture model approach, despite the fact that assessments like this have been, incorrectly in my view, published in the literature (te Beest et al. 2014). This inability to determine specificity and sensitivity is, in my opinion, an inevitable result of anonymized cross-sectional sampling.

A third critical limitation in this thesis is the lack of age-dependency in the epidemiological parameters. The original antigenic sin hypothesis states that infections at young ages and order of infections matter in terms of the titer that one should measure post-infection. Studies on seroconversion show that individuals of different ages have different distributions of their convalescent titer. Antibody dynamics are not necessarily the same across all age groups, with children maintaining higher titer levels for longer. It is likely that the SSE data combined with

clinical data with patient follow-up will be able to answer some of these questions. However, given that the analyses of the clinical data are still preliminary and unpublished, I was hesitant to put too much age dependency in the models, especially in Chapter 5. I plan to refine these analyses after the writing of this thesis, and expect that introducing age into the likelihood framework in Chapter 5 will have the largest qualitative effect on my results.

In general, in my analyses, I did not consider immunological cross-reaction among different influenza strains. Following natural infections, both heterosubtypic and homosubtypic titer rise have been observed in clinical studies (Todd 2016; Freeman et al. 2016). Even though the primary results of my thesis concern only the pandemic H1-09 virus, cross-reaction to the historic 1977 H1N1 lineage or the pre-1957 H1N1 strain could affect the titers measured in our population. For H1N1, it was known at the time of the 2009 pandemic that individuals over the age of 50 had antibody titers that appeared to neutralize the pandemic virus (Broberg, Nicoll, and Amato-Gauci 2011; Hancock et al. 2009; Miller et al. 2010; Rizzo et al. 2010; Veguilla et al. 2011). For H3N2, the frequent epidemics of H3N2 with multiple strains co-circulating (Holmes et al. 2005; Nelson et al. 2006; Le et al. 2013) and antigenic change every few years could mean that titers measured to a specific H3N2 strain (e.g. A/Victoria/361/2011, as in this thesis) are not as informative as antibody titer profiles measured to multiple H3N2 strains (Freidl et al. 2016).

Serological response to influenza infection is completely unknown for asymptomatic patients. This is a major gap in seroepidemiology that underlies all cross-sectional studies, with single or multiple cross-sections. All serological studies

are underpinned by the assumption that real individuals infected with influenza will seroconvert the same way as individuals enrolled into clinical observational studies (or trials) on influenza infection. Real individuals may have asymptomatic or sub-clinical influenza, which would mean that they would not present to a health provider where patients were being enrolled in a clinical trial. Some of these individuals would have mild infections for a very obvious reason, namely, that they were already partially protected from infection by a previous (possibly recent) influenza infection. Their post-infection immunological response in this case may be one primarily dominated by influenza antibodies targeting their recent infection or their older infection. It is not known which of these antibody populations should be dominant at the time of sampling and whether the severity of the infection would influence this outcome. In general, epidemiological analysis aiming to estimate attack rates or seroprevalence assumes that asymptomatically infected individuals would generate the same antibody response as symptomatic individuals. No study that I know of has begun to investigate to answer this question.

Finally, I would like to mention a small operational limitation. During the initial phase of the project when the implementation of the protocol was not yet perfect, sampling was mostly aggregated into one to two week windows before the cut-off time for each collection. This resulted in long time periods with complete sample missingness even though the total number of samples was quite high. For example, in the period from July 1, 2009 to Apr 30, 2010, there were more than 1000 samples collected in Hue; nevertheless, only eleven out of twenty-two biweekly periods had more than three samples present. The other eleven time windows had

two or fewer samples and many had zero. Because the beginning of the study (June 2009) coincided with the first wave of the 2009 pandemic, this 'sample clumping' in Hue caused us to miss out on a more precise reconstruction of the pandemic's dynamics in this province during the second half of 2009.

6.4 Areas for further exploration

For the stationary titer analysis in this thesis, the analysis could be expanded to include other strains of influenza. This may not have a large effect on the H3N2 analysis, but it may for H1N1 as different lineages of H1N1 have circulated in human populations over the past 100 years. The overall distribution of the titers themselves may not look any different (Figure 3.17). Nevertheless, an expanded analysis on how cross-reaction patterns among different H1N1 lineages affect a 2009 H1N1 titer may be informative in describing the history of individual samples. A potential analysis could be set up to determine if a particular titer pattern is more likely to be associated with 1977 H1N1 infection, 2009 H1N1 infection, or both. I did not examine cross-reactions in this thesis, but this will be an important area of serological research to take full advantage of the multi-antigen serological assays like the protein microarray.

For both the stationary analysis and the temporal analysis, I think it will be important to explore the large subset of samples that could not be tested past the upper limit of detection at 1:1280 dilution for H3N2 strains. Results from the clinical study accompanying these samples (Todd 2016) showed that more than 85% of H3N2 infected subjects seroconverted to the upper limit of assay detection; in many

of these patients little waning was observed during the seven-month follow-up period. Diluting out some of the samples past the current 1:1280 upper limit would allow us to perform statistics on uncensored values, and to confirm whether a fourth peak exists in the H3N2 titer histogram. In 2017, at the Oxford University Clinical Research Unit, the laboratory team did indeed dilute out a selection of these samples, to a 1:10240 dilution, and these new data will soon be used in the analysis of Dr Stacy Todd's clinical study, and eventually to improve the seroepidemiological analysis presented in this thesis.

In completing the analysis for Chapter 5, the next major improvement is to introduce a correlation parameter between consecutive time windows. Clearly, a true dynamic transmission process will produce a time series where infection counts during one time period are positively correlated with infection counts in the previous and following time periods. This correlation structure was ignored in Chapter 5 which was the reason causing the short sharp peaks of infections with all cases occurring during a brief time window. The first analysis I will attempt will be to compute the correlation values from the national sentinel data, in order to determine how auto-correlated a wave of influenza infection in Vietnam should be. Then, I will evaluate this correlation value in the likelihood analysis in Chapter 5 to determine by how much this additional feature improves the likelihood of the serological time series used in this inference.

Uncertainty will need to be presented for the likelihood analysis in Chapter 5. I considered a number of ways of presenting this, but the number of parameters made the computation too difficult. With a traditional likelihood analysis, I could

have made a likelihood profile for each of the 22 x_t parameters. Alternatively, I thought of re-computing the likelihood with one x_t value at a time set to zero, to determine if a zero value at any particular time point would alter the likelihood by a large amount. Ultimately, I realized that all of these approaches would involve separate uncertainty analyses for the 22 seroincidence parameters. A solution to this problem may be to take a Bayesian approach to the problem rather than maximizing the likelihood. With a Bayesian approach, posterior density functions will be available for each parameter and this will allow me to see how much uncertainty there is for the 22 seroincidence estimates inferred in Chapter 5.

In general, the likelihood framework in Chapter 5 can be improved by adding age-specific parameters (for waning or seroconversion), by combining the likelihoods for all three sites (so that they have common parameters for the individual processes of waning and seroconversion), and by adding in more sites to improve the situation of data missingness that I found when doing all of site analyses individually. This is the next area of analysis I will focus when following up and improving the research in this thesis. I believe that an analysis across all sites may have the disadvantage that it assumes a uniformly timed pandemic in all of southern Vietnam, but I feel that this is a small disadvantage given that the peak timings I inferred in Chapter 5 were quite similar. The benefit of combining sites here will give me more statistical power to infer individual-level antibody processes, and it will improve the temporal resolution of the inferred waves since there will be very few time windows with missing data. The end goal will be one that I believe is an important one in public health. I would like to determine if influenza virus is able to

cause silent and asymptomatic epidemics. While this seems impossible in temperate countries where winter causes strong, symptomatic bouts of respiratory disease outbreaks every year, this silent epidemic behavior may be possible in the tropics where waves of influenza tend to come and go in a slower milder rhythm than in temperate parts of the world.

7 References

Alonso, W. J., Viboud, C., Simonsen, L., Hirano, E. W., Daufenbach, L. Z., and Miller, M. A. 2007. "Seasonality of Influenza in Brazil: A Traveling Wave from the Amazon to the Subtropics." *American Journal of Epidemiology* 165 (12): 1434–42.

Angkasekwinai, N., Kaewnapha, B., Waywa, D., Werarak, P., Tongsai, S., Chokephaibulkit, K., Thamlikitkul, V., and Siritantikorn, S.. 2013. "Serological Response of Patients with Influenza A (H1N1) Pdm09-Associated Pneumonia: An Observational Study." *PLoS One* 8 (11): e81436.

Arnon, T. I., Lev, M., Katz, G., Chernobrov, Y., Porgador, A., and Mandelboim, O. 2001. "Recognition of Viral Hemagglutinins by NKp44 but Not by NKp30." *European Journal of Immunology* 31 (9): 2680–89.

Azziz Baumgartner, E., Dao, C. N., Nasreen, S., Bhuiyan, M. U., Mah-E-Muneer, S., Mamun, A. A., Sharker, M. A. Y., et al. 2012. "Seasonality, Timing, and Climate Drivers of Influenza Activity Worldwide." *The Journal of Infectious Diseases* 206 (6): 838–46.

Baas, D. C., Koopmans, M. P., de Bruin, E., Hulscher, H. I., Buisman, A. M., Hendrikx, L. H., van Beek, J., Godeke, G., Reimerink, J., and van Binnendijk, R. S. 2013. "Detection of Influenza A Virus Homo- and Heterosubtype-Specific Memory B-Cells Using a Novel Protein Microarray-Based Analysis Tool." *Journal of Medical Virology* 85: 899–909.

Baguelin, M., Hoschler, K., Stanford, e., Waight, P., Hardelid, P., Andrews, N., and Miller, E. 2011. "Age-Specific Incidence of A/H1N1 2009 Influenza Infection in England from Sequential Antibody Prevalence Data Using Likelihood-Based Estimation." *PloS One* 6 (2): e17074.

Bahl, J., Nelson, M. I., Chan, K. H., Chen, R., Vijaykrishna, D., Halpin, R. A., Stockwell, T. B., et al. 2011. "Temporally Structured Metapopulation Dynamics and Persistence of Influenza A H3N2 Virus in Humans." *Proceedings of the National Academy of Sciences of the United States of America* 108 (48): 19359–64.

Baughman, A. L., Bisgard K. M., Lynn, F., and Meade, B. D. 2006. "Mixture Model Analysis for Establishing a Diagnostic Cut-off Point for Pertussis Antibody Levels." *Statistics in Medicine* 25 (17): 2994–3010.

Bedford, T., Cobey, S., Beerli, P., and Pascual, M. 2010. "Global Migration Dynamics Underlie Evolution and Persistence of Human Influenza a (H3N2)." *PLoS Pathogens* 6 (5): e1000918.

Bedford, T., Riley, S., Barr, I. G., Broor, S., Chadha, M., Cox, N. J., Daniels, R. S., et al. 2015. "Global Circulation Patterns of Seasonal Influenza Viruses Vary with Antigenic Drift." *Nature* 523 (7559): 217–20.

Berto, A., Pham, H. A., Thao, T. T.N., Vy, N. H.T., Caddy, S. L., Hiraide, R., Tue, N. T., et al. 2017. "Hepatitis E in Southern Vietnam: Seroepidemiology in Humans and Molecular Epidemiology in Pigs." *Zoonoses Public Health*: 1–8.

Bloom-Feshbach, K., Alonso, W. J., Charu, V., Tamerius, J., Simonsen, L., Miller, M. A., and Viboud, C. 2013. "Latitudinal Variations in Seasonal Activity of Influenza and Respiratory Syncytial Virus (RSV): A Global Comparative Review." *PLoS One* 8 (2): 3–4.

Bollaerts, K., Aerts, M., Shkedy, Z., Faes, C., van der Stede, Y., Beutels, P., and Hens, K. 2012. "Estimating the Population Prevalence and Force of Infection Directly from Antibody Titres." *Statistical Modelling: An International Journal* 12 (5): 441–62.

Boni, M. F. 2008. "Vaccination and Antigenic Drift in Influenza." *Vaccine* 26 (Suppl. 3): 8–14.

Boni, M. F., Chau, N. V. V., Dong, N., Todd, S., Nhat, N. T. D., de Bruin, E., van Beek, J., et al. 2013. "Population-Level Antibody Estimates to Novel Influenza A/H7N9." *The Journal of Infectious Diseases* 208 (4): 554–58.

Boni, M. F., Gog, J. R., Andreasen, V., and Feldman, M. W. 2006. "Epidemic Dynamics and Antigenic Evolution in a Single Season of Influenza A." *Proceedings. Biological Sciences / The Royal Society* 273 (1592): 1307–16.

Borremans, B., Hens, N., Beutels, P., Leirs, H., and Reijniers, J. 2016. "Estimating Time of Infection Using Prior Serological and Individual Information Can Greatly Improve Incidence Estimation of Human and Wildlife Infections." *PLoS Computational Biology* 12 (5): 1–18.

Broberg, E., Nicoll, A., and Amato-gauci, A. 2011. "Seroprevalence to Influenza A (H1N1) 2009 Virus — Where Are We?" *Clinical and Vaccine Immunology* 18 (8): 1205–12.

Camacho, A., and Cazelles, B. 2013. "Does Homologous Reinfection Drive Multiple-Wave Influenza Outbreaks? Accounting for Immunodynamics in Epidemiological Models." *Epidemics* 5 (4): 187–96.

Cannell, J. J., Vieth, R., Umhau, J. C., Holick, M. F. , Grant, W. B. , Madronich, S. , Garland, C. F. and Giovannucci, E. 2006. "Epidemic Influenza and Vitamin D." *Epidemiology and Infection* 134 (6): 1129.

Carrat, F., Vergu, E., Ferguson, N. M., Lemaitre, M., Cauchemez, S., Leach, S., and Valleron, A. J. 2008. "Time Lines of Infection and Disease in Human Influenza: A Review of Volunteer Challenge Studies." *American Journal of Epidemiology* 167 (7): 775–85.

Cauchemez, S., Valleron, A. J., Boelle, P. Y., Flahault, A., and Ferguson, N. M. 2008. "Estimating the Impact of School Closure on Influenza Transmission from Sentinel Data." *Nature* 452 (1476–4687 (Electronic)): 750–54.

Cauchemez, S., Ferguson, N. M., Wachtel, C., Tegnell, A., Saour, G., Duncan, B., and Nicoll, A. 2009. "Closure of Schools during an Influenza Pandemic." *The Lancet Infectious Diseases* 9 (8): 473–81.

Cauchemez, S., Horby, P., Fox, A., Le, Q. M., Le, T. T., Thai, P. Q., Le, N. M. H., Nguyen, T. H., and Ferguson, N. M. 2012. "Influenza Infection Rates, Measurement Errors and the Interpretation of Paired Serology." *PLoS Pathogens* 8 (12): e1003061.

Cauchemez, S., Ferguson, N. M., Fox, A., Le, Q. M., Le, T. T., Pham, Q. T., Dang, D. T., et al. 2014. "Determinants of Influenza Transmission in South East Asia: Insights from a Household Cohort Study in Vietnam." *PLoS Pathogens* 10 (8): e1004310.

Chadha, M. S., Potdar, V. A., Saha, S., Koul, P. A., Broor, S., Dar, L., Chawla-Sarkar, M., et al. 2015. "Dynamics of Influenza Seasonality at Sub-Regional Levels in India and Implications for Vaccination Timing." *PLoS ONE* 10 (5): 1–14.

Chan, K.-H., To, K. K. W., Hung, I. F. N., Zhang, A. J. X., Chan, J. F. W., Cheng, V. C. C., Tse, H., Che, X.-Y., ChenH., and Yuen, K.-Y. 2011. "Differences in Antibody Responses of Individuals with Natural Infection and Those Vaccinated against Pandemic H1N1 2009 Influenza." *Clinical and Vaccine Immunology* 18 (5): 867–73.

Chen, M. I., Barr, I. G., Koh, G. C. H., Lee, V. J., Lee, C. P. S., Shaw, R., Lin, C., et al. 2010. "Serological Response in RT-PCR Confirmed H1N1-2009 Influenza A by Hemagglutination Inhibition and Virus Neutralization Assays: An Observational Study." *PLoS One* 5 (8): 1–7.

Chen, M. I. C. 2010. "2009 Influenza A(H1N1) Seroconversion Rates and Risk Factors Among Distinct Adult Cohorts in Singapore." *The Journal of the American Medical Association* 303 (14): 1383.

Cheng, C. K. Y., Cowling, B. J., Lau, E. H. Y., Ho, L. M., Leung, G. M., and Ip, D. K. M. 2012. "Electronic School Absenteeism Monitoring and Influenza Surveillance, Hong Kong." *Emerging Infectious Diseases* 18 (5): 885–87.

Cheng, X., Tan, Y., He, M., Lam, T. T. S., Lu, X., Viboud, C., He, J., et al. 2013. "Epidemiological Dynamics and Phylogeography of Influenza Virus in Southern China." *Journal of Infectious Diseases* 207 (1): 106–14.

Chew, F. T., and Ling, A. E. 1998. “Seasonal Trends of Viral Respiratory Tract Infections in the Tropics.” *Epidemioly and Infection* 121: 121–28.

Chirkova, T. V., Naykhin, A. N., Petukhova, G. D., Korenkov, D. A., Donina, S. A., Mironov, A. N., and Rudenko, L. G. 2011. “Memory T-Cell Immune Response in Healthy Young Adults Vaccinated with Live Attenuated Influenza A (H5N2) Vaccine.” *Clinical and Vaccine Immunology* 18 (10): 1710–18.

Chow, A., Ma, S., Ling, A. E., and Chew, S. K. 2006. “Influenza-Associated Deaths in Tropical Singapore.” *Emerging Infectious Diseases* 12 (1): 114–21.

Couch, R. B., and Kasel, J. A. 1983. “Immunity to Influenza in Man.” *Annual Review of Microbiology* 37: 529–49.

Cowling, B. J., Chan, K. H., Fang, V. J., Lau, L. L. H., So, H. C., Fung, R. O. P., Ma, E. S. K., Kwong, A. S. K., Chan, C. W., and Tsui, W. W. S. 2010. “Comparative Epidemiology of Pandemic and Seasonal Influenza A in Households.” *New England Journal of Medicine* 362: 2175–2184.

Cox, R. J., Brokstad, K. A., and Ogra, P. 2004. “Influenza Virus: Immunity and Vaccination Strategies. Comparison of the Immune Response to Inactivated and Live, Attenuated Influenza Vaccines.” *Scandinavian Journal of Immunology* 59 (1): 1–15.

Davenport, B. Y. F. M., Hennessy, A. V., and Francis, T. 1953. “Epidemiologic and Immunologic Significance of Age Distribution of Antibody to Antigenic Variants of Influenza Virus.” *Journal of Experimental Medicine* 98 (6): 641–56.

Dawood, F. S., Iuliano, A. D., Reed, C., Meltzer, M. I., Shay, D. K., Cheng, P., Bandaranayake, D., et al. 2012. “Estimated Global Mortality Associated with the First 12 Months of 2009 Pandemic Influenza A H1N1 Virus Circulation: A Modelling Study.” *The Lancet Infectious Diseases* 12 (9): 687–95.

de Angelis, D., Gilks, W. R., and Day, N. E. 1998. “Bayesian Projection of the Acquired Immune Deficiency Syndrome Epidemic.” *Journal of the Royal Statistical Society. Series C (Applied Statistics)* 47 (4): 449–98.

de Bruin, E., Loeber, J. G., Meijer, A., Castillo, G. M., Cepeda, M. L. G., Torres-Sepúlveda, M. R., Borrajo, G. J. C., et al. 2014. “Evolution of an Influenza Pandemic in 13 Countries from 5 Continents Monitored by Protein Microarray from Neonatal Screening Bloodspots.” *Journal of Clinical Virology* 61 (1): 74–80.

de Melker, H. E., Versteegh, F. G. A., Schellekens, J. F. P., Teunis, P. F. M., and Kretzschmar, M. 2006. “The Incidence of Bordetella Pertussis Infections Estimated in the Population from a Combination of Serological Surveys.” *Journal of Infection* 53 (2): 106–13.

de St Groth, S. F., and Webster, R. G. 1966. “Disquisitions of Origincal Antigenic Sin.” *The Journal of Experimental Medicine* 124 (3): 331–45.

de Vries, R. D., Altenburg, A. F., and Rimmelzwaan, G. F. 2015. “Universal Influenza Vaccines, Science Fiction or Soon Reality?” *Expert Review of Vaccines* 14 (10): 1299–1301.

Delabre, R. M., Salez, N., Lemaitre, M., Leruez-Ville, M., de Lamballerie, X., and Carrat, F. 2015. “Antibody Persistence and Serological Protection among Seasonal 2007 Influenza A(H1N1) Infected Subjects: Results from the FLUREC Cohort Study.” *Vaccine* 33 (49): 7015–21.

Deng, Y., Pand, X. H., Yang, P., Sshi, W. X., Tian, L. L., Liu, B. W., Li, S., et al. 2011. “Serological Survey of 2009 H1N1 Influenza in Residents of Beijing, China.” *Epidemiology and Infection* 139 (1): 52–58.

Deyle, E. R., Maher, M. C., Hernandez, R. D., Basu, S., and Sugihara, G. 2016. “Global Environmental Drivers of Influenza.” *Proceedings of the National Academy of Sciences of the United States of America* 113 (46): 201607747.

Falkenhorst, G., Simonsen, J., Ceper, T. H., van Pelt, W., de Valk, H., Sadkowska-todys, M., Zota, L., et al. 2012. "Serological Cross-Sectional Studies on Salmonella Incidence in Eight European Countries : No Correlation with Incidence of Reported Cases." *BioMed Central Public Health* 12: 523–31.

Fodor, E., and Brownlee, G. G. 2002. "Influenza Virus Replication." In *Influenza*, edited by C. W. Potter, 1–30. Elsevier.

Fonville, J. M., Wilks, S. H., James, S. L., Fox, A., Ventresca, M., Aban, M., Xue, L., et al. 2014. "Antibody Landscapes after Influenza Virus Infection or Vaccination." *Science* 346 (6212): 996–1000.

Francis, T. Jr. 1960. "On the Doctrine of Original Antigenic Sin." *Proceedings of the American Philosophical Society* 104 (6): 572–78.

Freeman, G., Perera, R. A. P. M., Ngan, E., Fang, V. J., Cauchemez, S., Ip, D. K. M., Peiris, J. S. M., and Cowling, B. J. 2016. "Quantifying Homologous and Heterologous Antibody Titre Rises after Influenza Virus Infection." *Epidemiology and Infection* 144 (11): 2306–16.

Freidl, G. S., de Bruin, E., van Beek, J., Reimerink, J., de Wit, S., Koch, G., Vervelde, L., van den Ham, H-J., and Koopmans, M. P. G. 2014. "Getting More Out of Less – A Quantitative Serological Screening Tool for Simultaneous Detection of Multiple Influenza A Hemagglutinin-Types in Chickens." *PLoS One* 9 (9): e108043.

Freidl, G. S., van den Ham, H., Boni, M. F., de Bruin, E., and Koopmans, M. P. G. 2016. "Changes in Heterosubtypic Antibody Responses during the First Year of the 2009 A(H1N1) Influenza Pandemic." *Scientific Reports* 6 (1): 20385.

Fujii, Y., Kaneko, S., Nzou, S. M., Mwau, M., Njenga, S. M., Tanigawa, C., Kimotho, J., et al. 2014. "Serological Surveillance Development for Tropical Infectious Diseases Using Simultaneous Microsphere-Based Multiplex Assays and Finite Mixture Models." *PLoS Neglected Tropical Diseases* 8 (7): e3040.

Gay, N J. 1996. "Analysis of Serological Surveys Using Mixture Models: Application to a Survey of Parvovirus B19." *Statistics in Medicine* 15: 1567–73.

Gay, N. J., Vyse, A. J., Enquselassie, F., Nigatu, W., and Nokes, D. J. 2003. "Improving Sensitivity of Oral Fluid Testing in IgG Prevalence Studies: Application of Mixture Models to a Rubella Antibody Survey." *Epidemiology and Infection* 130 (2): 285–91.

Gerhard, W. 2001. "The Role of the Antibody Response in Influenza Virus Infection." *Current Topics in Microbiology and Immunology* 260: 171–90.

Gillim-Ross, L., and Subbarao, K. 2006. "Emerging Respiratory Viruses: Challenges and Vaccine Strategies." *Clinical Microbiology Reviews* 19 (4): 614–36.

Gorman, O. T., Bean, W. J., Kawaoka, Y., and Webster, R. G. 1990. "Evolution of the Nucleoprotein Gene of Influenza A Virus." *Journal of Virology* 64 (4): 1487–97.

Greiner, M., Franke, C. R. , Bohning, D., and Schlattmann, P. 1994. "Construction of an Intrinsic Cut-off Value for the Sero-Epidemiological Study of Trypanosoma Evansi Infections in a Canine Population in Brazil: A New Approach towards an Unbiased Estimation of Prevalence." *Acta Tropica* 56 (1): 97–109.

Grilli, E. A., Davies, J. R., and Smith, A. J. 1986. "Infection with Influenza A H1N1. 1. Production and Persistence of Antibody." *The Journal of Hygiene* 96 (2): 335–43.

Gupta, V. Y., Dawood, F. S., Muangchana, C., Phan, T. L., Xeuatvongsa, A., Sovann, L., Olveda, R., et al. 2012. "Influenza Vaccination Guidelines and Vaccine Sales in Southeast Asia: 2008–2011." *PLoS One* 7 (12): e52842.

Hampson, Alan W. 2002. "Influenza Virus Antigens and 'Antigenic Drift.'" In *Influenza*, edited by CW Potter, 49–85. Elsevier.

Hancock, K., Veguilla, V., Lu, X., Zhong, W., Butler, E. N., Sun, H., Liu, F., et al. 2009. "Cross-Reactive Antibody Responses to the 2009 Pandemic H1N1 Influenza Virus." *The New England Journal of Medicine* 361 (20): 1945–52.

Hardelid, P., Williams, D., Dezateux, C., Tookey, P. A., Peckham, C. S., Cubitt, W. D., and Cortina-Borja, M. 2008. "Analysis of Rubella Antibody Distribution from Newborn Dried Blood Spots Using Finite Mixture Models." *Epidemiology and Infection* 136 (12): 1698–1706.

Hayward, A. C., Fragaszy, E. B., Bermingham, A., Wang, L., Copas, A., Edmunds, W. E., Ferguson, N., et al. 2014. "Comparative Community Burden and Severity of Seasonal and Pandemic Influenza: Results of the Flu Watch Cohort Study." *The Lancet Respiratory Medicine* 2 (6): 445–54.

Heisterkamp, S. H., de Vries, R., Sprenger, H. G., Hubben, G. A. A., and Postma, M. J. 2008. "Estimation and Prediction of the HIV–AIDS-Epidemic under Conditions of HAART Using Mixtures of Incubation Time Distributions." *Statistics in Medicine* 27 (6): 781–94.

Hens, N., Shkedy, Z., Aerts, M., Faes, C., van Damme, P., and Beutels, P. 2012. *Modeling Infectious Disease Parameters Based on Serological and Social Contact Data*. Vol. 63. Statistics for Biology and Health. New York, NY: Springer New York.

Hien, T. T., Boni, M. F., Bryant, J. E., Ngan, T. T., Wolbers, M., Nguyen, T. D., Truong, N. T., et al. 2010. "Early Pandemic Influenza (2009 H1N1) in Ho Chi Minh City, Vietnam: A Clinical Virological and Epidemiological Analysis." *PLoS Medicine* 7 (5): e1000277.

Hillaire, M. L. B., van Trierum, S. E., Kreijtz, J. H. C. M., Bodewes, R., Geelhoed-Mieras, M. M., Nieuwkoop, N. J., Fouchier, R. A. M., Kuiken, T., Osterhaus, A. D. M. E., and Rimmelzwaan, G. F. 2011. "Cross-Protective Immunity against Influenza pH1N1 2009 Viruses Induced by Seasonal Influenza A (H3N2) Virus Is Mediated by Virus-Specific T-Cells." *Journal of General Virology* 92 (10): 2339–49.

Hobson, D. 1974. "Assessment of the Efficacy of Influenza Vacines against Natural Challenge." *Developments in Biological Standardization Journal* 28: 285–94.

Hobson, D., Curry, R. L., Beare, A. S., and Ward-Gardner, A. 1972. "The Role of Serum Haemagglutination-Inhibiting Antibody in Protection against Challenge Infection with Influenza A2 and B Viruses." *Journal of Hygiene* 70: 767–77.

Holmes, E. C., Ghedin, E., Miller, N., Taylor, J., Bao, Y., St George, K., Grenfell, B. T., et al. 2005. "Whole-Genome Analysis of Human Influenza A Virus Reveals Multiple Persistent Lineages and Reassortment among Recent H3N2 Viruses." *PLoS Biology* 3 (9): 1579–89.

Hope-Simpson, R E. 1981. "The Role of Season in the Epidemiology of Influenza." *The Journal of Hygiene* 86 (1): 35–47. doi:10.1017/S0022172400068728.

Horby, P., Le, Q. M., Fox, A., Thai, P. Q., Yen, N. T. T., Thanh, L. T., Hang, N. L. K., et al. 2012. "The Epidemiology of Interpandemic and Pandemic Influenza in Vietnam, 2007-2010: The Ha Nam Household Cohort Study I." *American Journal of Epidemiology* 175 (10): 1062–74.

Horsfall, F. L., Hahn, R. G., and Rickard, E. R. 1940. "Four Recent Influenza Epidemics: An Experimental Study." *Journal of Clinical Investigation* 19 (2): 379–92.

Horsfall, F. L., and Richard, E. R. 1941. "Neutralizing Antibodies in Human Serum After Influenza A: The Lack of Strain-Specific in the Immunological Response." *The Journal of Experimental Medicine* 74 (5): 433–39.

Huijskens, E. G. W., Reimerink, J., Mulder, P. G. H., van Beek, J., Meijer, A., de Bruin, E., Friesema, I., et al. 2013. "Profiling of Humoral Response to Influenza A(H1N1)pdm09 Infection and Vaccination Measured by a Protein Microarray in Persons with and without History of Seasonal Vaccination." *PloS One* 8 (1): e54890.

Hung, I. F. N., To, K. K. W., Lee, C., Lin, C., Chan, J. F. W., Tse, H., Cheng, V. C. C., et al. 2010. "Effect of Clinical and Virological Parameters on the Level of Neutralizing Antibody against Pandemic Influenza A Virus H1N1 2009." *Clinical Infectious Diseases* 51 (3): 274–79.

Isakova-sivak, I., Rudenko, L., and Isakova-sivak, I. 2015. "Safety, Immunogenicity and Infectivity of New Live Attenuated Influenza Vaccines." *Expert Review of Vaccines* 14 (10): 1313–29.

Iwatsuki-Horimoto, K., Horimoto, T., Tamura, D., Kiso, M., Kawakami, E., Hatakeyama, S., Ebihara, Y., et al. 2011. "Seroprevalence of Pandemic 2009 (H1N1) Influenza A Virus among Schoolchildren and Their Parents in Tokyo, Japan." *Clinical and Vaccine Immunology* 18 (5): 860–66.

Jameson, J., Cruz, J., and Ennis, F. A. 1998. "Human Cytotoxic T-Lymphocyte Repertoire to Influenza A Viruses." *Journal of Virology* 72 (11): 8682–89.

Jang, Y. H., Byun, Y. H., Lee, Y. J., Lee, Y. H., Lee, K.-H., and Seong, B. L. 2012. "Cold-Adapted Pandemic 2009 H1N1 Influenza Virus Live Vaccine Elicits Cross-Reactive Immune Responses against Seasonal and H5 Influenza A Viruses." *Journal of Virology* 86 (10): 5953–58.

Kafatos, G., Andrews, N. J., McConway, K. J., Maple, P. a. C., Brown, K., and Farrington, C. P. 2015. "Is It Appropriate to Use Fixed Assay Cut-Offs for Estimating Seroprevalence?" *Epidemiology and Infection*: 1–9.

Kilbourne, E. D., Laver, W. G., Schulman, J. L., and Webster, R. G. 1968. "Antiviral Activity of Antiserum Specific for an Influenza Virus Neuraminidase." *Journal of Virology* 2 (4): 281–88.

Kilbourne, E. D. 1978. "Opinion : Influenza As a Problem in Immunology." *The Journal of Immunology* 120 (5): 1447–52.

Koopmans, M., de Bruin, E., Godeke, G-J., Friesema, I., van Gageldonk, R., Schipper, M., Meijer, A., et al. 2012. "Profiling of Humoral Immune Responses to Influenza Viruses by Using Protein Microarray." *Clinical Microbiology and Infection* 18 (8): 797–807.

Koul, Parvaiz A, Shobha Broor, Siddhartha Saha, John Barnes, Catherine Smith, Michael Shaw, Mandeep Chadha, and Renu B Lal. 2014. "Differences in Influenza Seasonality by Lattitude, Northern India." *Emerging Infectious Diseases* 20 (10): 1723–26.

Kreijtz, J.H.C.M., R.A.M. Fouchier, and G.F. Rimmelzwaan. 2011. "Immune Responses to Influenza Virus Infection." *Virus Research* 162 (1–2): 19–30.

Kucharski, Adam J, Justin Lessler, Jonathan M Read, Huachen Zhu, Chao Qiang Jiang, Yi Guan, Derek A T Cummings, and Steven Riley. 2015. "Estimating the Life Course of Influenza A(H3N2) Antibody Responses from Cross-Sectional Data." Edited by Andrew Fraser Read. *PLoS Biology* 13 (3): e1002082.

Lam, H. M., Wesolowski, A., Hung, N. T., Nhat, N. T. D., Todd, S., Vinh, D. N., et al. 2017. "Non-Annual Seasonality of Influenza-like Illness in a Tropical Urban Setting." *bioRxiv*, 100222.

Le, M. Q., Lam, H. M., Vuong, D. C., Lam, T. T., Halpin, R. A., Wentworth, A. E., Nguyen, T. H., Le, T. T., Hoang, V. M. P., et al. 2013. "Migration and Persistence of Human Influenza A Viruses, Vietnam, 2001-2008." *Emerging Infectious Diseases* 19 (11): 1756–65.

Lessler, J., Reich, N. G., Brookmeyer, R., Perl, T. M., Nelson, K. E., and Cummings, D. A. T. 2009. "Incubation periods of acute respiratory viral infections: a systematic review." *The Lancet Infectious Diseases* 9(5):291–300.

Lessler, J., Riley, S., Read, J. M., Wang, S., Zhu, H., Smith, G. J. D., Guan, Y., Jiang, C. Q., and Cummings, D. T. 2012. "Evidence for Antigenic Seniority in Influenza A (H3N2) Antibody Responses in Southern China." *PLoS Pathogens* 8 (7): e1002802.

Lindblade, K. A., Steinhardt, L., Samuels, A., Kachur, S. P., and Slutsker, L. 2013. "The Silent Threat: Asymptomatic Parasitemia and Malaria Transmission." *Expert Review of Anti-Infective Therapy* 11 (6): 623–39.

Liu, W., Ma, M. J., Tang, F., He, C., Zhang, X. A., Jiang, L. F., Xin, D. S., Hu, C. Y., Looman, C., and Cao, W. C. 2012. "Host Immune Response to A(H1N1)pdm09 Vaccination and Infection: A One-Year Prospective Study on Six Cohorts of Subjects." *Vaccine* 30 (32): 4785–89.

Liu, Y., Tao, H., Ma, F., Lu, P., Hu, Y., Ding, X., Liu, P., et al. 2011. "Sero-Epidemiology of Measles in General Population in Jiangsu Province of China: Application of Mixture Models to Interpret the Results from a Cross-Sectional Study." *Vaccine* 29 (5): 1000–1004.

Lowen, A. C., Mubareka, S.,. Steel, J., and Palese, P. 2007. "Influenza Virus Transmission Is Dependent on Relative Humidity and Temperature." *PLoS Pathogens* 3 (10): 1470–76.

Ly, S., Arashiro, T., Ieng, V., Tsuyuoka, R., Parry, A., Horwood, P., Heng, S., et al. 2017. "Establishing Seasonal and Alert Influenza Thresholds in Cambodia Using the WHO Method: Implications for Effective Utilization of Influenza Surveillance in the Tropics and Subtropics." *Western Pacific Surveillance and Response Journal* 8 (1): 22–32.

Matias, G., Taylor, R. J., Haguinet, F., Schuck-Paim, C., Lustig, R. L., and Fleming, D. M. 2016. "Modelling Estimates of Age-Specific Influenza-Related Hospitalisation and Mortality in the United Kingdom." *BMC Public Health* 16 (1): 481.

McLachlan, G., and Peel, D. 2000. *Finite Mixture Models*. New York, NY: John Wiley and Sons, Inc.

McLeish, N. J., Simmonds, P., Robertson, C., Handel, I., McGilchrist, M., Singh, B. K., Kerr, S., et al. 2011. "Sero-Prevalence and Incidence of A/H1N1 2009 Influenza Infection in Scotland in Winter 2009–2010." *PLoS ONE* 6 (6): e20358.

McMichael, A. J., Gotch, F. M., Noble, G. R., and Beare, P. A. 1983. "Cytotoxic T-Cell Immunity to Influenza." *New England Journal of Medicine* 309 (1): 13–17.

Miller, E., Hoschler, K., Hardelid, P., Stanford, E., Andrews, N., and Zambon, M. 2010. "Incidence of 2009 Pandemic Influenza A H1N1 Infection in England: A Cross-Sectional Serological Study." *The Lancet* 375 (9720): 1100–1108.

Miller, M. S., Gardner, T. J., Krammer, F., Aguado, L. C., Tortorella, D., Basler, C. F., and Palese, P. 2013. "Neutralizing Antibodies Against Previously Encountered Influenza Virus Strains Increase over Time: A Longitudinal Analysis." *Science Translational Medicine* 5 (198): 198ra107.

Ministry of Planning and Investment, General Statistics Office. 2011. "Vietnam Population and Housing Census 2009, Age-Sex Structure and Marital Status of the Population in Vietnam". Ha Noi, Vietnam.

Moura, Fernanda E A, Anne C B Perdigão, and Marilda M Siqueira. 2009. "Seasonality of Influenza in the Tropics : A Distinct Pattern in Northeastern Brazil." *American Journal of Epidemiology* 81 (1): 180–83.

Murphy, B. R., J. A. Kasel, and R. M. Chanock. 1972. "Association of Serum Anti-Neuraminidase Antibody with Resistance to Influenza in Man." *New England Journal of Medicine* 286 (25): 1329–32.

Murphy, B. R., and Clements, M. L. 1989. "The Systemic and Mucosal Immune Response of Humans to Influenza A Virus." In *New Strategies for Oral Immunization: International Symposium at the University of Alabama at Birmingham and Molecular Engineering Associates, Inc. Birmingham, AL, USA, March 21--22, 1988*, edited by Jiri Mestecky and Jerry R McGhee, 107–16.

Nelson, M. I., Njouom, R., Viboud, C., Niang, M. N. D., Kadjo, H., Ampofo, W., Adebayo, A., et al. 2014. "Multiyear Persistence of 2 Pandemic A/H1N1 Influenza Virus Lineages in West Africa." *Journal of Infectious Diseases* 210 (1): 121–25.

Nelson, M. I., Simonsen, L., Viboud, C., Miller, M. A., Taylor, J., St George, K., Griesemer, S., B., et al. 2006. "Stochastic Processes Are Key Determinants of Short-Term Evolution in Influenza A Virus." *PLoS Pathogens* 2 (12): 1145–51.

Neuenschwander, B. E., Zwahlen, M., Kim, S. J., Engel, R. R., and Rieder, H. L., 2000. "Trends in the Prevalence of Infection with Mycobacterium Tuberculosis in Korea from 1965 to 1995: An Analysis of Seven Surveys by Mixture Models." *International Journal of Tuberculosis and Lung Disease* 4 (8): 719–29.

Neuenschwander, B. E., Zwahlen, M., Kim, S. J., Lee, E. G., and Rieder, H. L. 2002. "Determination of the Prevalence of Infection with Mycobacterium Tuberculosis among Persons Vaccinated against Bacillus Calmette-Guérin in South Korea." *American Journal of Epidemiology* 155 (7): 654–63.

Ng, S., Fang, V. J., Ip, D. K. M., Chan, K-H., Leung, G. M., Peiris, J. S. M., and Cowling, B. J. 2013. "Estimation of the Association between Antibody Titers and Protection against Confirmed Influenza Virus Infection in Children." *The Journal of Infectious Diseases* 208 (8): 1320–24.

Ng, Sophia, and Gordon, A. 2015. "Influenza Burden and Transmission in the Tropics." *Current Epidemiology Reports* 2 (2): 89–100.

Nguyen, H. L. K., Saito, R., Ngiem, H. K., Nishikawa, M., Shobugawa, Y., Nguyen, D. C., Hoang, L. T., Huynh, L. P., and Suzuki, H. 2007. "Epidemiology of Influenza in Hanoi, Vietnam, from 2001 to 2003." *Journal of Infection* 55 (1): 58–63.

Nguyen, H. T., Dharan, N. J., Le, M. T. Q., Nguyen, N. B., Nguyen, C. T., Hoang, D. V., Tran, H. N., et al. 2009. "National Influenza Surveillance in Vietnam, 2006–2007." *Vaccine* 28 (2): 398–402.

Nguyen, Y. T., Graitcer, S. B., Nguyen, T. H., Tran, D. N., Pham, T. D., Le, M. T. Q., Tran, H. N., et al. 2013. "National Surveillance for Influenza and Influenza-like Illness in Vietnam, 2006-2010." *Vaccine* 31 (40): 4368–74.

Nicholson, K. G., Wood, J. M., and Zambon, M. 2003. "Influenza." *Lancet* 362: 1733–45.

Nielsen, S. S., Toft, N., Jørgensen, E., and Bibby, B. M. 2007. "Bayesian Mixture Models for within-Herd Prevalence Estimates of Bovine Paratuberculosis Based on a Continuous ELISA Response." *Preventive Veterinary Medicine* 81 (4): 290–305.

Pai, M., Dendukuri, N., Wang, L., Joshi, R., Kalantri, S., and Rieder, H. L. 2008. "Improving the Estimation of Tuberculosis Infection Prevalence Using T-Cell-Based Assay and Mixture Models." *The International Journal of Tuberculosis and Lung Disease* 12 (8): 895–902.

Palache, A., Abelin, A., Hollingsworth, R., Cracknell, W., Jacobs, C., Tsai, T., and Barbosa, P. 2017. "Survey of Distribution of Seasonal Influenza Vaccine Doses in 201 Countries (2004–2015): The 2003 World Health Assembly Resolution on Seasonal Influenza Vaccination Coverage and the 2009 Influenza Pandemic Have Had Very Little Impact on Improving Influenz." *Vaccine* 35 (36): 4681–86.

Patterson Ross, Z., Komadina, N., Deng, Y. M., Spirason, N., Kelly, H. A., Sullivan, S. G., Barr, A. G., and Holmes, E. C. 2015. "Inter-Seasonal Influenza Is Characterized by Extended Virus Transmission and Persistence." *PLoS Pathogens* 11 (6): 1–16.

Pollett, S., Nelson, M. I., Kasper, M., Tinoco, Y., Simons, M., Romero, C., Silva, M., et al. 2015. "Phylogeography of Influenza A(H3N2) Virus in Peru, 2010–2012." *Emerging Infectious Diseases* 21 (8): 1330–38.

Potter, C. W., and Oxford, J. S. 1979. "Determinants of Immunity to Influenza Infection in Man." *British Medical Bulletin* 35 (1): 69–75.

Rambaut, A., Pybus, O. G., Nelson, M. I., Viboud, C., Taubenberger, J. K., and Holmes, E. C. 2008. "The Genomic and Epidemiological Dynamics of Human Influenza A Virus." *Nature* 453 (7195): 615–20.

Rizzo, C., Rota, M. C., Bella, A., Alfonsi, V., Declich, S., Caporali, M. G., Ranghiasci, A., et al. 2010. "Cross-Reactive Antibody Responses to the 2009 A/H1N1v Influenza Virus in the Italian Population in the Pre-Pandemic Period." *Vaccine* 28 (20): 3558–62.

Rota, M. C., Massari, M., Gabutti, G., Guido, M., de Donno, A., and Atti, M. L. C. d. 2008. "Measles Serological Survey in the Italian Population: Interpretation of Results Using Mixture Model." *Vaccine* 26 (34): 4403–9.

Rothbarth, P. H., Groen, J., Bohnen, A. M., de Groot, R., and Osterhaus. A. D. M. E. 1999. "Influenza Virus Serology—a Comparative Study." *Journal of Virological Methods* 78 (1–2): 163–69.

Russell, C. A., Jones, T. C., Barr, I. G., Cox, N. J., Garten, R. J., Gregory, V., Gust, I. D., et al. 2008. "The Global Circulation of Seasonal Influenza A (H3N2) Viruses." *Science* 320 (5874): 340–46.

Saha, S., Chadha, M., Mamun, A. A., Rahman, M., Sturm-Ramirez, K., Chittaganpitch, M., Pattamadilok, S., et al. 2014. "Influenza Seasonality and Vaccination Timing in Tropical and Subtropical Areas of Southern and South-Eastern Asia." *Bulletin of the World Health Organization* 92 (5): 318–30.

Sangkawibha, N., Rojanasuphot, S., Ahandrik, S., Viriyapongse, S., Jatanasen, S., Salitul, V., Phanthumachinda, B., and Halstead, S. B. 1984. "Risk Factors in Dengue Shock Syndrome: A Prospective Epidemiologic Study in Rayong, Thailand. I. The 1980 Outbreak." *American Journal of Epidemiology* 120 (5): 653–69.

Scholtissek, C. 2002. "Pandemic Influenza: Antigenic Shift." In *Influenza*, edited by Potter, C. W. 87–100. Elsevier.

Schrauwen, E. J. A., and Fouchier, R. A. M. 2014. "Host Adaptation and Transmission of Influenza A Viruses in Mammals." *Emerging Microbes & Infections* 3 (2): e9.

Schulman, J. L., and Kilbourne, E. D. 1965. "Induction of Partial Specific Heterotypic Immunitv in Mice by a Single Infection with Influenza A Virus." *Journal of Bacteriology* 89 (1): 170–74.

Shaman, J., and Kohn, M. 2009. "Absolute Humidity Modulates Influenza Survival, Transmission, and Seasonality." *Proceedings of the National Academy of Sciences of the United States of America* 106 (9): 3243–48.

Shaman, J., Goldstein, E., and Lipsitch, M. 2011. "Absolute Humidity and Pandemic versus Epidemic Influenza." *American Journal of Epidemiology* 173 (2): 127–35.

Shaman, J., Pitzer, V. E., Viboud, C., Grenfell, B. T., and Lipsitch, M. 2010. "Absolute Humidity and the Seasonal Onset of Influenza in the Continental United States." *PLoS Biology* 8 (2): e1000316.

Shek, L. P., and Lee, B. 2003. "Epidemiology and Seasonality of Respiratory Tract Virus Infections in the Tropics." *Paediatric Respiratory Reviews* 4 (2): 105–11.

Simonsen, J., Strid, M. A., Mølbak, K., Krogfelt, K. A., Linneberg, A., and Teunis, P. 2008. "Sero-Epidemiology as a Tool to Study the Incidence of Salmonella Infections in Humans." *Epidemiology and Infection* 136 (7): 895–902.

Simonsen, J., Mølbak, K., Falkenhorst, G., Krogfelt, K. A., and Linneberg, A. 2009. "Estimation of Incidences of Infectious Diseases Based on Antibody Measurements." *Statistics in Medicine* 28 (14): 1882–95.

Smith, D. J., Lapedes, A. S., de Jong, J. C., Besterbroer, T. M., Rimmelzwaan, G. F., Osterhaus, A. D. M,. E., and Fouchier, R. A. M. 2004. "Mapping the Antigenic and Genetic Evolution of Influenza Virus." *Science* 305 (5682): 371–76.

Soh, S. E., Cook, A. R., Chen, M. I. C., Lee, V. J., Cutter, J. L., Chow, V. T. K., Tee, N. W. S., et al. 2012. "Teacher Led School-Based Surveillance Can Allow Accurate Tracking of Emerging Infectious Diseases - Evidence from Serial Cross-Sectional Surveys of Febrile Respiratory Illness during the H1N1 2009 Influenza Pandemic in Singapore." *BMC Infectious Diseases* 12 (1): 1–12.

Sonoguchi, T., Sakoh, M., Kunita, N., Satsuta, K., Noriki, H., and Fukumi, H. 1986. "Reinfection with Influenza A (H2N2, H3N2, and H1N1) Viruses in Soldiers and Students in Japan." *The Journal of Infectious Diseases* 153 (1): 33–40.

Sridhar, S., Begom, S., Hoschler, K., Bermingham, A., Adamson, W., Carman, W., Riley, S., and Lalvani, A. 2015. "Longevity and Determinants of Protective Humoral Immunity after Pandemic Influenza Infection." *American Journal of Respiratory and Critical Care Medicine* 191 (3): 325–32.

Steens, A., Waaijenborg, S., Teunis, P. F. M., Reimerink, J. H. J., Meijer, A., van der Lubben, M., Koopmans, M., van der Sande, M. a. B., Wallinga, J., and van Boven, M. 2011. "Age-Dependent Patterns of Infection and Severity Explaining the Low Impact of 2009 Influenza A (H1N1): Evidence from Serial Serologic Surveys in the Netherlands." *American Journal of Epidemiology* 174 (11): 1307–15.

Stöhr, K. 2002. "Influenza—WHO Cares." *The Lancet Infectious Diseases* 2 (9): 517.

Strid, M. A., Engberg, J., Larsen, L. B., Begtrup, K., Mølbak, K., and Krogfelt, K A. 2001. "Antibody Responses to CampylobacterInfections Determined by an Enzyme-Linked Immunosorbent Assay : 2-Year Follow-Up Study of 210 Patients Antibody Responses to Campylobacter Infections Determined by an Enzyme-Linked Immunosorbent Assay : 2-Year Follow-Up." *Clinical and Diagnostic Laboratory Immunology* 8 (2): 314–19.

Tamerius, J. D., Nelson, M. I., Zhou, S. Z., Viboud, C., Miller, M. A., and Alonso, W. 2011. "Review Global Influenza Seasonality : Reconciling Patterns across Temperate and Tropical Regions." *Environmental Health Perspectives* 119 (4): 439–45.

Tamerius, J. D., Shaman, J., Alonso, W. J., Bloom-Feshbach, K., Uejio, C. K., Comrie, A., and Viboud, C. 2013. "Environmental Predictors of Seasonal Influenza Epidemics across Temperate and Tropical Climates." *PLoS Pathogens* 9 (3): e1003194.

Taubenberger, J. K., and Reid, A. H. 2002. "The 1918 'Spanish' Influenza Pandemic and Characterization of the Virus That Caused It." In *Influenza*, edited by Potter, C. W. 101–22. Elsevier.

te Beest, D. E., Birrell, P. J., Wallinga, J., de Angelis, J., and van Boven, M. 2014a. "Joint Modelling of Serological and Hospitalization Data Reveals That High Levels of Pre-Existing Immunity and School Holidays Shaped the Influenza A Pandemic of 2009 in The Netherlands." *Journal of The Royal Society Interface* 12 (103): 20141244.

te Beest, D. E., de Bruin, E., Imholz, S., Wallinga, J., Teunis, P., Koopmans, M., and van Boven, M. 2014b. "Discrimination of Influenza Infection (A/2009 H1N1) from Prior Exposure by Antibody Protein Microarray Analysis." *PLoS One* 9 (11): e113021.

te Beest, D. E., de Bruin, E., Imholz, S. Koopmans, M., and van Boven, M. 2017. "Heterosubtypic Cross-Reactivity of HA1 Antibodies to Influenza A, with Emphasis on Nonhuman Subtypes (H5N1, H7N7, H9N2)." *PLoS One* 12 (7): 5–10.

Teunis, P. F. M., Eijkeren, J. C. H., Ang, C. W., Duynhoven, Y. T. H. P., Simonsen, J. B., Strid, M. A., and Pelt, W. 2012. "Biomarker Dynamics: Estimating Infection Rates from Serological Data." *Statistics in Medicine* 31 (20): 2240–48.

Thai, P. Q. 2014. "The Epidemiology and Control of Human Influenza in Vietnam." The Open University, United Kingdom. PhD Thesis.

Thai, P. Q., Choisy, M., Duong, T. N., Thiem, V. D., Yen, N. T., Hien, N. T., Weiss, D. J., Boni, M. F., and Horby, P. 2015. "Seasonality of Absolute Humidity Explains Seasonality of Influenza-like Illness in Vietnam." *Epidemics* 13: 65–73.

Todd, S. 2016. "Influenza in Vietnam: Cross Immunity from Prior Infection and Its Effect on Population-Level Estimates of Infection." University of Liverpool. PhD Thesis.

Todd, S., Nhat, N. T. D., Koopmans, M. P. G., and Boni, M. F. 2014. "Reply to Pawar et Al." *Journal of Infectious Diseases* 210 (1): 159–60.

Tsang, T. K., Cauchemez, S., Perera, R. A. P. M., Freeman, G., Fang, V. J., Ip, D. K. M., Leung, G. M., Peiris, J. S. M., and Cowling, B. J. 2014. "Association between Antibody Titers and Protection against Influenza Virus Infection within Households." *The Journal of Infectious Diseases* 210 (5): 684–92.

Tsang, T. K., Lau, L. L. H., Cauchemez, S., and Cowling, B. J. 2016. "Household Transmission of Influenza Virus." *Trends in Microbiology* 24 (2): 123–33.

United Nations Human Development Programme. 2016. "Human Development Report." http://hdr.undp.org/en/countries/profiles/VNM. (Accessed 31 July 2017).

Van Kerkhove, M. D, Asikainen, T., Becker, N. G., Bjorge, S., Desenclos, J-C., dos Santos, T., Fraser, C., et al. 2010. "Studies Needed to Address Public Health Challenges of the 2009 H1N1 Influenza Pandemic: Insights from Modeling." *PLoS Medicine* 7 (6): e1000275.

Van Kerkhove, M. D., Hirve, S., Koukounari, A., Mounts, A. W., Allwinn, R., Bandaranayake, D. D., Bella, A. A., et al. 2013. "Estimating Age-Specific Cumulative Incidence for the 2009 Influenza Pandemic: A Meta-Analysis of A(H1N1)pdm09 Serological Studies from 19 Countries." *Influenza and Other Respiratory Viruses* 7 (5): 872–86.

Veguilla, V., Hancock, K., Schiffer, J., Gargiullo, P., Lu, X., Aranio, D., Branch, A., et al. 2011. "Sensitivity and Specificity of Serologic Assays for Detection of Human Infection with 2009 Pandemic H1N1 Virus in U.S. Populations." *Journal of Clinical Microbiology* 49 (6):

Versteegh, F. G. A., Mertens, P. L. J. M., de Melker, H. E., Roord, J. J., Schellekens, J. F. P., and Teunis, P. F. M. 2005. "Age-Specific Long-Term Course of IgG Antibodies to Pertussis Toxin after Symptomatic Infection with Bordetella Pertussis." *Epidemiology and Infection* 133 (4): 737–48.

Viboud, C., Alonso, W. J., and Simonsen, L. 2006. "Influenza in Tropical Regions." *PLoS Medicine* 3 (4): e89.

Vinh, D. N., and Boni, M. F. 2015. "Statistical Identifiability and Sample Size Calculations for Serial Seroepidemiology." *Epidemics* 12: 30–39.

Vinh, D. N. 2015. "Influenza in Southern Vietnam: Serial Sero-Epidemiology Investigation." The Open University, United Kingdom. PhD Thesis.

Vink, M. A., van de Kassteele, J., Wallinga, J., Teunis, P. F. M., and Bogaards, J. A. 2015. "Estimating Seroprevalence of Human Papillomavirus Type 16 Using a Mixture Model with Smoothed Age-Dependent Mixing Proportions." *Epidemiology* 26 (1): 8–16.

Vuong, C. D., Hoang, P. M. V., Nguyen, H. L. K., Nguyen, H. T., Nguyen, T. C., Le, T. T., Dennis, D. T., Kapella, B. K., Kile, J. C., and Le, M. Q. 2013. "The Genetic Match between Vaccine Strains and Circulating Seasonal Influenza A Viruses in Vietnam, 2001-2009." *Influenza and Other Respiratory Viruses* 7 (6): 1151–57.

Vyse, A. J., Gay, N. J., Hesketh, L. M., Morgan-Capner, P., and Miller, E. 2004. "Seroprevalence of Antibody to Varicella Zoster Virus in England and Wales in Children and Young Adults." *Epidemiology and Infection* 132 (6): 1129–34.

Waicharoen, S., Thawatsupha, P., Chittaganpitch, M., and Maneewong, P. 2008. "Influenza Viruses Circulating in Thailand in 2004 and 2005." *Japanese Journal of Infectious Diseases* 61: 321–23.

Waldman, R. H., Wppd, S. H., Torres, E. J., and Small, P. A. 1970. "Influenza Antibody Response Following Aerosal Administration of Inactivated Virus." *American Journal of Epidemiology* 91 (6): 575–84.

Watson, D. S., Reddy, S. M., Brahmakshatriya, V., and Lupiani, B. 2009. "A Multiplexed Immunoassay for Detection of Antibodies against Avian Influenza Virus." *Journal of Immunological Methods* 340 (2): 123–31.

Webster, R. G., Bean, W. J., Gorman, O. T., Chambers, T. M., and Kawaoka, Y. 1992. "Evolution and Ecology of Influenza A Viruses." *Microbiological Reviews* 56 (1): 152–79.

Weibel, R. E., Woodhour, A. F., Stokes, J., Friedman, A., McAller, W. J., and Hilleman, M. R. 1970. "New Metabolizable Immunologic Adjuvant for Human Use X. Long-Term Serologi and Clinical Follow-Up." *The American Journal of Medicine* 48: 464–71.

WHO Global Influenza Surveillance Network. 2007. "A Description of the Process of Seasonal and H5N1 Influenza Vaccine Virus Selection and Development." http://apps.who.int/gb/pip/pdf_files/Fluvaccvirusselection.pdf?ua=1. (Accessed 31 July 2017).

WHO Global Influenza Surveillance Network. 2011. *Manual for the Laboratory Diagnosis and Virological Surveillance of Influenza*. http://apps.who.int/bookorders/MDIbookPDF/Book/11500806.pdf?ua=1. (Accessed 31 July 2017).

WHO Global Influenza Surveillance Network. 2016. "Influenza Vaccine Formulation". http://www.who.int/influenza/vaccines/tropics/Vaccine_formulation_1.jpg?ua=1. (Accessed 31 July 2017).

WHO. 2016. "Influenza (Seasonal)." http://www.who.int/mediacentre/factsheets/fs211/en/. (Accessed 31 July 2017).

Wilson, I. A., and Cox, N. J. 1990. "Structural Basis of Immune Recognition of Influenza Virus Hemagglutinin." *Annual Review of Immunology* 8: 737–71.

Wong, C. M., Yang, L., Chan, K. P., Leung, G. M., Chan, K. H., Guan, Y., Lam, T. H., Hedley, A. J., and Peiris, J. S. M. 2006. "Influenza-Associated Hospitalization in a Subtropical City." Edited by Paul Griffiths. *PLoS Medicine* 3 (4): e121.

Wood, J. M., Gaines-Das, R. E., Taylor, J., and Chakraverty, P. 1994. "Comparison of Influenza Serological Techniques by International Collaborative Study." *Vaccine* 12 (2): 167–74.

Word Bank. "World Health Organization Global Health Expenditure Database." 2014. https://data.worldbank.org/indicator/SH.XPD.TOTL.ZS?locations=VN. (Accessed 31 July 2017).

Wu, J. T., Ma, E. S. K., Lee, C. K., Chu, D. K. W., Ho, P. L., Shen, A. L., Ho, A., et al. 2010. "The Infection Attack Rate and Severity of 2009 Pandemic H1N1 Influenza in Hong Kong." *Clinical Infectious Diseases* 51 (10): 1184–91.

Wu, J. T., Ho, A., Ma, E. S. K, Lee, C. K., Chu, D. K. W., Ho, P-L., Hung, I. F. N., et al. 2011. "Estimating Infection Attack Rates and Severity in Real Time during an Influenza Pandemic: Analysis of Serial Cross-Sectional Serologic Surveillance Data." *PLoS Medicine* 8 (10): e1001103.

Wu, J. T., Leung, K., Perera, R. a P. M., Chu, D. K. W., Lee, C. K., Hung, I. F. N., Lin, C. K., et al. 2014. "Inferring Influenza Infection Attack Rate from Seroprevalence Data." *PLoS Pathogens* 10 (4): e1004054.

Yang, W., Cowling, B. J., Lau. E. H. Y., and Shaman, J. 2015. "Forecasting Influenza Epidemics in Hong Kong." *PLOS Computational Biology* 11 (7): e1004383.

Yang, Y., Sugimoto, J. D., Halloran, M. E., Basta, N. E., Chao, D. L., Matrajt, L., Potter, G., Kenah, E., and Longini, I. M. 2009. "The Transmissibility and Control of Pandemic Influenza A (H1N1) Virus." *Science* 326 (5953): 729–33.

Zhao, X., Siegel, K., Chen, M. I. C., and Cook, A. R. 2017. "Rethinking Thresholds for Serological Evidence of Influenza Virus Infection." *Influenza and Other Respiratory Viruses* 11 (3): 202–10.